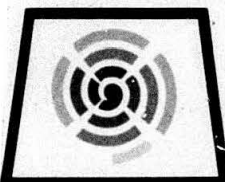


AD A101732



LEVEL III

A 083933

10

THE UNIVERSITY OF NEW MEXICO
COLLEGE OF ENGINEERING

BUREAU OF ENGINEERING RESEARCH

THE WAVY MECHANICAL FACE SEAL
THEORETICAL AND EXPERIMENTAL RESULTS

BY

A. O. LEBECK
and
L. A. YOUNG

SUMMARY REPORT ME-111(81)ONR-414-1

JANUARY 1981

DTIC
ELECTE

JUL 22 1981

D

Prepared for the Office of Naval Research under
Contract Number ONR-N-00014-76-C-0071

DISTRIBUTION STATEMENT A

Approved for public release;
Distribution Unlimited

01722009

DTIC FILE COPY

THE WAVY MECHANICAL FACE SEAL
THEORETICAL AND EXPERIMENTAL RESULTS

by

A. O. Lebeck
Professor of Mechanical Engineering

and

L. A. Young
Research Assistant

The University of New Mexico
Department of Mechanical Engineering
and
Bureau of Engineering Research
Albuquerque, New Mexico 87131

Summary Report ME-111(81)ONR-414-1

January 1981

Prepared for the Office of Naval
Research under Contract Number
ONR-N-00014-76-C-0071

Approved for public release;
distribution unlimited.

Reproduction in whole or in part
is permitted for any purpose of
the United States Government

Accession For	
NTIS GRA&I <input checked="" type="checkbox"/>	
DTIC TAB <input type="checkbox"/>	
Unannounced <input type="checkbox"/>	
Justification _____	
By _____	
Distribution/ _____	
Availability Codes _____	
Dist	Avail and/or Special
A	

DTIC
ELECTED
S JUL 22 1981 D
D

REPORT DOCUMENTATION PAGE		READ INSTRUCTIONS BEFORE COMPLETING FORM
1. REPORT NUMBER	2. GOVT ACCESSION NO.	3. RECIPIENT'S CATALOG NUMBER
	AD-A102 732	
4. TITLE (and Subtitle)	5. TYPE OF REPORT & PERIOD COVERED	
THE WAVY MECHANICAL FACE SEAL - THEORETICAL AND EXPERIMENTAL RESULTS.	Summary Report Dec. 1, 1979 - Nov. 30, 1980	
7. AUTHOR(s)	6. PERFORMING ORG. REPORT NUMBER	
A. O. Lebeck and L. A. Young	ME-111(81)ONR-414-1	
9. PERFORMING ORGANIZATION NAME AND ADDRESS	8. CONTRACT OR GRANT NUMBER(S)	
The University of New Mexico Albuquerque, New Mexico 87131	ONR-N-00014-76-C-0071	
11. CONTROLLING OFFICE NAME AND ADDRESS	10. PROGRAM ELEMENT, PROJECT, TASK AREA & WORK UNIT NUMBERS	
Director, Power Program Dept. of the Navy - Office of Naval Research Arlington, Virginia 22217	(14) 11	
14. MONITORING AGENCY NAME & ADDRESS// different from Controlling Office)	12. REPORT DATE January 1981	
(Tx) T	13. NUMBER OF PAGES 261	
16. DISTRIBUTION STATEMENT (of this Report)	15. SECURITY CLASS. (of this report)	
Approved for public release; distribution unlimited. <i>Approved for public release; distribution unlimited.</i>	Unclassified	
17. DISTRIBUTION STATEMENT (for the abstract entered in Block 20, if different from Report)	18a. DECLASSIFICATION/DOWNGRADING SCHEDULE	
<i>1100 76-35100-10</i>		
18. SUPPLEMENTARY NOTES		
19. KEY WORDS (Continue on reverse side if necessary and identify by block number)		
Mechanical Seals, Seals, Face Seals, Lubrication, Wear, Friction, Waviness		
20. ABSTRACT (Continue on reverse side if necessary and identify by block number)		
In this report the results of theoretical and experimental investigations on the effects of waviness on mechanical face seal performance are presented. In previous work it was shown how waviness imposed on a seal face leads to reduced friction and wear while creating only a small leakage in a water seal. It was also shown that the waviness must be moved slowly (continued on reverse)		

around the seal ring in order that the effect of waviness remain indefinitely. A new device for creating a moving wave with no internal moving parts is described. Experimental results show that the device operates reliably. Using this device, results from wavy seal experiments, show that a moving wave can reduce wear by at least a factor of 200 compared to a flat face seal.

A model for a wavy seal is presented and refined using the Elrod algorithm for determining cavitation. Predicted results for the wavy seal compare favorably to experimental results. Optimum wavy seal design conditions including the number of waves are established.

Theoretical and experimental results are given on the effects of radial taper and high temperature operation on seal performance. Thermal rotation is evaluated experimentally and predicted theoretically. A converging radial taper greatly reduces seal friction and wear during initial operation. Results show how wear progresses across the face. High temperature operation reduces seal friction.

A new concept of a self-forming offset-land seal is described. One ring of the seal continually machines an optimum shape into the mating face. Theoretical and experimental results are given.

APPLICATION OF RESEARCH TO THE NEEDS OF THE U.S. NAVY

Mechanical face seals are used in numerous applications in Naval machinery. These applications range from propeller shaft seals to boiler feed pump seals. In such equipment the mechanical seal plays a vital role. When such seals fail, repair is costly both in terms of lost time and direct costs, so any improvement in seal life and reliability would be of significant benefit.

As more advanced equipment is designed, it is sometimes difficult to achieve desired performance in more severe service environments with the present state of the art of seal design. Thus, an improvement in seal technology would serve this important application.

The immediate objective of the research herein is to further the understanding of mechanical face seal lubrication phenomena. The ultimate objective is to develop the capability of designing contacting face seals having a longer life, greater reliability, and for extreme environments. Thus, the objectives of this research are compatible with mechanical face seal needs for Naval machinery.

TABLE OF CONTENTS

	<u>Page</u>
Chapter 1 Introduction	1
Mechanical Face Seals.	1
Seal Lubrication	2
Wavy Face Seal	5
Chapter 2 Experimental Program and Results.	13
Test Apparatus Modification.	13
Waviness Drive	14
Friction and Wear Test Apparatus	21
Radial Taper Tests	25
Effects of Pressure Caused Rotation.	32
Surface Roughness.	34
Radial Surface Profiles.	43
High Temperature Tests	50
Long-Term Tests.	64
Offset Land Tests.	66
Speed Effects.	71
Nine-Wave Tests.	76
Chapter 3 Seal Theory Developments.	79
Waviness Drive	79
Waviness Model	82
Optimum Seal Design and Number of Waves.	91
Offset Land Theory	99
Chapter 4 Comparison of Theoretical and Experimental Results.	105
Three-Wave Seal Tests.	105
Radial Taper	105
High Temperature Tests	121
Offset Land Seal	143

TABLE OF CONTENTS (continued)

	<u>Page</u>
Speed Effects.143
Nine-Wave Seal150
Chapter 5 Summary, Conclusions, and Recommendations153
Experimental Results153
Theoretical Results.155
Comparison of Theoretical and Experimental Results156
General.157
References.158
Appendix.161

LIST OF FIGURES

<u>Figure</u>		<u>Page</u>
1-1	Mechanical Face Seal.	3
1-2	Wavy Seal Geometry.	7
1-3	Seal Roughness and Radial Profile	8
1-4	Moving Waviness Concept	12
2-1	Waviness Drive Assembly	15
2-2	Valve Assembly.	16
2-3	Flow Diagram of Waviness Drive System	18
2-4	Waviness Pressure with Time - Gas Supply.	19
2-5	Waviness Pressure with Time - Oil Supply.	20
2-6	Friction and Wear Test Apparatus.	23
2-7	Original and Modified Carbon Seals for Taper Tests. .	26
2-8	Tapering Devices.	27
2-9	Carbon Seal with Strain Gages	33
2-10	Face Taper Versus Strain.	35
2-11	Tangential Roughness Distribution - Test 68	39
2-12	Expanded Surface Profile - Test 68.	40
2-13	Electron Beam Microscope Image of Unworn Carbon . . .	41
2-14	Electron Beam Microscope Image of Worn Carbon	42
2-15	Initial and Final Radial Surface Profiles - Tests 64 and 65	44
2-16	Initial and Final Radial Surface Profiles - Tests 66 and 67	45
2-17	Initial and Final Radial Surface Profiles - Tests 68 and 75	46
2-18	Carbon and Mating Tungsten Carbide Ring - Test 75 . .	48
2-19	Resultant Profile - Test 75	48
2-20	Initial and Final Radial Surface Profiles - Test 76 .	49
2-21	Heating Element	51
2-22	Leakage Catcher	53
2-23	Thermocouple Position	54
2-24	High Temperature Continuous Test, B = 1.00.	60

LIST OF FIGURES (continued)

<u>Figure</u>		<u>Page</u>
2-25	High Temperature Continuous Test, $B = 0.75$	61
2-26	Radial Surface Profile, Seal #5	62
2-27	Radial Surface Profile, Seal #7	63
2-28	Offset Land Seal.	67
2-29	Surface Analyzer Trace of Diamond Indentor Produced Protrusion	69
2-30	Final Offset and Protrusion for Test #108	72
3-1	Pressure Pocket Arrangement for Moving Waviness Generator	80
3-2	Wavy Seal Geometry and Cavitation and Control Volume.	84
3-3	Node Arrangement for Elrod Solution	88
3-4	Film Thickness Distribution \bar{h}	92
3-5	Pressure Distribution - $\bar{p} \times 10^4$	92
3-6	Worn in Film Shape at Various $\bar{\phi}_0$	93
3-7	Torque and Leakage as a Function of Tilt - 1800 rpm .	94
3-8	Torque and Leakage as a Function of Tilt - 1 rpm. . .	94
3-9	Offset Land Seal.	100
3-10	Effect of Land Width on Performance	102
3-11	Effect of Offset on Performance	104
4-1	Effect of Waviness on Leakage, $n = 3$	107
4-2	Effect of Waviness on Torque, $n = 3$	107
4-3	Initial Torque Versus Initial Taper - $B = 0.75$. . .	110
4-4	Leakage Versus Initial Taper at 1 hr - $B = 0.75$. .	111
4-5	Initial Torque Versus Initial Taper - $B = 1.00$. . .	112
4-6	Leakage Versus Initial Taper at 1 hr - $B = 1.00$. .	113
4-7	Torque and Leakage Versus Time, Test 64 - $B = 0.75$. .	115
4-8	Torque and Leakage Versus Time, Test 64 - $B = 0.75$. .	116
4-9	Torque and Leakage Versus Time, Test 65 - $B = 0.75$. .	117
4-10	Torque and Leakage Versus Time, Test 65 - $B = 0.75$. .	118
4-11	Torque and Leakage Versus Time, Test 75 - $B = 0.75$. .	119

LIST OF FIGURES (continued)

<u>Figure</u>	Page
4-12 Torque and Leakage Versus Time, Test 75 - B = 0.75.	.120
4-13 Torque and Leakage Versus Time, Test 24 - B = 1.00.	.122
4-14 Torque and Leakage Versus Time, Test 43 - B = 1.00.	.123
4-15 Final Torque Versus Final Taper - B = 0.75.124
4-16 Final Torque Versus Final Taper - B = 1.00125
4-17 Seal Geometry for Two-Phase Model126
4-18 Torque as a Function of Temperature - B = 1.0130
4-19 Torque as a Function of Temperature - B = 0.75.131
4-20 ΔT Versus Torque, B = 1.0, F Varies133
4-21 ΔT as a Function of Temperature - B = 1.0134
4-22 ΔT as a Function of Temperature - B = 0.75.135
4-23 Theoretical Leakage at $\sigma = 0.5 \mu\text{m}$136
4-24 Geometry of Actual Seal Assembly and Heat Transfer Model138
4-25 Heat Transfer Parameters, B = 1.0140
4-26 Load Function142
4-27 Offset Land Seal Performance.144
4-28 Three Wave Seal Torque - Speed Effect148
4-29 Three Wave Seal Leakage - Speed Effect149

LIST OF TABLES

<u>Table</u>		
2-1	Radial Taper Test Results, $B = 0.75$	29
2-2	Experimental Results - Pressure Caused Rotation. . . .	36
2-3	Radial Taper Test Carbon Surface Statistics.	37
2-4	Initial Surface Data, High Temperature Tests	56
2-5	High Temperature Test Experimental Results, $B = 1.00$.	57
2-6	High Temperature Test Experimental Results, $B = 0.75$.	58
2-7	Long-Term Wear Test Results.	65
2-8	Offset Land Test Results	70
2-9	Wavy Seal Speed Effects.	73
2-10	Flat Face Speed Effects.	74
2-11	Wavy Seal Results, $n = 9$	77
4-1	Computed Results - Elrod Algorithm-Waviness Effect .	106
4-2	Theoretical Effect Results - Radial Taper.	109
4-3	Outside Convection Coefficients, H_0	129
4-4	Computed Results, Elrod Algorithm; Speed Effect at 0 Wear	145
4-5	Computed Results, Elrod Algorithm; Speed Effect at 100% Wear.	146
4-6	Computed Results, Elrod Algorithm; Speed Effect at $n = 9$	151

List of Symbols

$A = \frac{EJ_x}{GJ_\theta}$	Stiffness ratio - dimensionless
$B = \frac{r_o^2 - r_b^2}{r_o^2 - r_i^2}$	Balance ratio for an outside pressurized seal
c	One-half maximum roughness height - m
d	Diameter of gas pressure hole - m
e	Distance between gas pressure hole center and centroid - m
E	Youngs modulus - N/m ²
g	Parameter used in cavity solution
G	Shear modulus - N/m ²
h	Nominal film thickness - m
$\bar{h} = \frac{h}{c}$	Dimensionless film thickness
h_0	Nominal film thickness (between mean roughness heights) - m
H	Total film thickness or enthalpy - m or J/kg
H_i, H_o	Inside and outside convection coefficients - W/m ² K
$J_x = \int_A \frac{y^2}{I - x/r_c} dA$	Stiffness constant about x axis for ring cross section - m ⁴
$J_y = \int_A \frac{x^2}{I - x/r_c} dA$	Stiffness constant about the y axis for ring cross section - m ⁴
$J_{xy} = \int_A \frac{xy}{I - x/r_c} dA$	Stiffness constant - m ⁴
J_θ	Torsional stiffness constant for ring cross section - m ⁴

k_1, k_2	Thermal conductivities for seal materials - W/mK
m_θ, m_{θ_0}	Distributed moment and amplitude on seal ring - N • m/m
$m_{\theta_A}, m_{\theta_B}, m_{\theta_C}$	Moments as defined - N • m/m
\dot{m}_x, \dot{m}_y	Mass flow rate kg/s
n	Number of the harmonic or number of waves around seal face, or direction normal to cavity
p	Fluid pressure - N/m ²
p_c	Cavity pressure - N/m ²
p_g	Gas pressure amplitude causing waviness - N/m ²
$\bar{p} = \frac{pc^2}{r_o^2 \omega n}$	Dimensionless pressure
p_i	Seal inside pressure - N/m ²
p_m	Pressure at asperity contact--equals compressive strength - N/m ²
p_{ma}	Average mechanical contact pressure - N/m ²
p_o	Seal outside pressure - N/m ²
p_s	Shear strength of asperities - N/m ²
p_{sp}	Spring pressure on face - N/m ²
p_A, p_B, p_C	Pressures as defined - N/m ²
Q	Total leakage for the seal - m ³ /s
r	Radial coordinate
r, θ	Seal coordinates

$\bar{r} = \frac{r}{r_0}$	Dimensionless radial coordinate
r_b	Seal balance radius - m
r_c	Radius to centroid of seal ring - m
r_f	Friction radius - m
r_i	Inside radius of seal - m
r_o	Outside radius of seal - m
RWR	Relative wear rate
t	Time - s
T	Seal friction torque - N · m
T, T_∞	Temperature and environmental temperature - K
U	Velocity - m/s
v, v_0	Ring centroid displacement and amplitude - m
$\bar{v} = v/c$	Dimensionless v
v_{op}, v_{om_θ}	Amplitudes of wave caused by face pressure and gas pressure, respectively - m
α	Angle of normal to cavity
β	Compressibility - N/m ²
$\bar{\beta} = \frac{\beta c^2}{r_0^2 \omega n}$	Dimensionless compressibility
η	Viscosity - N · s/m ²
θ	Angular coordinate or flow variable
μ	Friction coefficient
μ_L, μ_G	Viscosities of liquid and gas - N · s/m ²

ρ	Density - kg/m ³
ρ_c	Density at cavity pressure - kg/m ³
λ	A flow variable - dimensionless
σ	Standard deviation of combined roughness - m
ϕ, ϕ_0	Rotation of seal ring about its centroid and amplitude
$\phi_{op_y}, \phi_{om_\theta}$	Tilt amplitude due to face pressures and gas pressures, respectively
$\bar{\phi} = \phi \frac{r_0}{c}$	Adjusted face rotation
ω	Angular speed
Ω	Speed of moving wave
%	Percent of load supported by fluid pressure
-	All symbols with a bar are dimensionless as defined

Chapter 1

Introduction

Mechanical Face Seals

In applications where a rotating shaft must pass from one fluid region to another, contacting mechanical face seals* play the essential role of minimizing the transfer of fluid between the regions. Applications of face seals range from water pump seals to process pump seals to propeller shaft seals. The performance and reliability of contacting mechanical face seals are of great importance for any type of equipment where minimal leakage, high reliability, and long life are necessary. Even for equipment where these factors are not so critical, seal failures and short seal life lead to high operating cost due to down time and maintenance cost.

Even though mechanical face seal technology has been steadily improving over the past several decades, further improvement in the state of the art of seal design would be most beneficial. Although seals having an acceptable life and reliability can be designed for many applications, further improvement in seal life and reliability would result in significant cost savings to the user. Also, there are numerous mechanical face seal applications where seal loading, reliability, life, and leakage requirements are difficult to achieve within the present state of the art. Examples of such applications are seals for pumps for nuclear power plants and seals for large diameter submarine propeller shafts. Additionally, the friction losses in face seals represent a significant fraction of energy consumed for pumping purposes. Within the present state of the art of seal design, it is very difficult to design a low leakage seal that also has a low friction loss.

*The class of low leakage face seals where there is definite contact and wear of the faces as opposed to some hydrostatic or hydrodynamic designs where a definite clearance is maintained.

The main barrier to the advancement of the state of the art in the past has been that the mechanics of seal operation were not well enough understood to be able to reasonably anticipate seal performance as a function of design parameters. It is essential that the lubrication mechanisms between the faces be well understood. In this work, the results from further research into hydrodynamic and hydrostatic lubrication mechanisms in face seals are reported. Much has been learned about these mechanisms. Based upon both theoretical and experimental work, there is a strong promise that effective use of hydrodynamic and hydrostatic mechanisms can now be made to dramatically improve contacting face seal performance.

Seal Lubrication

The mechanical face seal consists basically of two annular rings which rotate relative to each other and which are pressed together by spring and fluid pressures (see Figure 1-1). In conventional seals, the surfaces that rub together are generally manufactured as flat as possible initially so as to minimize leakage. The effective gap between the faces is ideally quite small (order of 1 μm) so that leakage flow across the faces will be quite small. The difficulty in designing a mechanical seal is in maintaining the gap at a very low value while at the same time providing a definite lubricant film between the faces.

The load that must be supported at the faces of a mechanical seal is due primarily to loading caused by the sealed pressure. The unit face load can be expressed as some fraction B of the sealed pressure where B can be made greater or less than unity by geometry selection. The load support at the faces is derived from fluid pressure and mechanical pressure. If the fluid pressure at the faces is large enough to support all of the load, then there will be no contact and no adhesive wear.* If none of

*There may still be abrasive or corrosive wear even if the surfaces do not touch.

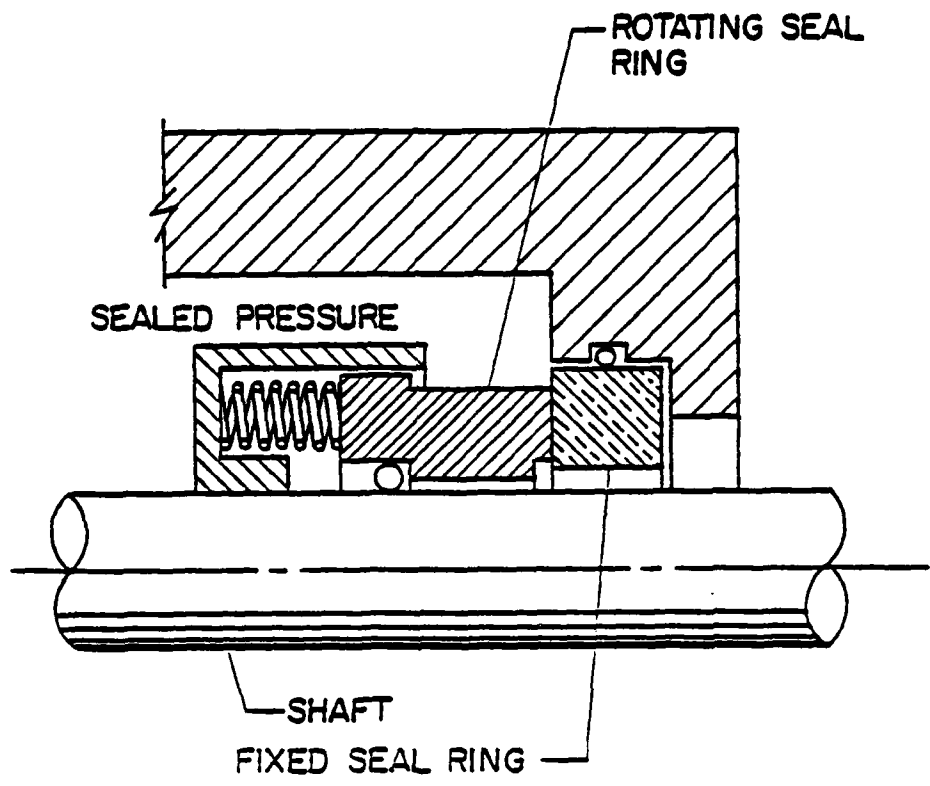


Figure 1-1. Mechanical Face Seal.

the load is supported by fluid pressure, the load must be carried by mechanical contact and the wear rate will be large.

In practice, conventional seals often operate at one of two extremes. At one extreme, a large gap will be created by hydrostatic or hydrodynamic pressure, all of the load will be supported by fluid pressure, and the seal will leak a large amount. At the opposite extreme, the gap will close completely and leakage will be very low. Only a small fraction of the load will be carried by fluid pressure, and wear and heat generation will increase.

Based on the above, it can be concluded that an effective seal should operate between these two extremes--having both adequate fluid pressure load support and low leakage. The seal should operate so that it just touches to minimize leakage but such that the load is carried by fluid pressure, not mechanical pressure. To do this requires that any fluid pressure generation mechanism used to provide load support to the seal must be very carefully controlled. At present, in commercial contacting face seals this lubrication is left primarily to chance, and often such seals operate at one of the extremes mentioned. Quite commonly such seals will operate in the low leakage condition where wear progresses at a definite rate. Such seals are quite satisfactory for many applications. However, when pressure or speed requirements are increased, then this mode of operation may lead to rapid failure through wear or heat checking.

In this research program, attention has been directed toward studying the effects of waviness as a source of hydrodynamic and hydrostatic pressure in face seals. Particular attention has been focused on hydrodynamic effects in relation to roughness and low viscosity applications where some touching is expected. Waviness was selected among the various mechanisms available because it is controllable in seals and a better understanding could lead to improved seal designs.

Wavy Face Seal

The concept of waviness is that the film thickness varies in some fashion circumferentially around the seal. Generally speaking, film thickness may vary radially as well as tangentially.

$$h = h(r, \theta) . \quad (1-1)$$

In the present work interest is focused upon film thickness shapes of the following functional form

$$h = h_0 + f_1(r) \cos n\theta + f_2(r) \sin n\theta . \quad (1-2)$$

At any particular radius r the film shape is periodic with n waves around the seal and is therefore wavy. However, film shape can also vary in some general manner with r .

If $f_1(r) = \text{const}$ and $f_2(r) = \text{const}$, then the faces are always radially parallel. This component of film thickness variation is commonly termed waviness. If the $f_i(r) \neq \text{const}$, then the faces are not in general radially parallel. The $f_i(r)$ are referred to as tilt. Thus, the film thickness shapes of interest are combinations of waviness and tilt. Since at any radius the film thickness is wavy, the combination of waviness and tilt defined above will also be called a wavy film shape.

The reason for choosing film shapes as described by equation (1-2) as a subject for study is that these shapes can conveniently be generated by planned mechanical distortions in a seal ring, and the shapes also include common modes of unplanned distortion found in operating seals. For example, generally seals undergo a uniform tilt due to pressure and thermal deformation. When rings are loaded by any nonaxisymmetric load they become wavy as described by equation (1-2).

Now, for the sake of illustration, assume a seal has a wavy film thickness shape given by equation (1-2) where $n = 2$. Assume a ring is pressed against a perfectly flat, moving, mating ring. For $n = 2$ there will generally be 2 or 4 regions where film

thickness is smallest (only 2 are shown) and where contact can be expected to occur (see Figures 1-2 and 1-3). In general, a fluid pressure distribution develops according to the Reynolds equation. Both hydrostatic and hydrodynamic components are included. Angular rotation of the mating face causes pressure to build up in the converging regions as the minimum film thickness region is approached. In diverging regions, cavitation will occur as the pressure attempts to become negative. For an outside pressurized seal the cavity may appear as shown in Figure 1-2 depending upon the $f_1(r)$. The fluid will flow in streamers across the cavity and a full film will again develop at the downstream cavity boundary.

The problem to be solved is to determine the fluid and mechanical pressure distribution for the given configuration. Given the pressure distribution, then load support and leakage can be calculated, and the effect of various parameters can be studied. Given this tool, then waviness shapes which provide improved performance can be found.

During the first portion of this research program only radially parallel face waviness was considered. Much effort was spent in developing solution methods and studying predicted results.

As background, the pressure distribution for wavy parallel faces has been solved by various methods by Findlay [1], Pape [2], and Stanghan-Batch and Iny [3] for perfectly smooth faces. These results show that even a small waviness produces sufficient load support for complete liftoff. However, heavily loaded or low viscosity seals do not operate with full fluid pressure load support and complete separation. A definite wear results. Surfaces of such seals contact during operation, and pressure distribution is affected by interactions with surface roughness (see Figure 1-3). Seals of this type operate in a mixed friction regime. Fluid pressure load support due to waviness may provide

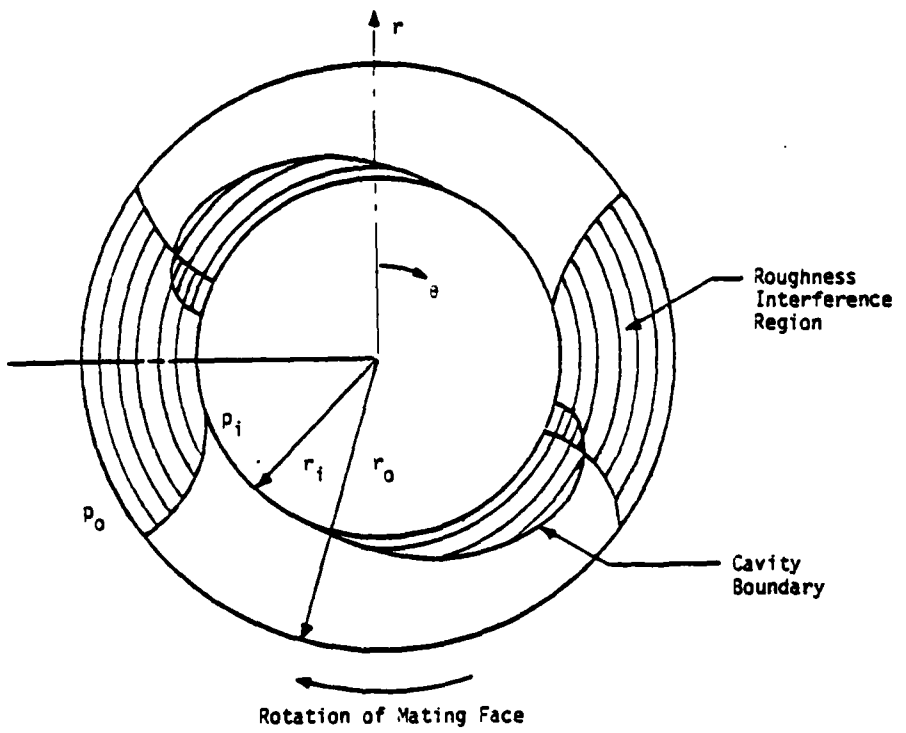


Figure 1-2. Wavy Seal Geometry.

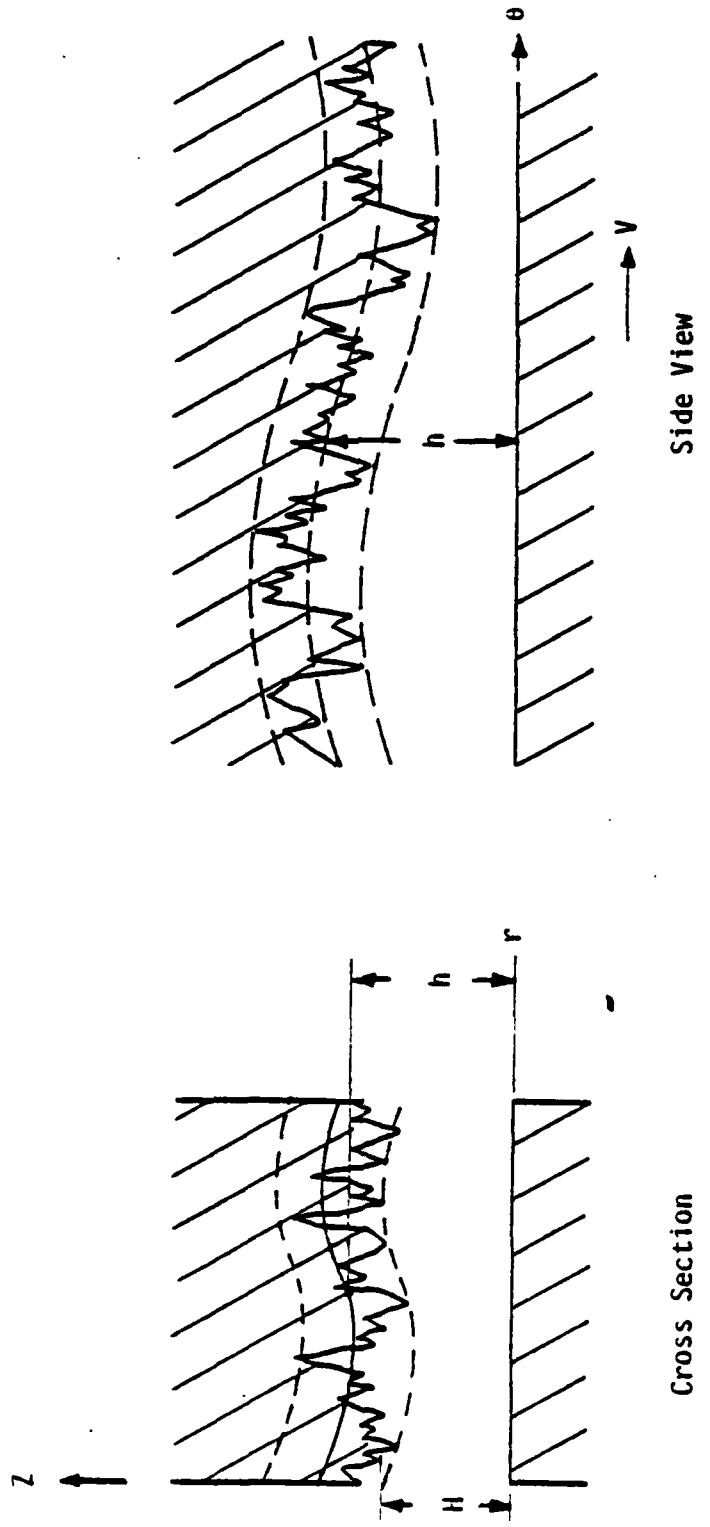


Figure 1-3. Seal Roughness and Radial Profile.

a significant fraction of the load support, but asperity contact must provide the balance.

As a starting point for this research program, these important effects were included in a wavy seal lubrication model. In the first annual report for this project, reference [4], this more general problem was solved using a one-dimensional theory. In the second annual report, [5], the much more complex two-dimensional solution to the above problem was solved. The effects of waviness, roughness, asperity contact, wear, cavitation, and elastic deflection were included in this model. Using this model, predictions were made for the relative wear rate, friction, and leakage as a function of roughness, waviness, speed, size, pressure, viscosity, and material.

A number of conclusions were reached based on these first two annual reports:

- 1) The effects of roughness on hydrodynamic lubrication are not completely understood. Certain fundamental questions remain concerning the roughness model used.
- 2) As to the potential of utilizing hydrodynamic effects caused by parallel face waviness to advantage by design, the results show that wear rate and friction can be greatly reduced while maintaining leakage at acceptable levels.
- 3) While a comparison of predicted results to experimental results given in the literature is generally good, data contained in the literature is incomplete, so more complete experimental data are needed for comparison.
- 4) In low viscosity or heavily loaded applications where some touching is expected to occur, waviness will wear away with time and any benefit derived will be lost.
- 5) Based upon data for some commercial seals and using the model, it was determined that there was insufficient accidentally caused waviness to produce significant

hydrodynamic effects in water. One cannot generalize to say that such effects do not occur in commercial seals. However, the model is provided so that the question can be answered on a case by case basis.

Item 1) was treated extensively in the third annual report [6]. Even after this analysis certain fundamental questions remain concerning how to deal with roughness in lubrication problems. A contribution to the literature on the subject was made [7]. This thorough analysis led to conclusions allowing certain simplifying assumptions discussed in the previous annual report [8].

Item 2) was also treated extensively in the third annual report [6]. A methodology for the design of a wavy face seal was developed and applied. Theoretical results showed large reduction in friction and wear rate compared to conventional designs whereas leakage could be controlled.

Concerning Item 3), the second and third annual reports [5,6] describe a test apparatus designed to test the wavy seal theory. This apparatus has been in operation for more than two years and many tests have been conducted. These test results are reported in Chapter 2 and compared to theory in Chapter 4 of this report. The previous annual report includes additional results [8].

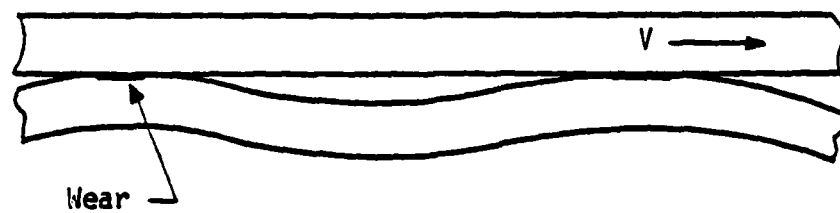
Early in the test program it was observed that the type of waviness which can be practically applied is not of the radially parallel type. Waviness generally consists of alternating tilt plus radially parallel waviness as described by equation (1-2). Based on these considerations, a new model for predicting performance was developed and appears in the previous annual report [8]. In the present report, significant improvements on the model have been made, and a comparison to experimental results has been made.

Concerning Item 4) above, a solution to this problem was first proposed in the first annual report [4]. It was proposed to move the waviness slowly around the seal so that whatever wear occurred would be uniformly distributed. Then the shape of the wave would be preserved and tests using a constant wave could be made. The concept is illustrated in Figure 1-4. This concept was incorporated into the test apparatus and is described in detail in references [5] and [6]. In this report, a new concept to move the waviness with no internal moving parts is described in detail.

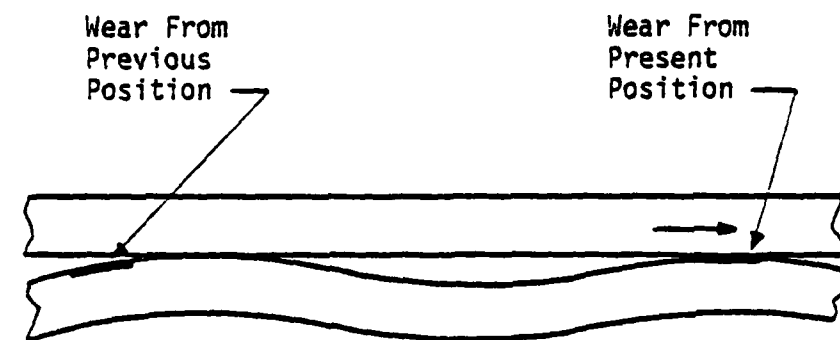
In summary, in this report additional experimental results using waviness are presented, the wavy seal model is further improved, and theory and experiment are compared. The results using a new concept, that of a self-generating seal profile, are reported. Results from tests of the effects of radial taper and high temperature environment are also reported and compared to theory.



Distorted Ring Under Zero Pressure



Distorted Ring Under Pressure



Distorted Ring Under Pressure
After Wave Has Moved

Figure 1-4. Moving Waviness Concept.

Chapter 2

Experimental Program and Results

Since the time the previous report [8] was written, several series of tests have been conducted using the seal test apparatus, several improvements have been made, and a new type of waviness device has been designed, fabricated and tested. These activities will now be described in detail.

Test Apparatus Modification

During the past year several minor improvements were made which are not related directly to a test. First, an electronic tachometer was installed. A gear was mounted on the drive shaft adjacent to a proximity probe such that the output voltage undergoes a cycle as each tooth passes. This signal is fed into a pulse counter card in the HP 6940 multiprogrammer. Using a counting period of 400 ms, controlled by a timer card, a subprogram in the HP 9835 calculates the rpm directly and displays the information during a test.

Second, a reversing control was installed on the main drive motor. Whereas previously a torque zero was found by hand cranking the system first forward and then backward, this procedure is now carried out using the drive motor itself to provide forward and backward rotation at low speed. This procedure has the advantage that it is quicker and more consistent than the hand method.

Third, a fixture was designed to provide a support for the pressure vessel when the vessel is installed. Formerly, installation of the vessel was somewhat awkward and required two people. The device is designed to be removed from contact with the vessel after installation so that torque readings are not affected. Although fabricated, the device has not been installed at this time.

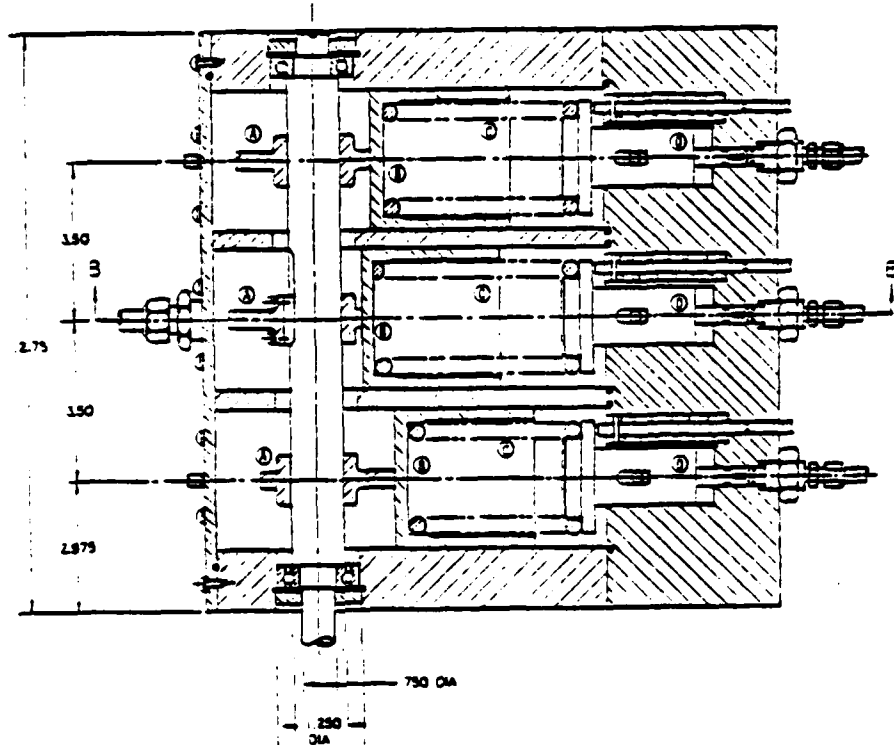
Waviness Drive

As discussed previously [8], moving the wave by physically rotating the pressure pockets relative to the seal ring has the disadvantages that the O-rings slide tangentially and are subject to wear and that a turning mechanism is required within the seal assembly. As will be shown in Chapter 3, the sliding and the turning mechanism can be eliminated by providing three waviness causing pressures, each varying sinusoidally with time, to three separate sets of pressure pockets under the seal. By superposition of deflections, this causes the wave to move.

A device to provide these pressures has been designed, fabricated, and tested on a three-wave seal. Figure 2-1 shows the waviness drive assembly. The three cams **(A)** are driven by a low-speed drive (the same drive as used previously for the waviness drive) at 5.3 revolutions per hour. Each cam is spaced 120° from the other two. The cams are circular in shape and move the flat face followers **(B)**. The circular shape of the cam displaces the follower in a simple harmonic motion. Then the linear spring **(C)** produces a simple harmonic sinusoidal force as a function of time. These forces act on pistons **(D)**. The pistons are sealed off by O-rings.

At the bottom of each piston cylinder is a valve assembly shown in detail in Figure 2-2. Oil hydraulic pressure is supplied at point **(E)**. If the piston is too low (meaning that the pressure in chamber **(F)** is lower than it should be as dictated by the spring force), then the needle valve seat at **(G)** opens, admitting high pressure oil into the chamber **(F)**. If the pressure is too high, then the piston will raise and open the needle valve at **(H)**, thus releasing pressure from the chamber. In this manner the pressure in the chamber is controlled to follow the spring force so that the chamber pressure (connected to the seal pressure pockets) also varies sinusoidally with time.

Section on A-A



Section on B-B

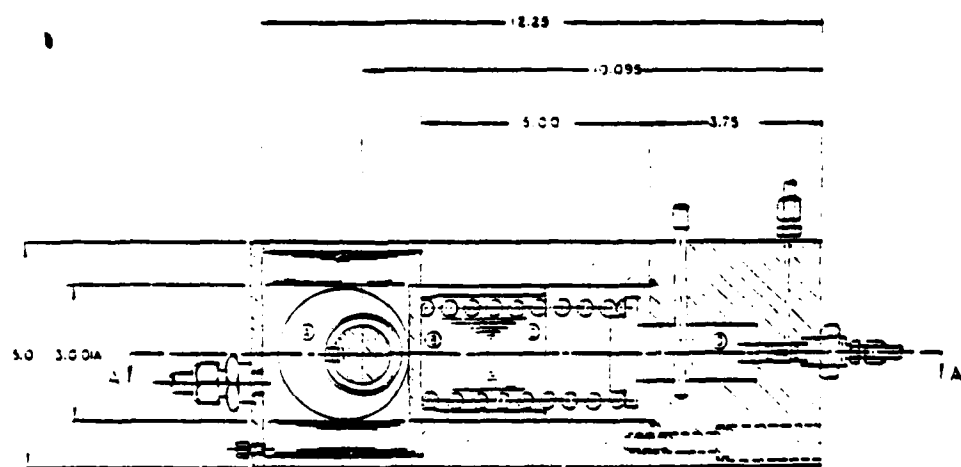


Figure 2-1. Waviness Drive Assembly.

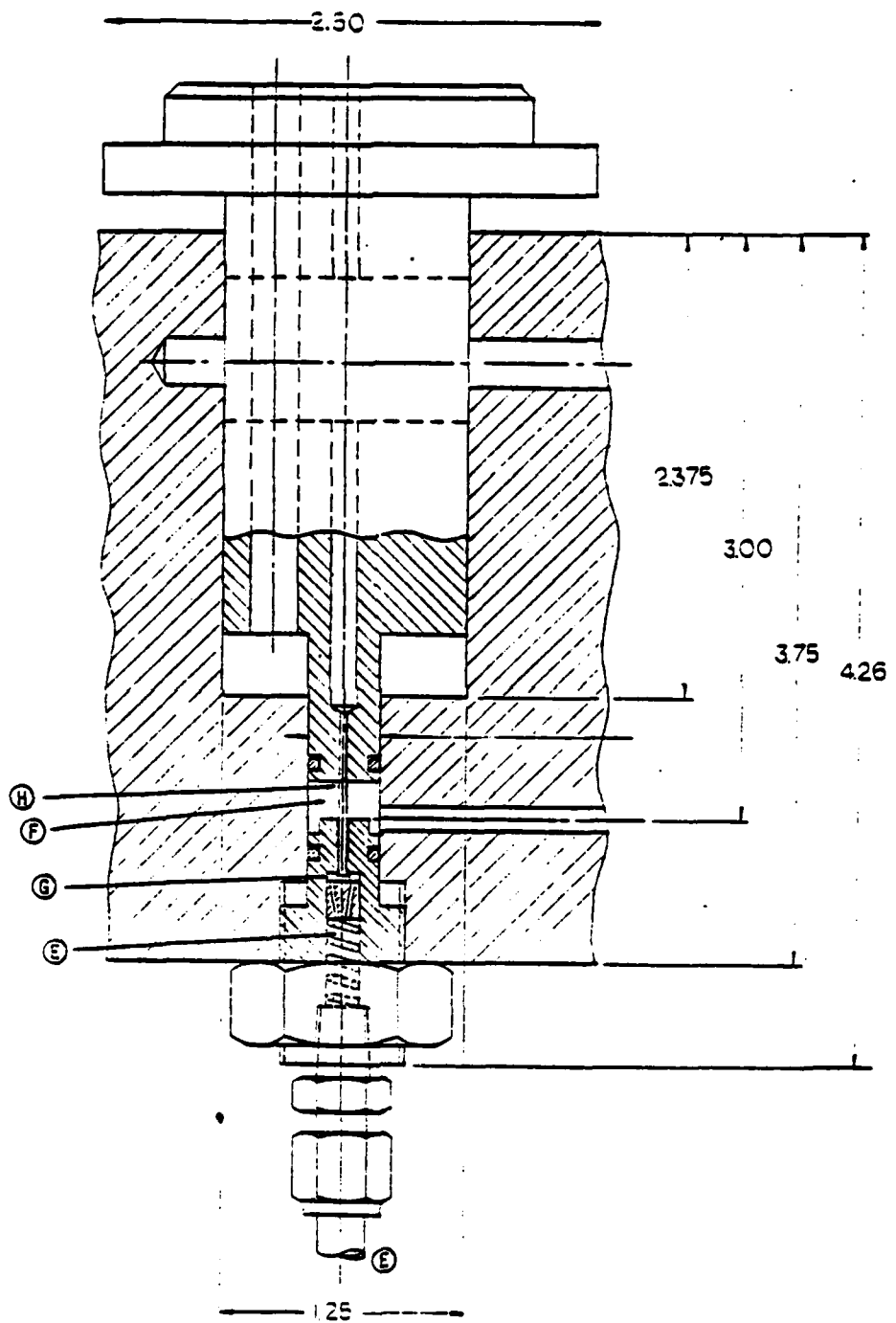


Figure 2-2. Valve Assembly.

The mechanism in essence consists of three programmed pressure regulators. One major difference between this device and a normal pressure regulator, however, is that both an increasing pressure and a decreasing pressure can be provided as needed as the required pressure both increases and then decreases with time.

As first conceived and fabricated the valve assembly in Figure 2-2 was not installed. Instead, each of the three chambers (F) and the lines to the seal were filled with grease. Theoretically, this will provide the same result, given an incompressible system. However, it was found that this approach did not work because of uneven thermal expansion of various parts of the system and because of deflection interactions at the seal itself. That is, as one pressure increased, the seal would deflect and this deflection would increase the volume of the adjacent pressure system. The system was unable to compensate for these errors so an active system using the valves was installed.

A flow diagram of the waviness drive as connected to the seal is shown in Figure 2-3. Hydraulic pressure is maintained by an air driven oil pump. The accumulator reduces pulsation caused by the pump. The oil is supplied to the valves as described. The three regulated pressures are transmitted to three sets of pockets under the seal as shown. Leakage flow through the valves is returned to the sump.

The operation of the waviness drive was verified experimentally by measuring pressure as a function of time. Figure 2-4 shows how the system responded using high pressure nitrogen as a supply rather than oil. The curve has a sinusoidal shape with time. The flattening at the top and bottom is caused by friction in the system and the error introduced by the valve opening force.

Figure 2-5 shows the time response using high pressure oil. Although the general shape is clearly sinusoidal, there are

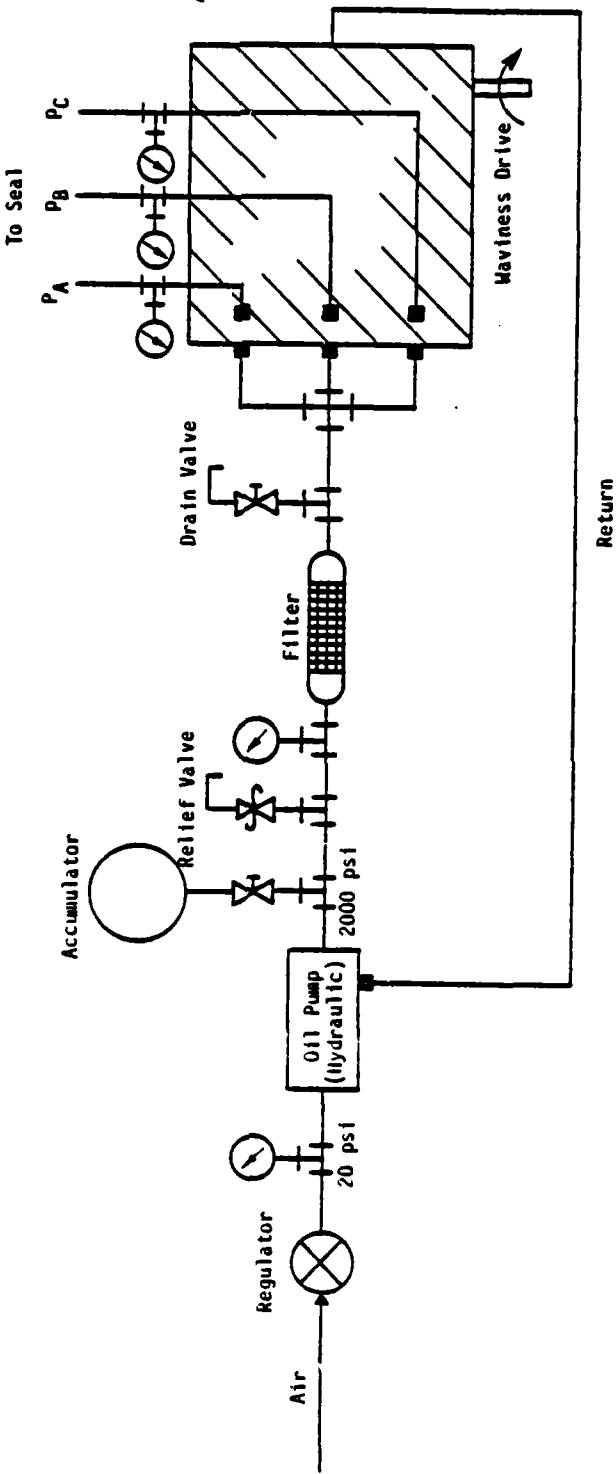


Figure 2-3. Flow Diagram for Waviness Drive System.

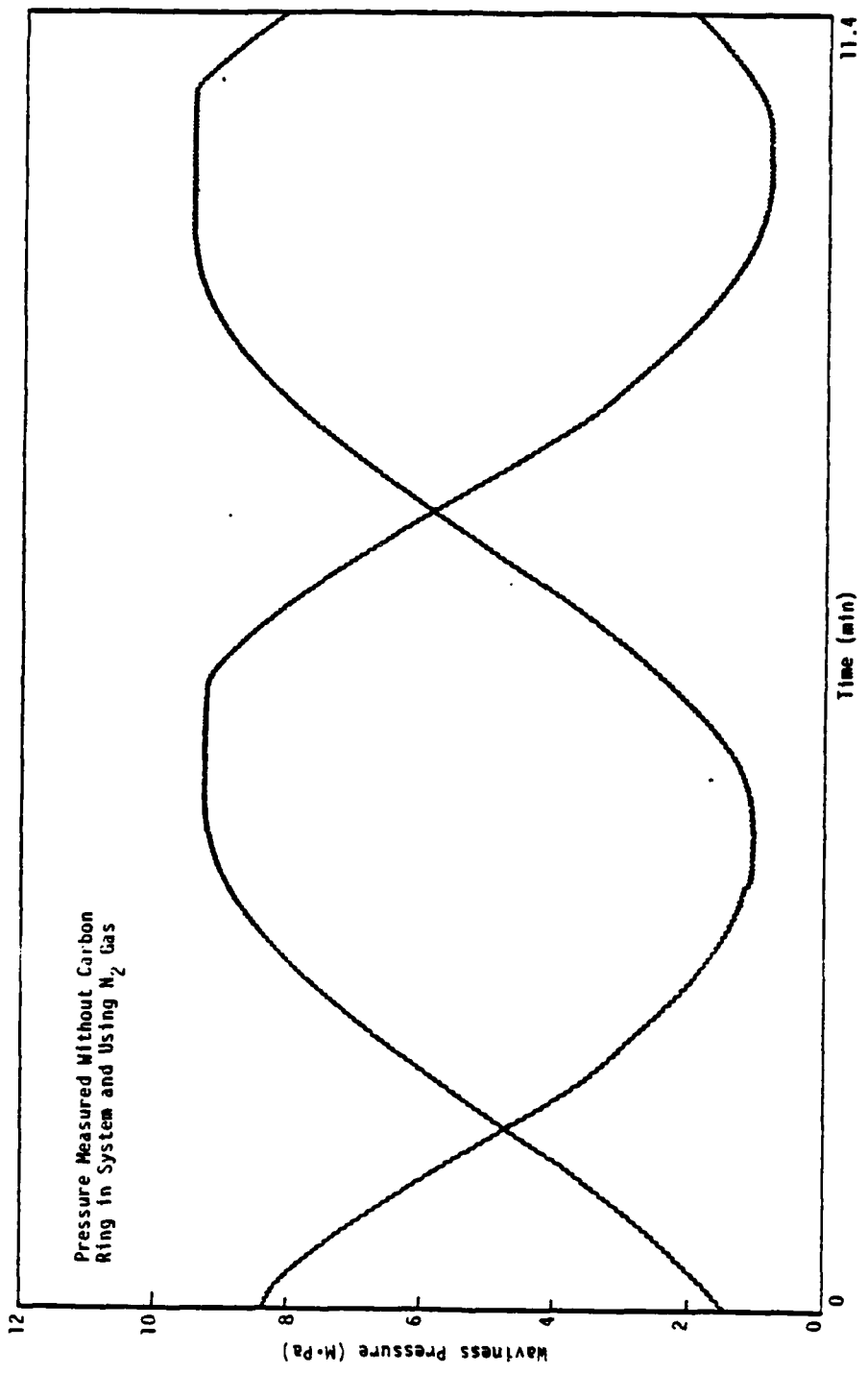


Figure 2-4. Waviness Pressure with Time - Gas Supply.

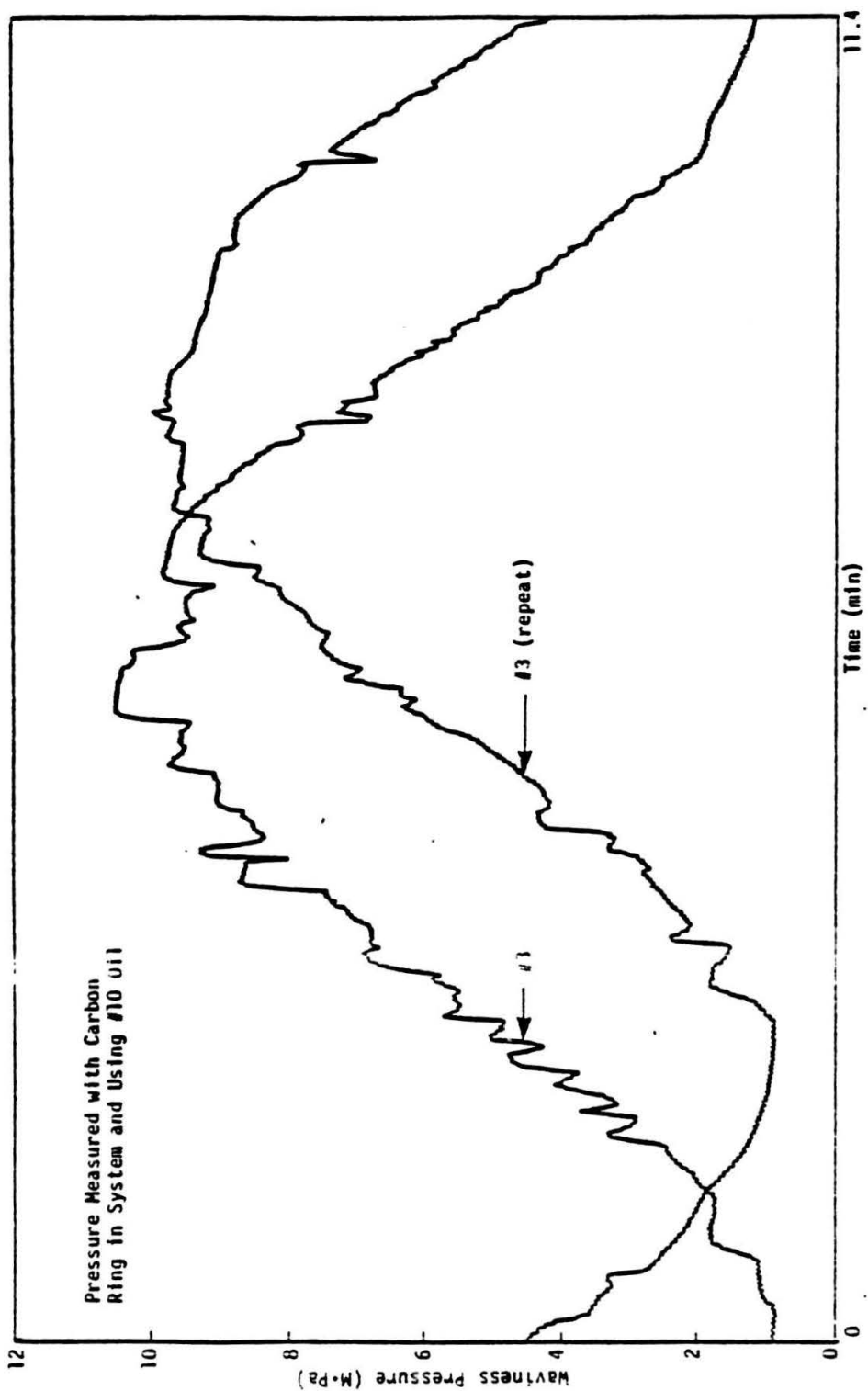


Figure 2-5. Waviness Pressure with Time - Oil Supply.

clearly jumps in the pressure. Again, these are believed to be caused by O-ring friction coupled with the higher viscosity of the oil. It is expected that some refinements will be made to the system to reduce these errors, although it is thought that there is little effect on actual seal operation.

Even though the time-dependent behavior of the pressure is better using gas than oil, it was decided to use oil for the system because an oil supply system is simple and there are no problems with corrosion. Long-term reliability is expected to be better.

Using this device one 500-hour test has been completed (Test 110 in Appendix). No difficulties were encountered in the test; the device operated reliably. A comparison of test results for the seal shows that seal performance is quite close to that obtained using the previous moving waviness device. Thus, it has been demonstrated that the waviness drive concept works. Given the inherent reliability of the waviness drive system, it is expected that it will operate indefinitely, whereas the sliding O-ring approach would be expected to fail because of O-ring wear. (The 500-hour test using sliding O-rings did show signs of deterioration.)

Friction and Wear Test Apparatus

In comparing the results of certain experiments to the prediction of theoretical models, it has become clear that the mechanical coefficient of friction between carbon and tungsten carbide is not a constant but varies widely depending on contact pressure, temperature, and the amount of water present. Similar inconsistencies are observed for wear in that the wear coefficient used in the simple wear law is apparently not a constant.

What is needed is a set of fundamental experimental data relating friction and wear to various operating conditions. A search of the literature has shown that such data does not exist for tungsten carbide versus carbon operating in water. It is

known that mechanical friction coefficient is sensitive to the presence of water, so dry friction measurements are not very useful. Such data does exist for these materials in a mechanical seal configuration. However, this data is of little use because, as is well known now, there is no way to separate the actual mechanical contact pressure from the fluid pressure in a seal, so any estimate of mechanical friction coefficient based on seal operation is a guess at best. Mechanical friction coefficient must be measured outside of the context of a seal where fluid pressure load support can be eliminated or at least limited to microasperity lubrication caused by surface roughness.

Given that such data does not exist and is important for the development of refined seal models, the design of a friction and wear test apparatus has been undertaken. Figure 2-6 shows the design. The friction pair consists of three carbon cylindrical plugs ④ being pressed against a rotating W-C ring ⑤. Three plugs are used to provide symmetry of load which simplifies the design. The plugs are small enough such that hydrodynamic and hydrostatic effects should be minimized relative to the applied mechanical load. Load is applied by air cylinder ⑥ acting on the end of shaft ⑦ and in turn onto the mounting ring for the three plugs. Shaft ⑦ is designed to easily bend to compensate for uneven wear of the plugs and wobble of the face of the rotating ring. Shaft ⑦ transmits the friction torque to reaction arm ⑧ on which strain gages are mounted to indicate torque. The entire assembly is housed in a pressure vessel ⑨ so that the contacts can be flooded with water and the water can be heated under pressure up to 400°F. The pressure is contained at the drive shaft end by mechanical seal ⑩ and at the torque shaft end by a small diameter O-ring. The O-ring is calculated to introduce only a small error into the torque readings. A variable speed drive motor is connected to the drive shaft.

At the present time detail drawings of the apparatus have been completed, and fabrication will begin soon. The first

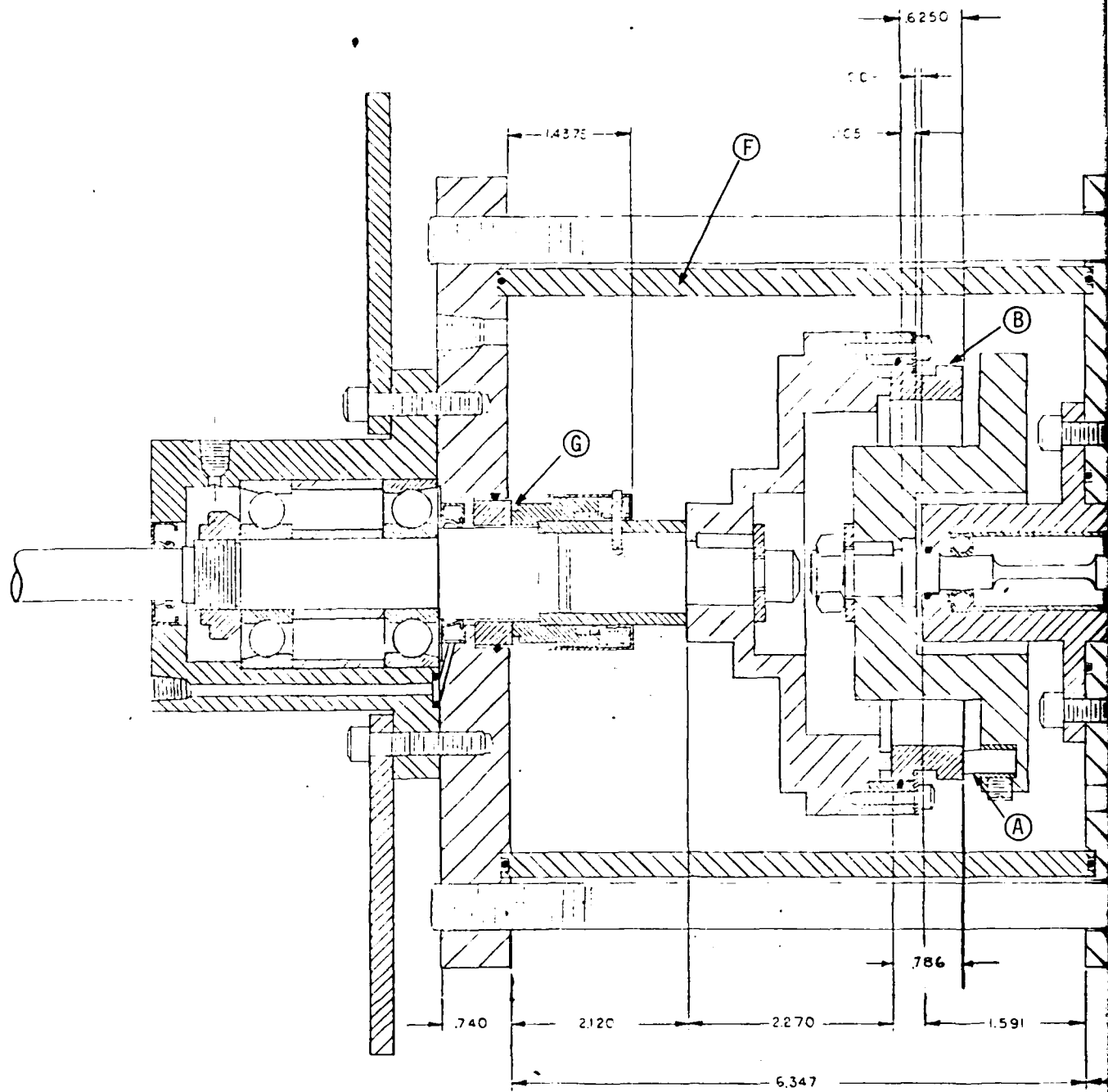
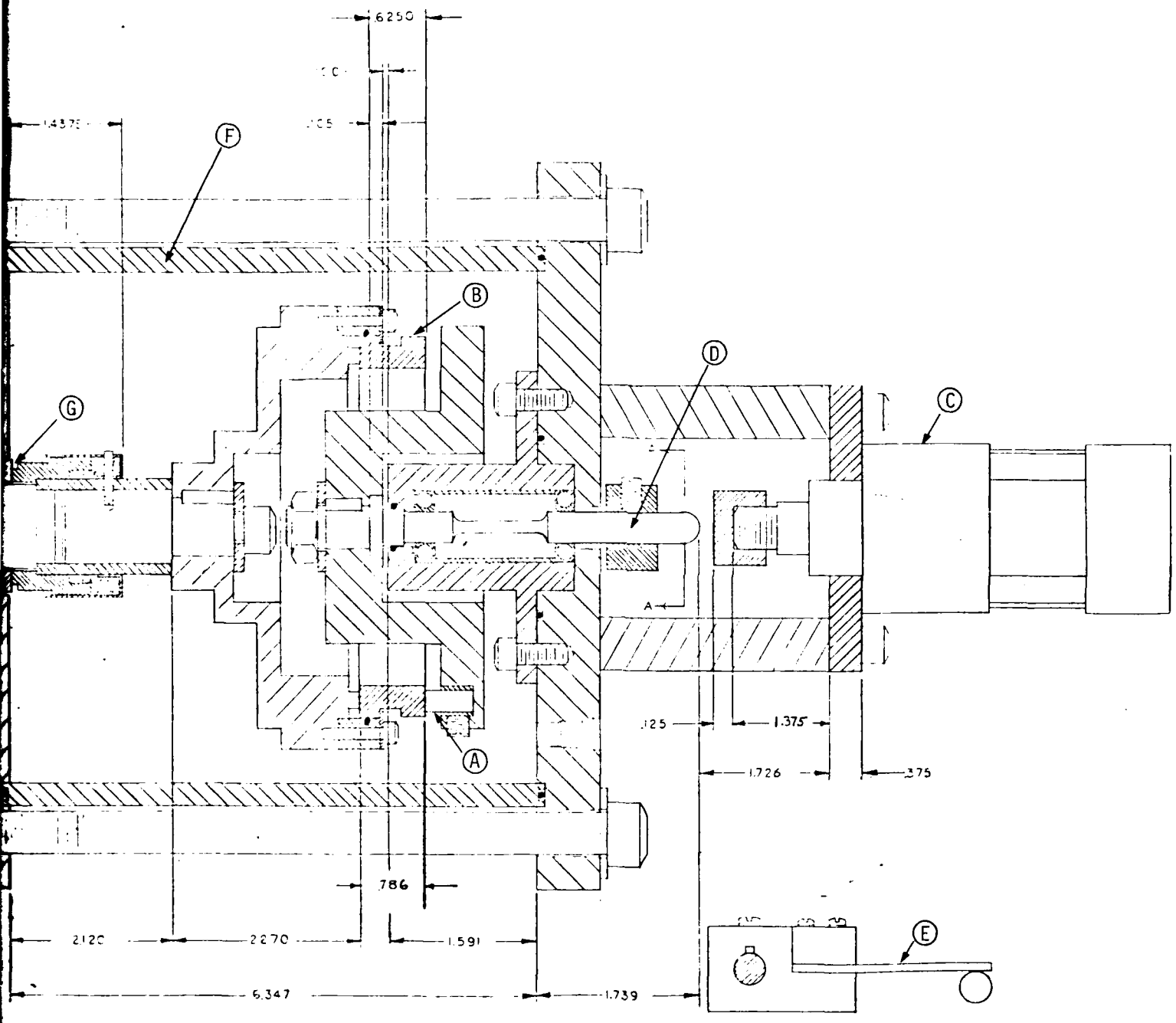


Figure 2-6. Friction and Wear Test Apparatus.



SECTION A-A

Test Apparatus.

series of tests will be conducted at room temperature under both dry and flooded conditions at various speeds and mechanical contact pressures. Both friction and wear will be measured.

Radial Taper Tests

A series of tests was conducted for the purpose of evaluating the effects of various initial radial tapers on seal performance, both short term and long term, and for the purpose of comparing to results based on a theoretical model developed previously in relation to this project. The model considers the effect of initial taper, thermally-caused taper, and wear on seal performance [9].

A series of 14 tests beyond those reported previously [8] were conducted. These tests were conducted for a balance ratio $B = 0.75$ so the original seal design was modified as shown in Figure 2-7. The purpose of using $B = 0.75$ was to be able to achieve complete liftoff at high convergent tapers.

Snapp and Sasdelli [10] produced a radial taper by lapping seal rings on a commercial lapping machine and manipulating the machine's operating conditions. Experience shows that this method is effective but can be slow and unpredictable. The needed manipulation is that of moving the lapping rings in toward the center of the lapping plate or out. Moving the lapping rings inward causes the lapping plate to wear convex, thereby producing a carbon ring with a converging radial taper. Moving the rings outward has the opposite effect. This method takes time to wear the lapping plate to the desired shape and it is not easily controlled.

The two devices shown in Figure 2-8 have proven to be both reliable and easy to use for producing a uniform moment about the ring centroid causing the faces to either converge or diverge. Device A is used to create a net divergent taper by placing it into the seal ring close to the sealing face. It is then

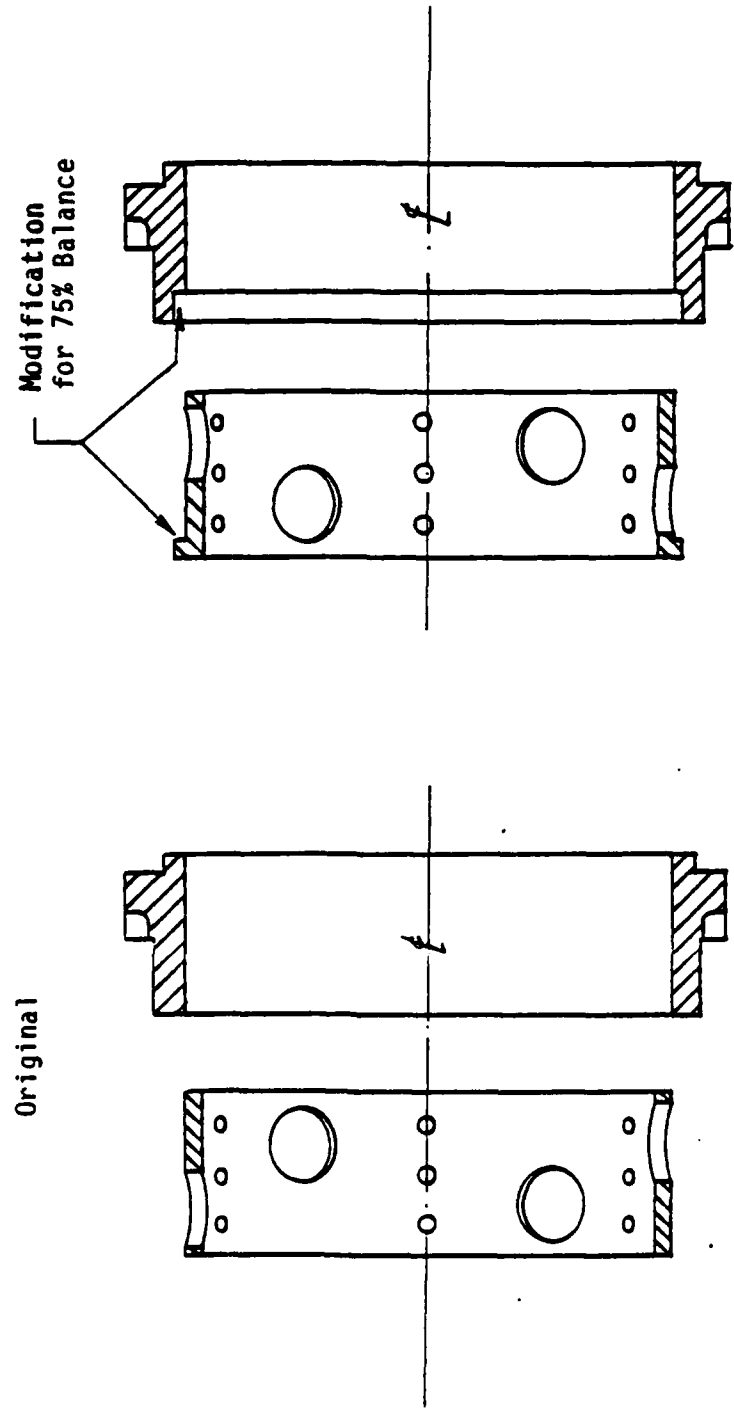


Figure 2-7. Original and Modified Carbon Seals for Taper Tests.

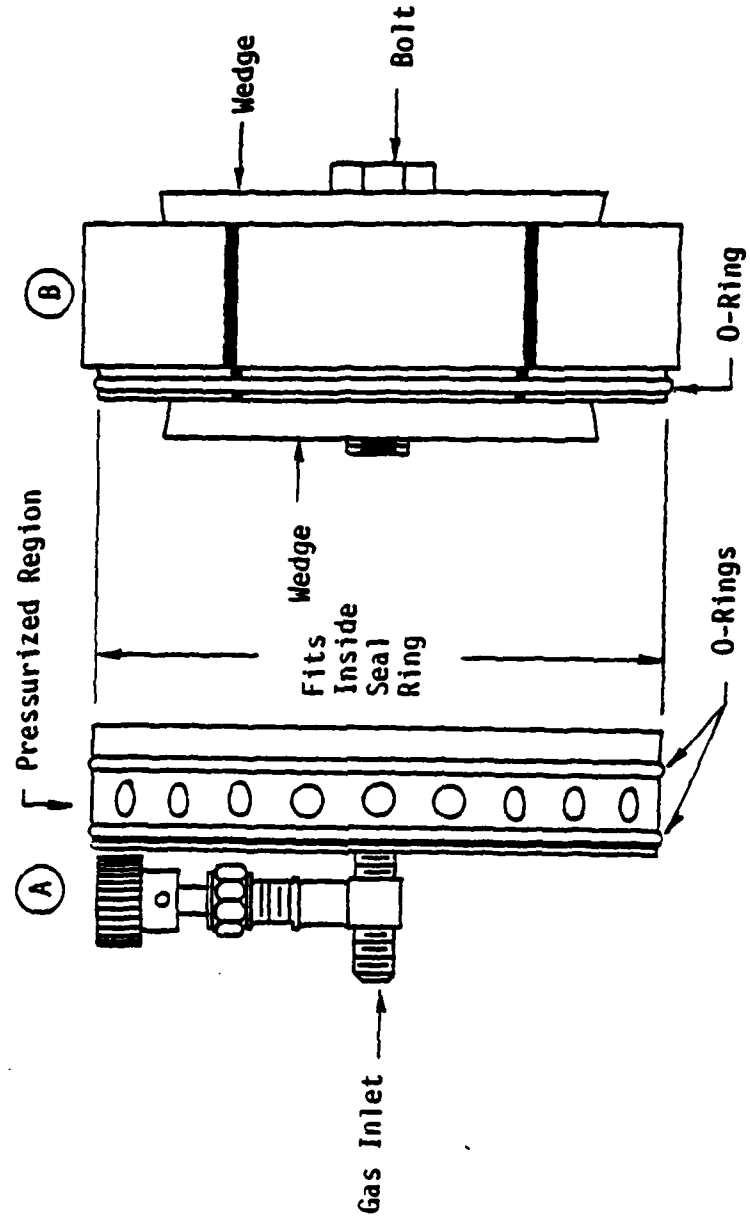


Figure 2-8. Tapering Devices.

pressurized and the resultant profile becomes convergent. The seal is then lapped flat, the device depressurized and the result is a divergent taper. Device B, an expanding mandrel, is placed at the extreme opposite end from the face of the seal. Because of the slots in the device, when the bolt is tightened, the wedges move inward expanding the apparatus. The O-ring is used to help even the load around the circumference. This expansion causes a divergent taper which when lapped flat and the device removed results in a net converging taper.

The test procedure used for the tapered seal tests is similar to that reported previously [8]. The Appendix (Tests 64-68, 75, 76, 97-101) contains performance curves for the experiments conducted. Table 2-1 is a summary of results. Test 64 was run with a carbon seal which had an initial slope of $1013 \mu\text{m/m}$ convergent taper. It was expected that torque would be quite low and leakage high. Table 2-1 shows that the torque was $0.05 \text{ N}\cdot\text{m}$ and the leakage very high at $58 \text{ cm}^3/\text{min}$.

Test 64 in the Appendix shows an erratic operation with a sudden increase in torque and seal face temperature approximately 4.5 hours after start and a sudden decrease at approximately 25 hours after start. This closely corresponds to 18:45 and 05:30 clock time. These jumps are also seen in Test 65. The periodic nature exhibited called for a closer examination. Several tests were made with the drive motor off and a constant torque applied. The same behavior persisted, leading to the belief that periodic voltage surges were affecting the 6940 multiprogrammer unit. During this period of testing, the University physical plant was shutting down at night all nonessential electrical items, such as circulation fans in the ventilation system, in the building in which the test apparatus was located to conserve energy. Full power was brought back up early in the morning and it was thought that this may have been the cause of the problem. The 6940 unit was removed from the system and sent to be serviced. Nothing

Table 2-1. Radial Taper Test Results, $B = 0.75$
 $p_0 = 3.45 \text{ MPa}$ (500 psi)
 Speed = 1800 rpm

Test No.	Test Duration (hr)	ϕ_i ($\mu\text{m}/\text{m}$)	Initial Torque N·m (in.-lb)	Final Torque* N·m (in.-lb)	Leakage** @ 1.0 hrs (cm $^3/\text{min}$)	Final Leakage* (cm $^3/\text{min}$)
64	24.0	1013	0.05 (0.4)	-0.40 (-3.6)	58.0	60.4
65	64.0	613	0.68 (6.0)	0.29 (2.6)	18.0	27.0
66	118.3	40	4.05 (35.8)	1.76 (15.6)	4.0	5.28
67	63.8	-320	6.10 (54.0)	4.12 (36.5)	3.0	0.80
68	65.3	-750	8.75 (77.4)	7.71 (68.2)	2.5	0.043
75	71.5	-1110	11.48 (101.6)	11.92 (105.5)	2.0	0.000
76	138.6	-778	6.89 (61.0)	10.93 (96.7)	0.0	0.0072
97***	66.7	960	1.02 (9.0)	0.64 (5.7)	0.0	3.55
98	15.6	1200	0.17 (1.5)	0.43 (3.8)	88.0	89.1
99	4.1	400	0.17 (1.5)	0.30 (2.6)	23.0	23.8
100	24.4	643	0.83 (7.4)	0.78 (6.9)	42.0	45.6

*Averaged over last 10 hours.

**Leakage delayed due to the filling of inner cavities of the waviness cylinder.

***Torque and leakage data for Test 97 are not comparable to other tests because of the zeroing process at the beginning of the test were away the initial taper.

could be found defective with the unit so it was again installed and testing continued. Further tests after reassembly showed no abnormal behavior. No satisfactory answer has been found to explain the erratic operation discussed. It is thought that the negative torques for Test 64 are caused by the fact that the output is subjected to some error and the voltage surges discussed.

Test 65 was run with a carbon seal having an initial convergent taper of 613 $\mu\text{m}/\text{m}$. The torque is still quite low at 0.68 N·m but the leakage dropped considerably to 18 cm^3/min . This test was run for 64 hours and displayed the jumps in torque and seal face temperature as discussed earlier.

After reinstalling the 6940 multiprogrammer unit, Test 66 was run for 118 hours. The initial taper was 48 $\mu\text{m}/\text{m}$ convergent (nearly initially parallel faces). Test 66 in the Appendix shows that the torque increased a little more compared to the previous test, up to 2.83 N·m. The leakage has again dropped considerably, down to 4 cm^3/min . The operation is quite smooth except for the slightly erratic leakage at the beginning.

It was thought that a parallel face operating condition could be achieved if the test ran long enough. However, because of thermal rotation, hydrostatic effects were predominant allowing sufficient lift off so wear was quite small. After 118 hours torque and leakage had not changed enough to expect parallel face conditions to be established in any reasonable length of time, so the test was ended.

In the next test (Test 67, Appendix), the carbon seal had a divergent taper of -320 $\mu\text{m}/\text{m}$ lapped into it. At start up, the torque was measured at approximately 6.2 N·m (54.8 in.-lb) and then decreased rapidly to 4.86 N·m (43 in.-lb) one hour later. The torque then approached a constant 4.12 N·m (36.5 in.-lb). Leakage started out at 3 cm^3/min and slowly reduced to 0.8 cm^3/min after 32 hours of operation.

It should be noted here that the delay in leakage at the start of each test, as shown in the Appendix figures, is caused by the fact that it takes about 20 cm^3 of leakage to fill the inner cavities of the waviness cylinder and leakage catcher before leakage is able to flow into the leakage measuring device.

An even higher divergent taper was used on the seal for Test 68. The initial slope was $-750 \mu\text{m/m}$. Test 68 in the Appendix shows that the initial torque starts out at approximately $8.8 \text{ N}\cdot\text{m}$ (77.8 in.-lb) and drops off quite fast to $7.63 \text{ N}\cdot\text{m}$ (67.5 in.-lb) after one hour. Initial leakage is about $2 \text{ cm}^3/\text{min}$ and slowly decreases to $0.043 \text{ cm}^3/\text{min}$ after 65 hours of operation. The sharp drop in torque and temperature readings at approximately 19 hours was due to a momentary (less than one second) shutdown of the test apparatus. The motor drive was not allowed to stop before power was reapplied. It appears that the seal was able to operate in two stable conditions as evidenced by the torque prior to and after the shutdown. The slopes of the torque and temperature before and after shutdown are quite similar although leakage did not seem to be affected. The final torque averaged out to $7.71 \text{ N}\cdot\text{m}$ (68.2 in.-lb) after 65 hours.

Test 75 was run with a divergent taper of $-1110 \mu\text{m/in}$. The starting trend is the same as that of the previous tests. The torque started out at approximately $11.8 \text{ N}\cdot\text{m}$ (100 in.-lb) and decreased to $9.49 \text{ N}\cdot\text{m}$ (84 in.-lb) after one hour. Operational trends appeared to be the same as Tests 66 through 68. However, after four hours the performance was quite different from previous tests. Apparently, the seal had reached a parallel face condition. Leakage had dropped off very fast with no measurable leakage after eight hours. The sudden changes in torque may be caused by the faces drying out, the result of the fluid being sealed off at the outside diameter. Since dry carbon has a higher friction coefficient than wet carbon, the increased friction results in a sharp increase in torque and temperature. As

the temperature increases, additional thermal rotation occurs such that some fluid reenters the gap and friction is reduced [9]. The final corrected torque averaged at 11.92 N·m (105.5 in.-lb) after 71.5 hours of operation.

Test 76 was a repeat of Test 68 so as to obtain additional wear data. The initial taper was -778 $\mu\text{m}/\text{m}$. Test 76 in the Appendix shows the initial torque at 6.89 N·m (61 in.-lb) and then decreasing. After about one hour the torque began to rise and become erratic. Apparently, a parallel face condition had developed quite quickly. The face temperature was very high due to the fact that there was no leakage initially. A shutdown occurred at approximately 16 hours into the test due to excessive face temperature. The maximum level was reset and the test continued.

At about 17 hours leakage began, which in turn reduced the face temperature and torque dramatically. The amount of this initial leakage was very small (approximately $0.1 \text{ cm}^3/\text{min}$) and shows how sensitive torque and face temperature are to this quantity. As the leakage decreased, the torque and face temperature once again began to increase. The performance steadied after 36 hours. The final corrected torque was 10.93 N·m (96.74 in.-lb) and leakage was $0.00719 \text{ cm}^3/\text{min}$. These values were averaged over the last 24 hours of operation.

Effects of Pressure Caused Rotation

After Test 66 was run, a separate test was performed to check the zero moment design, i.e., a check to insure little or no rotation of the seal faces occurred due to sealed pressure. Two strain gauges were mounted on the seal ring as shown in Figure 2-9. With the strain gauges in these locations, a divergent rotation would put the gauge on the left into tension and the gauge on the right into compression. Calibration was accomplished by the use of the pressure type radial tapering device.

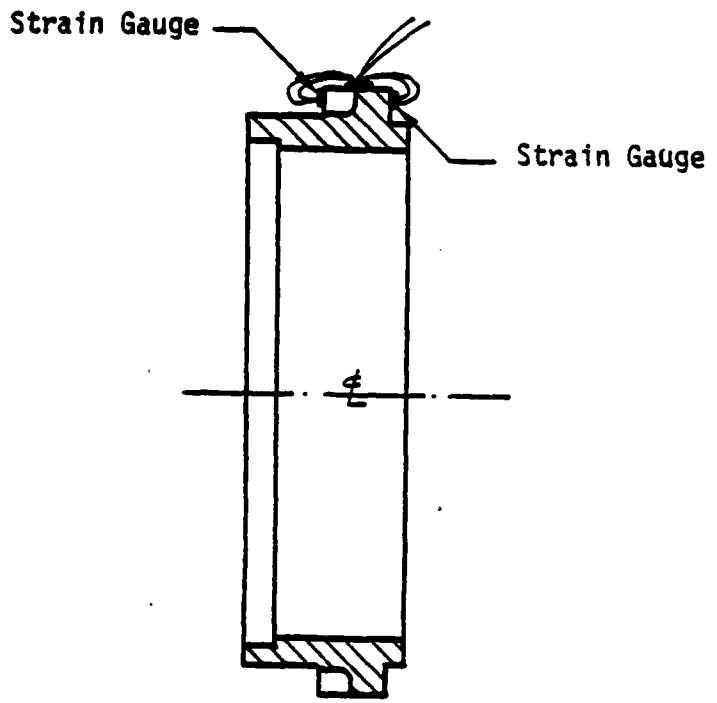


Figure 2-9. Carbon Seal with Strain Gages.

The device was inserted into the seal ring toward the face. A spacer was used to control the location of the tapering device relative to the face. After the tapering device was pressurized, a radial surface profile was made across both faces to record the face rotation; then the resultant strain was measured from a strain indicator. The results of calibration are shown in Figure 2-10. The seal was then mounted on the seal test apparatus and the strain gauge leads were run through a small brass tube which exited from the left-hand end plate through a pressure fitting. The gauge wires were epoxied at the tube opening inside the pressure vessel to prevent leakage. The pressure vessel was installed and the system was pressurized with water to 3.45 MPa (500 psi). The results of the experimentation are given in Table 2-2. The average tilt was 103 $\mu\text{m}/\text{m}$ divergent. This is considered within acceptable limits since such an amount would affect the performance curves very little.

Surface Roughness

All mixed friction theoretical models to date are based on the assumption of Gaussian or similar surface roughness. It is now recognized that this may lead to considerable error in the prediction of leakage because carbon surfaces are not Gaussian by any means.

To better understand the nature of carbon surfaces, a series of measurements was made as a part of the radial taper test series. Table 2-3 contains the surface statistics before and after the test in both the radial and tangential directions. These data were obtained using a surface analyzer. The initial radial and tangential σ are quite close, leading to the conclusion that the initial lapped surface characteristics are independent of direction. The final values show a considerable reduction in the standard deviation in both the radial and tangential directions.

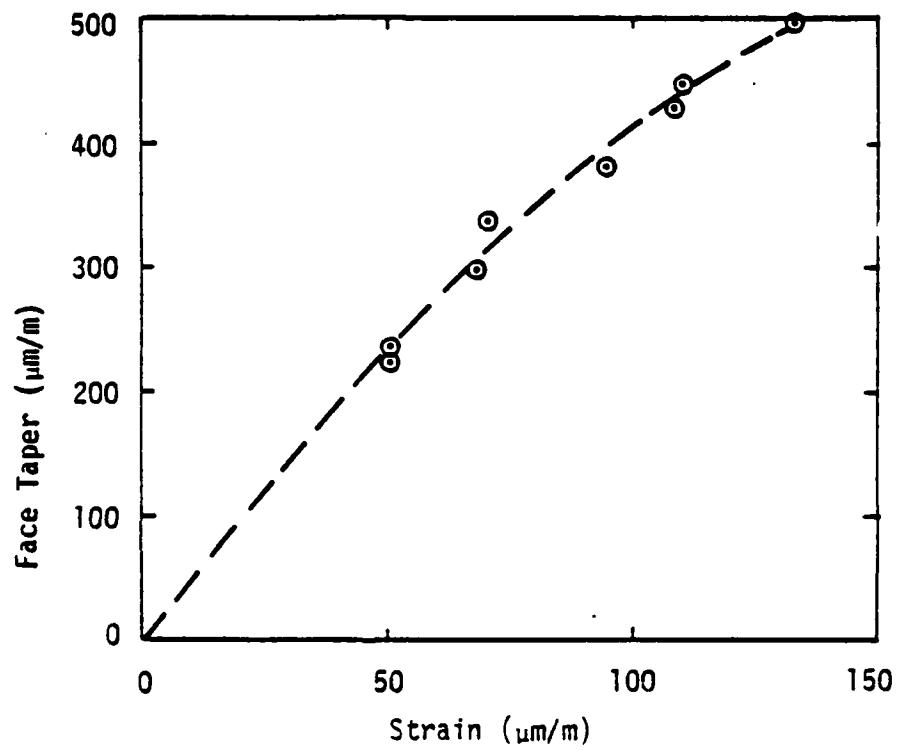


Figure 2-10. Face Taper Versus Strain.

Table 2-2. Experimental Results--Pressure Caused Rotation

Strain μm/m	Resultant Tilt μm/m
-20	-92.8
-22	-102.2
-24	-111.4
-23	-106.8
Average = -103 μm/m	

Table 2-3. Radial Taper Tests Carbon Surface Statistics

Test No.	Initial $\sigma \mu m$ ($\mu in.$)		Final $\sigma \mu m$ ($\mu in.$)	
	Radial	Tangential	Radial	Tangential
64	0.79 (31.3)	0.83 (32.5)	0.79 (31.3)	0.70 (27.5)
65	0.70 (27.5)	0.70 (27.5)	0.64 (25.0)	0.57 (22.5)
66	0.70 (27.5)	0.79 (31.3)	0.57 (22.5)	0.51 (20.0)
67	0.73 (28.8)	0.79 (31.3)	0.70 (27.5)	0.70 (27.5)
68	0.67 (26.3)	0.76 (30.0)	0.41 (16.3)	0.38 (15.0)
75	0.73 (28.8)	0.76 (30.0)	0.35 (13.75)	0.38 (15.0)
Avg.	0.72 (28.4)	0.77 (30.4)	0.58 (22.7)	0.54 (21.3)

With these values and using the mathematical models mentioned, one would expect a significant leakage in the parallel face tests. This was not the case (see Tests 75 and 76 and all $B = 1$ parallel face tests) [8]. To further examine this question, a histogram was generated for the carbon surface of Test 68 as described previously [8] and is shown in Figure 2-11. An expanded surface profile is shown in Figure 2-12. The histogram is characteristic of a worn carbon surface having a series of valleys with the higher asperities being chopped off. Figure 2-12 also shows this surface characteristic.

The question that has arisen is whether or not the valleys, as seen in Figure 2-12, are connected or are they simply isolated pockets. If they are connected, the measured standard deviation would be justified, but if they are not connected, the surface should be characterized for purposes of calculating leakage by the much smaller standard deviation of the relatively "flat" peaks. For the sake of future discussion, the idea that while the valleys contribute to the measured roughness, they do not significantly influence flow is called the "pocket theory."

Proving the pocket theory by use of the trace shown in Figure 2-12 is not possible. A three-dimensional view is needed. It was decided that an electron beam microscope scan of the carbon surface would be useful. This requires the destruction of a carbon ring. Seal 11, which was used for Test 68, was chosen since a final trace of the surface showed that the inside radius had no evidence of wear while the remainder of the surface showed some wear. This provided the opportunity to see both worn and unworn surface characteristics on a single seal.

Figure 2-13 is the image of the unworn section viewed radially from inside to outside at an angle of 10° from the horizontal. The dark area in the foreground is the vertical edge at the inside radius of the ring. This section shows the inherently rough nature of the surface due to lapping. Figure 2-14, on the

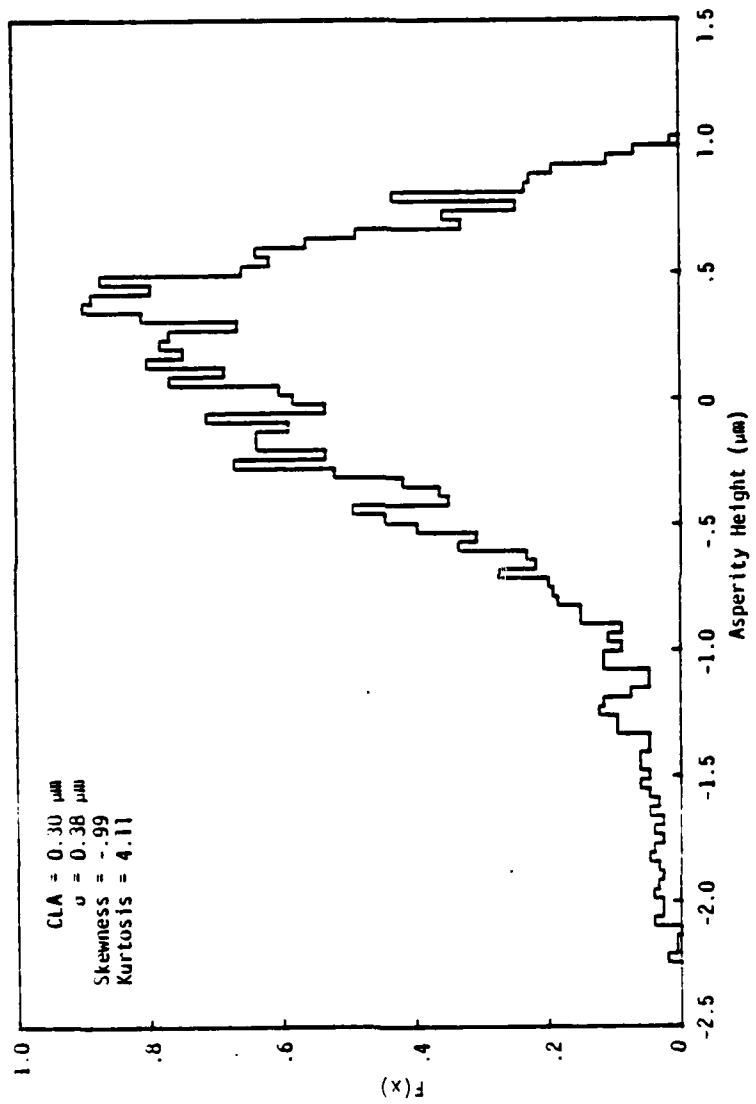


Figure 2-11. Tangential Roughness Distribution - Test 68.

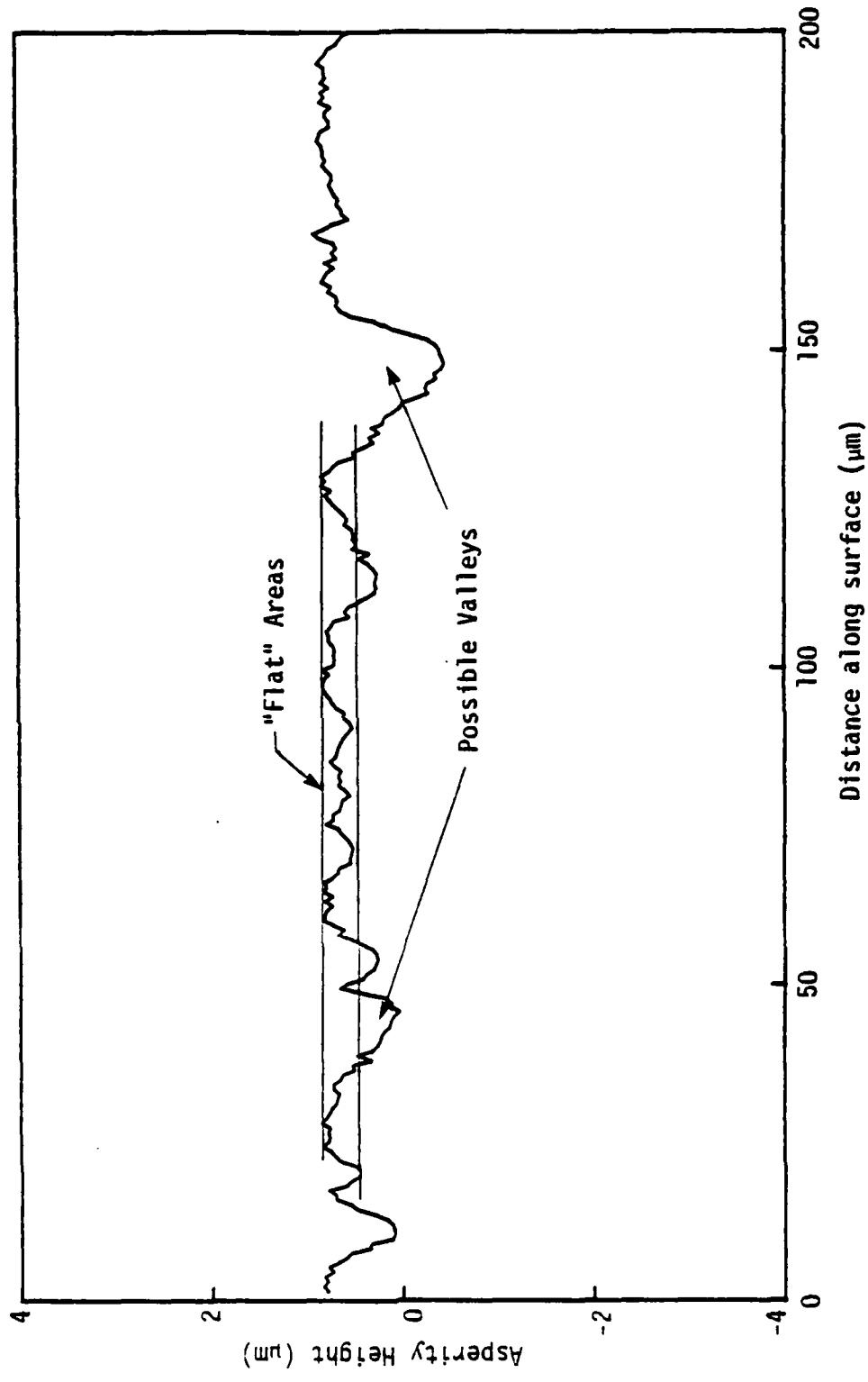


Figure 2-12. Expanded Surface Profile - Test 68.

Figure 2-13. Electron Beam Microscope Image of Unworn Section - Test 68.

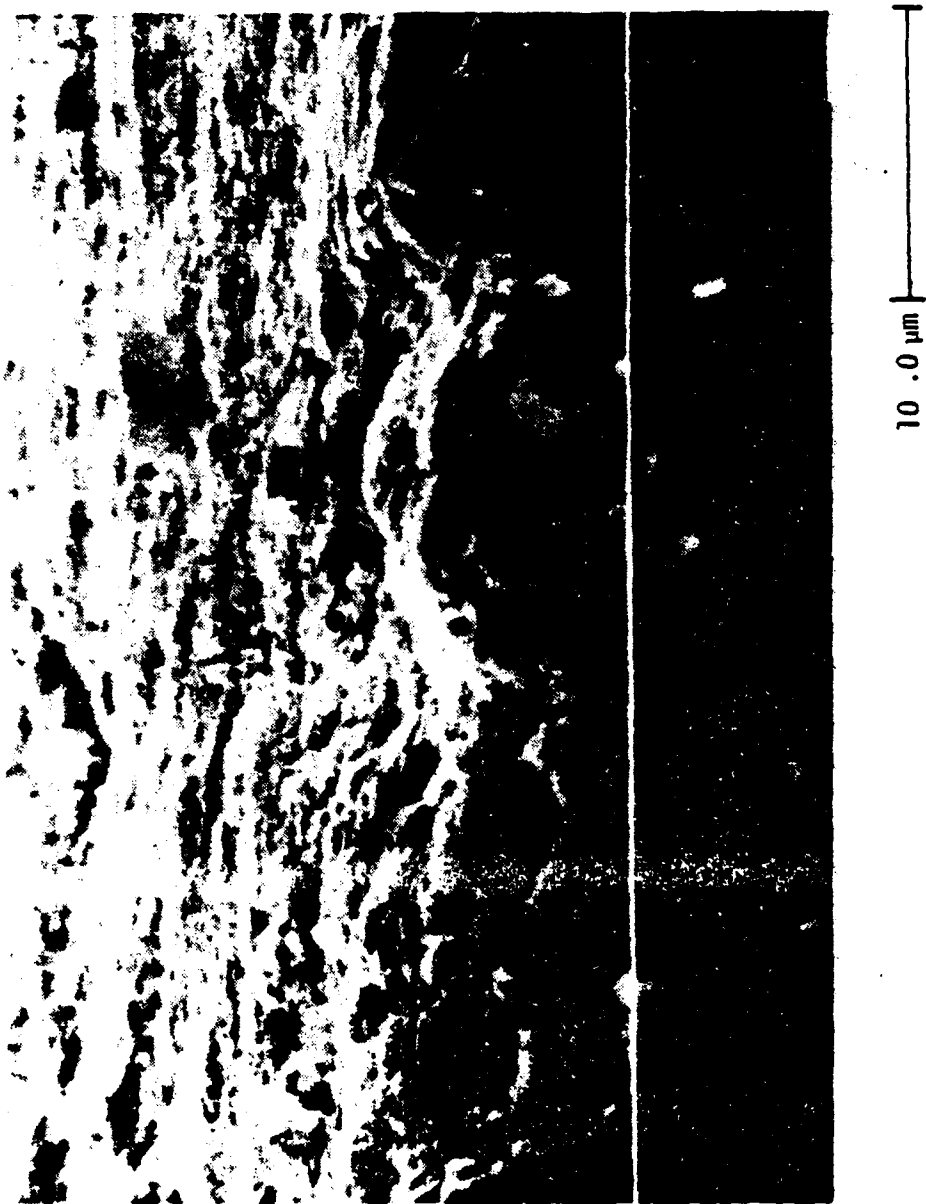




Figure 2-14. Electron Beam Microscope Image of Worn Section - Test 68.

other hand, shows the worn section of the surface. Again, this is viewed radially from inside to outside at an angle of 10° from the horizontal. Both scans are magnified 1800 times. Figure 2-14 confirms the pocket theory. These pockets are not conducive to fluid flow in the radial direction because liquid becomes trapped in them. Therefore, the actual surface should be characterized from a leakage standpoint by a smaller standard deviation than actually measured.

Radial Surface Profiles

Figure 2-15 shows the initial and final radial traces for Tests 64 and 65. Looking at these two tests and the corresponding initial and final surface roughness statistics in Table 2-3 indicates clearly that no measurable wear had taken place. Although the final slopes are not exactly the same as the initial, they are essentially unchanged, since measurement of the slopes is no better than $\pm 50 \mu\text{m/m}$. This result explains why the performance curves changed very little during testing.

Figure 2-16 also shows no measurable wear or significant change in surface roughness for both Tests 66 and 67. The thermal rotation was apparently large enough in Test 67 to produce a net convergent taper during operation which was sufficient to give enough hydrostatic load support so that the minimum film thickness was greater than the surface roughness and hence no wear. The initial and final tapers are again comparable.

Tests 68 and 75, Figure 2-17, do show measurable wear. This is also seen in Table 2-3 where the surface roughness decreases from the beginning of the test to the end. The seal in Test 68 has not completely worn to a flat face condition. The inside radius shows little wear on this trace. The asperities on the inside were still quite distinct while the remainder of the face shows that these higher asperities had been chopped off. The electron microscope images, Figures 2-13 and 2-14, were made from

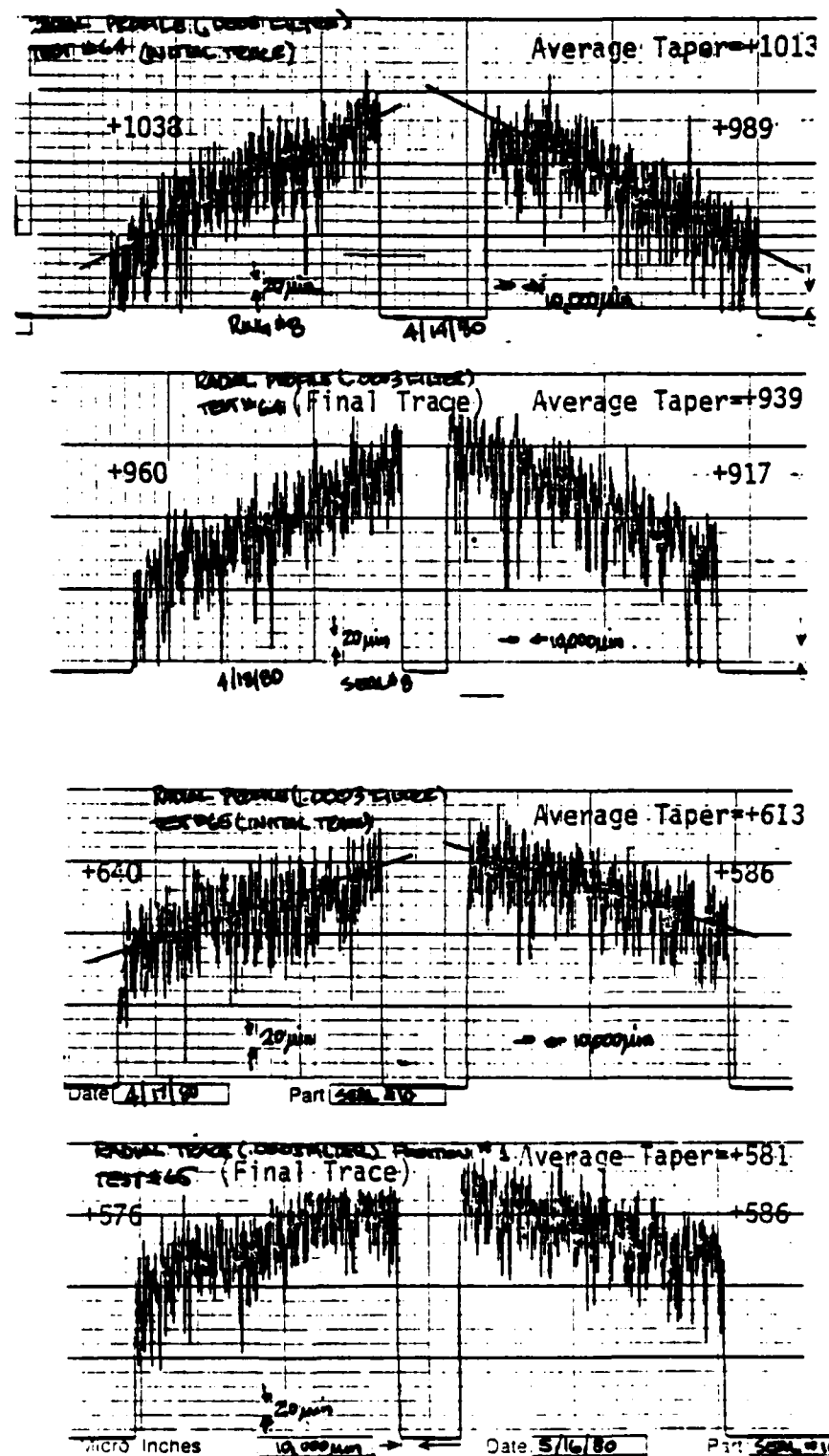


Figure 2-15. Initial and Final Surface Profiles - Tests 64 and 65.

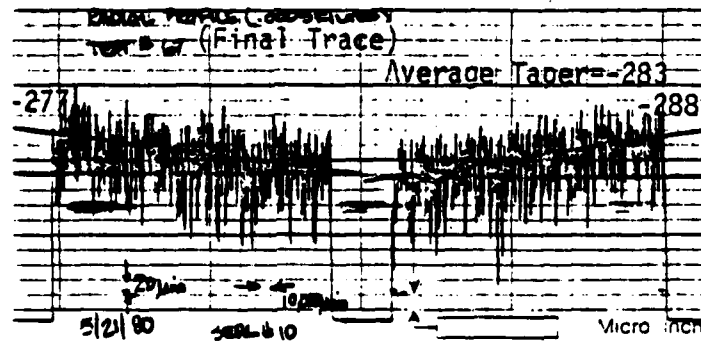
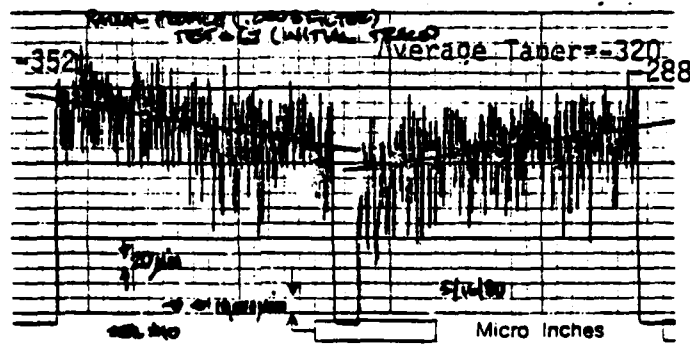
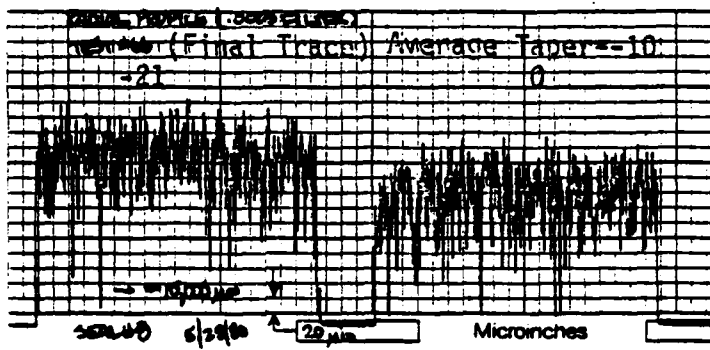
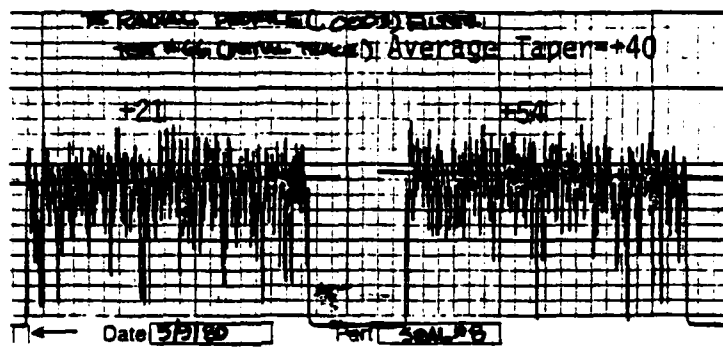
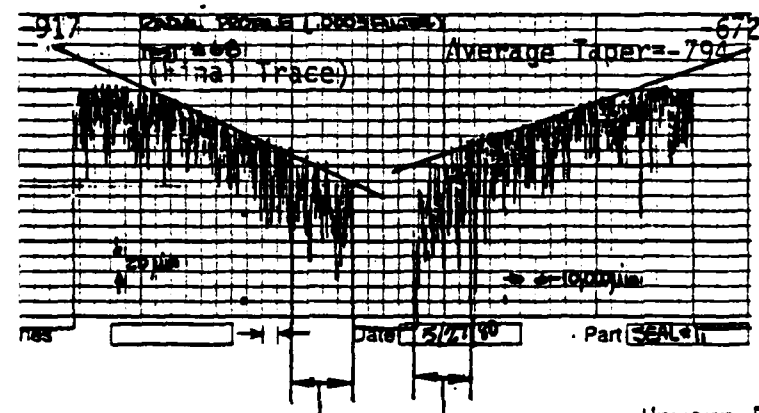
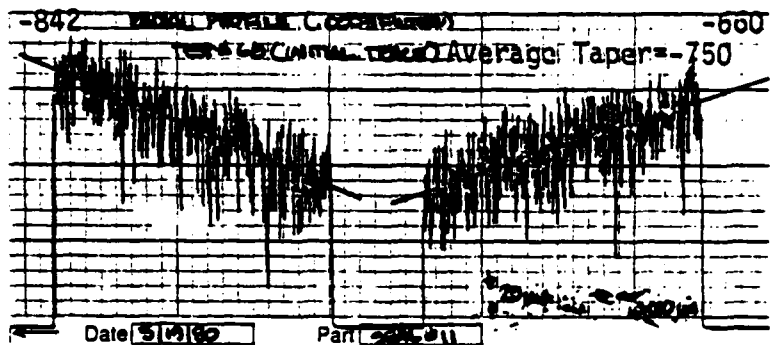


Figure 2-16. Initial and Final Surface Profiles - Tests 66 and 67.



Unworn Portions

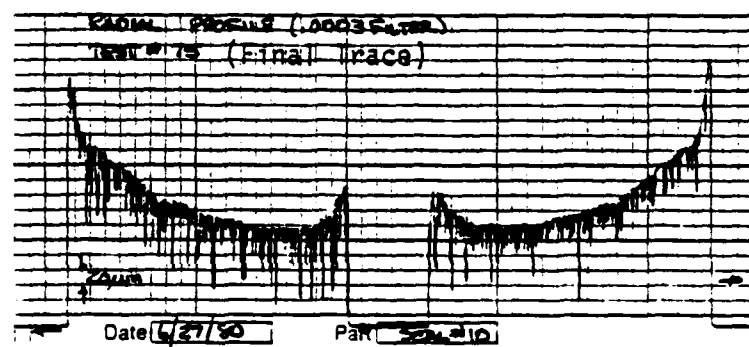
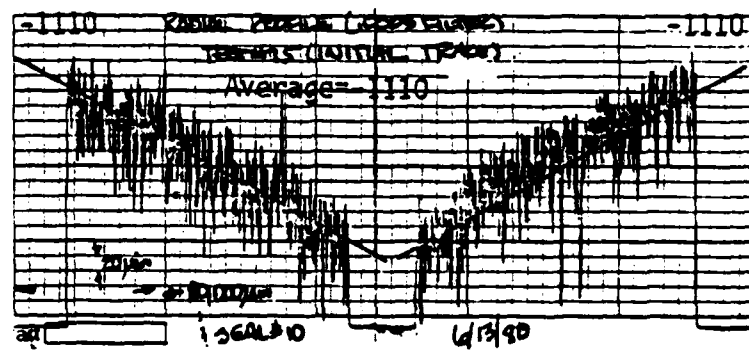


Figure 2-17. Initial and Final Surface Profiles - Tests 68 and 75.

this surface. The final trace in Test 68 does not represent the equilibrium thermal rotation, but is probably close. As the seal continues to wear in, the friction will increase and so will the thermal rotation. Therefore, it would be expected that the final tilt would be slightly more divergent. The flat portions on the outside edge were probably caused by initial start-up and finding the zero torque level.

The final trace of Test 75 shows a concave shape. Determining the taper is quite difficult in this case, so the profile of the mating tungsten carbide ring is shown in Figure 2-18. The tungsten carbide ring has deep circumferential grooves that correspond to the exaggerated peaks at the inner and outer radii of the carbon ring. Figure 2-18 shows how these sections match up. By taking a reference point at the outside radius as being zero and finding the difference between heights of the two surfaces from that reference, a resultant profile is obtained and is presented in Figure 2-19. This trace still poses some difficulty in determining a taper so a least squares fit was made. The final average taper was $-710 \mu\text{m/m}$ and is at best an approximation under the circumstances. The reason for this concave shape is due most likely to the fact that the seal face temperature was quite high locally and local thermal deformations were superimposed over the thermally caused tilt. Tests 68 and 75 together show that the thermal rotation at the parallel face operating condition is from 700 - $800 \mu\text{m/m}$. This will be compared to theory later.

Test 76, Figure 2-20, is a repeat of Test 68 to get additional wear data. Once it was determined from Tests 68 and 75 that the equilibrium thermal rotation for parallel faces is about $-750 \mu\text{m/m}$, Test 76 was run at an initial taper of $-778 \mu\text{m/m}$. Figure 2-20 shows a thermal taper which is higher than the results above. For some unexplained reason, Test 76 ended up operating at a higher torque than Tests 68 or 75, thus resulting in the higher thermal taper.

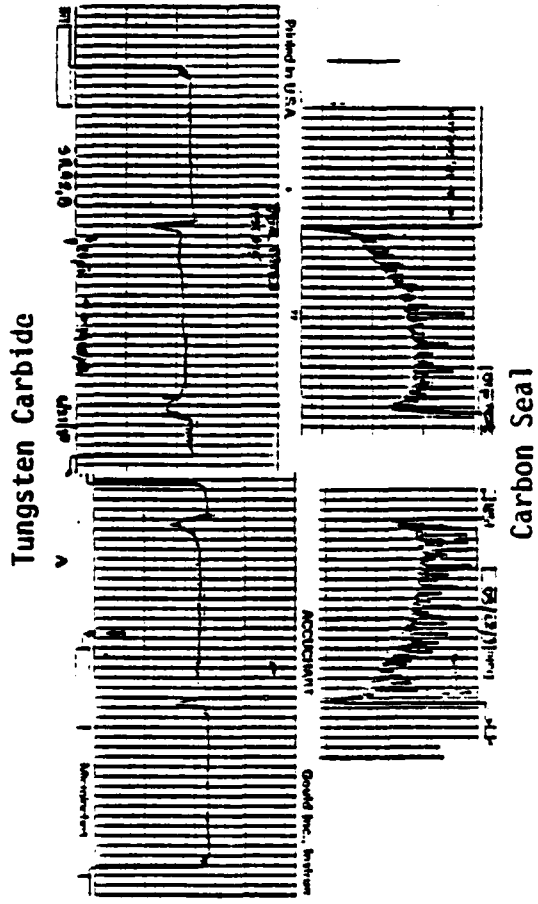


Figure 2-18. Carbon and Mating Tungsten Carbide Ring - Test 75.

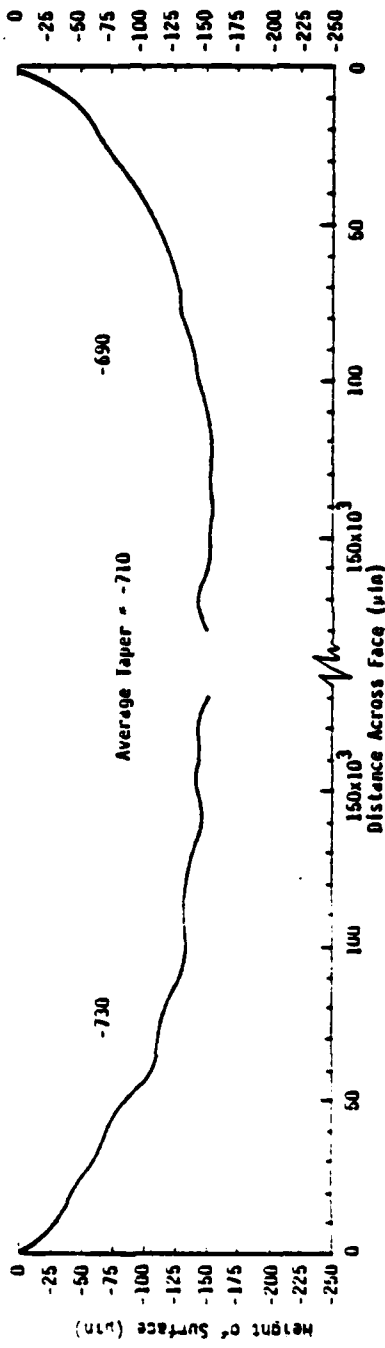


Figure 2-19. Resultant Profile - Test 75.

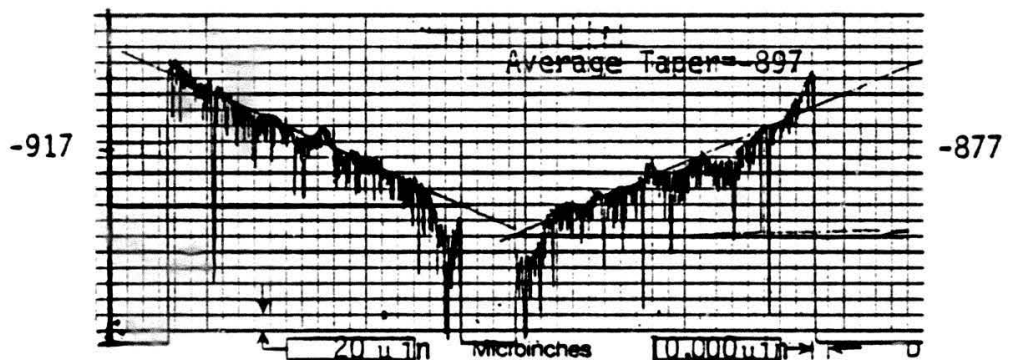
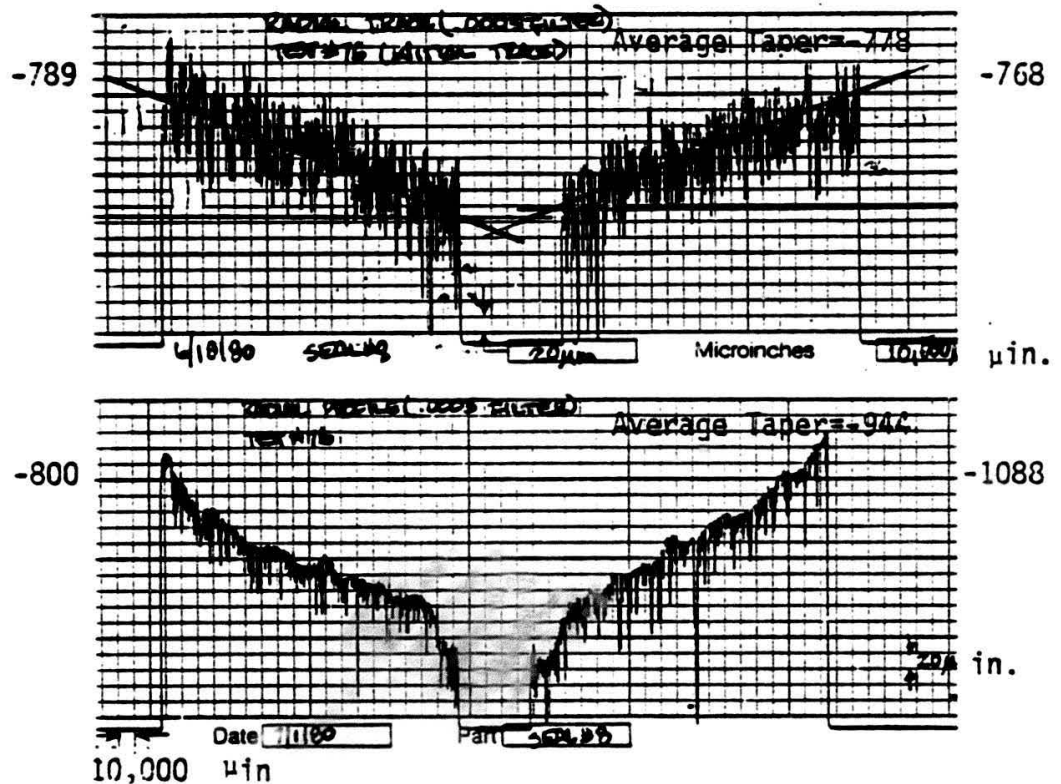


Figure 2-20. Initial and Final Radial Surface Profiles - Test 76.

Wear measurements were made for both Tests 75 and 76. The wear values are 7.04 and 10.67 μm per 100 hours, respectively. Both of these values are lower than obtained for the $B = 1.0$ tests as shown in the previous annual report [8].

High Temperature Tests

A series of twenty-nine tests were conducted in water with nominally flat face seals at elevated temperatures up to 190°C for both $B = 0.75$ and $B = 1.00$. The purpose of these tests was to provide data to compare to results predicted by a two-phase model [11] which was developed in part during this research program. In essence the model predicts that seal friction should decrease with increasing temperatures because more of the load is carried by fluid pressure as the phase change boundary moves across the seal face. This trend will continue up to some critical temperature after which the friction will again increase. Theoretically, leakage will suddenly increase at this critical point and seal puffing may occur.

Several modifications of the test apparatus were required to make these tests. The first of these was to provide a means to maintain the high temperatures required. After investigating the heat loss through the pressure vessel and the space available inside the pressure vessel, it was determined that a tubular heating element with a capability of 2 kW was adequate. It was bent and placed inside the pressure vessel to heat the system (Figure 2-21). The water temperature is sensed by a thermocouple and monitored by computer. Whenever the water temperature goes above the set temperature, the control program opens a relay which stops the electrical heating.

It was discovered early in this test series that both heating and cooling were necessary to be able to control the temperature under all operating conditions. At the lower test temperatures the cooling system described previously [8] was used.

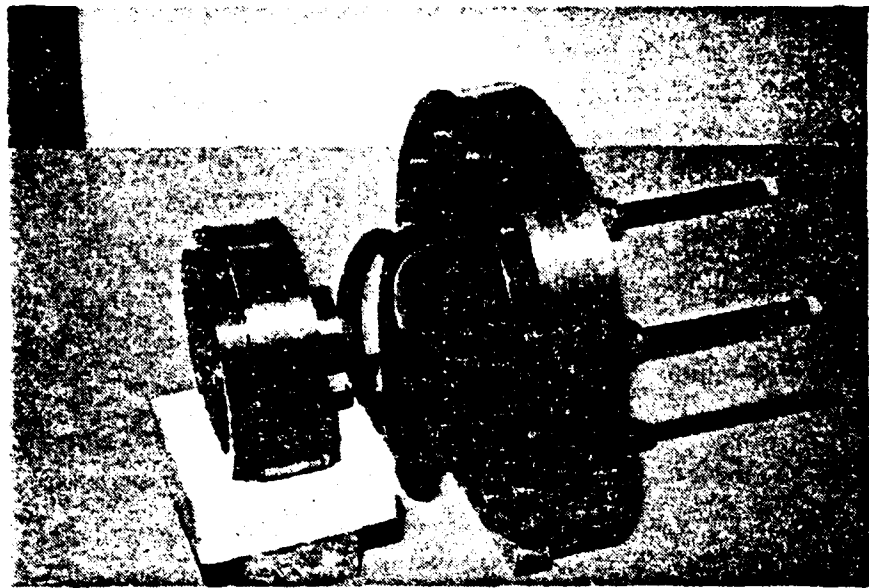


Figure 2-21. Heating Element.

The cooling control temperature was set a few degrees above the heating temperature. Since the water temperature was higher than the temperature limit of the circulation pump for some of the high temperature tests, the circulation pump was by-passed to avoid damage. A small re-circulation vane was attached on the left-hand end plate of the pressure vessel to increase circulation and cooling. Experimental results show that temperature control is in the range of $\pm 3^{\circ}\text{C}$ for most of the tests.

When conducting a test at a high temperature, vapor leakage would be expected when two-phase operation is occurring. After the vapor passes the seal face, it will condense on cooler seal parts, and the observed leakage will be in the form of a liquid. A newly designed leakage catcher (Figure 2-22) with an O-ring at the right-hand end of the leakage sleeve was used during the test. The vapor leakage is sealed and condensed to a liquid within the sleeve. Then, the entire leakage is collected and measured by the leakage measuring device.

Based on the experimental evidence, the minimum measurable leakage for the measuring device is about $0.05 \text{ cm}^3/\text{min}$. Below such rates it is expected that water evaporates from the leakage counter before it can be registered. Since no leakage was detected for all the tests after the seals were worn in, leakage rates below this value must have occurred.

A Type J thermocouple was used to measure the seal face temperature. The thermocouple is placed at a specific position beneath the seal face (Figure 2-23). The thermocouple is read several times per minute, converted to temperature, averaged, plotted, and the data stored on tape. There are three sources of error for temperature measurement: 1) the accuracy of the thermocouple ($\pm 2.2^{\circ}\text{C}$); 2) the accuracy of the low-level A/D card ($\pm 0.7^{\circ}\text{C}$); and 3) the error caused by the thermocouple position error. Based upon the theoretical temperature distribution, there is a temperature gradient of about $30^{\circ}\text{C}/\text{cm}$ near the end of

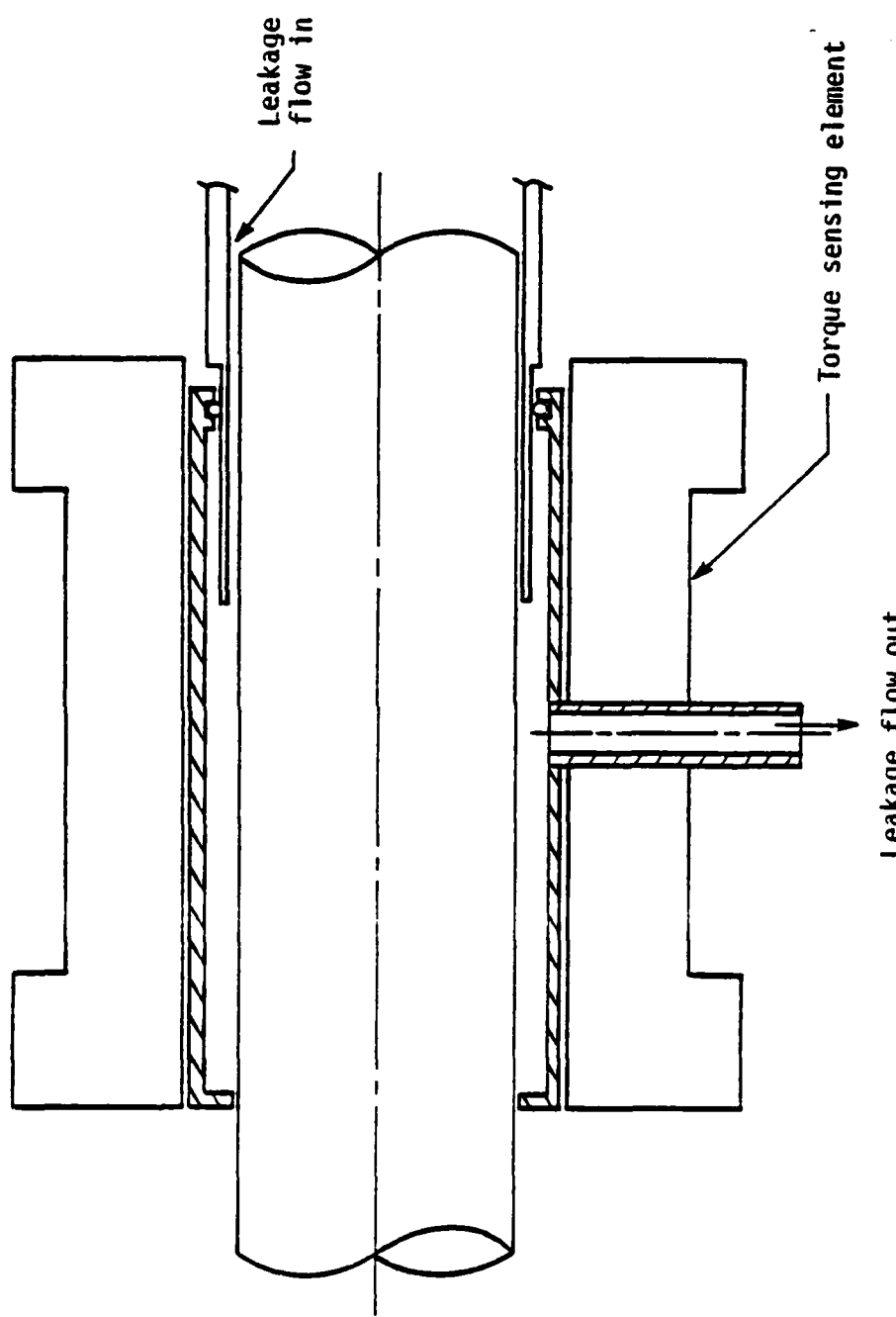


Figure 2-22. Leakage Catcher.

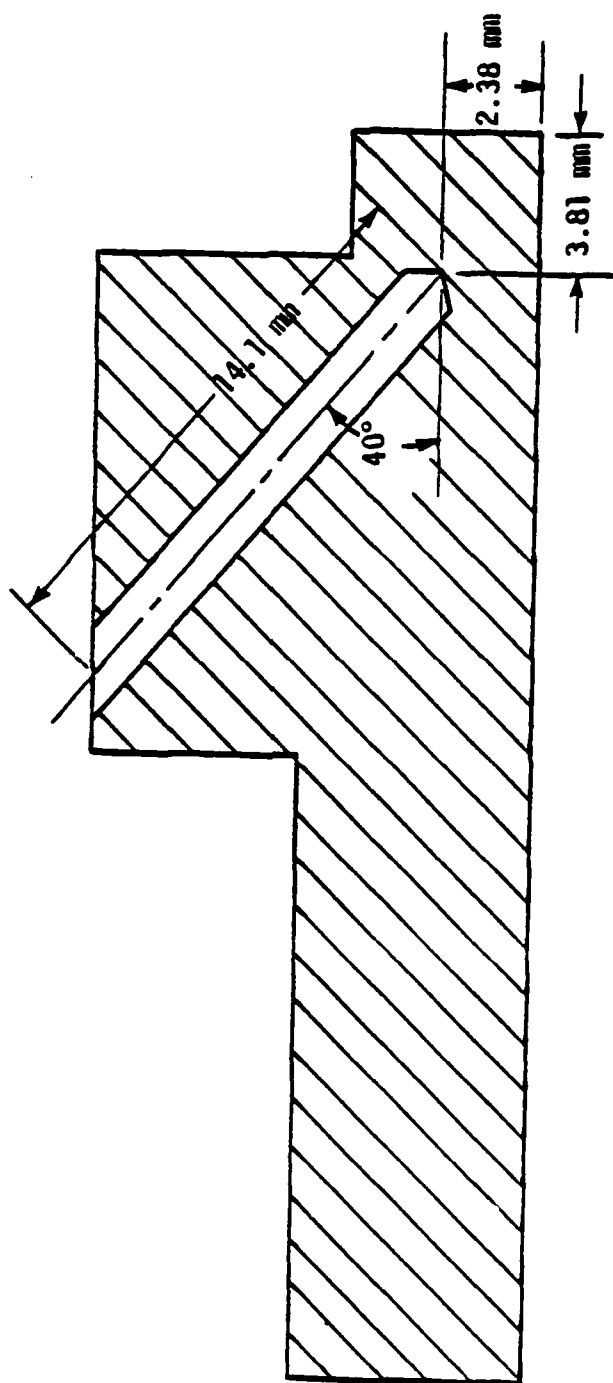


Figure 2-23. Thermocouple Position.

thermocouple. The thermocouple position error is about ± 0.025 cm. This will cause an error of $\pm 0.75^\circ\text{C}$. Therefore, the total absolute error for seal face temperature measurement could be as much as $\pm 3.7^\circ\text{C}$. The comparative error from one test to another and within one test is much smaller.

In all of the experiments performed, the outside pressure and the drive speed were adjusted to 1.72 MPa absolute (250 psia) and 1800 rpm, respectively. Ordinarily, the seal was started with the desired pressure and accelerated immediately to the operating speed. The system was heated gradually up to the desired operating temperature within about one hour. Test duration varied from 1 hour to 89 hours. The seal was lapped only once before installation and run through several tests. The initial surface parameters of test seals are shown in Table 2-4.

Immediately after starting a new or relapped seal, there was a certain period characterized by relatively low torque and seal face temperature (see Appendix) during which leakage was detected. This behavior agrees with the theory presented in reference [9] which suggests that during initial operation, thermal coning produces a convergent film shape and reduces friction. As the face wears flat, the friction increases. Within 10 hours or less, conditions stabilized and the seals appeared to have run-in.

No measurable leakage was detected after the run-in period. After the seals had worn in, a fluctuating torque and seal face temperature were recorded. The mean value of torque and seal face temperature stabilized at a certain level. At this point, it was assumed that the seal faces had been worn parallel.

Tests were conducted on four seals with operating temperature varying from 37.8°C (100°F) to 190.6°C (375°F) as shown in Tables 2-5 and 2-6. Most of the data are averages over the last 8 hours of the test. The Appendix contains all the detailed performance data for these tests.

Table 2-4. Initial Surface Data, High Temperature Tests

Seal No.	Radial Taper	Tangential CLA (μm)	Radial CLA (μm)
5	Flat	0.51	0.58
7	Flat	0.43	0.66
9	Flat	0.43	0.28
10	-570.10^{-6}	0.58	0.61
10*	Flat	0.46	0.41

*Lapped after Test 73.

Table 2-5. High Temperature Test Experimental Results,
 $B = 1.00$, $P_{H_2O} = 1.72$ MPa, 1800 rpm

Test No.	Seal No.	Test Duration (h)	T_∞ (°C)	Average Torque (N-m)	Average Face Temp (°C)	Average Leakage (cm³/min)
46	5	29.7	93.3	6.8	98.5	0.0
47	5	24.9	121.1	9.1	125.2	0.0
48	5	29.4	148.9	8.9	154.1	0.0
49	5	32.7	121.1	8.2	125.8	0.0
50	5	15.3	148.9	8.6	152.8	0.0
51	5	23.9	93.3	12.8	100.5	0.0
52	5	41.2	65.6	11.1	73.5	0.0
53	5	46.5	37.8	11.4	45.7	0.0
54	7	72.0	93.3	9.1	98.7	0.0
55	7	26.8	137.8	6.8	140.7	0.0
56	7	43.7	165.6	7.4	168.9	0.0
58	9	1.2	176.7	20.9	192.2	0.5
59	9	0.8	176.7	21.1	192.5	0.0
60	9	44.2	165.6	8.3	171.0	0.0
61	9	46.0	137.8	10.9	145.7	0.0
62	9	4.8	37.8 to 176.7			
63	9	4.7	37.8 to 176.7			

Table 2-6. High Temperature Test Experimental Results,
 $B = 0.75$, $P_{H_2O} = 1.72$ MPa, 1800 rpm

Test No.	Seal No.	Test Duration (h)	T_a (°C)	Average Torque (N-m)	Average Face Temp (°C)	Average Leakage (cm³/min)
69	10	24.1	37.8	4.6	44.1	0.2
70	10	24.1	93.3	6.9	98.1	0.0
71	10	24.0	148.9	6.7	153.2	0.0
72	10	89.2	37.8	1.7	41.1	0.0
73	10	5.0	37.8 to 190.6			
78	10*	37.1	37.8	7.6	47.1	0.0
79	10	12.2	65.6	5.3	71.0	0.0
80	10	10.0	93.3	7.4	100.8	0.0
81	10	12.0	121.1	6.5	126.7	0.0
82	10	11.7	176.7	4.2	180.4	0.0
83	10	3.8	148.9	4.0	152.8	0.1
84	10	2.1	190.6	10.1	199.7	0.0

*Lapped flat after Test 73.

Tests 58 and 59 are short because of a shut down due to overload of the drive motor immediately after the operating temperature reached 176.7°C (350°F). Three short period tests (Tests 62, 63, and 73) were run for the purpose of observing the effects of operating temperature on seal performance on a continuous basis. Tests 62 and 63 were shut down by control program due to overload of the drive motor at $T_{\infty} = 176.7^{\circ}\text{C}$ (350°F). Test 73 was shut down manually when puffing occurred at $T_{\infty} = 191^{\circ}\text{C}$.

In order to verify the parallel face operation, an examination of the torque curves was made after all tests had been completed. Results show that most of the torque curves, except for Tests 69, 72, and 79 are characterized by a wide variation in torque level (see Appendix), which is characteristic of a parallel face operation. The torque curves of Tests 69, 72, and 79 were quite steady and the torque levels were much lower compared to the others. It is thought that these seals were operating with a convergent taper, and this resulted in a sufficient hydrostatic load support which prevented wear-in. Thus, they are excluded from the data which will be used for later comparison to theory.

Figures 2-24 and 2-25 show the results of the continuous Tests 62 and 73. In these tests temperatures were gradually increased with time. The data show the decreasing and then increasing trend in ΔT (or equivalently torque) as discussed earlier.

Surface profiles were made before and after each test series using the surface analyzer. The divergent radial taper caused by the thermal coning effect, shown in Figure 2-26, agrees with the theory presented in reference [9]. But, the convergent profile shown typically by Figure 2-27 is in disagreement with theory. Close examination of the operational history of each test seal shows that the final operating temperature for the convergent

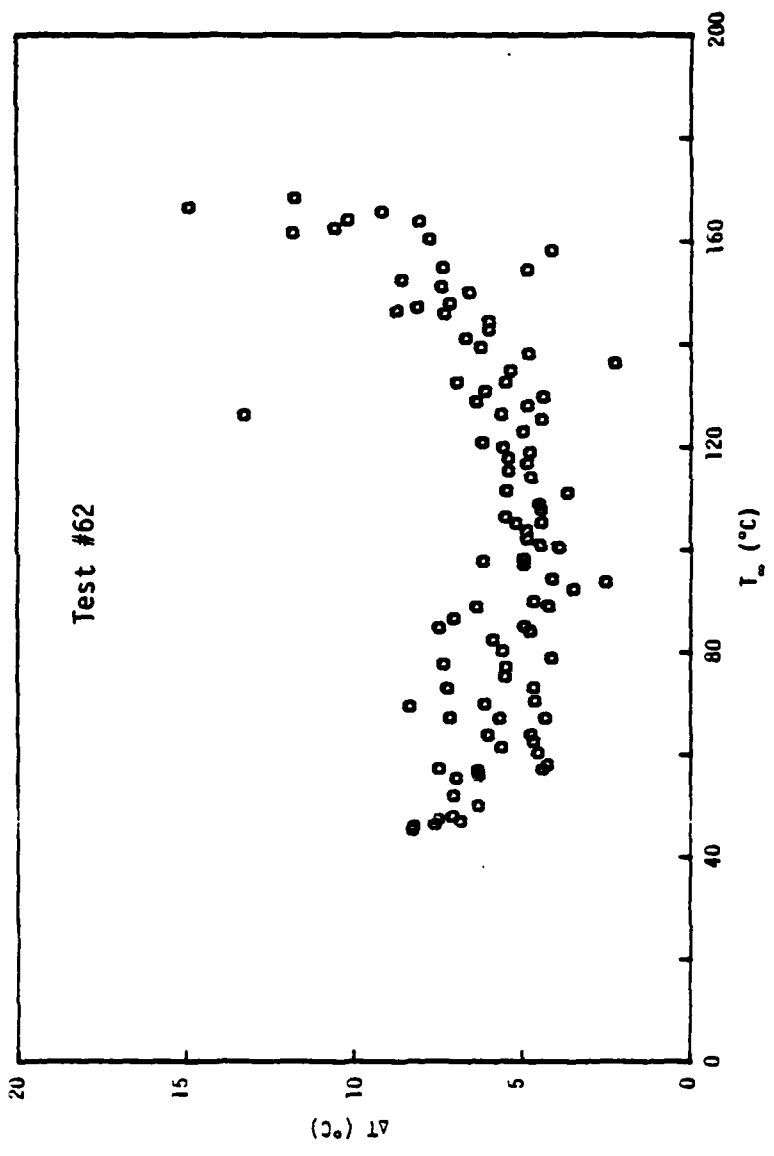


Figure 2-24. High Temperature Continuous Test, $B = 1.0$.

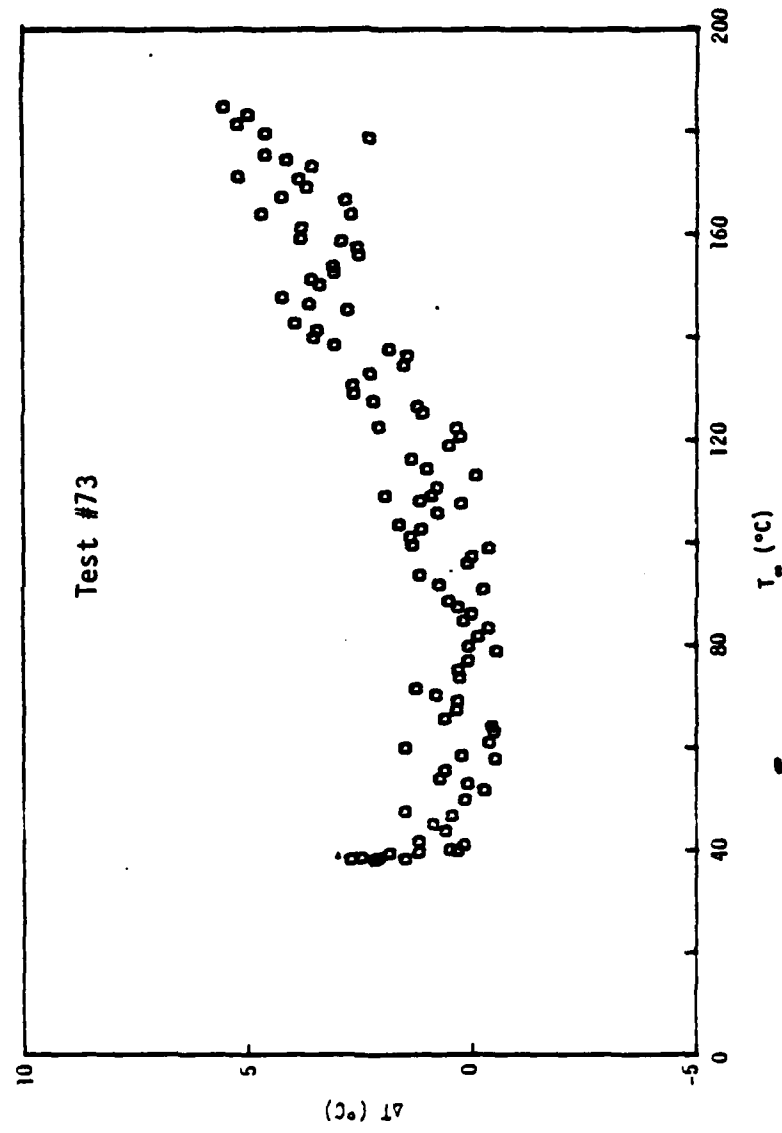
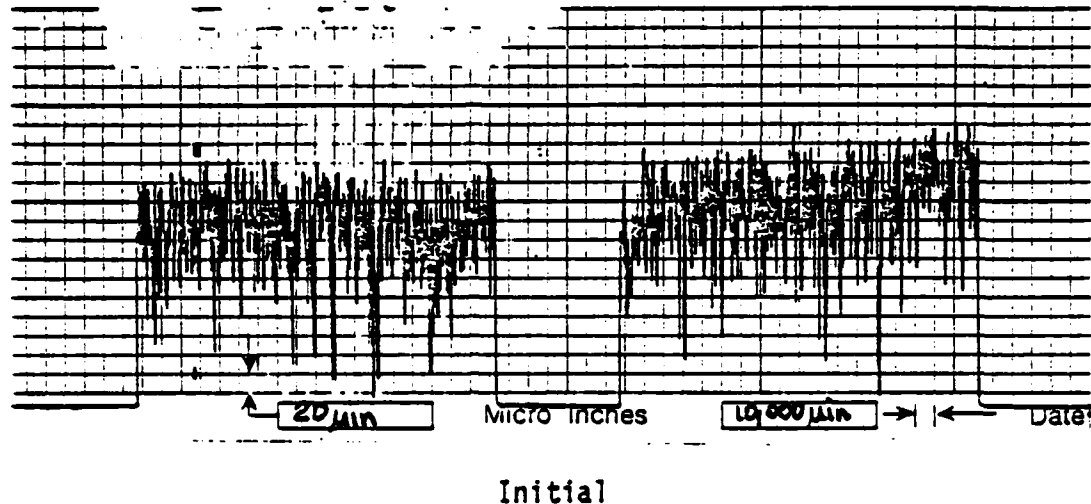


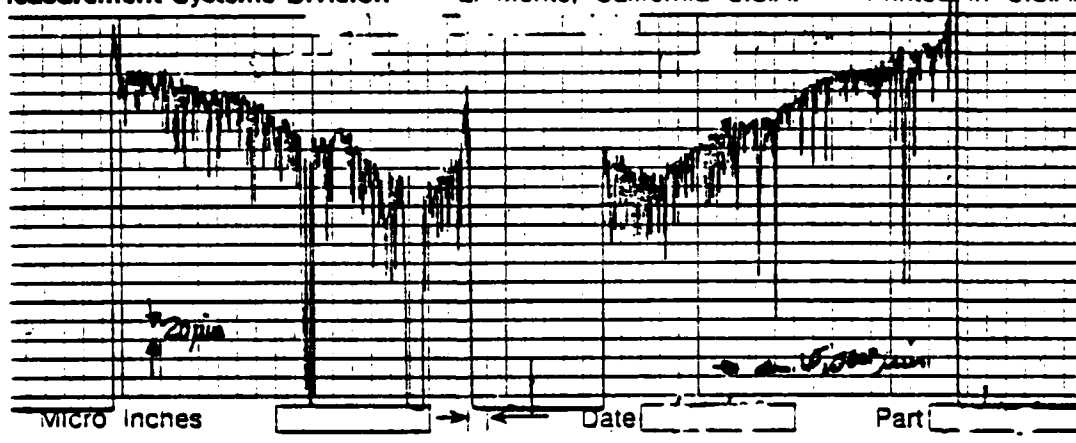
Figure 2-25. High Temperature Continuous Test, $B = 0.75$.

Gould Inc., Measurement Systems Division El Monte, Calif



Initial

Measurement Systems Division El Monte, California U.S.A. Printed in U.S.A.

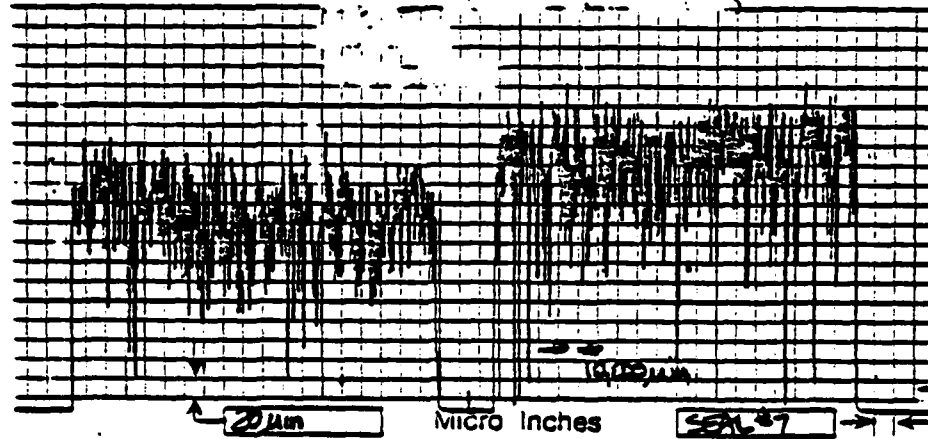


Final

Figure 2-26. Radial Surface Profile - Seal #5

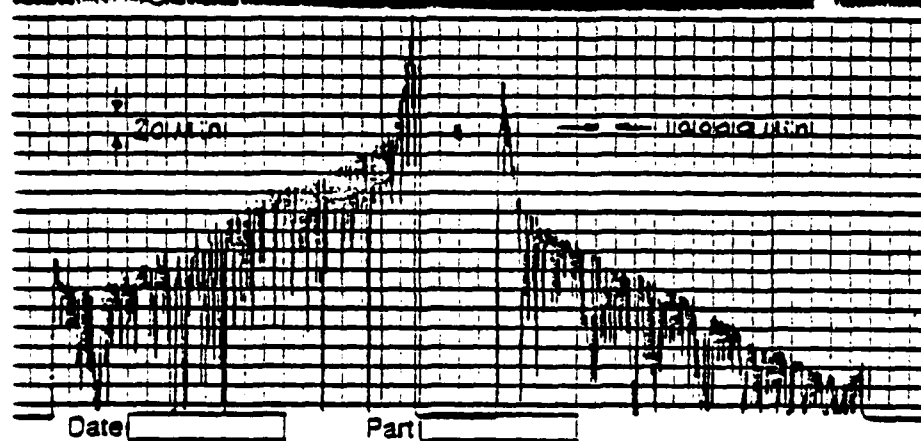
Gould Inc., Measurement Systems Division

E.I.M.



Initial

Date: _____ Cleveland, Ohio Printed in U.S.A.



Final

Figure 2-27. Radial Surface Profile - Seal #7.

seal was above 176.7°C (350°F), whereas for the divergent seal it was 100°F (30°C). It was thought that at high operating temperatures, the thermal expansion of the waviness ring might cause interference with the seal and cause it to become divergent during operating. To investigate this, the inside diameter of a carbon ring (Seal 10*) was increased by 0.5 mm and run through several tests. The final trace still indicates a convergent profile. This means that there must be another kind of thermal distortion taking place for high temperature operation. Further investigation is needed to understand how the carbon ring deforms in the high temperature environment.

Although this behavior may have influenced the test results, in most tests the period of operation was long enough that the faces became parallel in spite of the additional apparent thermally-caused rotation.

Long-Term Tests

Wear tests results on the wavy seals reported in the previous report [8] show some inconsistency and in some cases are clearly beyond the capability of measurement techniques. To get better wear data, it was decided to run a series of long-term wear tests of 500 hours each. Table 2-7 shows the results of two such tests. Test 45 was run using the original waviness drive concept with sliding O-rings, whereas Test 110 was run using the new waviness generator described previously. Comparing the actual test data between Test 45 [8] and Test 110 (see Appendix) shows that much more uniform performance was obtained using the new waviness generator than the previous method. The leakage oscillations in Test 110 are much smaller. Recalling that the oscillations are caused by the superpositions of the second harmonic drive force caused waviness over the three intentional waves, the oscillation in Test 110 is smaller because torque on the drive lugs is small since there is no friction torque on the seal ring caused by sliding gas pocket O-ring friction.

Table 2-7. Long-Term Wear Test Results
 1800 rpm, $p_0 = 3.45$ MPa, $p_g = 6.90$ MPa, $B = 1$, $n = 3$

Test No.	Duration (h)	Torque* N·m	Leakage* (ml/min)	Face Temp (°C)	Avg. Carbon Wear (μm)
45	507	3.39	6.8	32.2	0.31
110	500	1.28	1.54	39.3	-0.84

*Average over last 9.47 hours of test.

Average leakage for the final 9.47 hours of Test 110 is lower than for Test 45. It is thought that leakage is smaller because there are no large oscillations as in Test 45. Test 45 in fact shows that the oscillation amplitude increases toward the end of the test as O-ring friction presumably becomes higher. The opposite is true of Test 110 (see Appendix). After the first 24 hours the amplitude of the leakage oscillations decrease as the seal wears in. Likewise, torque in Test 110 is lower than in Test 45.

Table 2-7 shows the wear rate for Test 45 to be very small, 0.3 $\mu\text{m}/500$ hours. Test 110 shows a negative wear rate meaning that wear is less than the distortion of the nose of the seal. Comparing the lowest wear rate from the parallel face tests of the previous report [8] to the worst case above (Test 45) shows that the wear rate for the wavy seal is a factor of at least 200 times lower than for the parallel face seal. At such a low wear rate a wavy seal could be designed such that a ten year face life in continuous operation could be anticipated.

Offset Land Tests

As will be discussed later, it can be shown theoretically that a flat face seal constructed with an offset will have a lower wear rate than a parallel face seal. This seal can be made to operate theoretically with a low leakage rate for an indefinite period of time by in essence machining the offset into the soft face on a continuous basis. This concept is shown in Figure 2-28. The hard face operates hydrostatically as if it were a flat face. The only purpose of the protrusion is to machine the offset into the mating soft face as shown.

To produce such a seal it is necessary to provide the protrusion as shown while the remainder of the face is left undisturbed. The height of the protrusion is of the order of 1-5 μm depending on performance desired. As a first attempt an electron beam deposition device was used to produce the protrusion on the

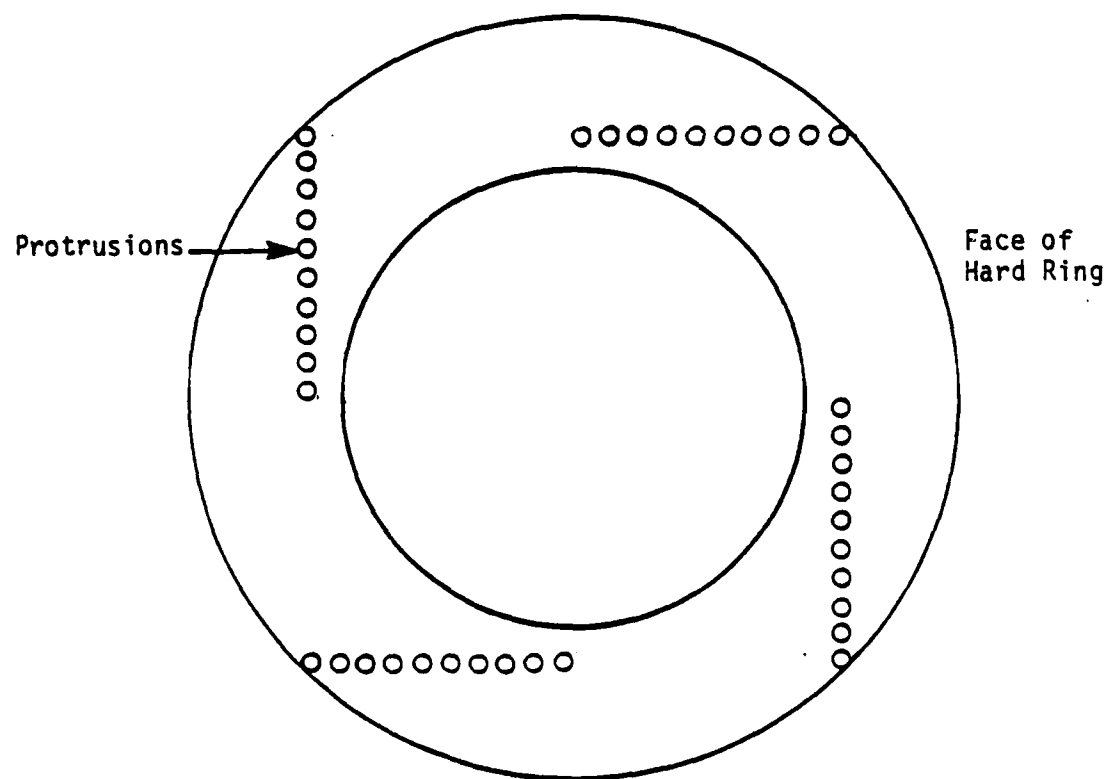
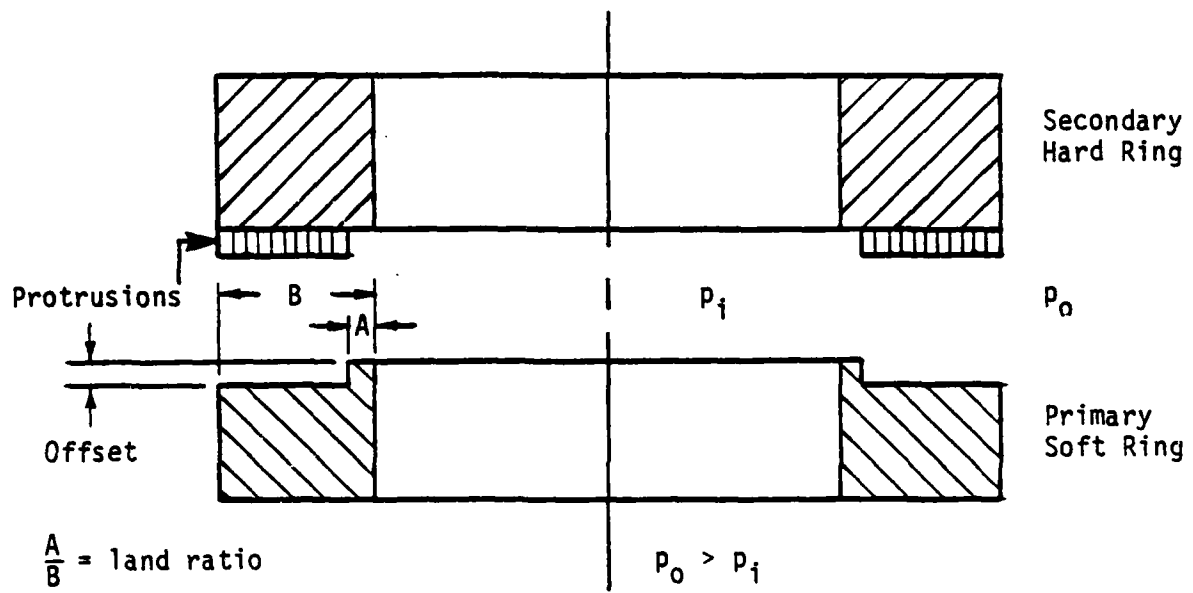


Figure 2-28. Offset Land Seal.

hard face. Tungsten carbide powder was vaporized and deposited on the face using a mask to obtain the desired pattern of protrusions similar to that shown. It was found that the deposits would not bond tightly to the seal face. After several trials using different techniques, this method was abandoned.

The technique which was found to work was to use the diamond indentor from a Rockwell tester under load. This technique produces a protrusion of the form shown by the surface analyzer trace of Figure 2-29. The height of the protrusion can be controlled by lapping with diamond compound and by varying the indentor load. The protrusion produced in this way is actually a round crater with the actual protrusion being formed by the walls of the crater. This type of protrusion has the disadvantage that in nonconductile materials the crater walls may have a tendency to break off as discussed later.

Using this technique, seal faces were prepared with $A/B = 0.2$ as shown in Figure 2-28, and four tests were run as shown in Table 2-8. The Appendix shows the actual performance data for these tests. Test 105 was started up with no special procedure. The running torque is, in fact, higher than observed on previous tests for parallel face seals and the theoretical mechanism was clearly not operating. Test 106 was started at 400 rpm under full water pressure and run for approximately 5 minutes. Then speed was increased to 1800 rpm. Again here, torque was higher than in parallel face tests. In both Tests 105 and 106 it appeared that the protrusions were acting to grind away the mating face and, in fact, causing a higher torque than for the parallel face test. Judging by the low leakage, the fluid never had the opportunity to become distributed properly across the face to relieve the mechanical load.

Test 107 was set up with much larger protrusions. It was started up under about 60 psi and run at 400 rpm for nearly one hour after which speed and pressure were increased to test

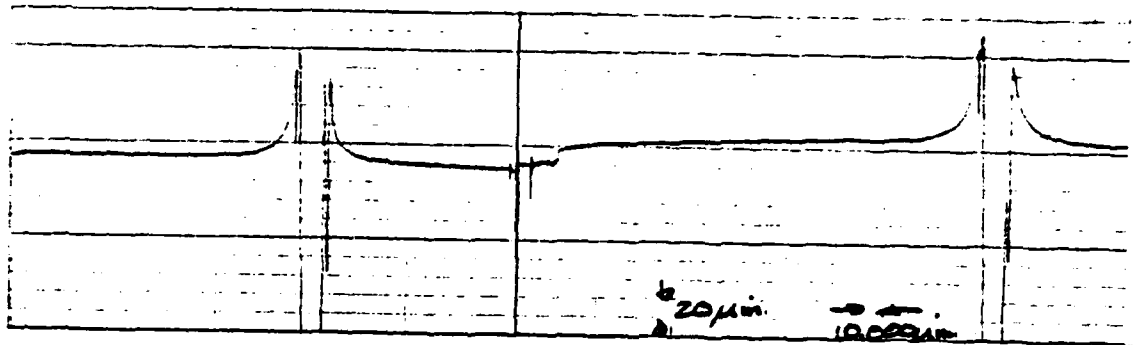


Figure 2-29. Surface Analyzer Trace of Diamond Indentor-Produced Protrusions.

Table 2-8. Offset Land Test Results
 $P_0 = 3.45 \text{ MPa}$, 1800 rpm, $B = 0.75$, $A/B = 0.2$

Test No.	Initial WC Offset (μm)	Final WC Offset (μm)	Final Carbon Offset (μm)	Test Duration (h)	Avg. Face Temp ($^{\circ}\text{C}$)	Avg. Torque (in.-lb)	Avg. Leakage cm^3/min	Avg. Wear (μm)
105	1.52	1.52	--*	22.5	52.2	13.2(117)	0.02	--*
106	1.52	1.52	--*	20.6	52.0	13.8(122)	0.008	--*
107	5.08	--*	3.30	3.3	38.0	0.32(2.8)	71.9	0.55
108	2.54	1.52	1.02	162.2	38.3	0.32(2.8)	19.3	0.17

*Not measured.

values. In contrast this seal clearly lifted off. Leakage was quite high and torque was extremely low. Test 108 was run in an identical manner but using a smaller protrusion. Leakage became more moderate and torque was still quite low. Figure 2-30 shows the final offset and protrusion for Test 108, and it can be clearly seen how the offset is machined into the carbon. The data for Test 108 also shows that wear is quite low as predicted even for the 162 hour test. Table 2-8 also shows that the protrusions wear down.

In summary, the concept appears to work. However, there are certain limitations and unknowns. First, from Test 108, the protrusions appear to wear down. It is not known whether they will wear down to a still useful level or simply wear away over a long period of time. Second, observing that Tests 105, 106, and 107 have the same final W-C offset, there may be serious problems in repeatedly starting up such a seal in the low-friction mode. The seal can clearly start also in a high-friction mode, at least at the lower offset values. This is a real disadvantage because only at low offset values will the leakage assume a low value-- which is one of the theoretical advantages of this seal over other types of hydrostatic seals which characteristically have high leakage. Further work is needed to see what is required to make the seal start up in the proper mode. One possibility to be considered is to use an offset taper arrangement which has a similar theoretical performance but may have a stronger tendency to start properly.

Speed Effects

Several additional tests were run at varying speeds for both the wavy seal and the flat face seal. The results of these tests plus similar tests run during the previous year are shown in Tables 2-9 and 2-10. In Table 2-9 for the wavy tests, the most striking result is the very high friction coefficient at 1.4 rpm

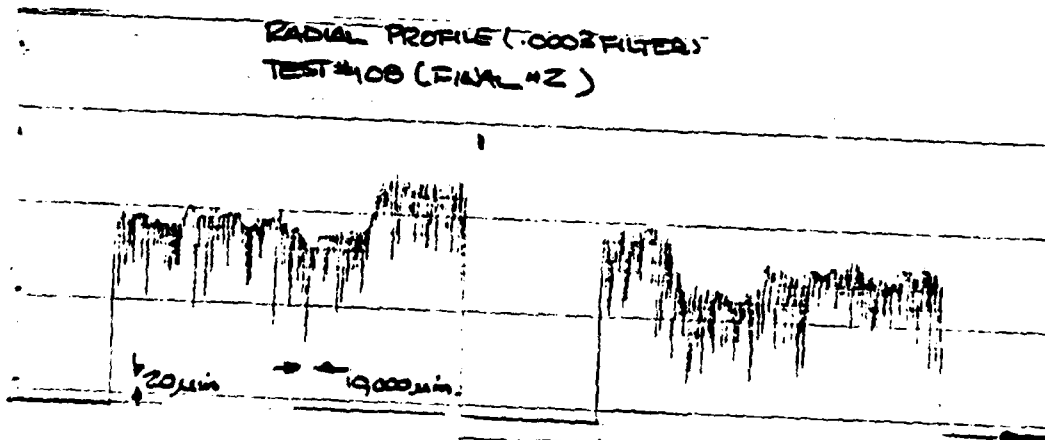
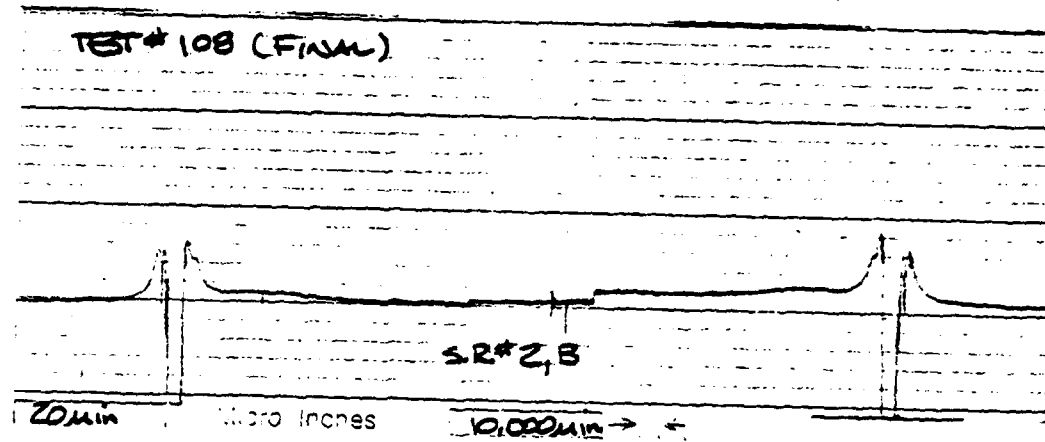


Figure 2-30. Final Offset and Protrusions
for Test No. 108.

Table 2-9. Wavy Seal Speed Effect at
 $p_0 = 3.45 \text{ MPa}$, $p_g = 6.90 \text{ MPa}$, $n = 3$, $B = 1.0$

Test No.	Speed RPM	Test Duration (h)	Avg. Face Temp (°C)	Avg. Torque N·M (in.-lb)	Avg. Leakage cm³/min.
91	1.4	20.6	37	29.0 (255)	1.2
103	1.4	48	38	30.7 (272)	1.3
90	400	72.4	38	0.6 (6)	2.3
102	400	47.8	38	0.7 (6)	1.9
26	500	4	40	1.6 (14)	0.3
33	900	20	40	1.8 (16)	0.2
104	900	28.7	38	0.3 (3)	1.4
89	900	50	39	2.2 (19)	0.6
34	1800	100	39	1.4 (12)	1.4
39	1800	100	39	1.6 (14)	3.2
21	1800	100	40	1.5 (13)	1.1
30	2700	46	41	3.2 (28)	4.5
31	3600	6	43	5.0 (44)	1.8

Table 2-10. Flat Face Speed Effects,
 $p_0 = 3.45$ MPa, $B = 1.0$

Test No.	Speed RPM	Test Duration (h)	Avg. Face Temp (°C)	Avg. Torque N·M (in.-lb)	Avg. Leakage cm³/min.
92	1.4	13.1	37	18.6 (164)	0.0
93	400	23.6	41	9.1 (80)	0.0
94	900	25.1	43	8.6 (76)	0.0
35	1800	100	44	8.4 (74)	0.0
40	1800	111	43	9.2 (81)	0.0
95	2700	22	47	6.2 (54)	0.0
96	3600	0.8	50	6.2 (55)	0.0

and the dramatic reduction in torque at a relatively slow speed of 400 rpm. After 400 rpm, friction torque generally increases with increasing speed.

Looking at the flat face speed effects in Table 2-10, again torque is very high at 1.4 rpm, drops off rapidly at 400 rpm, and then continues to decrease with increasing speed. The flat face results can be explained in two ways. Assuming that the seal has worn to a parallel face configuration in all cases, then there must exist a reduction in mechanical coefficient of friction with increasing speed or microasperity hydrodynamic lubrication reduces the effective mechanical coefficient of friction, or both. Unfortunately, there is no way to distinguish between the two effects. Alternatively, part of the decrease might be attributable to an increase in thermal coning with increasing speed if the faces are not worn parallel in each instance. However, this effect could not account for the large difference between 1.4 and 1800 rpm because it is known that the 1800 rpm cases have been well worn in. Thus, this large difference must be explained by one of the first two mechanisms. A better distinction between the thermal coning mechanism and changing friction coefficient will become available using the friction and wear tester discussed previously because thermal coning and related hydrostatic effects can be eliminated.

Now considering the trends in the waviness tests in Table 2-9, the same effect as in the flat face test must be operating. However, the decrease is greater, and this is attributable to the greater global hydrodynamic effect caused by the waves. The reason for the subsequent increase can be explained in part by the fact that the wave changes in amplitude with speed as discussed later in Chapter 4. It is expected that when the nine-wave, redesigned seal is tested, this confusing behavior will be eliminated and the wavy seal speed-dependent behavior as caused

by hydrodynamic action will be established conclusively.

Nine-Wave Tests

The waviness cylinder under the seal ring was modified to have 18 pressure pockets. If each pocket is pressurized equally, nine waves result and these can be moved in the original fashion by rotating the waviness cylinder.. Thus, Table 2-11 shows four tests conducted using nine waves. In all cases friction is quite high and leakage is zero or quite small. This indicates that neither significant enhanced hydrostatic support or hydrodynamic load support occurred. As will be discussed later, analysis predicts this behavior in general. It occurs because the resultant deflection of the original seal ring deflected to nine waves takes on a disadvantageous shape and does not, in fact, mean that a nine-wave shape of the proper deflection characteristic will behave poorly. This case serves as an example that simply deflecting a seal into a wavy shape will not necessarily be of advantage. The exact nature of the shape that creates an advantage must be understood and properly imposed.

Table 2-11. Wavy Seal Results, $n = 9$,
 $p_0 = 3.45 \text{ MPa}$, $p_g = 6.90 \text{ MPa}$, $B = 1.0$

Test No.	Speed RPM	Test Duration (h)	Avg. Face Temp (°C)	Avg. Torque N·m (in.-lb)	Avg. Leakage cm³/min.
85	1800	24.5	53	13.2 (117)	0
86	900	48.5	40	5.1 (45)	0
87	1800	44.3	46	7.2 (64)	0
88	2700	44.8	53	8.7 (77)	0.03

Chapter 3

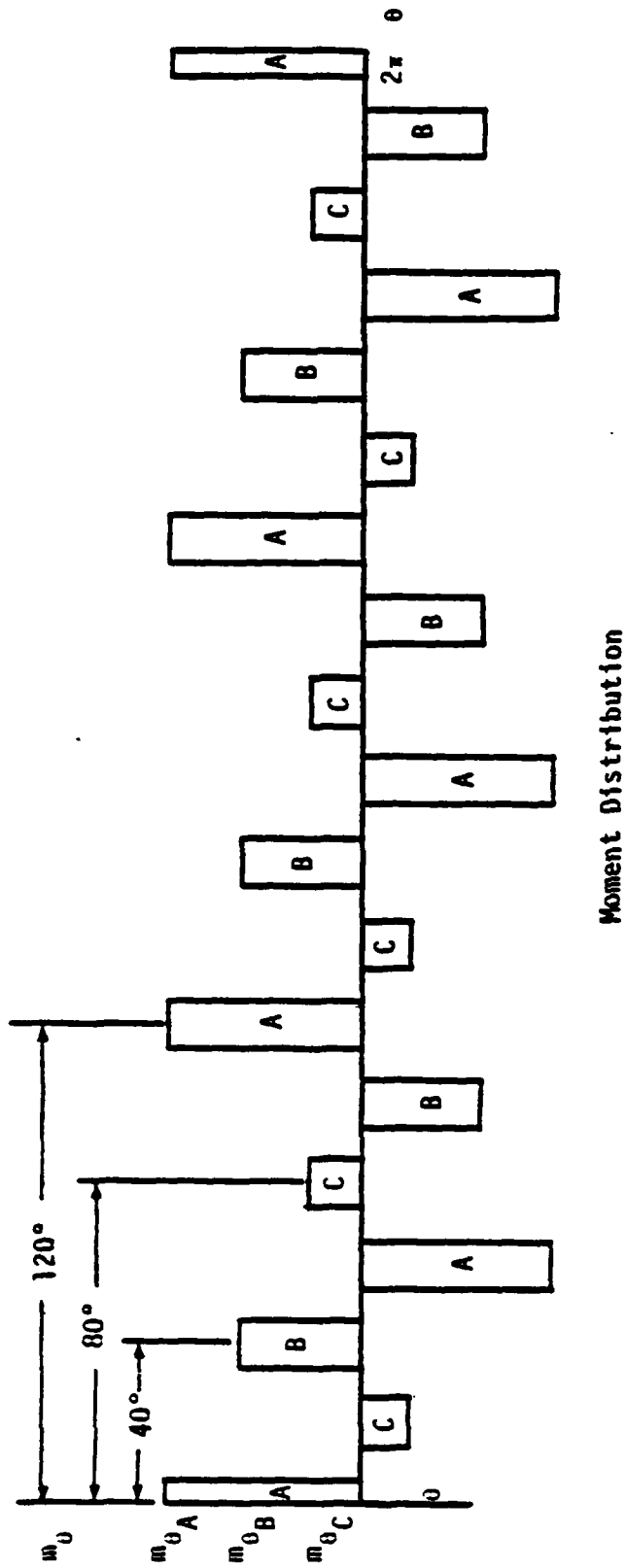
Seal Theory Developments

Waviness Drive

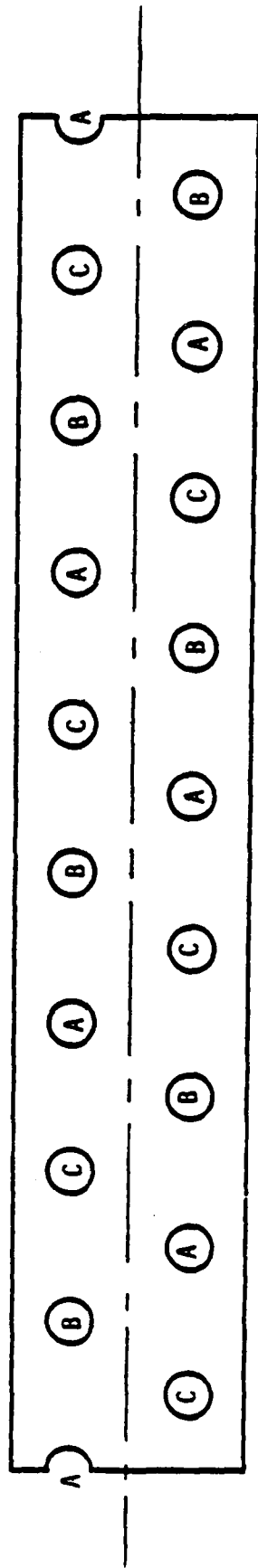
It became clear soon after the moving wavy seal was first tested that moving the wave by moving pressure pockets with sliding O-rings represented a serious limitation on what is otherwise an extremely long-life seal design. The 500-hour test (Test 45) shown in the previous report [8] is a case in point. Toward the end of the test, leakage amplitude became large and erratic. After disassembly the O-rings showed considerable wear, and it is thought that O-ring friction became high toward the end of the test. This caused the second harmonic distortion to become large giving rise to a larger leakage amplitude.

Although other mechanical means of moving the wave, such as pressure loaded rollers, were considered, it was decided that the most reliable operation could be obtained if there were no internal moving parts except the seal faces themselves. There are various concepts which can be used to move the distortion pattern with no internal moving parts. The method selected for development is similar conceptually to that of a three-phase electric motor where three voltages, each at a different phase angle, are applied to three sets of windings giving rise to a rotating magnetic field. In the case of the seal, three pressures, each different in phase, are applied to three sets of pressure pockets causing the resulting distortion to move.

With reference to Figure 3-1, three sets of pressure pockets similar to those described previously [8] are shown. Each set of six pockets A, B, or C will produce three waves around the seal because of the alternating moment produced on the ring. It can be shown that the first and most significant term of the Fourier series approximation to the moment produced by each set of pockets is given by [8]



Moment Distribution



Pressure Pockets - Developed

Figure 3-1. Pressure Pocket Arrangement for Moving Waviness Generator.

$$m_{\theta A} = p_A \frac{dr_i e}{r_c} \sin\left(\frac{nd}{2r_i}\right) \cos n\theta , \quad (3-1)$$

$$m_{\theta B} = p_B \frac{dr_i e}{r_c} \sin\left(\frac{nd}{2r_i}\right) \cos\left(n\theta - \frac{2\pi}{3}\right) , \quad (3-2)$$

$$m_{\theta C} = p_C \frac{dr_i e}{r_c} \sin\left(\frac{nd}{2r_i}\right) \cos\left(n\theta - \frac{4\pi}{3}\right) . \quad (3-3)$$

where

$$n = 3 \quad (3-4)$$

for the example in Figure 3-1. The predominant term for deflection due to an nth harmonic distribution such as m_θ is

$$v = \frac{r_c^3(1 + A)}{EJ_x(n^2 - 1)^2} m_\theta . \quad (3-5)$$

Therefore, the total deflection v at any θ is

$$v = \frac{r_c^3(1 + A)}{EJ_x(n^2 - 1)^2} (m_{\theta A} + m_{\theta B} + m_{\theta C}) , \quad (3-6)$$

$$v = \frac{r_c^3(1 + A)}{EJ_x(n^2 - 1)^2} \frac{dr_i e}{r_c} \sin\left(\frac{nd}{2r_i}\right) \left[p_A \cos n\theta + p_B \cos\left(n\theta - \frac{2\pi}{3}\right) + p_C \cos\left(n\theta - \frac{4\pi}{3}\right) \right] . \quad (3-7)$$

Now assume the pressure p_A , p_B , and p_C are functions of time as follows:

$$p_A = p_g \cos \Omega t + p_0 , \quad (3-8)$$

$$p_B = p_g \cos\left(\Omega t + \frac{2\pi}{3}\right) + p_0 , \quad (3-9)$$

$$p_C = p_g \cos\left(\Omega t + \frac{4\pi}{3}\right) + p_0 . \quad (3-10)$$

Substitution of equations (3-8), (3-9), and (3-10) into (3-7) gives

$$v = K \cos(n\theta - \Omega t) , \quad (3-11)$$

where

$$K = \frac{3}{2} \frac{p_g r_c^2 dr_i e}{EJ_x} \frac{(1 + A)}{(n^2 - 1)^2} \sin\left(\frac{\pi d}{2r_i}\right) . \quad (3-12)$$

A similar derivation applies for the face tilt ϕ . Thus, equation (3-11) represents a deflection of n waves which moves at angular speed Ω around the face of the seal. This is accomplished by supplying three pressures, varying sinusoidally with time and spaced 120° apart, to three separate sets of pockets. The theory equally applies to any number of waves n , only the number of pockets need be changed. Three pressures only are required.

Pressures of the form of equation (3-8), (3-9), and (3-10) can be obtained by several means including the waviness generator described in detail in Chapter 2. It is to be noted that each pressure must have the same amplitude p_g and the same mean value p_0 . If these are not equal, then some more complex moving wave is created which does not have a time-independent amplitude.

Waviness Model

In the previous report [8] it was noted that the analytical model for predicting performance of the wavy seal was based on assuming all negative fluid pressures equal to zero. This was done in the interest of simplicity because the problem solution becomes quite difficult for the wavy and tilted seal when deflection must be considered. The cavitation solution model developed previously [5] could not accommodate the tilted wavy seal because

the cavity shape may change character from one solution to the next. Using the approximation it was recognized that some error would be introduced into the solution because the correct cavity boundary conditions were not satisfied.

Since the time the previous report was written, a paper has been presented by Elrod [12] which provides a solution algorithm for the cavitation problem which is much more general than those developed previously [5]. It provides relatively fast, consistent solutions to the cavity problem using the proper cavity boundary conditions. This algorithm was incorporated into the seal model, and previously given solutions were recalculated. The algorithm and its incorporation into the seal model will now be described.

Considering Figure 3-2 which shows two waves as an example, the proper boundary conditions for the Reynolds equations are as follows. At the inside and outside,

$$p(r_i) = p_i , \quad (3-13)$$

$$p(r_o) = p_o . \quad (3-14)$$

Cavitation is most properly accounted for at the upstream boundary by

$$p = p_c , \quad (3-15)$$

$$\frac{\partial p}{\partial n} = 0 . \quad (3-16)$$

At the downstream boundary, the proper boundary conditions are considered to be those given by Jakobson and Floberg [13].

$$p = p_c , \quad (3-17)$$

$$\frac{\partial p}{\partial n} = \frac{6 \cos \alpha_2}{h_2^3} (h_2 - h_1) , \quad (3-18)$$

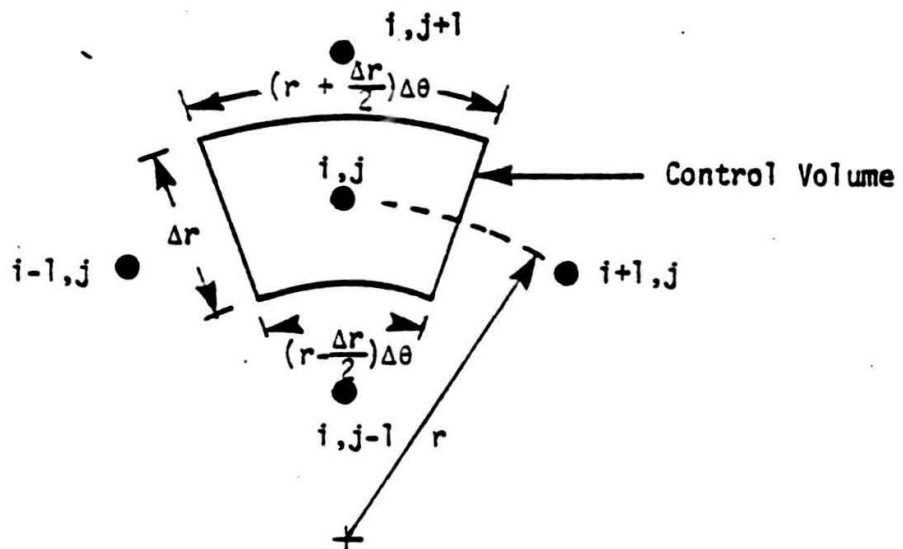
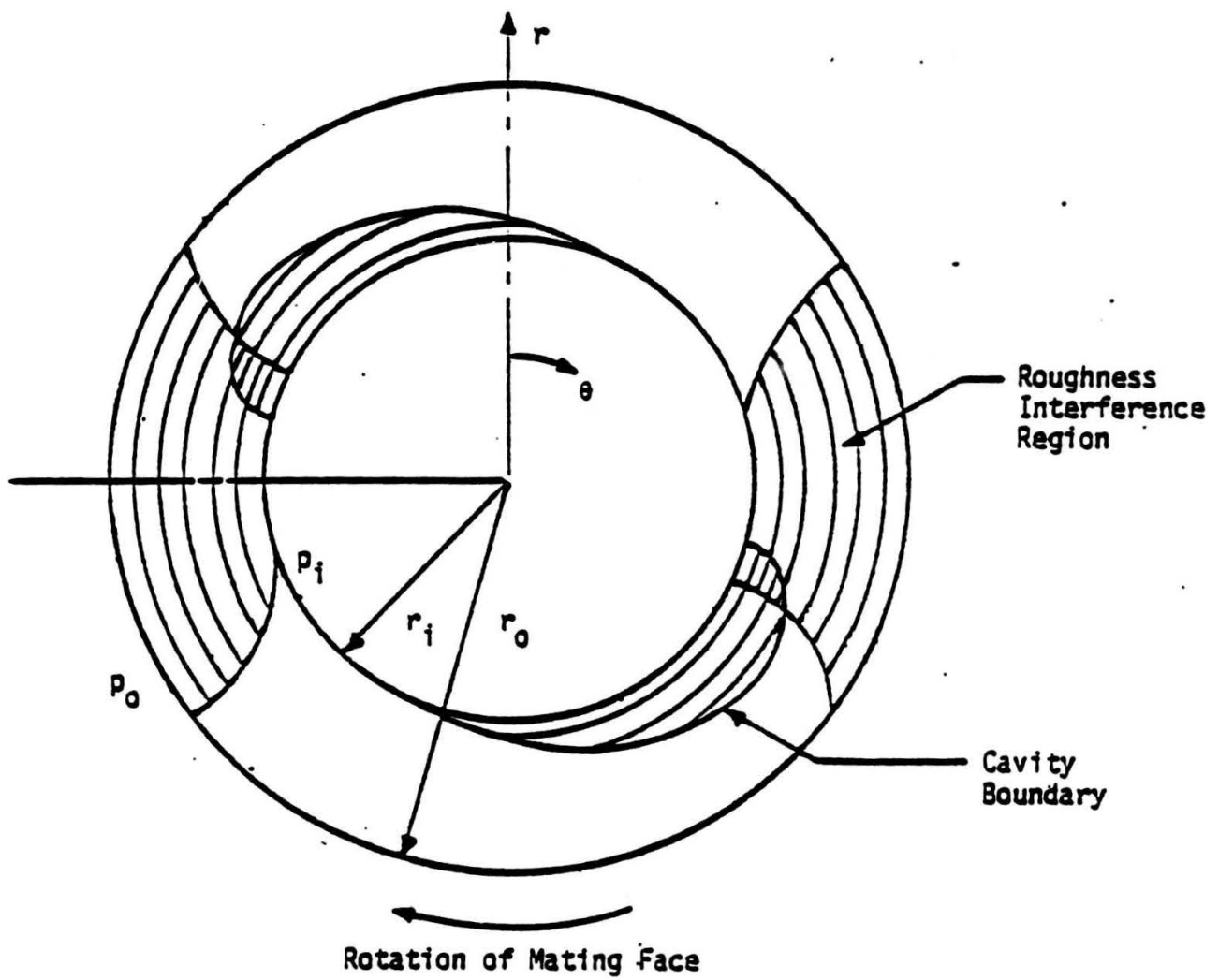


Figure 3-2. Wavy Seal Geometry, Cavitation, and Control Volume.

where ② represents the downstream cavity boundary and ① represents the upstream cavity boundary. The use of (3-15), (3-16), (3-17), and (3-18) provides continuity across the boundary.

The above equations were used as stated in the previous cavity solutions [5]. Their use requires that the general shape of the cavity be known or the method can be defeated. Elrod [12] uses a different approach. A dimensionless variable λ (ϵ in the original paper) is introduced to provide continuity. When λ is less than unity, it represents the fraction of flow in the cavity. When λ is greater than unity, it represents the compression of the fluid. Thus, the same variable is used throughout the region and can be solved for given certain assumptions.

In particular, Elrod [12] provides the following relationships:

$$(\dot{m}_x)_{\text{convection}} = \rho_c \frac{U}{Z} \left[\lambda_{-1} h_{-1} (1 - g_{-1}) + g_{-1} h_{-1} + \frac{g_{-1} g_0}{2} (h_0 - h_{-1}) \right], \quad (3-19)$$

$$(\dot{m}_x)_{\text{pressure}} = \left(\frac{h^3}{12n} \right)_{\text{avg}} \beta \rho_c \left[\frac{g_{-1} (\lambda_{-1} - 1) - g_0 \cdot (\lambda_0 - 1)}{\Delta x} \right], \quad (3-20)$$

where

$$p = p_c + \beta(\lambda - 1) \quad \text{and} \quad g = 1 \quad \text{for } \lambda \geq 1, \quad (3-21)$$

$$p = p_c \quad \text{and} \quad g = 0 \quad \text{for } \lambda < 1. \quad (3-22)$$

β represents compressibility, and for this essentially incompressible problem, a convenient arbitrary value can be used. The subscripts -1 and 0 represent node locations in the x (ϵ in the problem of interest) direction (see Figure 3-2). Equation (3-19) applies only to the tangential direction. An equation similar to equation (3-20) can be written for the y (radial in the problem

of interest) direction. Both equations (3-19) and (3-20) are written to describe flow across the left-hand boundary of a control volume. Similar expressions with the subscripts changed apply to the right-hand boundary.

Considering a complete control volume in polar coordinates, as shown in Figure 3-2, the above and similar expressions can be used to write a difference equation applicable to all node points.

$$\begin{aligned}
 & - \left[\bar{\beta} g_{ij} \left\{ \left(\frac{\bar{h}_{ij} + \bar{h}_{i-1j}}{2} \right)^3 \frac{\Delta r}{r \Delta \theta} + \left(\frac{\bar{h}_{ij} + \bar{h}_{ij-1}}{2} \right)^3 \left(\frac{\bar{r} - \frac{\Delta \bar{r}}{2}}{\Delta \bar{r}} \right) \Delta \theta \right. \right. \\
 & \quad \left. \left. + \left(\frac{\bar{h}_{ij} + \bar{h}_{ij+1}}{2} \right)^3 \left(\frac{\bar{r} + \frac{\Delta \bar{r}}{2}}{\Delta \bar{r}} \right) \Delta \theta + \left(\frac{\bar{h}_{ij} + \bar{h}_{i+1j}}{2} \right)^3 \frac{\Delta \bar{r}}{r \Delta \theta} \right\} \right. \\
 & \quad \left. + 6 \bar{r} \bar{h}_{ij} (1 - g_{ij}) \Delta \bar{r} \right] \lambda_{ij} \\
 & + \left[6 \bar{r} \Delta \bar{r} \bar{h}_{i-1j} (1 - g_{i-1j}) + \bar{\beta} \left(\frac{\bar{h}_{ij} + \bar{h}_{i-1j}}{2} \right)^3 g_{i-1j} \frac{\Delta \bar{r}}{r \Delta \theta} \right] \lambda_{i-1j} \\
 & + \left[\bar{\beta} \left(\frac{\bar{h}_{ij} + \bar{h}_{i+1j}}{2} \right)^3 g_{i+1j} \frac{\Delta \bar{r}}{r \Delta \theta} \right] \lambda_{i+1j} \\
 & + \left[\bar{\beta} \left(\frac{\bar{h}_{ij} + \bar{h}_{ij+1}}{2} \right)^3 g_{ij+1} \left(\frac{\bar{r} + \frac{\Delta \bar{r}}{2}}{\Delta \bar{r}} \right) \Delta \theta \right] \lambda_{ij+1}
 \end{aligned}$$

(Note: Equation (3-23) is continued on the next page.)

$$\begin{aligned}
& + \left[\frac{\bar{\beta}}{\beta} \left(\frac{\bar{h}_{ij} + \bar{h}_{ij-1}}{2} \right)^3 g_{ij-1} \left(\frac{\bar{r} - \frac{\Delta \bar{r}}{2}}{\Delta \bar{r}} \right) \Delta \theta \right] \lambda_{ij-1} \\
& + 6 \bar{r} \Delta \bar{r} \left[g_{i-1j} \bar{h}_{i-1j} + g_{i-1j} g_{ij} \left(\frac{\bar{h}_{ij} - \bar{h}_{i-1j}}{2} \right) - g_{ij} \bar{h}_{ij} \right. \\
& \quad \left. - g_{ij} g_{i+1j} \left(\frac{\bar{h}_{i+1j} - \bar{h}_{ij}}{2} \right) \right] \\
& + \frac{\bar{\beta}}{\beta} \left(\frac{\bar{h}_{ij} + \bar{h}_{i-1j}}{2} \right)^3 (g_{ij} - g_{i-1j}) \frac{\Delta \bar{r}}{\bar{r} \Delta \theta} \\
& + \frac{\bar{\beta}}{\beta} \left(\frac{\bar{h}_{ij} + \bar{h}_{ij-1}}{2} \right)^3 (g_{ij} - g_{ij-1}) \left(\frac{\bar{r} - \frac{\Delta \bar{r}}{2}}{\Delta \bar{r}} \right) \Delta \theta \\
& - \frac{\bar{\beta}}{\beta} \left(\frac{\bar{h}_{ij} + \bar{h}_{ij+1}}{2} \right)^3 (g_{ij+1} - g_{ij}) \left(\frac{\bar{r} + \frac{\Delta \bar{r}}{2}}{\Delta \bar{r}} \right) \Delta \theta \\
& - \frac{\bar{\beta}}{\beta} \left(\frac{\bar{h}_{i+1j} + \bar{h}_{ij}}{2} \right)^3 (g_{i+1j} - g_{ij}) \frac{\Delta \bar{r}}{\bar{r} \Delta \theta} = 0 . \tag{3-23}
\end{aligned}$$

Equation (3-23) represents the difference equation in nondimensional terms. The g_{ij} are as defined previously. $\bar{\beta}$ is dimensionless compressibility. For a grid of nodes ij (Figure 3-3), application of equation (3-23) results in a system of $(IMAX-1) \times (JMAX-2)$ linear equations in the unknown flow factors λ_{ij} . Values of g_{ij} must be assumed at the start. The five diagonal coefficient matrix of λ_{ij} has a bandwidth of $2(JMAX-2) + 1$ assuming equations are numbered in the r direction skipping from end to end to reduce bandwidth. The matrix is nonsymmetrical because of convective flow equation (3-19). U (r_w in the problem here) must be a positive number or the equations are invalid.

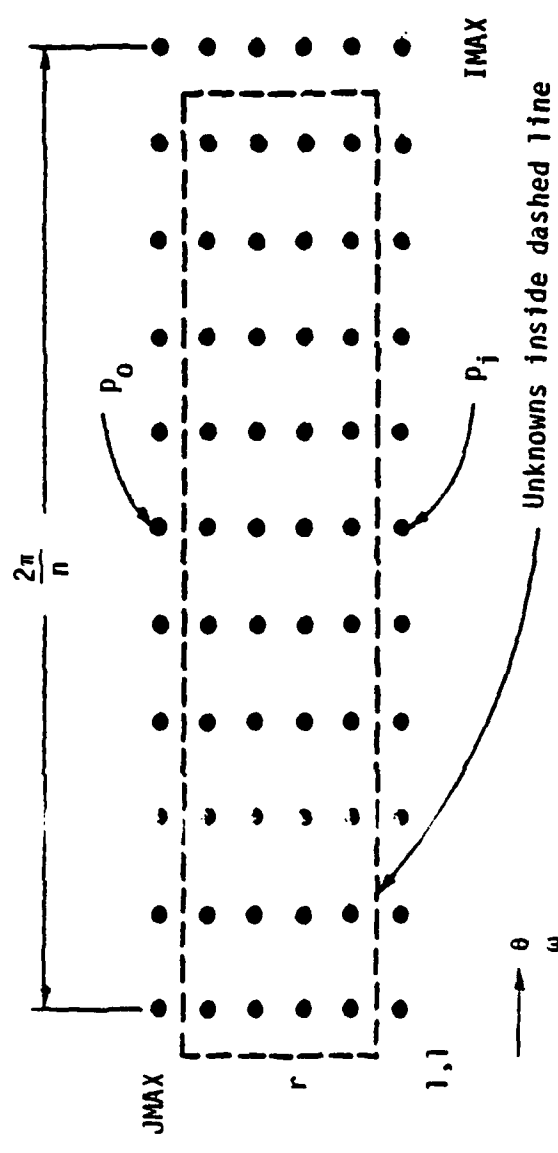


Figure 3-3. Node Arrangement for Elrod Solution.

Solution of equations (3-23) for the wavy seal was carried out as follows.

- 1) All g_{ij} were set equal to 1 at the start.
- 2) Values of λ_{ij} on the boundaries were calculated using equation (3-21) and the known pressures.
- 3) The coefficients in equation (3-23) were solved for and stored in a compacted form (Bandwidth x number of equations matrix).
- 4) A gauss elimination and back substitution technique were used to solve for λ_{ij} .
- 5) Using (3-21) and (3-22), p_{ij} and g_{ij} were solved for.
- 6) Using the p_{ij} , load support and leakage were calculated.
- 7) If no convergence, the new g_{ij} were used and steps 3) through 6) were repeated.

Convergence was established by noting the fact that the solution eventually reached a stable oscillation. That is, the set of values g_{ij} found after a particular iteration would after a few iterations repeat itself, which means that the solution cycle would start over again. Once such a repetition began, it was concluded that the solution converged (to the extent possible). Values of p_{ij} used for subsequent calculations were based on average values within a cycle. It was found that in some cases the g_{ij} would repeat each iteration and in other cases several iterations occurred before the cycle repeated. The change in load support within a cycle was generally small. It was concluded that the method could not generally lead to an absolute convergence because of the finite grid.

Using the above technique a check was made with the solution of the Findlay problem discussed in detail and solved in reference [5]. Agreement with the previous work was found to be excellent, thus establishing complete confidence in the method.

The above method does use relatively large amounts of computer time compared to the approach of using the incorrect cavity

boundary conditions. However, it is still fast enough that solutions to pressure-caused deflection problems could be obtained at a grid spacing of JMAX=12 and IMAX=14, somewhat coarser than ideal but fine enough to obtain approximate solutions. A typical solution using the algorithm was obtained for the base case problem in this work with an ideal combination of waviness and tilt at $n = 9$. The case presented is:

$$\begin{aligned}
 p_i &= 0 \\
 p_0 &= 3.45 \text{ MPa} \\
 p_m &= 262 \text{ MPa} \\
 p_s &= 0.1 p_m \\
 p_{sp} &= 0.207 \text{ MPa} \\
 C &= 0.51 \mu\text{m} \\
 B &= 1.0 \\
 n &= 6.83 \cdot 10^{-4} \text{ Pa} \cdot \text{s} \\
 \text{rpm} &= 1800 \\
 r_i &= 48.26 \text{ mm} \\
 r_o &= 54.04 \text{ mm} \\
 r_c &= 49.05 \text{ mm} \\
 n &= 9
 \end{aligned} \tag{3-24}$$

Nondimensional constants are:

$$\begin{aligned}
 \bar{p}_0 &= 2.46 \cdot 10^{-3} \\
 \bar{p}_m &= 1.87 \cdot 10^{-1} \\
 \bar{p}_s &= 1.87 \cdot 10^{-2} \\
 \bar{p}_{sp} &= 1.48 \cdot 10^{-4} \\
 r_o/c &= 1.044 \cdot 10^5 \\
 \bar{r}_i &= 0.910 \\
 \bar{r}_c &= 0.925
 \end{aligned} \tag{3-25}$$

Waviness selected is:

$$\begin{aligned}\bar{v}_0 &= 0.36 \\ \bar{\phi}_0 &= 24\end{aligned}\tag{3-26}$$

Using the new algorithm, the computed values are:

1800 rpm	1 rpm	
$\mu = 0.0019$	$\mu = 0.0277$	
$Q = 2.3 \text{ ml/min}$	$Q = 0.6 \text{ ml/min}$	
$T = 0.54 \text{ N} \cdot \text{m}$	$T = 7.8 \text{ N} \cdot \text{m}$	(3-27)
$\% = 100$	$\% = 72.0$	
$\bar{h}_0 = 1.23$	$\bar{h}_0 = 0.66$	

Figure 3-4 shows the film thickness distribution and Figure 3-5 shows the pressure distribution for 1800 rpm. The cavity is identified as the region of zero pressure.

The new algorithm has been used for calculating all of the theoretical results shown in Chapter 4.

Optimum Seal Design and Number of Waves

Since the previous report was written [8], further work on optimum seal design and number of waves has been done and presented in reference [14]. This work was carried out using the new algorithm above. The essential features of this work will be given here.

Considering the base case values of (3-24) and optimum conditions, reference is made to Figure 3-7 where dynamic performance is shown as a function of $\bar{\phi}_0$ for given value of \bar{v}_0 . Consider first the case for $\bar{v}_0 = 5.0$ which is also shown by Figure 3-6. As $\bar{\phi}_0$ increases leakage begins to decrease rapidly and torque slowly begins to increase. In the static case shown in Figure 3-8, there is a distinct minimum in the torque curve at a particular value of ϕ . This value corresponds to the middle

$\theta = 0^\circ$	1.24	1.63	2.01	2.40	2.79	3.17	3.56	3.95	4.34	4.72	5.11	5.50
	1.24	1.60	1.97	2.33	2.70	3.06	3.43	3.79	4.16	4.52	4.88	5.25
	1.24	1.54	1.84	2.14	2.45	2.75	3.05	3.35	3.66	3.96	4.26	4.56
	1.24	1.45	1.66	1.88	2.09	2.31	2.52	2.74	2.95	3.16	3.38	3.59
	1.23	1.35	1.48	1.60	1.72	1.84	1.96	2.08	2.20	2.32	2.44	2.57
	1.23	1.28	1.32	1.36	1.41	1.45	1.49	1.54	1.58	1.63	1.67	1.71
	1.23	1.23	1.23	1.23	1.23	1.23	1.23	1.23	1.23	1.23	1.23	1.23
	1.23	1.23	1.23	1.23	1.23	1.23	1.23	1.23	1.23	1.23	1.23	1.23
	1.23	1.28	1.32	1.36	1.41	1.45	1.49	1.54	1.58	1.63	1.67	1.71
	1.23	1.35	1.48	1.60	1.72	1.84	1.96	2.08	2.20	2.32	2.44	2.57
	1.24	1.45	1.66	1.88	2.09	2.31	2.52	2.74	2.95	3.16	3.38	3.59
	1.24	1.54	1.84	2.14	2.45	2.75	3.05	3.35	3.66	3.96	4.26	4.56
	1.24	1.60	1.97	2.33	2.70	3.06	3.43	3.79	4.16	4.52	4.88	5.25
$\theta = 40^\circ$	1.24	1.63	2.01	2.40	2.79	3.17	3.56	3.95	4.34	4.72	5.11	5.50
	r_i										r_o	

Figure 3.4. Film Thickness Distribution \bar{h}

$\theta = 0^\circ$	0.	0.	0.	3.	10.	15.	18.	20.	22.	23.	24.	25.
	0.	8.	16.	22.	25.	26.	27.	27.	27.	26.	25.	25.
	0.	21.	31.	36.	38.	38.	37.	35.	33.	30.	27.	25.
	0.	28.	44.	52.	56.	56.	53.	49.	44.	38.	32.	25.
	0.	34.	57.	72.	81.	83.	81.	75.	66.	54.	40.	25.
	0.	33.	61.	82.	98.	107.	109.	105.	95.	78.	55.	25.
	0.	19.	36.	52.	65.	75.	80.	81.	77.	67.	50.	25.
	0.	4.	8.	11.	13.	15.	15.	14.	12.	9.	13.	25.
w	0.	0.	0.	0.	0.	0.	0.	0.	0.	0.	8.	25.
	0.	0.	0.	0.	0.	0.	0.	0.	0.	0.	13.	25.
	0.	0.	0.	0.	0.	0.	0.	0.	4.	11.	17.	25.
	0.	0.	0.	0.	0.	0.	1.	6.	11.	16.	20.	25.
	0.	0.	0.	0.	0.	3.	9.	13.	17.	20.	22.	25.
$\theta = 40^\circ$	0.	0.	0.	3.	10.	15.	18.	20.	22.	23.	24.	25.
	r_i										r_o	

Figure 3.5. Pressure Distribution - $\bar{p} \times 10^4$

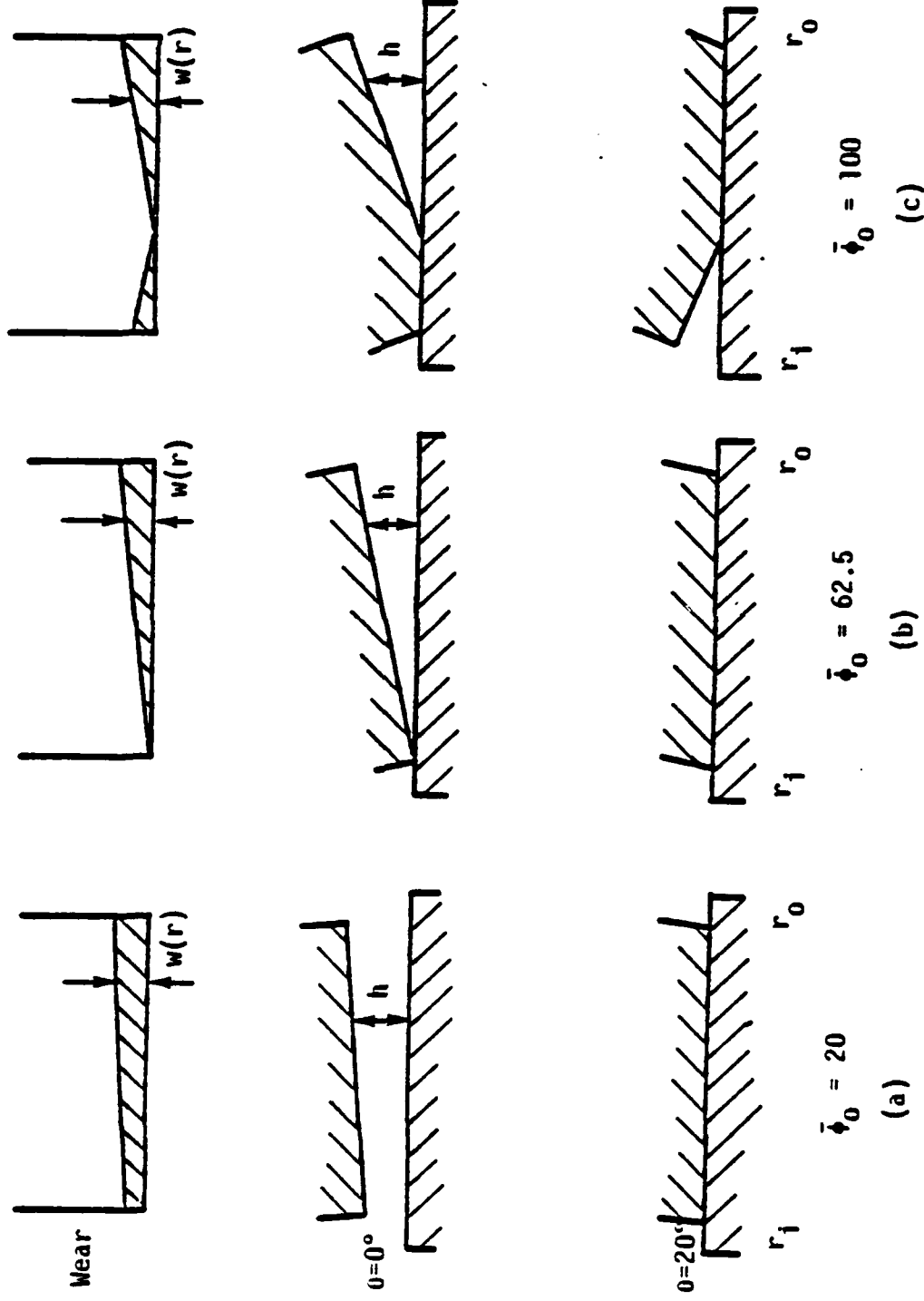


Figure 3-6. Worn Film Shape at Various $\bar{\Phi}_0$ With $f_0 = 0$.

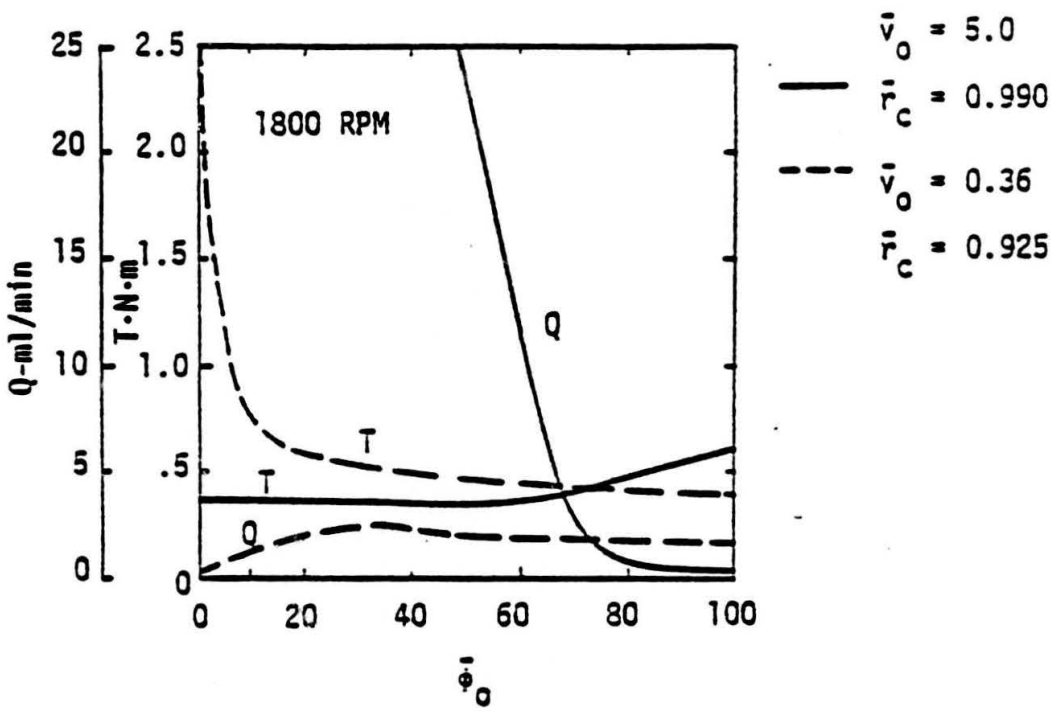


Figure 3.7. Torque and Leakage as a Function of Tilt -
1800 RPM.

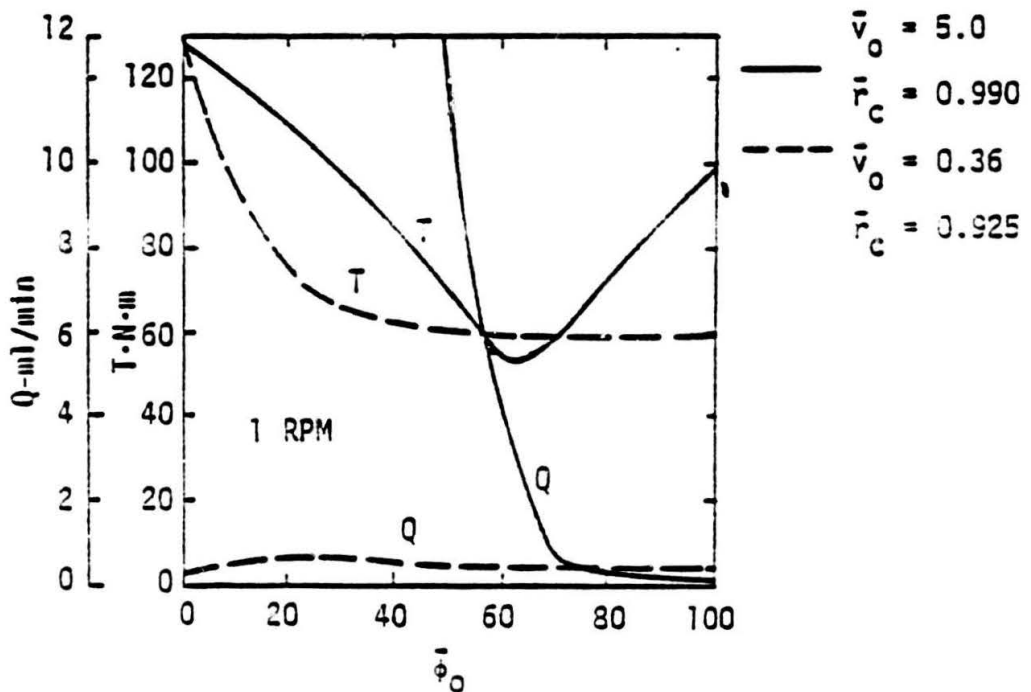


Figure 3.8. Torque and Leakage as a Function of Tilt -
1 RPM.

film thickness configuration shown by Figure 3-6, which is the condition where touching just begins to occur completely around the seal at r_j . As discussed previously [8], this condition can be shown to be where

$$\bar{\phi}_{\text{optimum}} = \frac{\bar{v}_0}{\bar{r}_c - \bar{r}_i} \quad (3-28)$$

For $\bar{v}_c = 5$ and $\bar{r}_o = 0.99$, $\bar{\phi}_{\text{optimum}} = 62.5$. Understandably as $\bar{\phi}_o$ is increased beyond this point, leakage becomes quite low both statically and dynamically because a continuous sealing band is formed. It is also clear that as $\bar{\phi}_o$ increases the friction torque begins to increase for the static case because, as shown in Figure 3-6, a portion of the converging film which reduces hydrostatic load support is lost. For $\bar{\phi}_o$ values lower than the point above, leakage is high because of large gaps, and static torque is high because the effect of taper is lost at large gaps.

This illustration shows how a combination of waviness and tilt leads to better performance than waviness alone. With the proper combination, leakage can be much smaller because there are no large gaps as caused by parallel face waviness. Friction, particularly static friction, can be made much lower than for radially parallel waviness because the tilt introduces a converging taper over much of the face of the seal.

For $n = 9$, $\bar{v}_o = 5$ is not practical as will be shown later and has been used to demonstrate the conditions where performance approaches an optimum. The case where $\bar{v}_o = 0.36$ illustrated in Figures 3-7 and 3-8 is physically possible but represents a departure from the behavior of the previous case. The optimum point is at $\bar{\phi}_o = 24$. In Figure 3-7 it is clear that friction is high for $\bar{\phi}_o$ less than 24. However, friction and leakage both continue to decrease with increasing $\bar{\phi}_o$ far beyond the optimum point. The reason for this behavior is that the seal radius at which continuous contact occurs (see Figure 3.6c) moves in

very slowly with respect to ϕ for this case as compared to the previous case. Thus, some slight improvement is found beyond the optimum point whereas in the previous case the change to less advantageous operating conditions occurs so rapidly the potential slight improvement with ϕ beyond the optimum point is hardly noticed. In any case, the designer can choose any physically achievable operating point beyond the optimum point where performance is best or where performance is most satisfactory. The selection of \bar{v}_0 depends to a large extent on what is physically achievable as well as acceptable maximum leakage. According to reference [8] for a three-wave study, for the optimum point there is a tradeoff between leakage and wear rate which depends on \bar{v}_0 . To achieve maximum benefit one should choose an operating point with less than desired leakage and with % fluid film load support such that the ratio $0.5/(1 - F)^*$ gives a suitable wear reduction factor compared to parallel face performance. It is also desirable that static torque be minimized so that low speed operation or startup will not damage the seal.

The means selected in this work to produce alternating tilt and waviness is to apply a moving cosinusoidally-distributed moment to the ring, i.e.,

$$m_\theta = m_{\theta 0} \cos(n\theta + \omega t) \quad (\text{N} \cdot \text{m/m}) , \quad (3-29)$$

where the moment must be expressed as moment/unit length of circumference. From reference [8], it can be shown that the above moment produces a sinusoidal v and ϕ with amplitudes given by

$$v_0 = \frac{m_{\theta 0} r_c^3}{EJ_x} \frac{(1 + A)}{(n^2 - 1)^2} \quad (3-30)$$

*The 0.5 refers to a 50 percent fluid pressure load support for a parallel face balance ratio one seal.

$$\phi_0 = \frac{m_{\theta 0} r_c^2}{EJ_x} \frac{1 + An^2}{(n^2 - 1)^2} . \quad (3-31)$$

The physical forces producing the moment need not be literally cosinusoidally distributed. Any means of applying concentrated loads or discrete length distributed loads whose nth term Fourier series representation corresponds to equation (3-29) is sufficient. For example, in the device shown in Figure 3-1, the loads are derived from gas pressure acting over a circular area. The Fourier analysis of the staggered pattern of the holes gives

$$m_{\theta 0} = \frac{p_g d r_i e}{r_c} \sin \frac{3nd}{2r_i} . \quad (3-32)$$

Higher harmonic terms are also present, but these generally give negligibly small deflections. On the other hand, one must be certain that unwanted lower harmonics are not introduced by whatever method is used to apply force.

Now if the method selected for applying the moment is that above, to obtain the optimum ratio of ϕ_0 to v_0 , substitution of equations (3-30) and (3-31) into (3-28) gives

$$\frac{r_c}{r_c - r_i} = \frac{1 + An^2}{1 + A} . \quad (3-33)$$

For the data given by (3-25), this would require that $A = 3.14$, a realistic value. Clearly, if A does not satisfy this requirement, or any other non-optimum case requirement involving the ratio of equations (3-30) and (3-31), then the geometry must be adjusted, changing r_c and A , until equation (3-28) is satisfied. In general, the ratio ϕ_0/v_0 has definite limits imposed by the method of application. Some design experimentation must be performed both in choosing a ratio ϕ_0/v_0 which gives suitable performance and which is physically achievable.

In practical applications, there are errors of approximation associated with the calculations of both r_c and A such that a less than optimum condition might in fact result. To avoid this possibility, it has been determined that the contact point as shown in Figure 3-6 should be designed to be at some radius greater than the inside radius as shown by 3-6c. The condition

$$\bar{r} = -\frac{\bar{v}_0}{\bar{\phi}_0} + r_c \quad (3-34)$$

defines the contact radius. If the design contact radius r_d is specified to be some fraction f of the face width outside of the inside radius, then

$$r_d = r_i + f(r_o - r_i) . \quad (3-35)$$

Then the required ratio for $\bar{v}_0/\bar{\phi}_0$ is

$$\frac{\bar{v}_0}{\bar{\phi}_0} = \bar{r}_c - \bar{r}_i - f(\bar{r}_o - \bar{r}_i) \quad (3-36)$$

and equations (3-30) and (3-31) may be applied to determine the necessary geometry to provide for this more realistic design condition.

The number of waves to be used is not arbitrary, particularly if the seal is to operate under various operating conditions. It is shown in reference [8] that the deflection due to face pressure, referred to above, changes with operating pressure and speed. This means that the faces must wear into a new equilibrium shape for each change of conditions. This will accelerate wear and is undesirable.

To counter this problem, it is possible to design the seal ring so that the desired deflection is large relative to the changing face pressure deflection. Thus, when operating conditions change, there will be no significant change in the

equilibrium face profile. This objective can be achieved by noting the results of the ratios of the face pressure-caused deflection to the desired deflection as given by equations (4-47) and (4-68) of reference [8].

$$\frac{v_{op}}{v_{om_\theta}} = \frac{p_{yo} r_c}{m_{\theta 0}} \frac{A + n^2}{n^2(A + 1)}, \quad (3-37)$$

$$\frac{\phi_{op}}{\phi_{om_\theta}} = \frac{p_{yo} r_c}{m_{\theta 0}} \frac{A + 1}{An^2 + 1}. \quad (3-38)$$

As n becomes large, the second of these two ratios becomes small. This means that the tilt angle ϕ_0 is not significantly influenced by face pressure p_y and therefore not influenced significantly by changing operating conditions. v_0 is not greatly affected by n . However, it is the change in ϕ_0 with operating conditions that leads to accelerated wear. Thus, by using large n , the detrimental effect of unwanted deflection can be minimized. For the particular example under study with $n = 9$, changes in ϕ due to changes in operating conditions were less than one percent.

The above considerations have been made for the design of a new experimental seal using $n = 9$ and the off-optimum condition mentioned. It is expected that the new design will be insensitive from a wear standpoint to the operating pressure and speed.

Offset-Land Theory

The offset-land seal is shown in Figure 3-9. The offset portion of the seal is continuously machined away by protrusions attached to the hard face as described in the previous chapter. To calculate performance of the offset-land seal, a computer program developed previously [9] was modified to accommodate the offset geometry. Leakage, load support, and friction torque are calculated as usual. To compare the anticipated wear rate of the

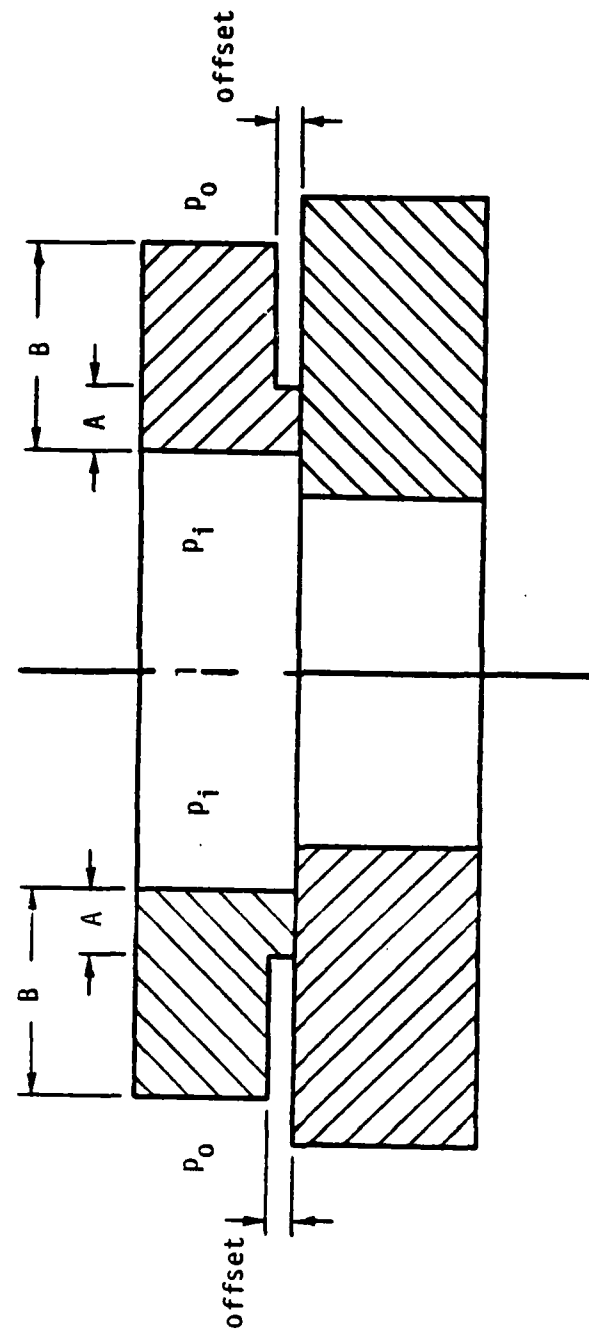


Figure 3-9. Offset - Land Seal.

offset design to a conventional parallel face design, the mechanical contact pressure, to which wear rate is proportional, was calculated. Thus, the relative wear rate is given by

$$RWR = \frac{p_{ma}(\text{offset})}{p_{ma}(\text{parallel})} . \quad (3-39)$$

When this ratio is 1.0, the wear ratio of the land of the offset land is the same as that of a parallel face seal. As the ratio becomes smaller, the wear rate of the offset-land seal would be expected to be the RWR fraction of the parallel face wear rate.

Performance was evaluated over a wide range of variables. It was determined that the concept is useful only for seals having a balance ratio less than 1.0. The following studies for $B = 0.75$ were based on the following parameter values.

$$\begin{aligned} p_i &= 0 \\ p_o &= 3.45 \text{ MPa} \\ p_m &= 262 \text{ MPa} \\ p_s &= 0.1 p_m \\ p_{sp} &= 0.207 \text{ MPa} \\ \sigma &= 0.17 \mu\text{m} \\ n &= 6.83 \cdot 10^{-4} \text{ Pa} \cdot \text{s} \\ \text{rpm} &= 1800 \\ r_i &= 48.26 \text{ mm} \\ r_o &= 54.04 \text{ mm} \\ h_{\text{offset}} &- \text{variable} \\ A/B &- \text{variable} \end{aligned} \quad (3-40)$$

Also,

$$\bar{h}_{\text{offset}} = h_{\text{offset}} / \sigma . \quad (3-41)$$

Figure 3-10 shows the effect of land width on performance holding $\bar{h}_{\text{offset}} = 5$ ($h_{\text{offset}} = 0.85 \mu\text{m}$). From the standpoint of minimizing both torque and relative wear rate, there appears to be an

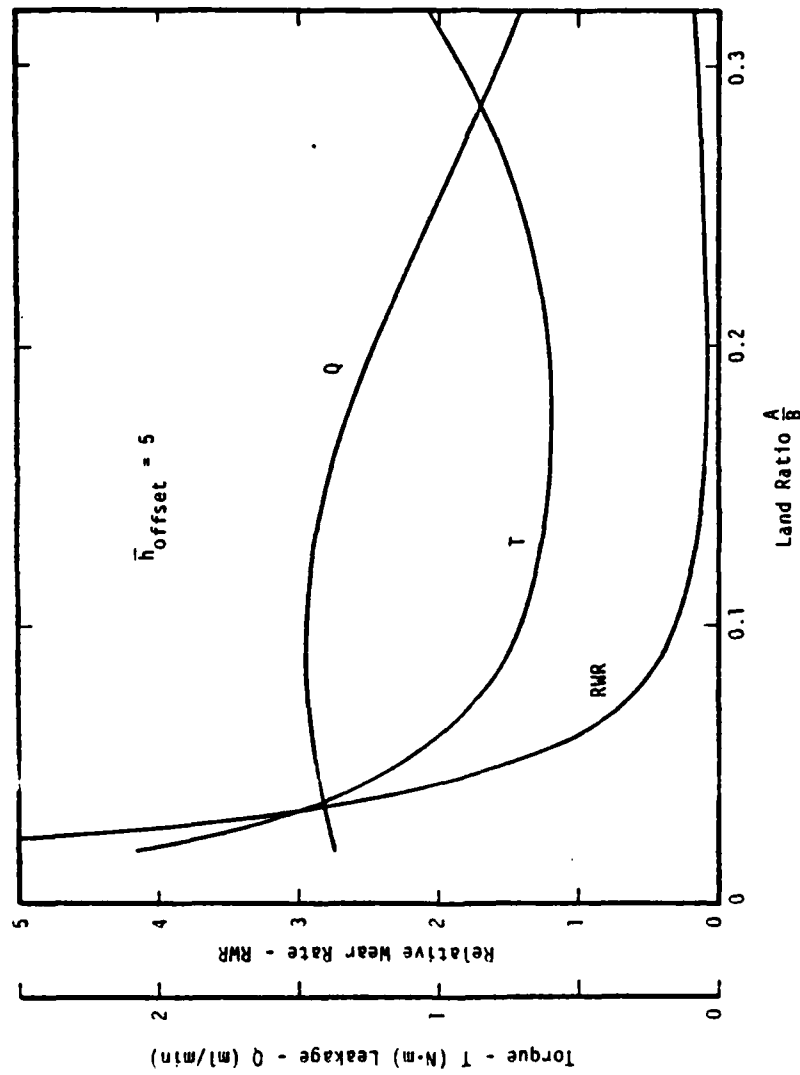


Figure 3-10. Effect of Land Width on Performance.

optimum land ratio around 0.2. Wear rate becomes less than 0.1 that of a comparable parallel face seal. Leakage values at $\bar{h}_{\text{offset}} = 5$ are modest.

Figure 3-11 shows the effect of h_{offset} on performance with land ratio held constant at 0.2. The relative wear rate quickly drops to insignificant values as \bar{h}_{offset} increases beyond 8. Further increases in h_{offset} do little to decrease torque and cause leakage to increase to large values. Based on these studies, a good design point would be for an \bar{h}_{offset} between 6 and 10 (1.0 - 1.7 μm). This would result in wear rates at least a factor of 10 lower than parallel face seals and low torque while leakage would be less than 10 ml/min.

The results of the theory described here are compared to experimental results in the next chapter.

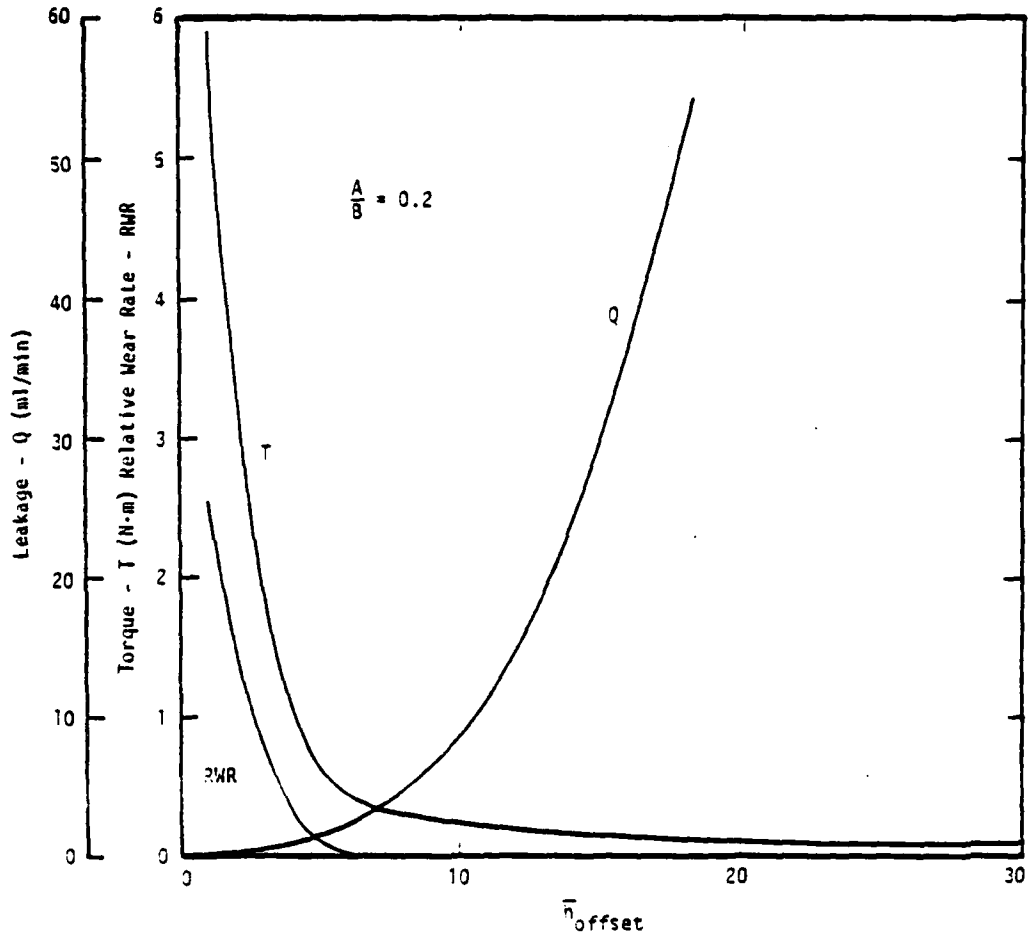


Figure 3-11. Effect of Offset on Performance.

Chapter 4

Comparison of Theoretical and Experimental Results

Three-Wave Seal Tests

Using the new algorithm described in the previous chapter, the theoretical results for the base case, three-wave, moving waviness test as a function of waviness pressure were recomputed. These results are shown in Table 4-1. The results are similar to those in Table 4-4 in the previous report [8] which were obtained using an approximate method. The two columns for h_{pb} and $h_{pb\text{calc}}$ have signs opposite to those in the previous results. This occurs because the direction of rotation was reversed for the present calculations as is required by the new algorithm. The other significant difference is that the predicted leakage values are lower than the previous predictions. The leakage is compared to experimental results in Figure 4-1. Agreement is better than that obtained using the previously calculated results. Torque values were adjusted by reducing the friction coefficient from the value used for computation. These values are compared to experimental results in Figure 4-2. Agreement is reasonable and similar to that obtained previously.

In summary, the use of the more correct algorithm makes some improvement in predicting leakage for the three-wave seal. Although the difference here is not large, it was found for the nine-wave case that the approximate model was totally in error because of the extensive cavitation in that case. Without the use of the new algorithm, total disagreement for the nine-wave case was found.

Radial Taper

Using the theoretical model presented in detail in reference [9], calculations were made to predict performance for the radial taper tests. The model predicts both short-term (initial) and

Table 4.1. Computed Results--Firod Algorithm Wear Effect at 1600 rpm
 $p_0 = 3.45 \text{ MPa}$, 100% wear, $B = 1$, 12×14 Grid

p_g MPa	h_{pa}	h_{pb} calc	h_{pb}	h_{pb} calc	h_a net	h_b net	ϕ_a net $\times 10^6$	ϕ_b net $\times 10^6$	\bar{h}_{ma}	\bar{h}_{mb}	u	T (N-mm)	Q (ml/min)	x	\bar{h}_o	p_g corrected MPa
6.90	-10.99	-9.99	1.39	1.57	4.94	1.39	719	70	1.05	-0.09	0.013	3.8	2.00	89.1	0.681	6.41
5.17	-8.26	-8.32	0.69	0.63	3.01	0.69	503	28	0.45	0.40	0.025	7.1	0.53	78.0	0.629	4.97
3.45	-5.77	-5.73	0.33	0.16	1.74	0.16	327	7	-0.22	0.70	0.035	9.7	0.24	69.6	0.622	3.56
0.0	0	0	0	0	0	0	0	0	0	0	0.060	16.8	0.09	48.5	0.740	0

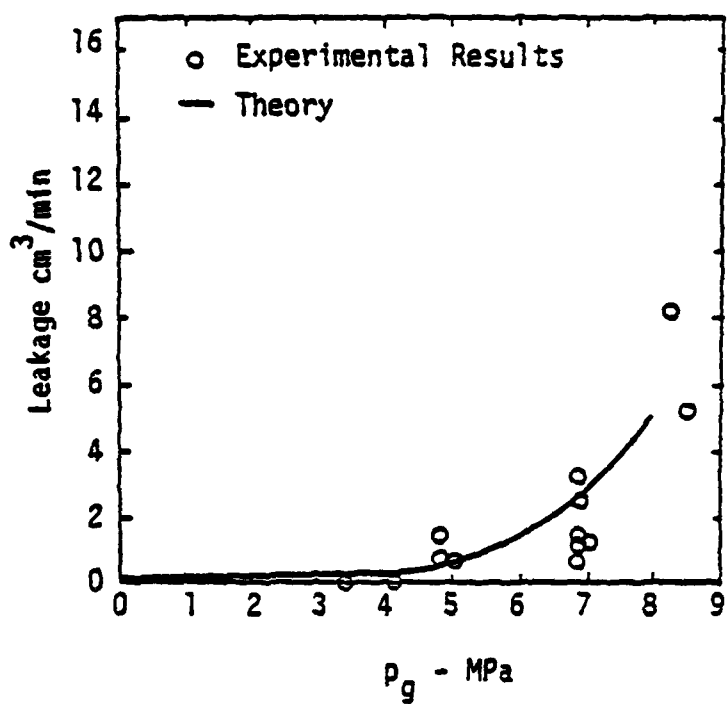


Figure 4-1. Wavy Seal Leakage - $n = 3$.

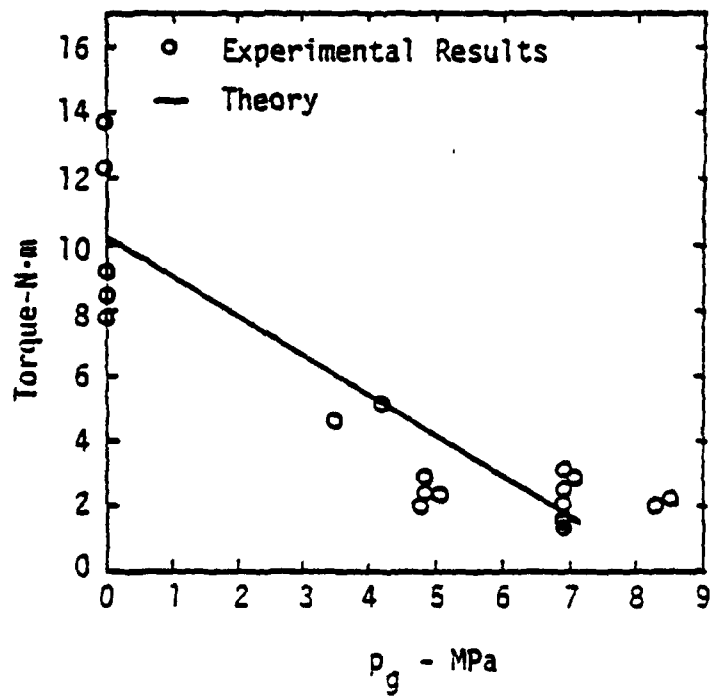


Figure 4-2. Wavy Seal Torque - $n = 3$.

long-term performance. Table 4-2 presents typical computed results for $B = 0.75$ and a roughness of $\sigma = 0.54 \mu\text{m}$ which was the average final roughness for these tests. The computed values show a reduction in leakage and an increase in torque as the radial taper goes from convergent to divergent as previously discussed.

Considering first the initial performance, Figures 4-3 and 4-4 show predicted torque and leakage as functions of radial taper for the $B = 0.75$ cases compared to experimental results. Two theoretical curves are given, one for $\sigma = 0.54 \mu\text{m}$ as discussed above and one for $\sigma = 0.15 \mu\text{m}$. The reason for the second curve will become apparent later. The data on both figures agrees reasonably well with theory at $\sigma = 0.54$ thus substantiating the model.

Figures 4-5 and 4-6 show a similar comparison made for the $B = 1.0$ tests whose results were reported in the previous report [8]. Figure 4-5 shows good agreement between theory and experiment at $\sigma = 0.54$. Figure 4-6 shows that $\sigma = 0.54$ greatly overestimates leakage. $\sigma = 0.15$ provides a better appreciation for leakage (which was unmeasurable on three of the four tests).

This discrepancy points out the reason for advancing the pocket theory in Chapter 2. It is clear from Figure 4-6 (and other data to be discussed) that using the actual roughness can overestimate the leakage in many cases. The effective value of the roughness may be much smaller than the actual roughness as explained previously. What is not clear is why the higher value of roughness more accurately predicted the results in the $B = 0.75$ cases. It is clear that the theory is inadequate. Neither the original theory nor the pocket theory are consistent. One thing that is known is that the surface roughness changes during the course of a test. This may in part explain these differences in that the surfaces evolve differently in the two types of tests because the mechanical contact pressures are different. While

Table 4-2. Theoretical Results--Radial Taper
 $\sigma = 0.54 \mu\text{m}$ (21.25 $\mu\text{in.}$), $B = 0.75$

ϕ_i ($\mu\text{m}/\text{m}$)	Initial Torque N·m (in.-lb)	Final Torque* N·m (in.-lb)	Leakage @ 1 hr (cm^3/min)	Final Leakage* (cm^3/min)
1013	0.2 (1.5)	0.19 (1.7)	48.5	41.4
613	0.8 (6.6)	8.12 (71.9)	18.0	4.18
40	3.5 (31.3)	8.18 (71.4)	6.43	4.17
-320	6.9 (60.6)	8.17 (72.3)	4.25	4.17
-750	11.5 (101.7)	8.18 (72.4)	3.75	4.17
-1110	15.0 (132.4)	8.18 (72.4)	3.79	4.17

*Based on length of corresponding test.

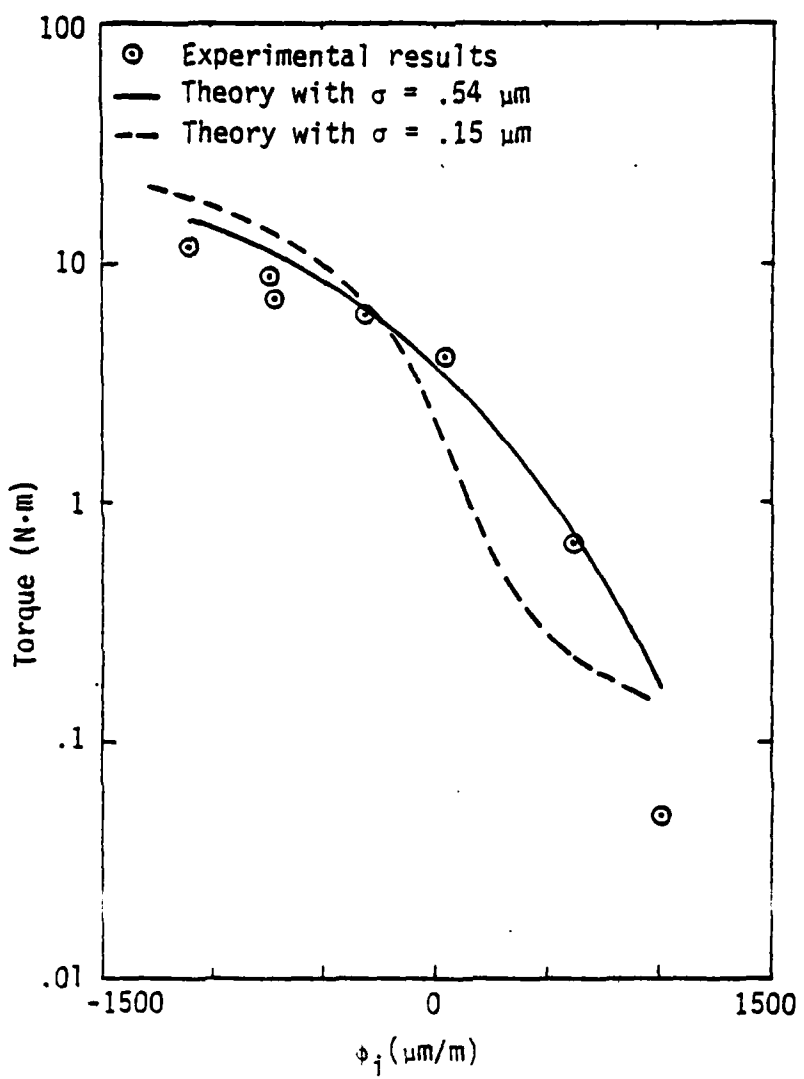


Figure 4-3. Initial Torque Versus Initial Taper - $B = 0.75$.

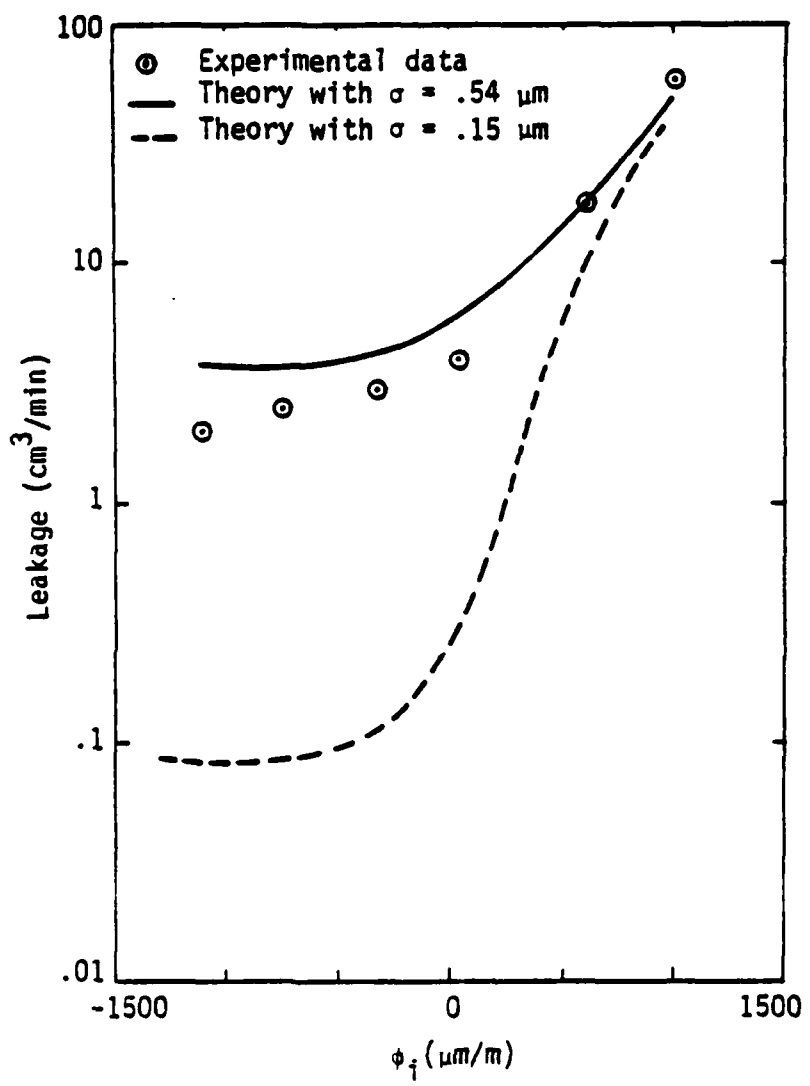


Figure 4-4. Leakage Versus Initial Taper at 1 hr - $B = 0.75$.

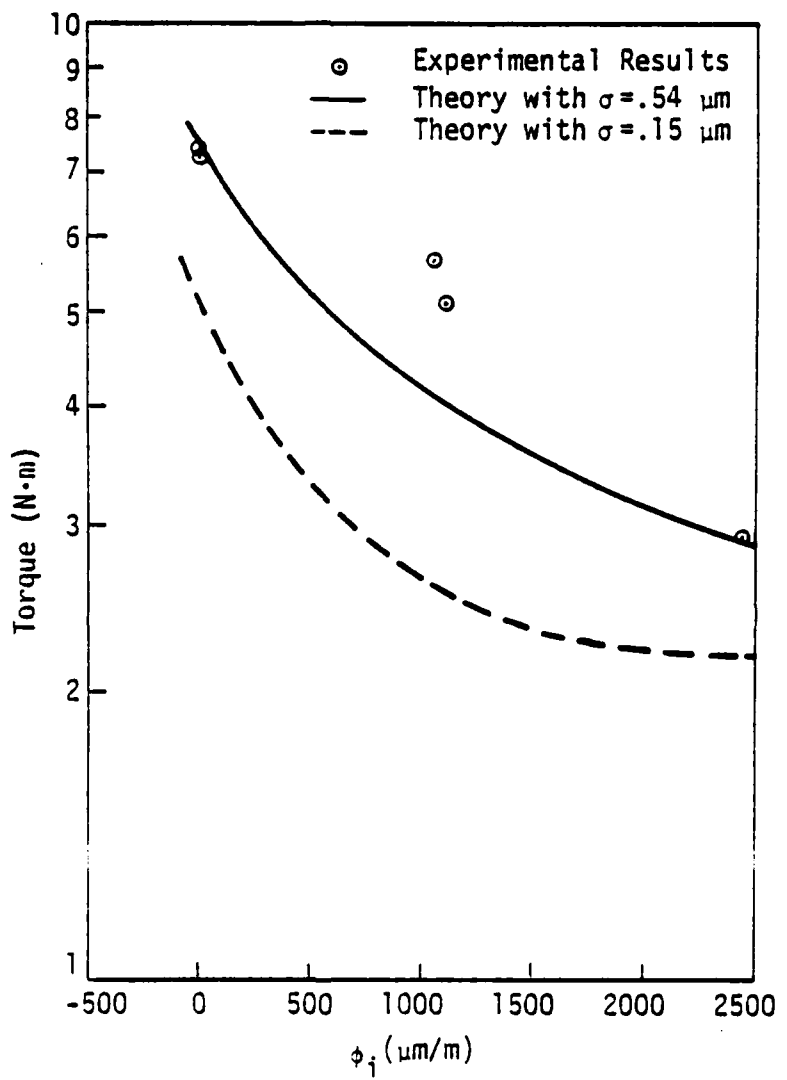


Figure 4-5. Initial Torque Versus Initial Taper - $B = 1.00$.

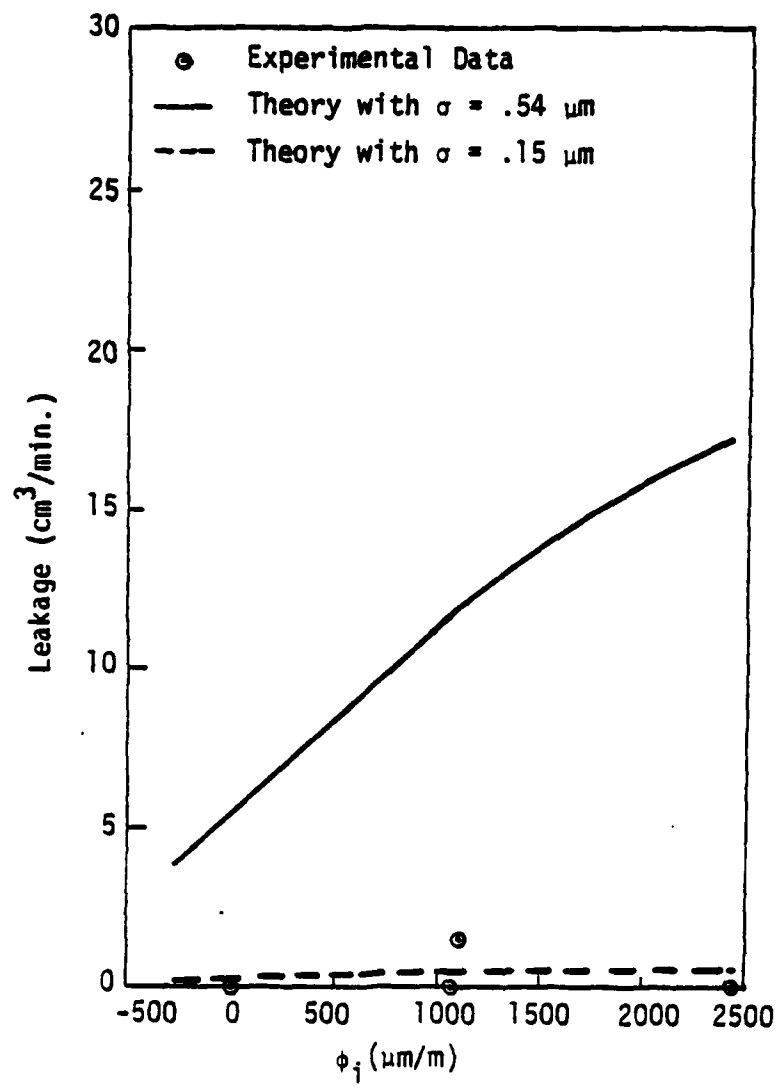


Figure 4-6. Leakage Versus Initial Taper at 1 hr - $B = 1.00$.

the theory does predict leakage trends, much more work will be needed to understand the nature of surface roughness as it affects leakage in order to accurately predict leakage quantitatively.

Figures 4-7 and 4-8 show torque and leakage versus time for a highly convergent $B = 0.75$ case. The experimental data are compared to theoretical data computed based on the time-dependent mode of the radial taper model [9]. The experimental results are scattered and there is no discernable trend. The theoretical values change very little over this time interval, and one can say that theory and experiment agree to some extent.

In Figures 4-9 and 4-10, the inadequacy of the time-dependent model becomes apparent for this slightly less converging case. In Figure 4-10 for $\sigma = 0.54 \mu\text{m}$, it is predicted that some of the converging taper will wear away causing the torque to increase and leakage to decrease with time. This is clearly not the case. Using $\sigma = 0.15 \mu\text{m}$ helps very little. Torque agrees in that there is virtually no change with time, but predicted leakage is now too low. It is likely that not only does the model suffer from an inadequate characterization of the surface roughness as discussed previously, it also suffers because the wear model used is not sufficiently accurate, even though the wear constant used is based on experimental data. In general, it has been found for the converging cases that very little wear occurs during a test, much less than predicted based on the model and parallel face test results.

Figures 4-11 and 4-12 are for a highly divergent case. Here in Figure 4-11 some agreement is found in that experimental torque does decrease with time, although not as much as predicted. Measured leakage again agrees much better with the $\sigma = 0.15 \mu\text{m}$ analysis. Figure 4-12 shows that in the long run torque varies widely with time which is characteristic of a parallel face test.

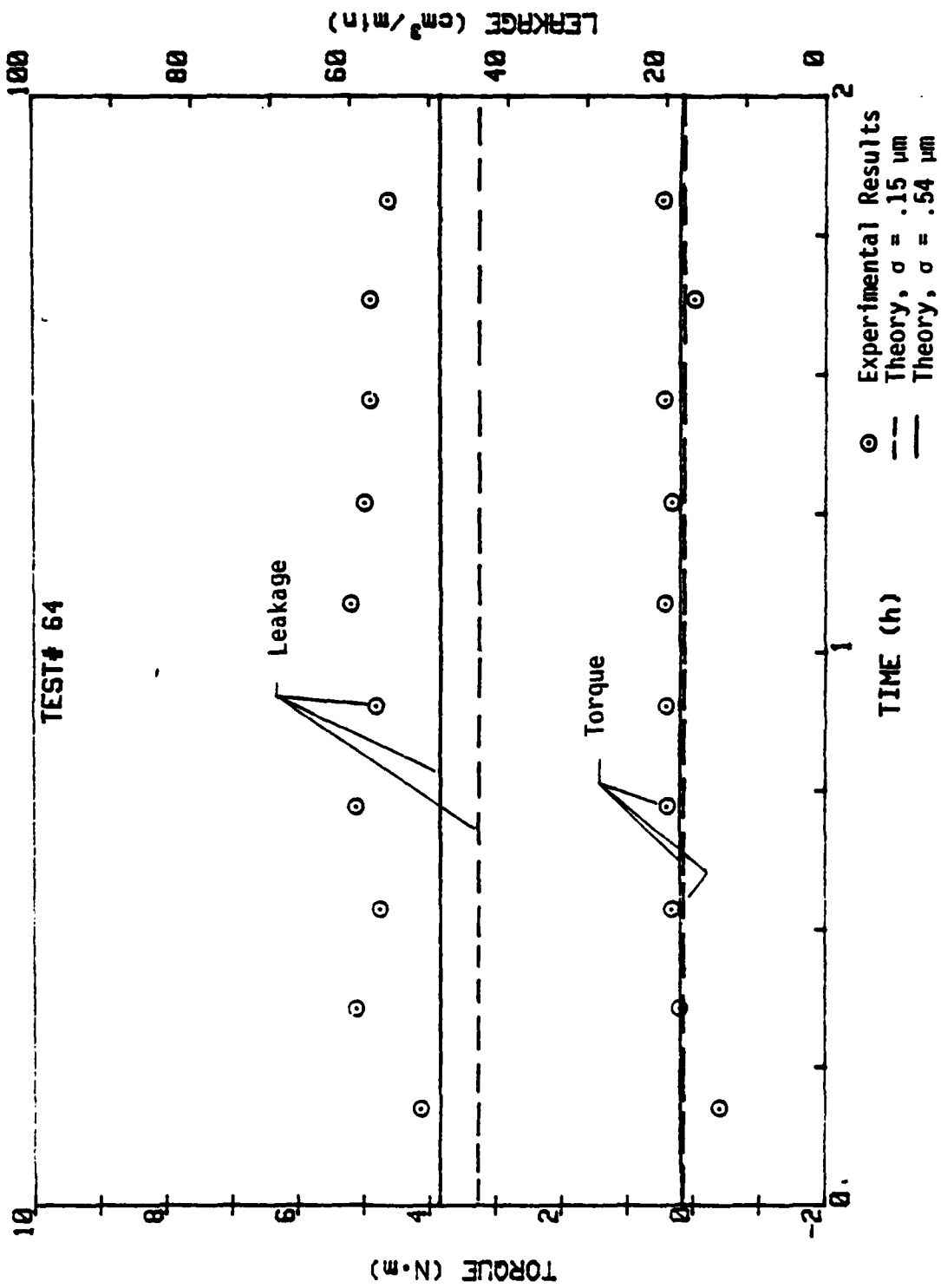


Figure 4-7. Torque and Leakage Versus Time, Test 64 - $B = 0.75$.

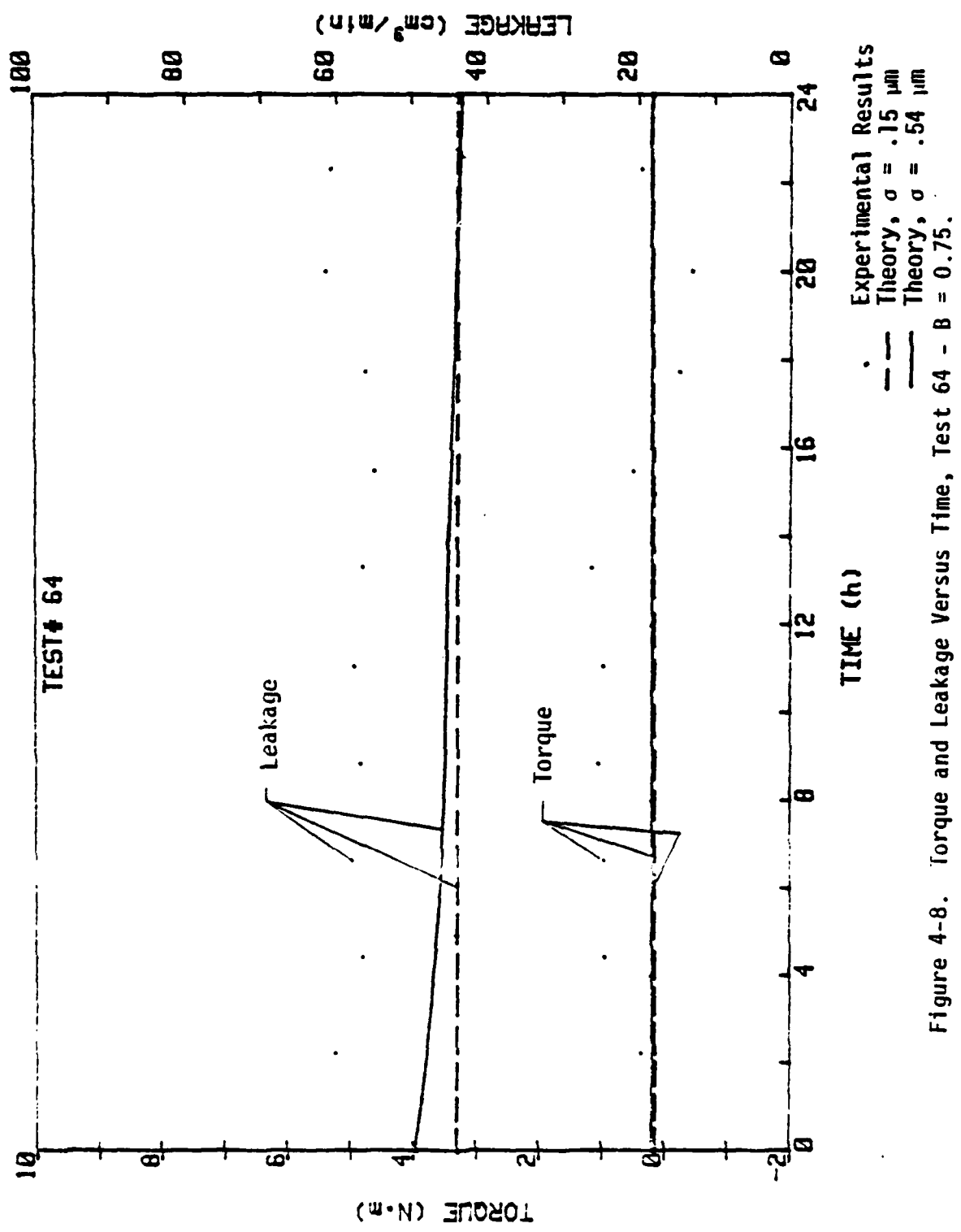


Figure 4-8. Torque and Leakage Versus Time. Test 64 - B = 0.75.

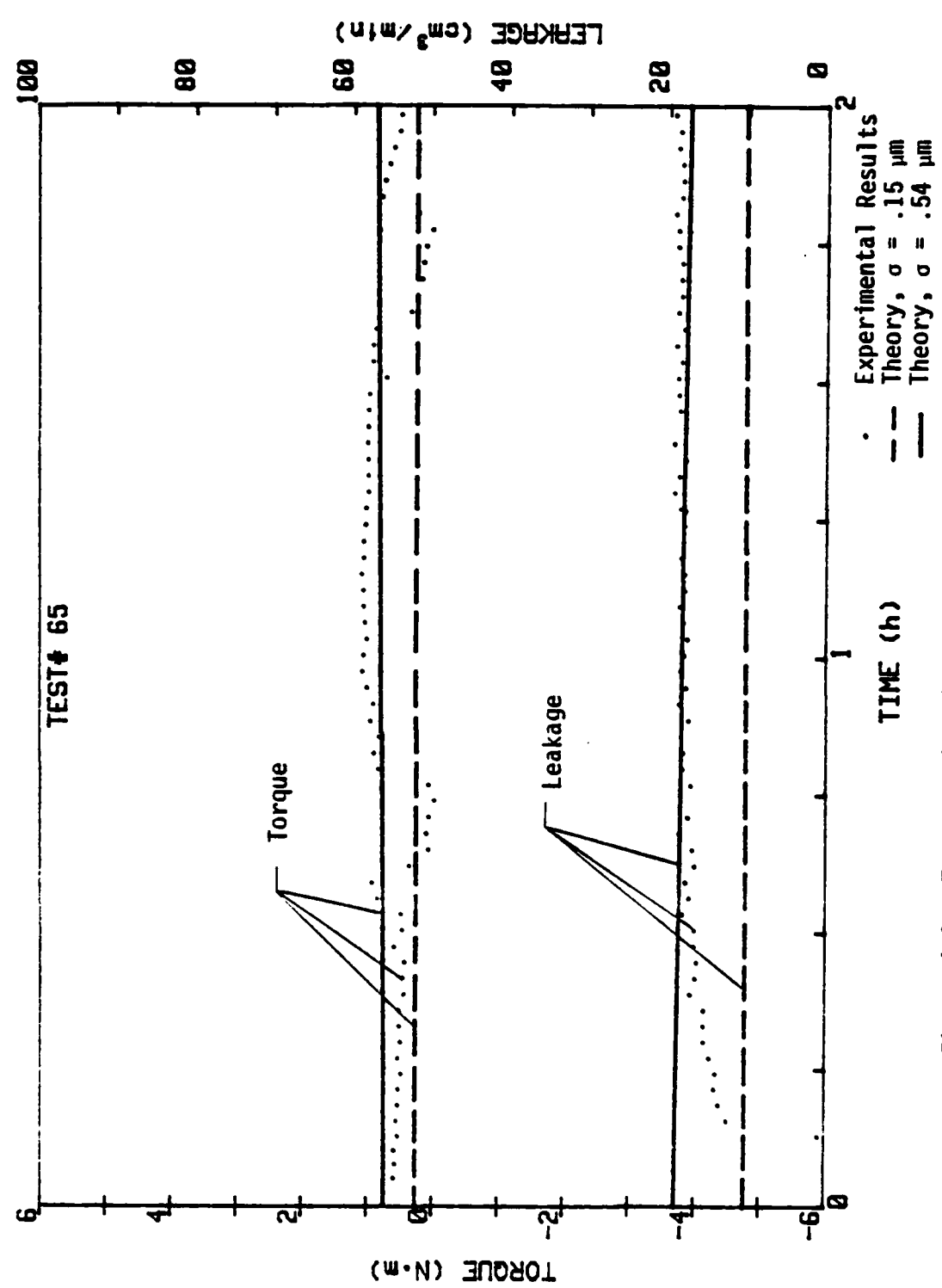


Figure 4-9. Torque and Leakage Versus Time, Test 65 - $B = 0.75$.

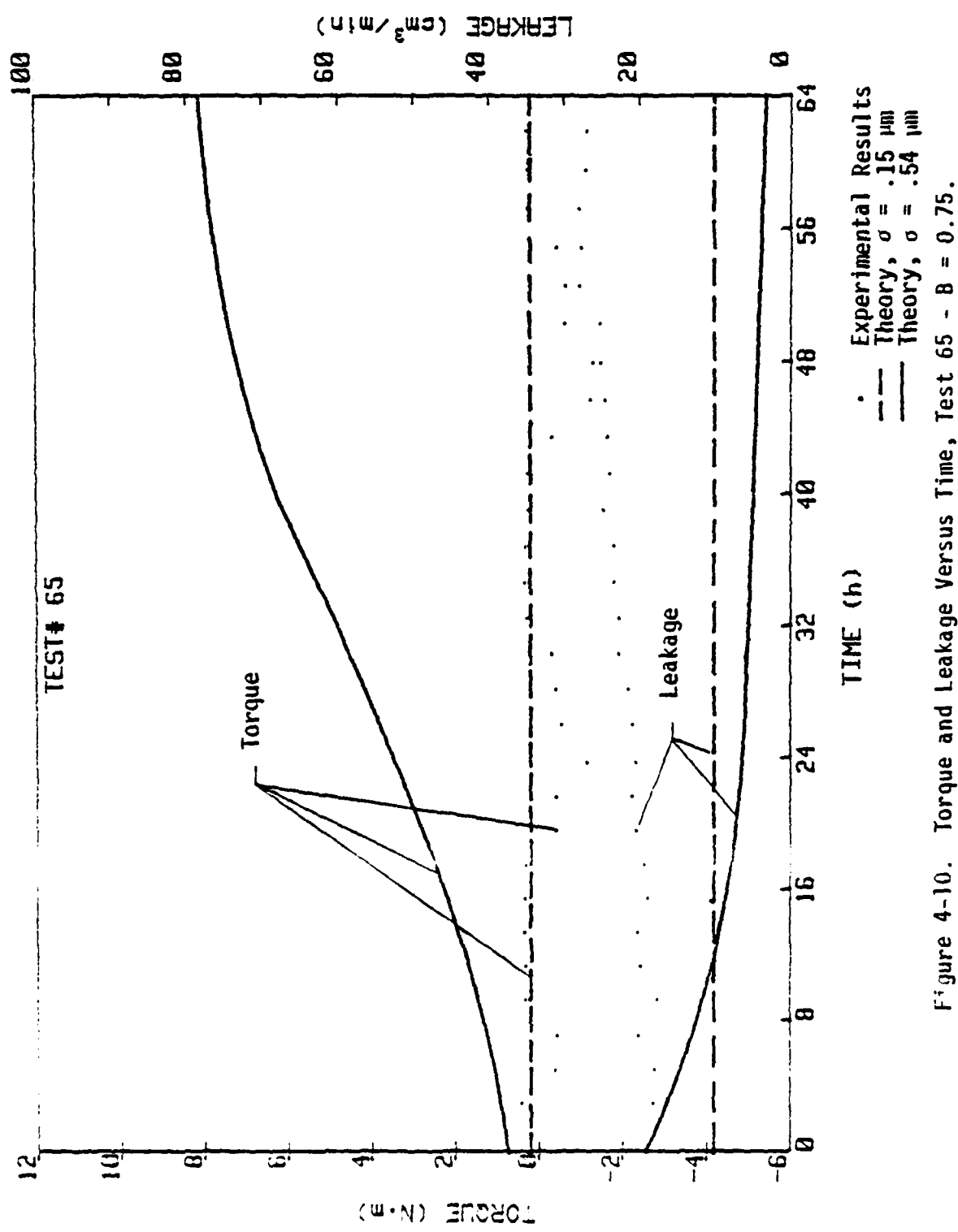


Figure 4-10. Torque and Leakage Versus Time, Test 65 - $B = 0.75$.

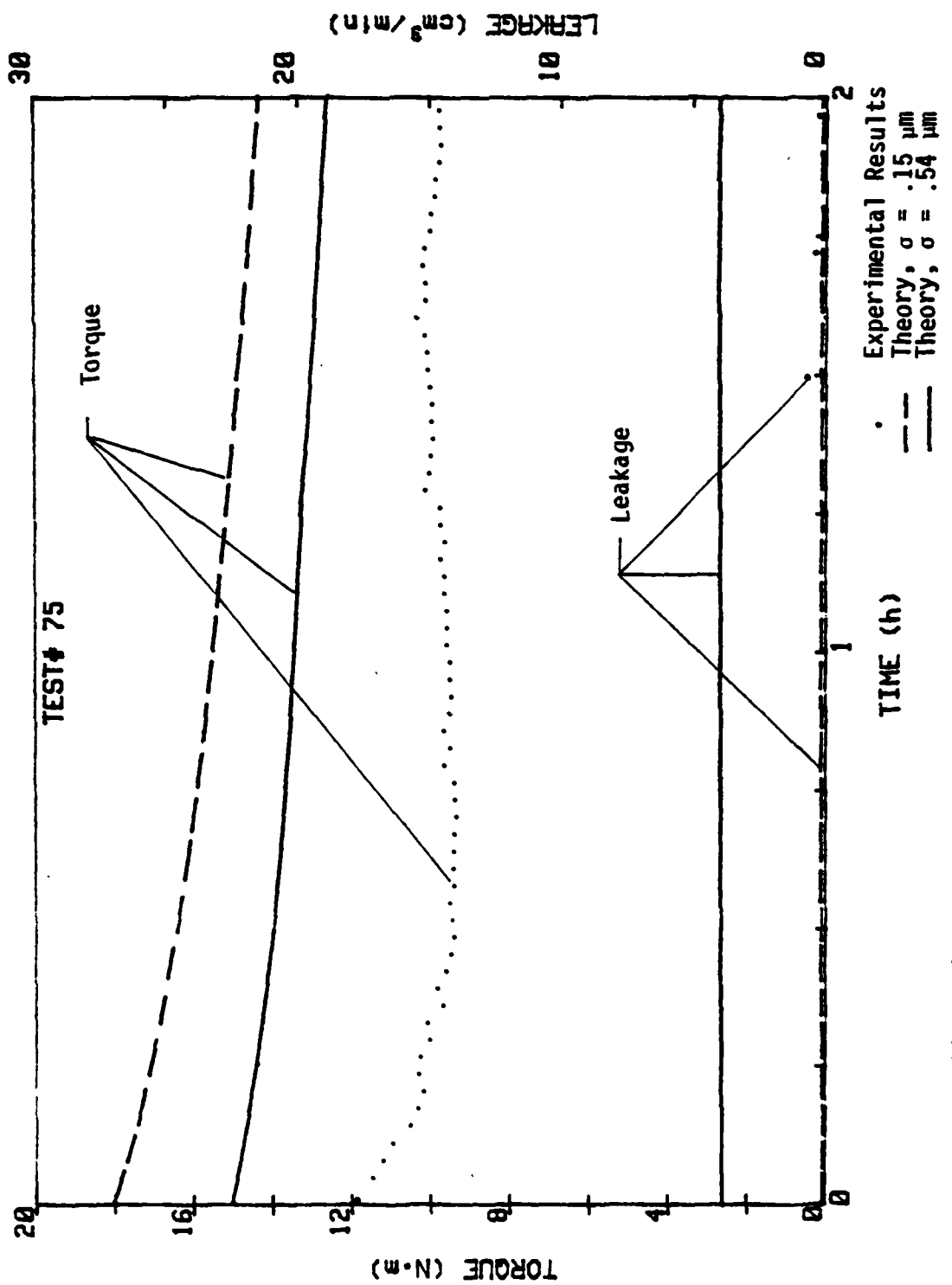


Figure 4-11. Torque and Leakage Versus Time, Test 75 - $B = 0.75$.

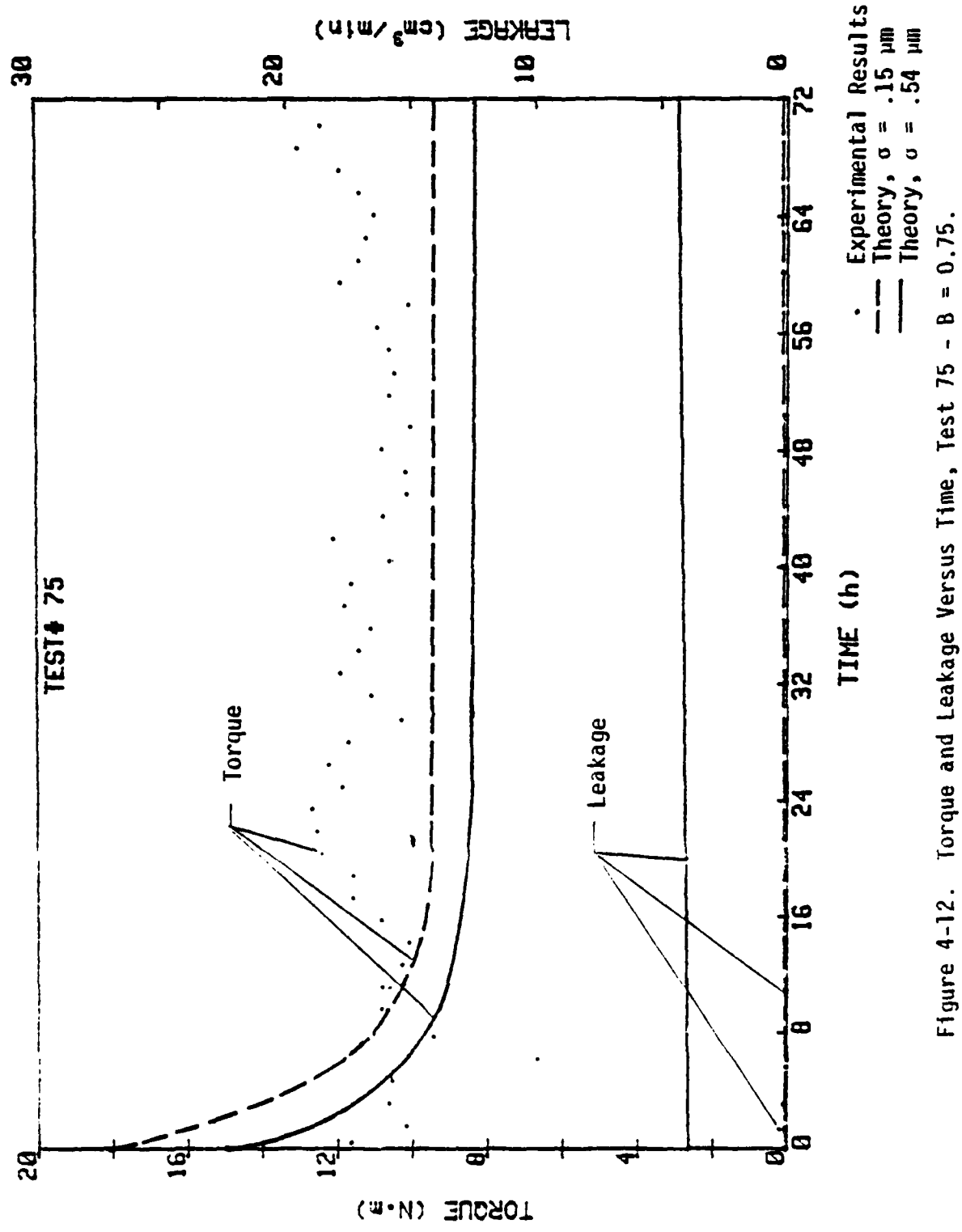


Figure 4-12. Torque and Leakage Versus Time, Test 75 - $B = 0.75$.

Figures 4-13 and 4-14 for two tests at $B = 1.00$ illustrate further the problems with the model. Wear is predicted to occur much faster than it actually does. The wear constant used is clearly not a constant but apparently is a strong function of the mechanical contact pressure and other factors.

When operation is such that parallel face operation results over a sufficient portion of the face that a worn in slope can be determined, then one may determine the radial taper or rotation caused by thermal effects. Figures 4-15 and 4-16 show experimentally determined radial taper compared to predicted thermal taper as a function of final measured torque. These results were not based strictly on the radial taper tests but included a number of originally parallel face cases particularly for the $B = 1.00$ cases. The lower experimental values for $B = 1.00$ correspond well to the theory. The $B = 0.75$ values indicate that the model underestimates the thermal taper. This is thought to be a result of the fact that the model uses film coefficients based on experiments which are for a geometry somewhat different than that of a seal. By plotting taper as a function of torque, errors caused by imprecise friction coefficient estimates are eliminated. In spite of the difference, the model does provide a good first approximation to predicting thermal rotation.

High Temperature Tests

As discussed previously, when a seal is operated at a temperature such that the seal face temperature is above the saturation temperature of the fluid at the discharge pressure, performance may change dramatically. In previous work [11], a model was developed to predict this behavior. The model has been applied to the test seal geometry.

The details of the geometry are shown in Figure 4-17. The parameter values for the computer solutions are as follows.

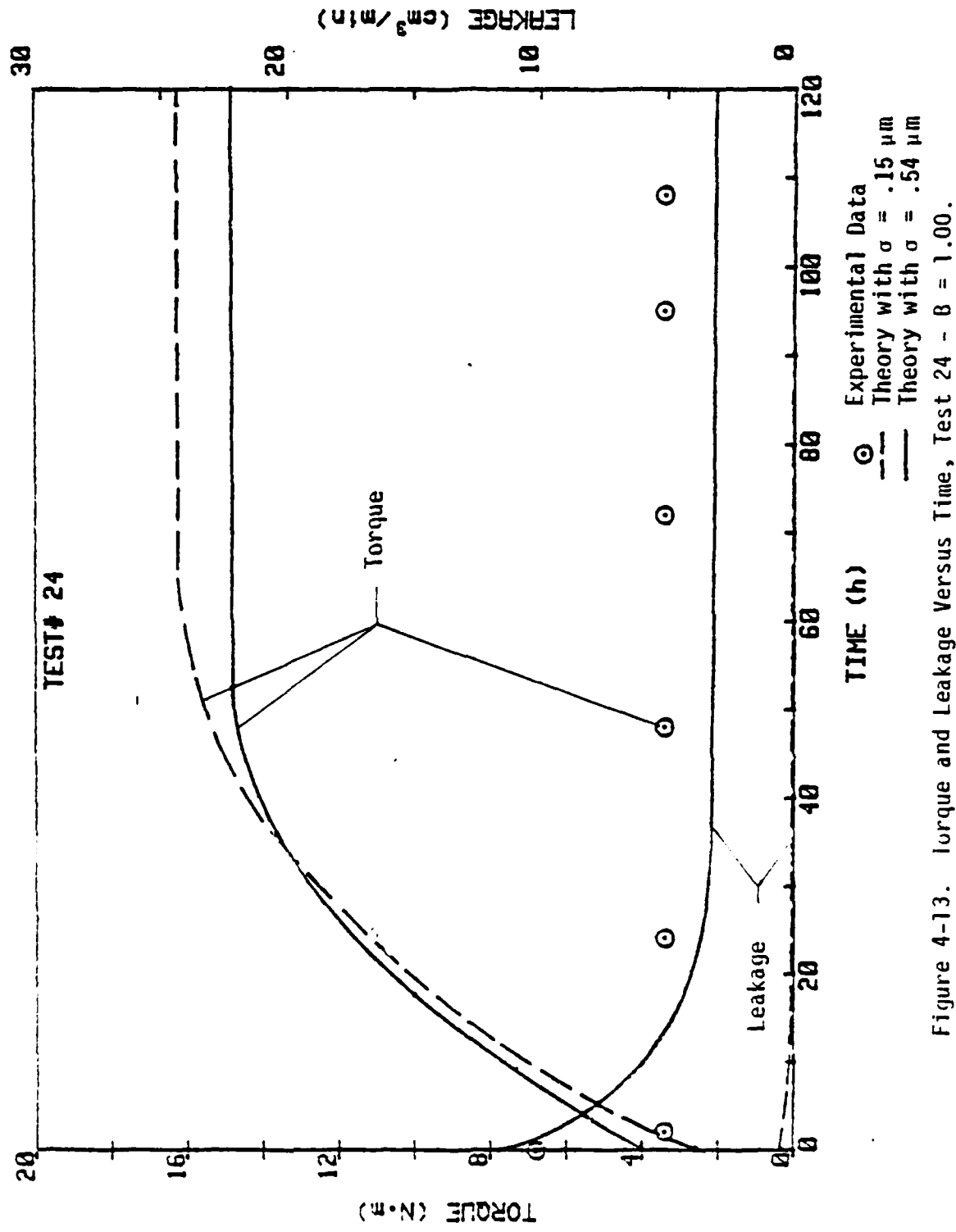


Figure 4-13. Torque and Leakage Versus Time, Test 24 - $\beta = 1.00$.

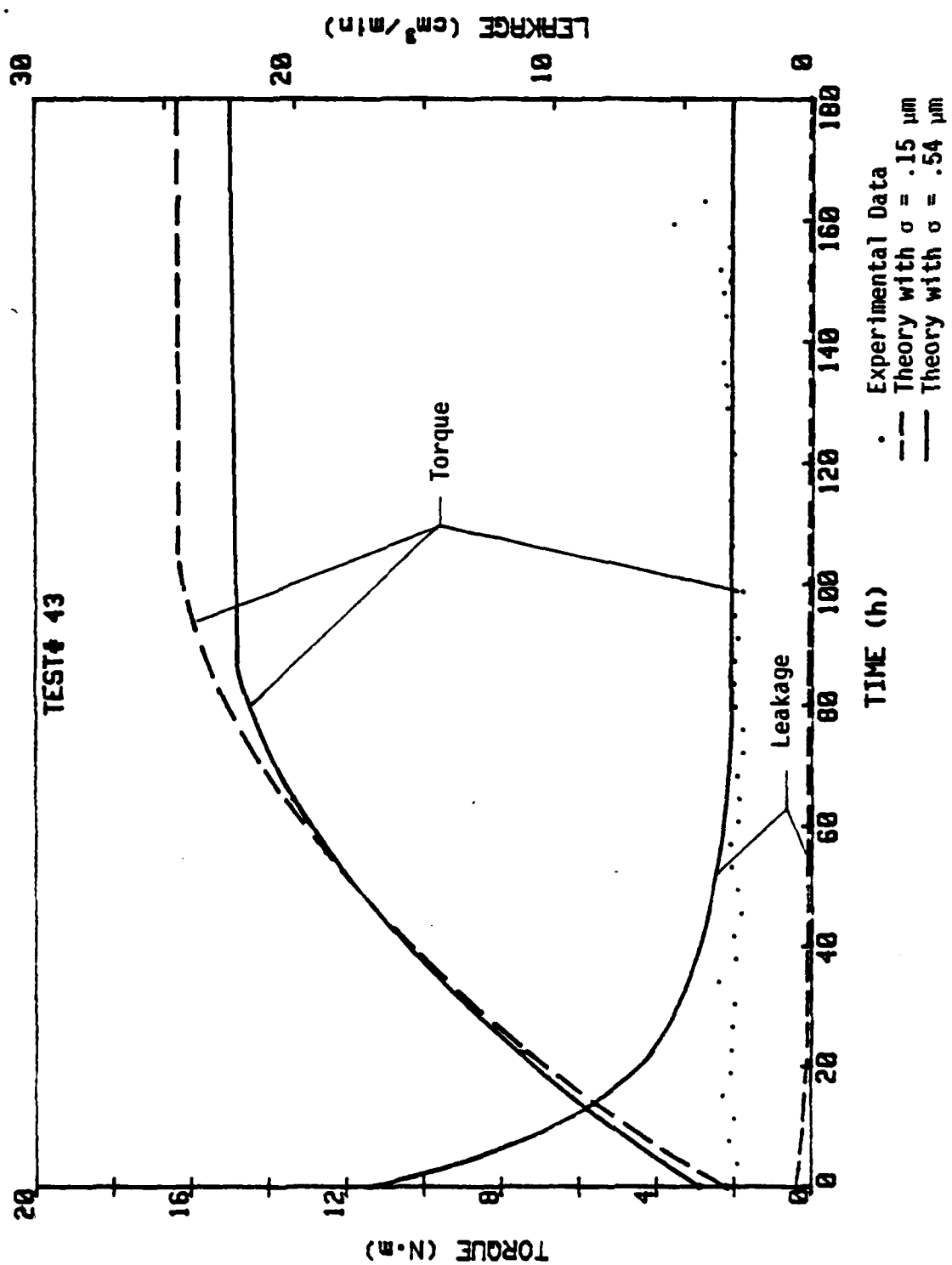


Figure 4-14. Torque and Leakage Versus Time, Test 43, $B = 1.00$.

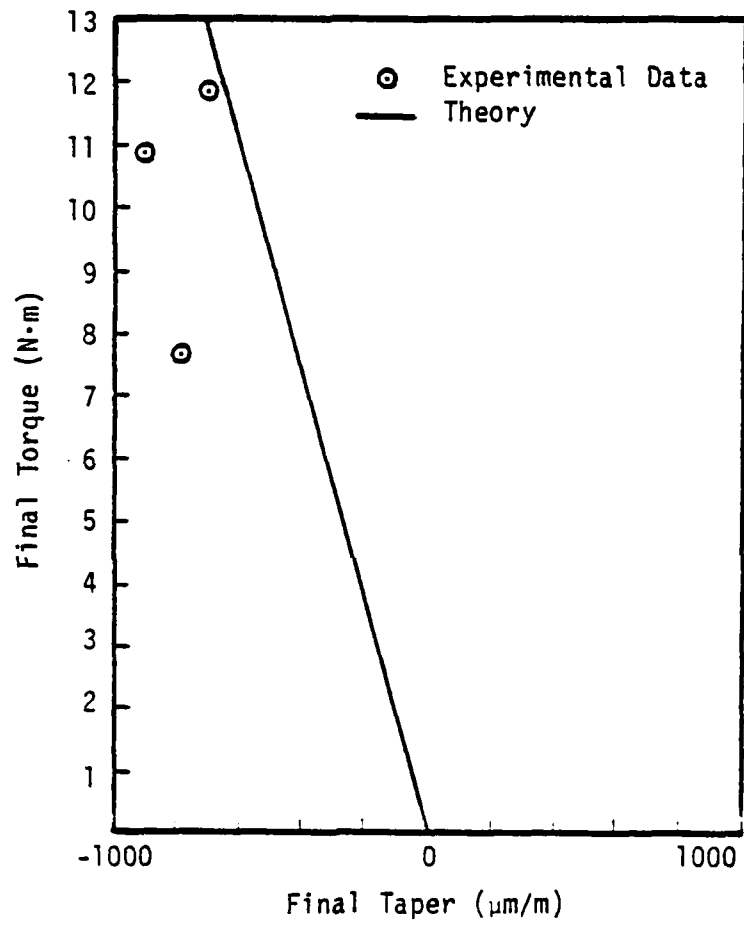


Figure 4-15. Final Torque Versus Final Taper, $B = 0.75$.

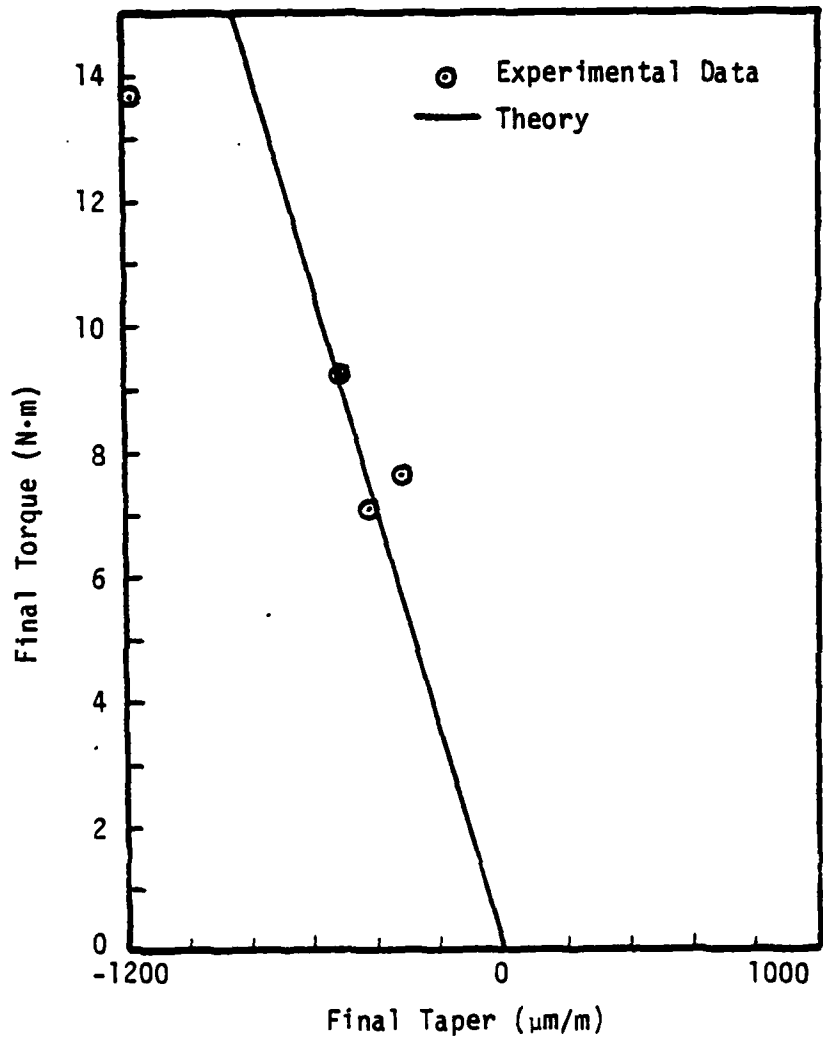


Figure 4-16. Final Torque Versus Final Taper, $B = 1.00$.

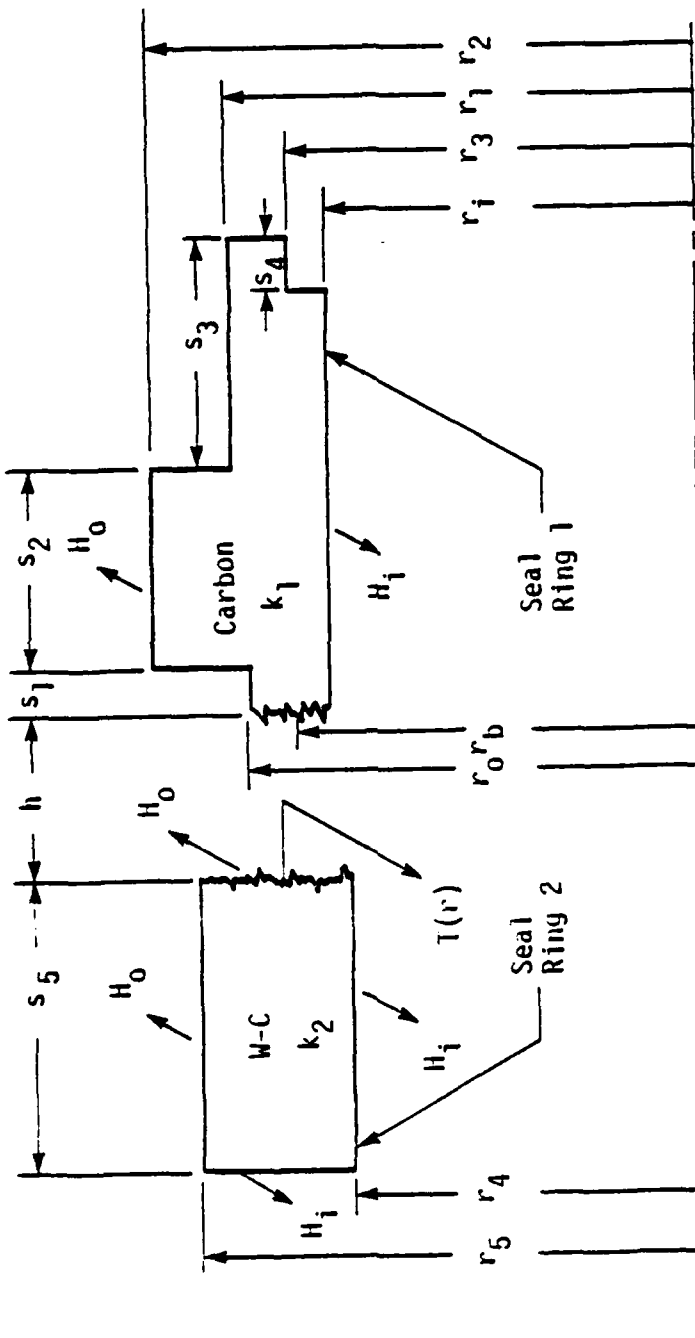


Figure 4-17. Seal Geometry for Two-Phase Model.

Seal Parameters:

$r_0 = 53.04 \text{ mm (2.088 in.)}$
 $r_i = 48.26 \text{ mm (1.900 in.)}$
 $r_1 = 54.28 \text{ mm (2.137 in.)}$
 $r_2 = 59.69 \text{ mm (2.350 in.)}$
 $r_3 = 48.26 \text{ mm (1.900 in.) for } B = 1.0;$
 $\quad \quad \quad 49.49 \text{ mm (1.949 in.) for } B = 0.75$
 $s_1 = 3.18 \text{ mm (0.125 in.)}$
 $s_2 = 13.34 \text{ mm (0.525 in.)}$
 $s_3 = 15.24 \text{ mm (0.600 in.)}$
 $s_4 = 0.0 \text{ mm for } B = 1.0;$
 $\quad \quad \quad 6.45 \text{ mm (0.254 in.) for } B = 0.75$
 $r_4 = 47.19 \text{ mm (1.858 in.)}$
 $r_5 = 57.14 \text{ mm (2.250 in.)}$
 $s_5 = 19.96 \text{ mm (0.786 in.)}$
 $p_{sp} = 2.07 \times 10^5 \text{ N/m}^2 (30.0 \text{ lb/in.}^2)$
 $p_m = 2.62 \times 10^8 \text{ N/m}^2 (38000 \text{ lb/in.}^2)$
 $p_s = 2.62 \times 10^7 \text{ N/m}^2 (3800 \text{ lb/in.}^2)$
 $\sigma = 0.5 \mu\text{m (19.69 }\mu\text{in.)}$

Heat Transfer Parameters:

$H_0 = (\text{given later})$
 $H_i = (\text{given later})$
 $k_1 = 11.25 \text{ W/m}^\circ\text{K (6.5 Btu/hr.ft.}^\circ\text{F)}$
 $k_2 = 70.00 \text{ W/m}^\circ\text{K (40.0 Btu/hr.ft.}^\circ\text{F)}$

Operating Conditions:

$p_0 = 1.72 \times 10^6 \text{ N/m}^2 (250 \text{ lb/in.}^2 \text{ absolute})$
 $p_i = 8.43 \times 10^4 \text{ N/m}^2 (\text{local atmospheric pressure}$
 $\quad \quad \quad (12.2 \text{ lb/in.}^2))$
 $\omega = 188 \text{ l/s (1800 rev./min)}$

Fluid Properties:

$R_{H_2O} = 460 \text{ N.m/kg}^\circ\text{K (0.110 Btu/lb}_m^\circ\text{F)}$

$\mu_g, \mu_f, \rho_g, \rho_{sat}, H_f, H_{fg} \text{ -- from steam table data.}$

The value selected for p_s gives the mechanical friction coefficient $F = 0.1$ when all of the load is supported by mechanical contact. Seal ring 1 properties of k_1 and p_m are typical of a carbon material. The thermal conductivity of seal ring 2, k_2 , is typical of tungsten-carbide. The RMS combined roughness σ is the approximate roughness value that evolves during test operation.

Two different convection coefficients H_0 and H_i have been included in the heat transfer model. H_0 is approximated by using the convection coefficient of a horizontal cylinder rotating in a tank of water [15]. By using the formula

$$N_{Nu} = 0.133 \times Re^{2/3} \times Pr^{1/3} \quad (4-1)$$

the convection coefficient, H_0 , for different operating conditions can be determined. The H_0 values used for $p_0 = 1.72 \times 10^6 \text{ N/m}^2$ and different operating temperatures are shown in Table 4-3. Due to the complexity of the seal assembly, it is not easy to determine the H_i value accurately. An approximate value of $H_i = 7000 \text{ w/m}^2\text{K}$ is used in computation. As discussed later, this value is justified by investigating the equivalent convection coefficients on different seal parts and then making an overall approximation for H_i .

Using these data and the model, theoretical performance for test seal torque has been calculated and is compared to experimental results in Figures 4-18 and 4-19 for $B = 1.00$ and $B = 0.75$. Two values of mechanical friction coefficient were used for the calculation as shown. At $F = 0.15$, agreement with theory is reasonable up to the transition point. The approximate temperature of the transition point is predicted. Beyond the transition point, experimental friction torque is much higher than predicted. It is thought that this is probably caused by extremely high coefficients of mechanical friction associated with

Table 4-3. Outside Convection Coefficients, H_0
 $p_0 = 1.72 \text{ MPa}$

T_∞ (°C)	T_∞ (°F)	H_0 (Btu/hr.ft ² ·°F)	H_0 (W/m ² ·K)
37.8	100	3120	17700
65.6	150	3980	22600
93.3	200	4400	25000
121.1	250	4670	26500
148.9	300	5070	28800
176.7	350	5350	30400
182.2	360	5370	30500
187.8	370	5400	30700
193.3	380	5420	30800
198.9	390	5440	30900

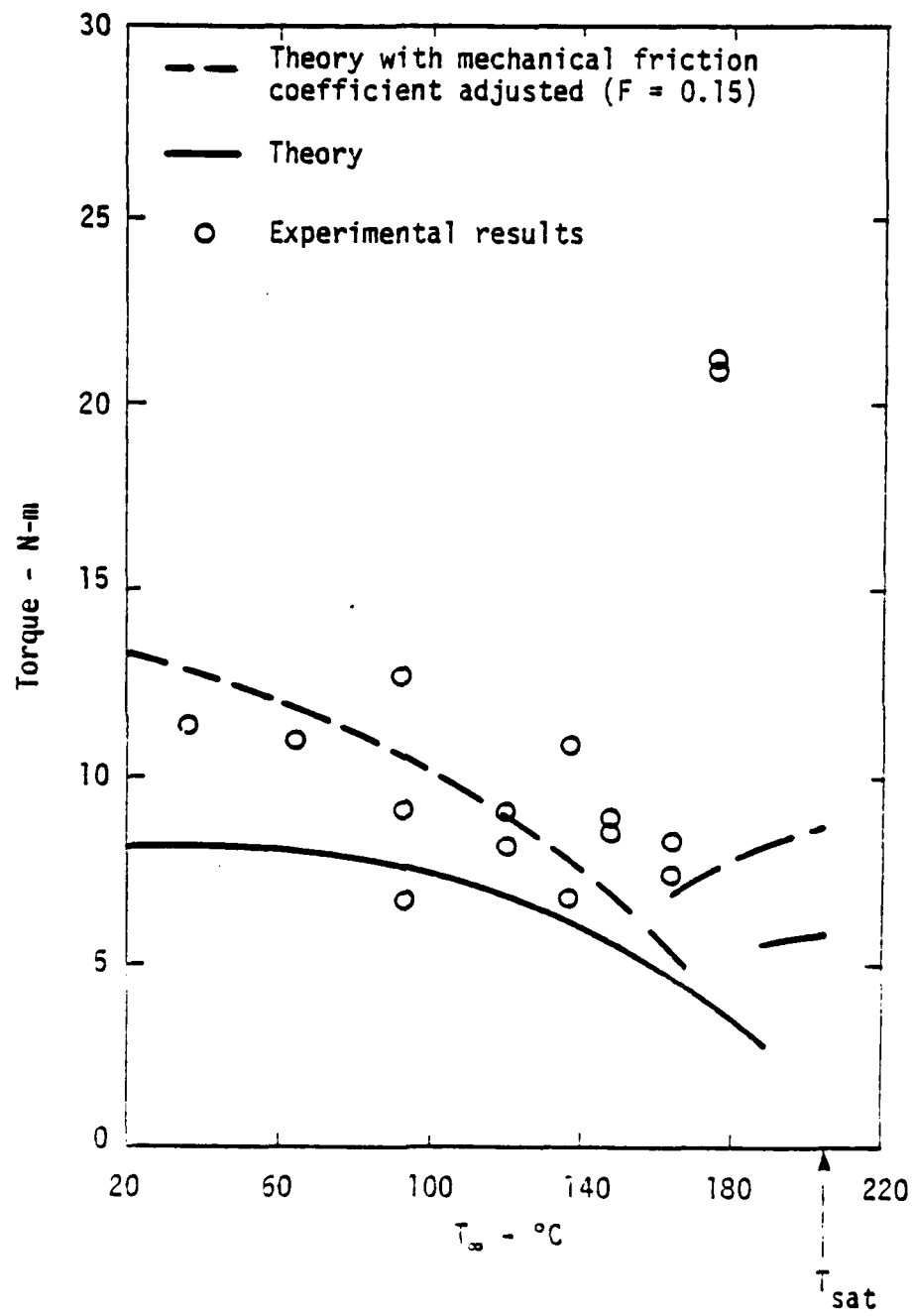


Figure 4-18. Torque as a Function of Temperature - $B = 1.0$.

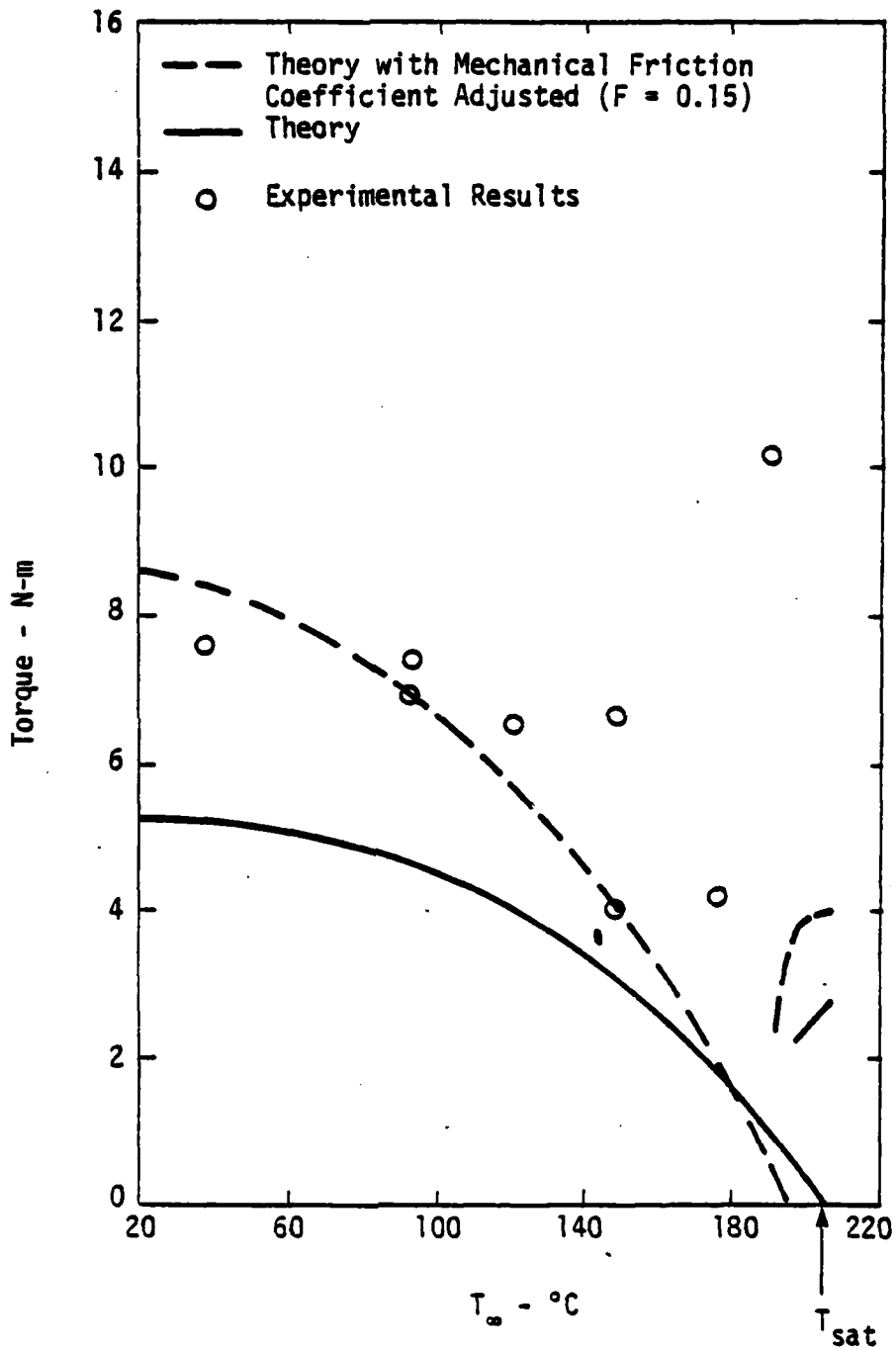


Figure 4-19. Torque as a Function of Temperature,
 $B = 0.75$.

operation of the faces in essentially superheated vapor. Experiments are needed to verify this hypothesis; such data is not available in the literature.

It can be shown theoretically that the temperature difference, $T_f - T_\infty = \Delta T$, is proportional to the friction torque for different operating temperatures. As shown in Figure 4-20, experimental results also show this trend, although theory overestimates the ΔT . Thus, the ΔT data can be used as an indication of friction. In Figures 4-21 and 4-22, such experimental results are compared to theory. The experimental values of ΔT are averaged over the last few hours of the test. The theoretical temperature estimate is based on the calculated temperatures at the point in the seal body where temperature is measured.

Considering Figure 4-18 and Figure 4-21 (or Figure 4-19 and Figure 4-22), the prediction of the effect of operating temperature on friction is consistent between that based on ΔT and that based on torque. Given that ΔT is a reliable measurement, this also suggests that the measurement of torque is satisfactory.

Experimental results in Chapter 2 show that after a running in period no leakage has ever been measured for the high temperature tests. Based upon the theoretical analysis, the leakage rate is determined primarily by the surface roughness (a cubic relationship). The standard deviation of surface roughness of the carbon after test was found to vary from 0.4 to 1.0 μm . Leakage results shown in Figure 4-23 are based on $\sigma = 0.5 \mu\text{m}$, which compares favorably to measured values. Since no leakage has been measured, it is thought that the effective roughness is lower than the measured value as discussed with regard to the radial taper model. The pocket theory previously discussed suggests that flow is controlled primarily by the roughness magnitude associated with the flat peaks. This value amounts to approximately 0.1 μm of standard deviation, much less than the

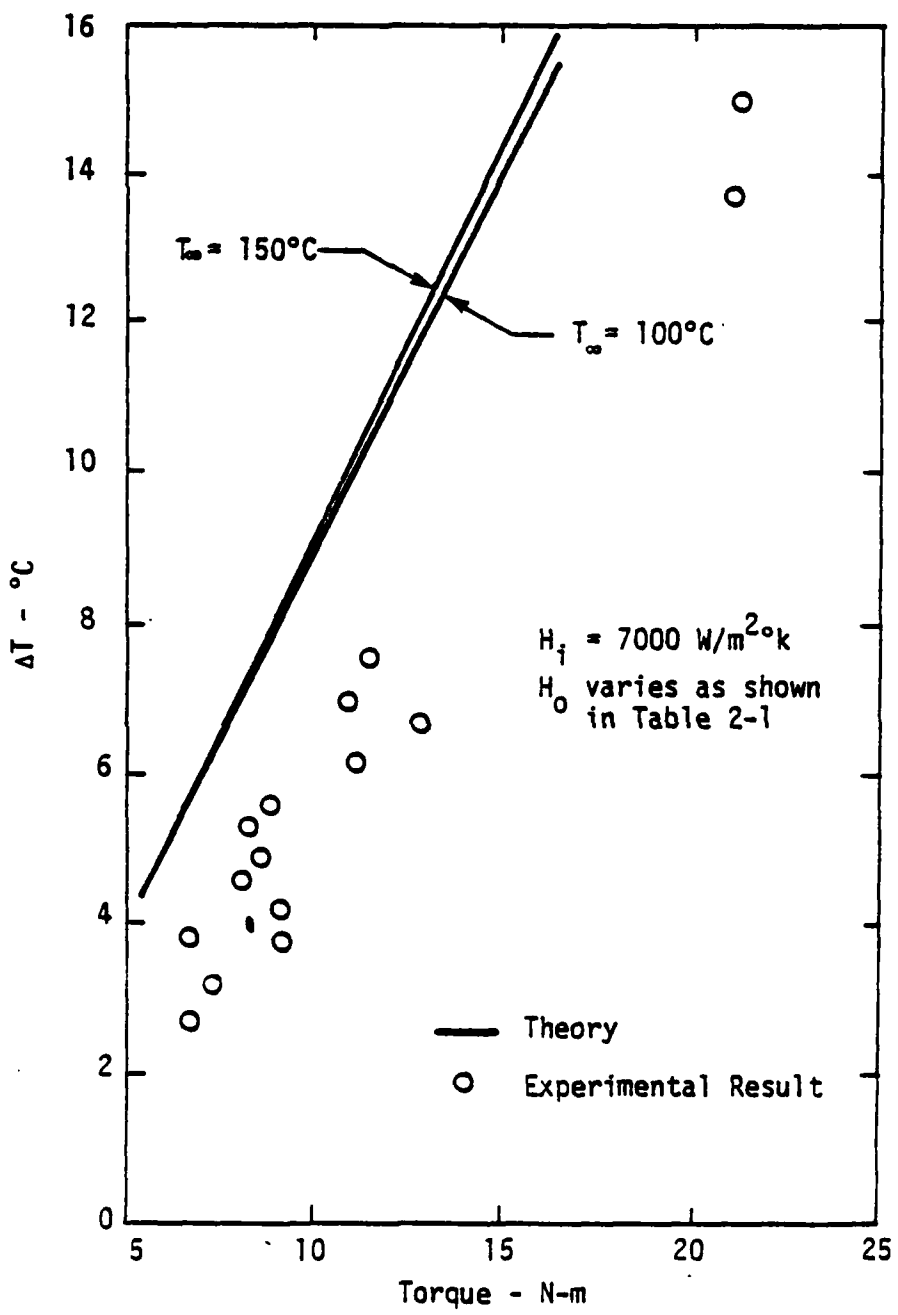


Figure 4-20. ΔT Versus Torque, $B = 1.0$, F Varies

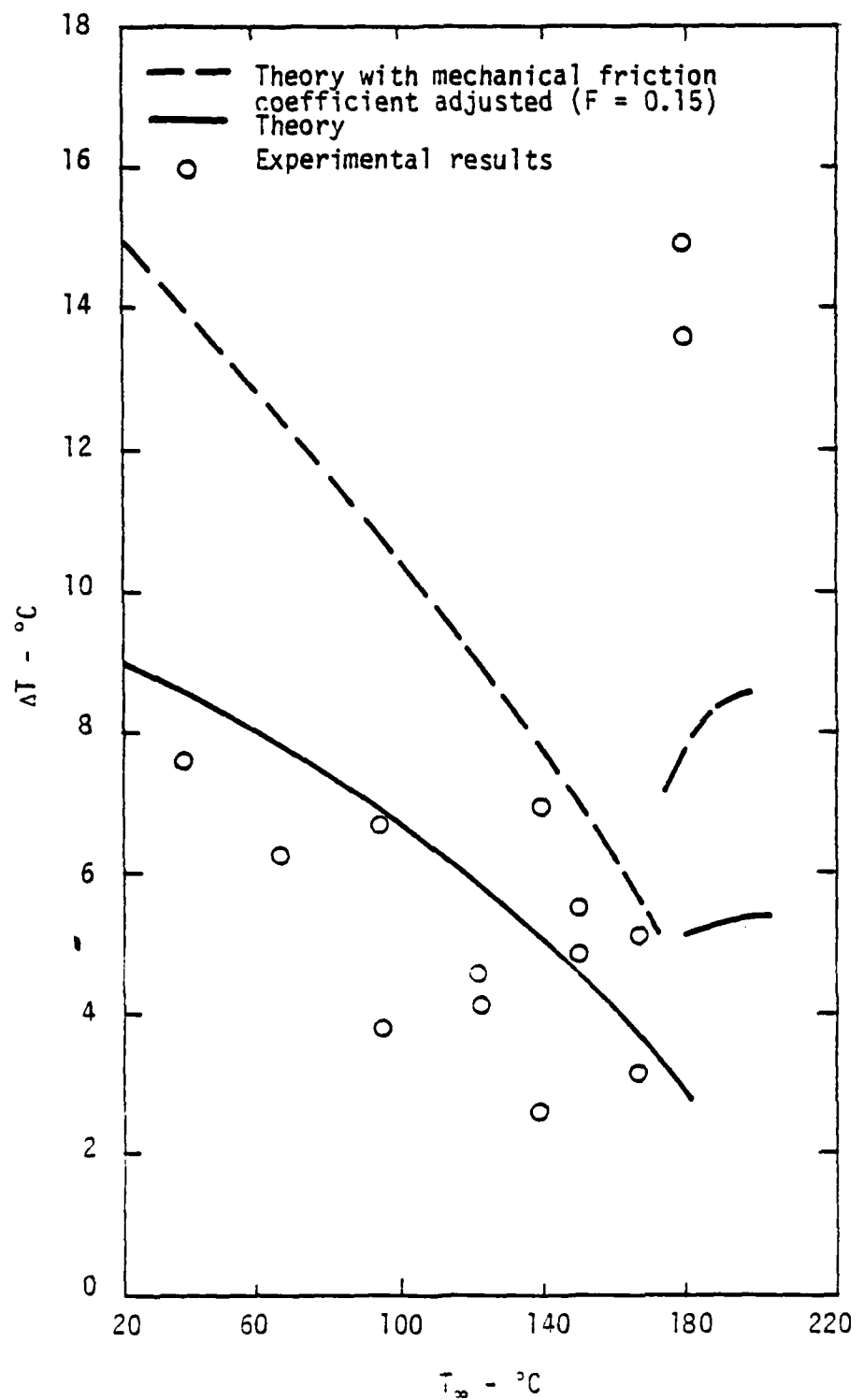


Figure 4-21. ΔT as a Function of Temperature - $B = 1.0$.

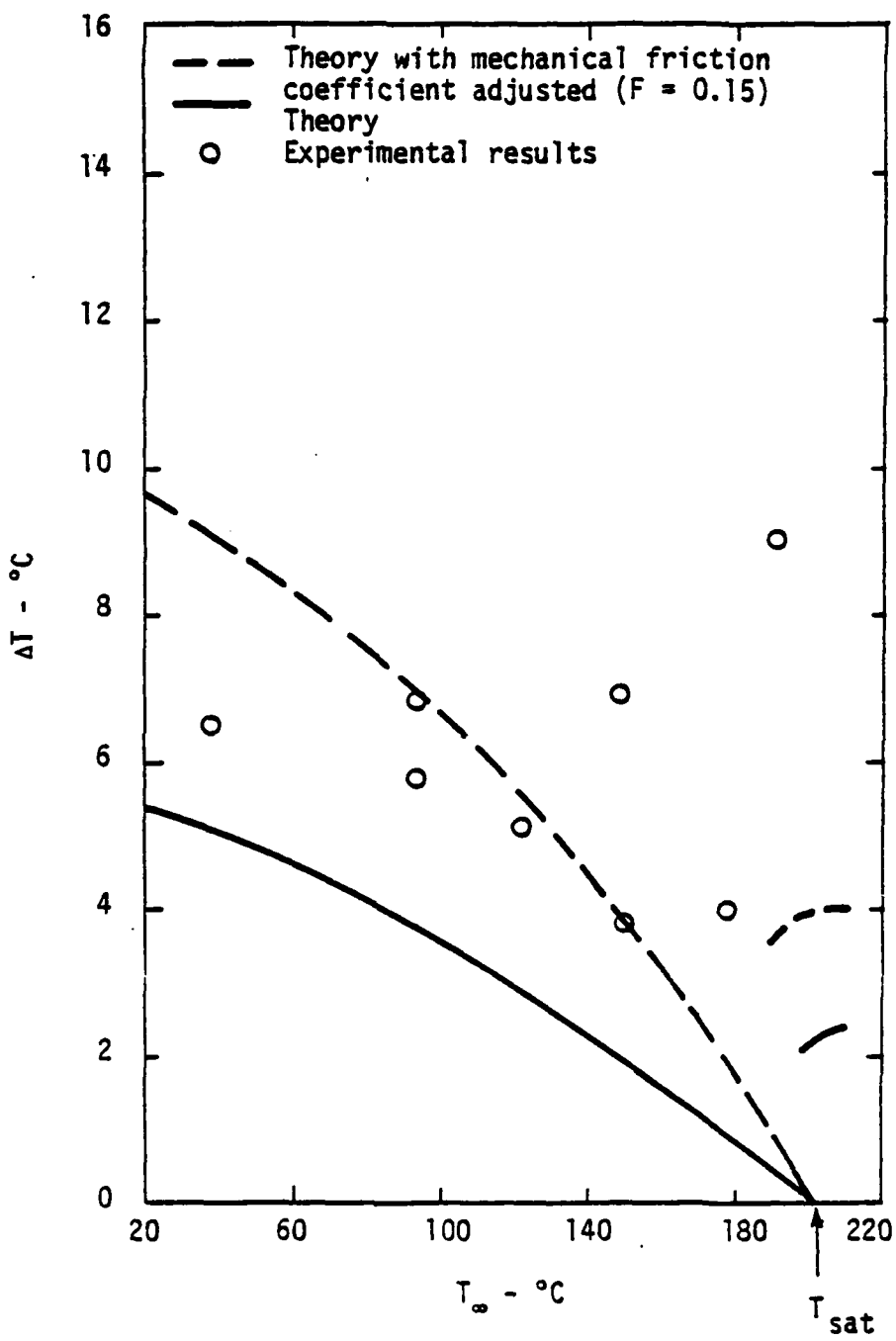


Figure 4-22. ΔT as a Function of Temperature, $B = 0.75$.

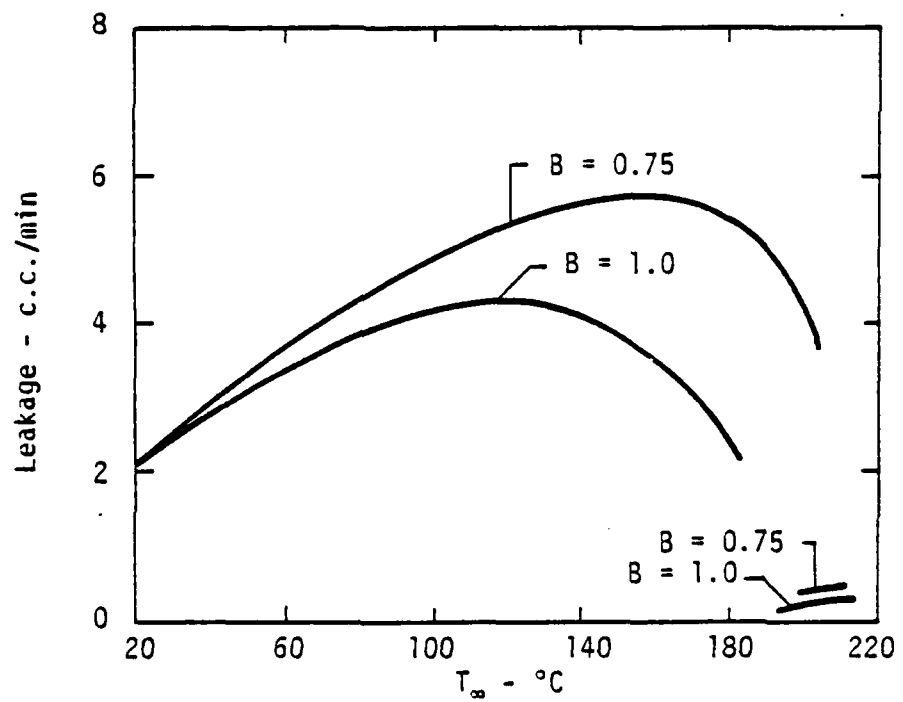


Figure 4-23. Theoretical Leakage at $\sigma = 0.5 \mu\text{m}$.

standard deviation measured by taking the entire surface into account. By using the value $\sigma = 0.1 \mu\text{m}$, the computed results of leakage are less than $0.05 \text{ cm}^3/\text{min}$. At this low rate it is expected that water will evaporate from the leakage counter before it can be registered. Thus, the experimental results are consistent with the theory as modified.

Considering Figures 4-18 and 4-19, it has been shown that the higher mechanical friction coefficient ($F = 0.15$) may be used such that the theoretical curve of torque intersects the experimental data. In Figure 4-21, it can be seen that the theoretical ΔT value based on this mechanical friction coefficient is somewhat higher than the experimental results. This indicates that the validity of the heat transfer model must be examined more closely.

Figure 4-24 shows the geometry of the actual seal assembly and that of the heat transfer model. It can be seen that the geometry of the actual seal is somewhat different from that of the heat transfer model particularly in region D. However, modification of the geometry of the heat transfer model to fit the actual seal geometry has been shown to be unnecessary since the theoretical temperature distribution in the portion D is very close to T_∞ .

In the following paragraphs, the selection of heat transfer parameter values for the $B = 1.0$ seal and the sensitivity of T_f to the change of each parameter value are examined.

1. During operation, the W-C ring is rotating while the carbon ring remains stationary. The calculated value of H_0 using equation (4-1) is a convection coefficient of a rotating cylinder in water. Thus, there might be an error in the convection coefficient for the stationary carbon ring. However, considering the flow around the seal rings and the complexity of the seal assembly, the assumption used might be the best approximation which can be made.

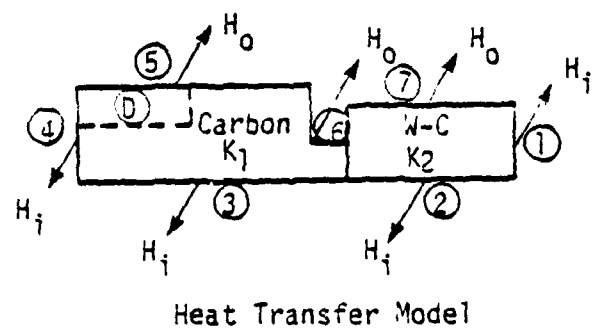
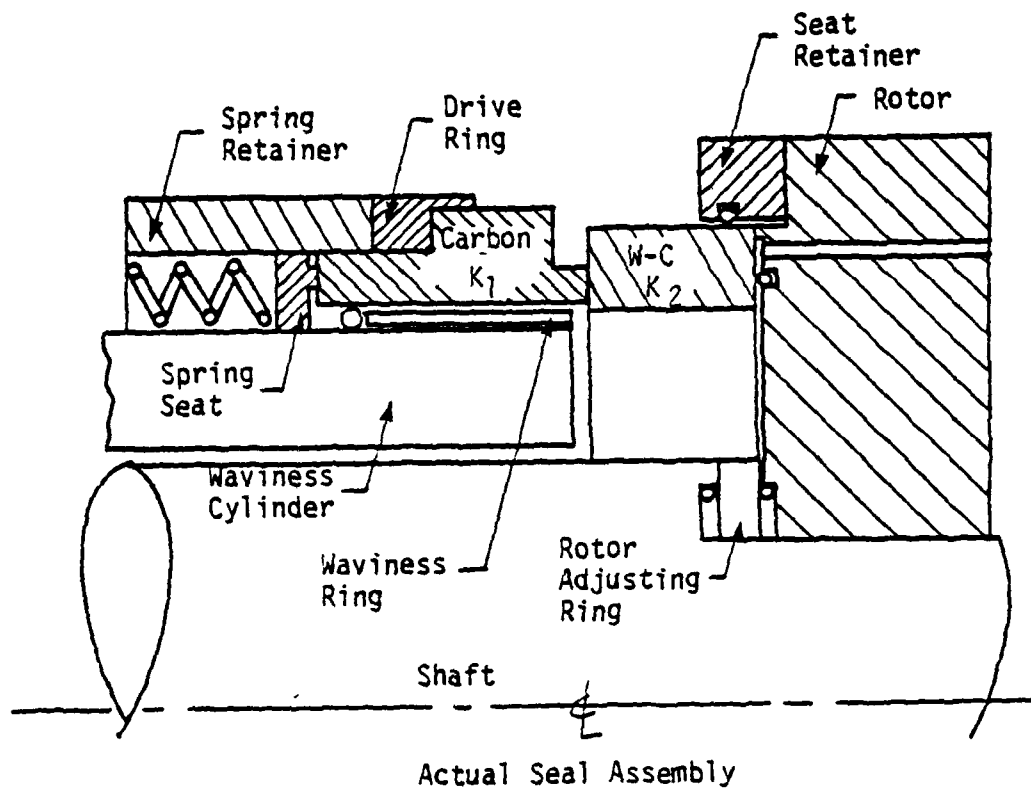
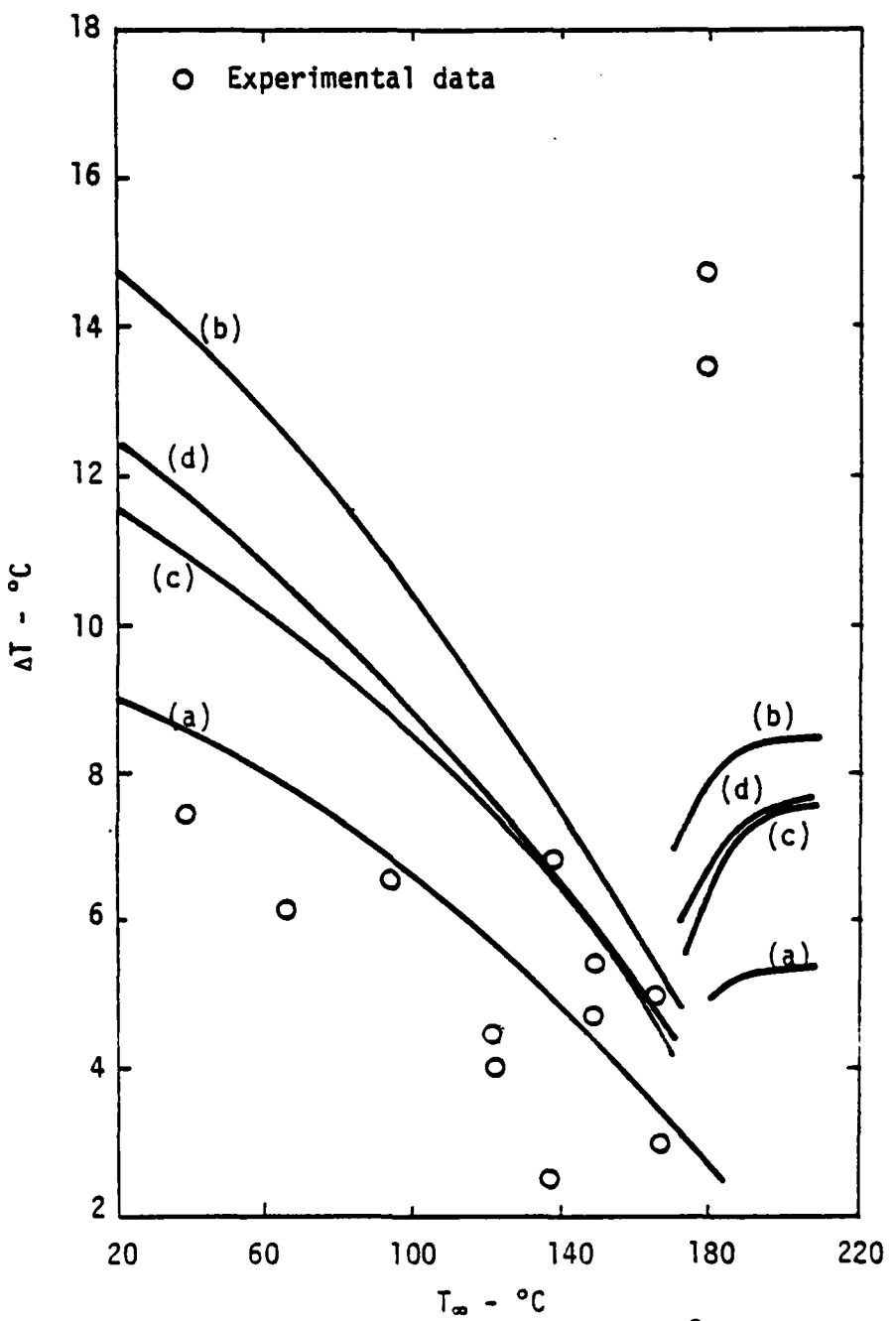


Figure 4-24. Geometry of Actual Seal Assembly and Heat Transfer Model.

2. The thermal conductivities, k_1 and k_2 , are typical values for carbon and W-C. However, they are not actually measured values. It is known that the value of k_2 is in the range of 43 to 86 $\text{W/m}^\circ\text{K}$. Based upon theoretical analysis using $k_2 = 86 \text{ W/m}^\circ\text{K}$, the ΔT curve is generated as shown in Figure 4-25 as curve c. Curve b is based on the value $k = 70 \text{ W/m}^\circ\text{K}$ assumed for the previously given results. The result shows that the ΔT prediction is quite sensitive to the value of k_2 .
3. Due to the complexity of seal assembly, it is not easy to accurately determine the inside convection H_i . Considering Figure 4-24, it is believed that positions 1, 3, and 4 are filled with water with temperature T_∞ during operation when operation is below the saturation temperature. By investigating the thermal conductivity of water and the gap thickness between the seal and the surrounding components and assuming these components are at temperature T_∞ , equivalent H_i (thermal conductivity of water divided by the gap thickness) can be determined. The H_i value at position 2, assuming air is around this area, is determined by using equation (4-1). After H_i values on different seal parts have been obtained, an overall approximated value of $H_i = 7000 \text{ W/m}^2\text{K}$ was selected for computation. In order to observe the effect of the H_i value on the ΔT prediction, a ΔT curve based on $H_i = 9000 \text{ W/m}^2\text{K}$ is shown in Figure 4-25 as curve d. Results show that theoretical prediction of ΔT is quite sensitive to the H_i value.

Thus, for more accurate temperature prediction, further investigation of these heat transfer parameters is required. However, considering the numerous approximations and uncertainties in



- (a): $K_{W-C} = 70 \text{ W/m}^{\circ}\text{K}$, $H_i = 7000 \text{ W/m}^2\text{K}$, $F = 0.1$
 (b): $K_{W-C} = 70 \text{ W/m}^{\circ}\text{K}$, $H_i = 7000 \text{ W/m}^2\text{K}$, $F = 0.15$
 (c): $K_{W-C} = 86 \text{ W/m}^{\circ}\text{K}$, $H_i = 7000 \text{ W/m}^2\text{K}$, $F = 0.15$
 (d): $K_{W-C} = 70 \text{ W/m}^{\circ}\text{K}$, $H_i = 9000 \text{ W/m}^2\text{K}$, $F = 0.15$

Figure 4-25. Heat Transfer Parameters - $B = 1.0$.

both theory and experiment, the heat transfer model used is considered adequate for the purpose of this investigation.

From the comparison of torque and leakage, it is known that using $\sigma = 0.1 \mu\text{m}$ and $F = 0.15$ provides a reasonable prediction of performance. Thus, a set of load versus film thickness curves using $\sigma = 0.1 \mu\text{m}$ and $F = 0.15$ should provide some prediction about puffing of the seal. These curves are shown in Figure 4-26. The progression of curves shows that for $B = 1.0$ seal there are three roots for the $T_\infty = 445^\circ\text{K}$ curve. However, they are close together such that puffing would not occur. This agrees with the experimental result.

As for $B = 0.75$ seal, considering the curve of $T_\infty = 472^\circ\text{K}$ (199°C), although there are three roots, the right-hand root does not move very far to the right before disappearing. This means that noticeable puffing may not occur for $B = 0.75$ seal either. However, puffing has been observed at $T_\infty = 464^\circ\text{K}$ (191°C) during Test 73. One possible explanation for this is that the balance ratio of the pressurized seal ring might change due to mechanical and thermal distortion in operation. If it changed to as little as $B = 0.74$, then the horizontal line of applied load would be lower and the right-hand root would move far to the right. This would cause puffing.

Therefore, based on the comparison above, the theoretical model cannot provide an accurate prediction for puffing. However, the model does have some use in that it indicates the approximate temperature at which puffing would be expected to occur.

Both the torque versus temperature and ΔT versus temperature data display a wide scatter in spite of being averaged over many hours of testing. As shown in Chapter 2, numerous attempts were made to get repeatable results at a given temperature. This scatter is similar to scatter found in all previous tests for parallel face seals. It is believed that certain random

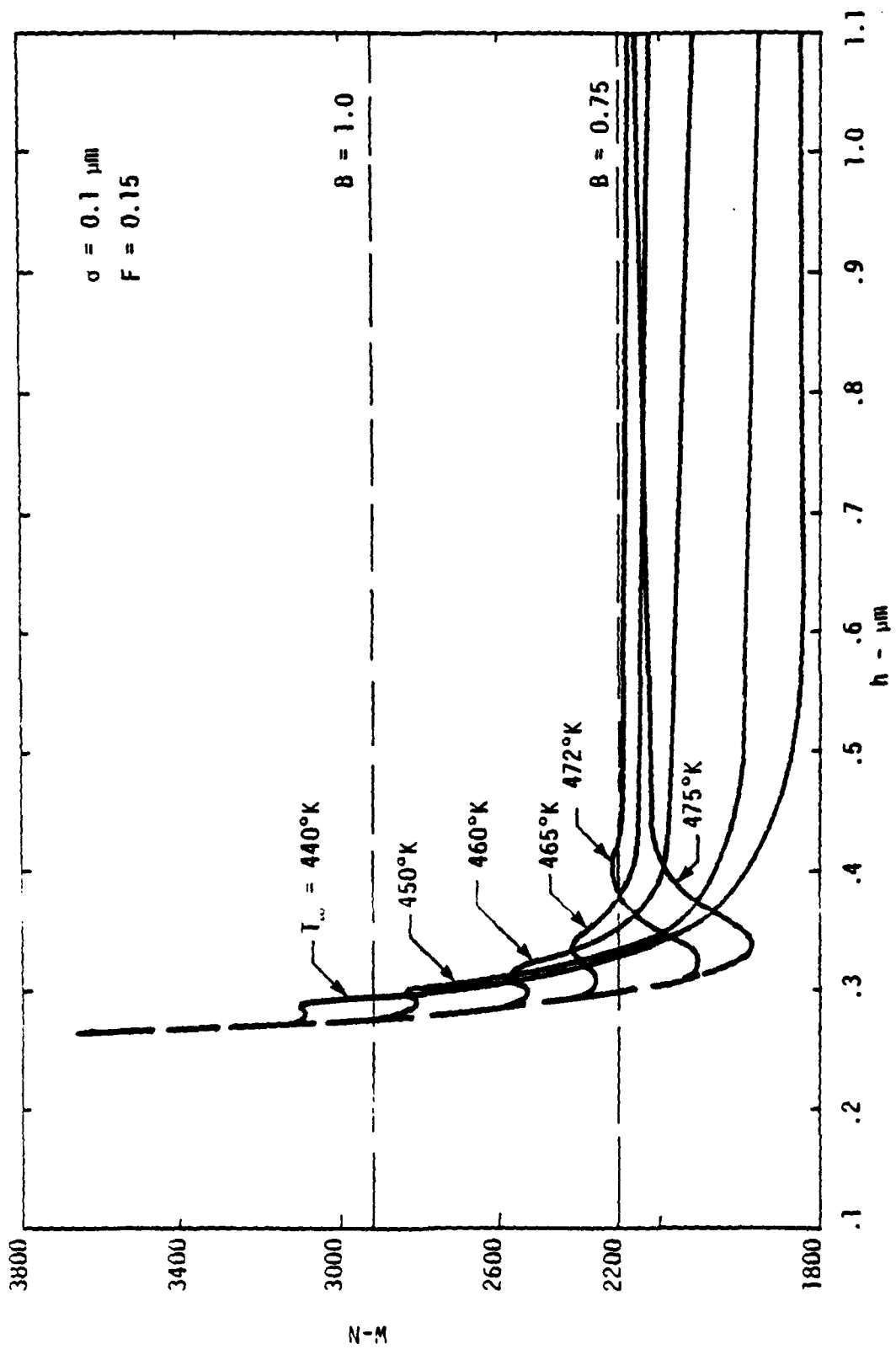


Figure 4-26. Load Function.

processes are occurring to cause this. The deterministic model used to predict performance is simply not adequate. It is thought that there is an interaction between wear (global and local), thermal deformation (global and local), friction coefficient (local) and fluid flow (local) which, in fact, may allow a seal to operate at different average conditions from time to time. Clearly, more investigation of the basic friction and wear processes is needed to explain this type of behavior.

Offset-Land Seal

Using the methods outlined in the previous chapter, performance was calculated for the experimental offset-land seal described in Chapter 2. The computed results are shown compared to experimental results in Figure 4-27. Only two experimental points were plotted because in only two of the tests could the final offset be determined. It is no surprise that one of the torque readings is poorly predicted since the torque values are at the limit of accurate resolution of the torque measuring device. Considering leakage, the theory underpredicts at the lower offset case. This probably occurs because the roughness of the surface of the land was larger than assumed in the calculations.

In summary, some agreement between theory and experiment is observed. Clearly, many more experimental results will be needed before any final judgement can be made concerning the validity of the theory.

Speed Effects

In the previous report [8], computations of the speed effects were made and compared to experimental results. These calculations have now been remade using the new algorithm described previously and compared to all of the speed effect data now available. Tables 4-4 and 4-5 show the computed values assuming 0%

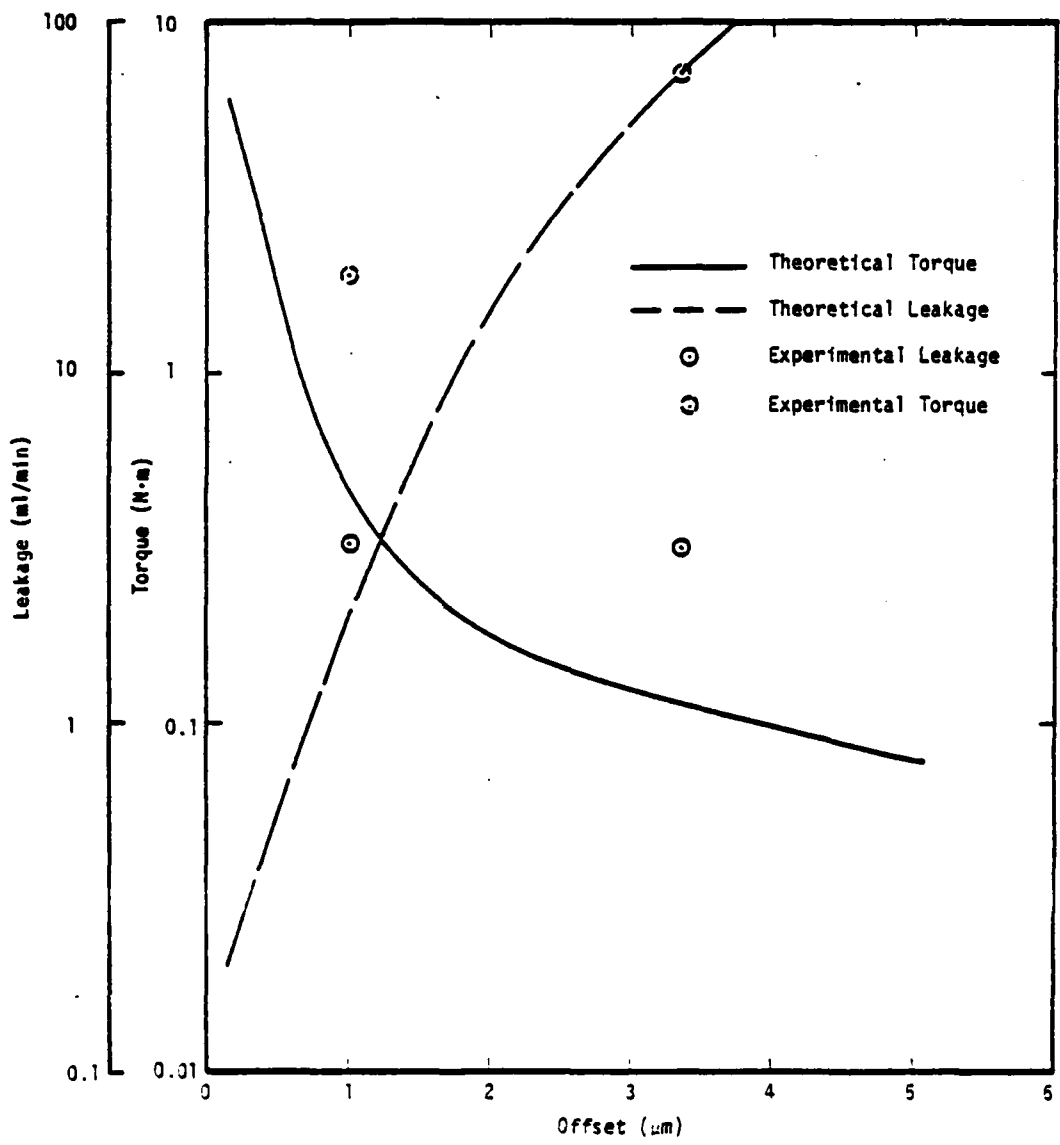


Figure 4-27. Offset Land Seal Performance.

Table 4-4. Computed Results--Elrod Algorithm Speed Effect at
 $p_0 = 3.45$ MPa, 0% Water, $B = 1$, 12 R \times 14 0 Grid, $n = 3$, $p_g = 6.90$ MPa

RPM	h_{pa}	h_{pa} calc	h_{pb}	h_{pb} calc	h_b net	h_a net	ϕ_a net $\times 10^6$	ϕ_b net $\times 10^6$	\bar{h}_{ma}	\bar{h}_{mb}	u	$(N \cdot m)$	θ_{min}	x	\bar{h}_o	p_g corrected MPa
1	-11.77	-11.96	0.00	0.00	3.26	0.00	640	0	-1.59	0	0.057	15.9	4.0	45.8	-0.175	7.63
400	-11.82	-11.76	0.09	0.08	3.21	0.09	638	4	-1.62	-0.05	0.056	15.8	3.8	46.5	-0.188	7.64
900	-11.83	-11.87	0.19	0.18	3.20	0.19	637	8	-1.58	-0.11	0.055	15.6	4.0	47.6	-0.197	7.62
1400	-11.90	-11.93	0.34	0.34	3.13	0.34	634	15	-1.52	-0.15	0.055	15.3	4.2	49.3	-0.203	7.59
3600	-12.00	-12.05	0.49	0.49	3.03	0.49	629	22	-1.41	-0.10	0.052	14.7	5.0	53.2	-0.175	7.54

Table 4-5. Computed Results--Elrod Algorithm Speed Effect at
 $p_0 = 3.45$ MPa, 100% Wear, $B = 1$, $12 R \times 14 \theta$ Grid, $n = 3$, $p_g = 6.90$ MPa

RPM	\bar{h}_{μ_a}	\bar{h}_{p_a} calc	\bar{h}_{p_b}	\bar{h}_{pb} calc	\bar{h}_a net	\bar{h}_b net	ϕ_a net $\times 10^6$	ϕ_b net $\times 10^6$	\bar{h}_{ma}	\bar{h}_{mb}	μ	T (N-mm)	Q (ml/min)	χ	\bar{h}_0	p_g corrected MPa
1	-6.36	-6.50	0.00	0.00	8.67	0.00	880	0	1.08	0	0.024	6.6	20.4	76.4	0.648	6.40
400	-6.80	-6.80	0.94	0.92	8.23	0.94	861	41	1.23	-0.08	0.017	4.9	15.9	83.0	0.623	6.33
900	-7.10	-7.71	1.60	1.70	7.33	1.60	821	71	1.26	-0.22	0.008	2.2	11.0	93.4	0.713	6.32
1300	-10.09	-9.99	1.39	1.57	4.94	1.39	719	70	1.05	-0.09	0.013	3.8	2.0	89.1	0.681	6.41
2700	-10.86	-10.89	1.27	1.40	4.17	1.27	681	56	0.70	0.06	0.015	4.1	2.3*	89.2	0.681	6.57
3600	-11.41	-11.58	0.94	0.93	3.62	0.94	656	42	0.92	0.28	0.016	4.5	1.4*	89.4	0.690	6.47

*Average over last two iterations.

wear and 100% wear, respectively. The 0% wear case represents expected performance if little wear occurred and should predict performance at start up or under conditions where the worn shape of the face was not fully developed. The 100% wear case represents expected performance for a well run in case.

Figures 4-28 and 4-29 compare the theoretical and experimental results. All of the speed effect experimental results for $n = 3$ are plotted. Considering torque, agreement with the 100% wear case at and above 900 rpm is satisfactory. At 0 rpm, experimental torque is much higher than predicted by even the 0% wear case. Furthermore, experimental results consistently show a torque minimum around 450 rpm, whereas theory shows the minimum at just above 900 rpm. At these lower speeds the theory is clearly missing some important physical behavior. One good possibility is that the assumed mechanical coefficient of friction is not constant but may drop off quickly with increasing speed due to microasperity lubrication effects. That is, at the lowest speeds tested (1.4 rpm) microasperity lubrication does not function and the mechanical coefficient of friction is much higher than assumed. Such behavior could well explain the discrepancy in the torque prediction, and this question will probably become resolved as better data for mechanical friction coefficients in water become available using the friction test apparatus described in Chapter 2.

Considering leakage in 4-29, disagreement at the lower speeds is pronounced. It is probable that at the lower speeds 100% wear has not been achieved and the lower leakage values might correspond better to the 0% wear case which they do. It is also possible that there are additional deflection components of the carbon that have not been accounted for. Finally, it is likely that the surface roughness used in the calculation does not accurately characterize the actual roughness as discussed previously.

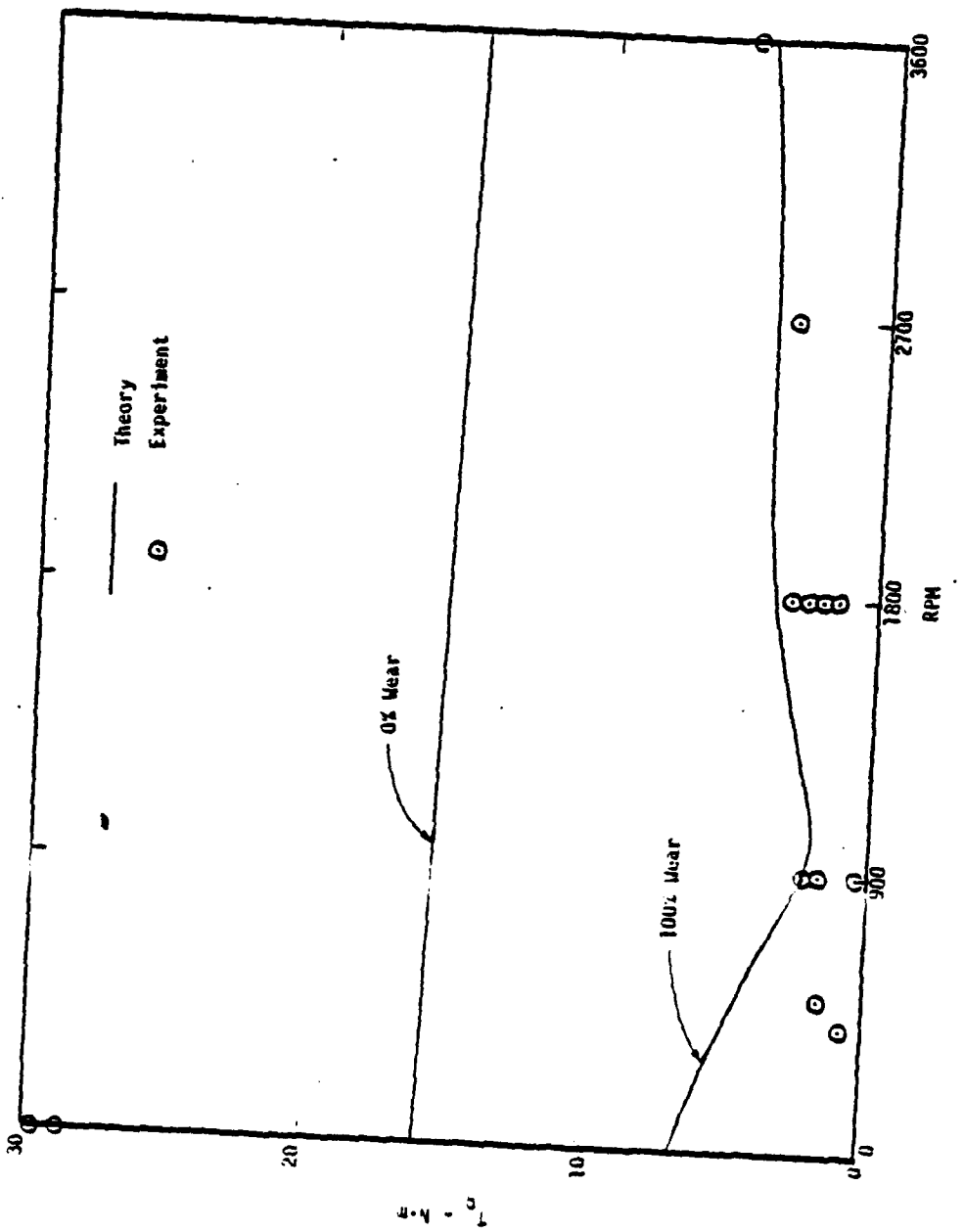


Figure 4-28. Three-Wave Seal Torque - Speed Effect.

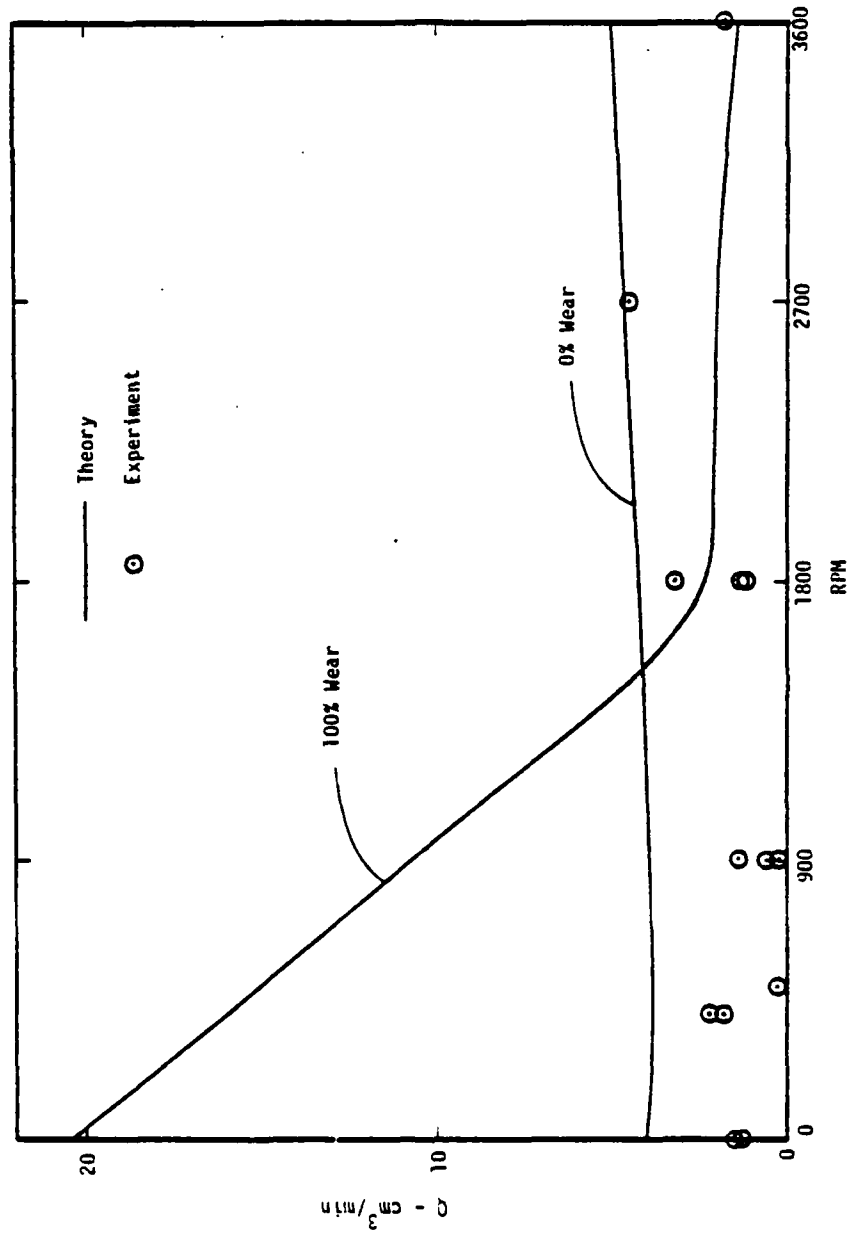


Figure 4-29. Three-Wave Seal Leakage - Speed Effect.

In any case the wavy seal theory appears to be inadequate at the lower speeds even though Figures 4-1, 4-2, 4-28 and 4-29 show reasonable agreement at higher speeds. It is thought that some insight into these problems may arise from data from a new nine-wave optimum design which has negligible deflection and from the friction and wear test apparatus. As new information becomes available, the wavy seal model will be modified accordingly.

Nine-Wave Seal

As described in Chapter 2 tests were run using the original three-wave seal as a nine-wave seal. Results using the wavy seal model have been computed and are shown in Table 4-6. Friction torque is seen to be consistently high at all speeds as it was in the tests and leakage is negligibly small as in the tests. The calculations show that this particular nine-wave seal performs very poorly as it, in fact, did.

It is interesting to note that using the original seal model algorithm a good performance was predicted. This occurred because the original algorithm could not create the lubricant starvation that, in fact, occurs as shown by the Elrod algorithm seal model. In this case, lubrication starvation is caused by the fact that the effective sealing radius is predicted to be near the outside diameter and not close to the inside diameter as it must be to approach optimum performance. Because of this an insufficient amount of fluid is present in the highly converging-diverging region of the seal to provide a significant hydrodynamic effect. In the original algorithm, this did not occur because negative pressures were allowed to pull fluid in from the low pressure side.

In summary, the seal model predicts the poor measured performance of this particular nine-wave seal. This example also serves to illustrate how the original seal model based on approximate cavity boundary conditions could lead to very poor design because of its inaccuracy.

Table 4-6. Computed Results--Elrod Algorithm Speed Effect at
 $p_0 = 3.45 \text{ MPa}$, 100% Wear, $\theta = 1$, 128×148 Grid, $n = 9$, $p_g = 6.90 \text{ MPa}$

RPM	$h_p a$	\bar{h}_{pa} calc	\bar{h}_{pb} calc	\bar{h}_a net	\bar{h}_b net	ϕ_a net $\times 10^6$	ϕ_b net $\times 10^6$	\bar{h}_{ma}	\bar{h}_{mb}	T (N-mm)	Q (ml/min)	x	\bar{h}_0	p_g corrected MPa		
900	0.078	0.079	-0.009	0.009	0.284	-0.009	243	-1	-0.034	0.004	0.068	19.1	0.03	35.8	0.571	7.54
1800	0.072	0.072	-0.002	-0.001	0.290	-0.002	244	0	-0.032	0.002	0.075	21.0	0.03	31.6	0.565	7.50
2700	0.069	0.069	0.002	0.001	0.293	0.002	244	0	-0.032	0.002	0.076	21.5	0.02	32.4	0.566	7.50

Chapter 5

Summary, Conclusions, and Recommendations

Experimental Results

- 1) The waviness drive provides a means of producing a moving wave using no moving parts internal to the seal. The device designed performed with no problems for a 500-hour test. Seal performance with time does not deteriorate using this device as compared to sliding O-rings. Minor modifications and improvements of the device to smooth out the pressure versus time functions are anticipated.
- 2) For the purpose of obtaining friction and wear data in water but independently of hydrostatic pressure, a friction and wear test apparatus has been designed. It is thought that data obtained from this device will explain some of the discrepancies between theory and experiment found using the simple wear and friction relationships built into the present seal models.
- 3) Experimental results from a series of tests at different radial tapers show that thermally caused radial taper has a strong influence on initial seal performance. A large initial divergent taper must be lapped onto the seal faces such that initial operation will have the faces parallel. Results also show that initially convergent faces result in very low friction but some wear at the inside corners occurs. This will eventually lead to parallel face operation. However, the amount of time required to establish parallel face operation after starting at a high convergent value is much larger than the few hundred hours of test used herein. Initial seal wear can definitely be reduced by starting with a convergent taper. The disadvantage of doing this is that long-term performance cannot be anticipated by short-term testing. It is thought, in fact, that long-term performance can best be simulated bylapping a divergent radial taper equivalent to the thermal taper onto the seal. It was found that the behavior of a balanced seal operating as described

was much different from seals where no significant initial radial taper was provided. Thus, testing seals with no initial taper can be misleading because of the thermal rotation effect.

4) Results from the high temperature tests show that as the seal operating temperature goes above the saturation temperature of the liquid at discharge pressure, seal friction is reduced. This trend continues until just before saturation temperature at the seal inlet pressure is reached. At this point, friction greatly increases with increasing temperature. There is a great amount of scatter in the data which cannot be attributed to experimental error. It appears possible that multiple states of equilibrium can be set up for a high temperature parallel face seal just as for a normal temperature parallel face seal. The question of why the high temperature seals formed a converging final taper instead of the normal diverging taper remains unanswered.

5) The radial taper tests, the high temperature tests, and parallel face tests show that for parallel faces the use of the Patir-Cheng [16] surface roughness model to calculate leakage overestimates the leakage flow by at least an order of magnitude. Investigation of the worn carbon surface shows that the surface consists of mostly high regions having a small roughness and deep craters which are generally not interconnected. Thus, while the craters add to the roughness value of the surface, they do not promote flow. It is clear that the surfaces are not Gaussian as assumed for the purpose of using the model and have some very special function. More work needs to be done to characterize the flow between the rough surfaces of seals. It is thought that a model similar to that of Patir and Cheng could be developed based on actual surface characteristics. A better rough surface flow model is needed to use in the various other seal models to improve their predictive capabilities.

6) The results from two 500-hour test show that the waviness concept reduces wear by a minimum of a factor of 200 compared to a flat-faced test. Wear is so small that it is of the same order of magnitude as the carbon nose distortions and sometimes negative wear values are measured. Improved wear measuring techniques are being incorporated into future seal tests.

7) The offset land seal concept works in principle. However, it is not known if the protrusions will, in fact, wear away over a long period of operation. It was not possible to start a seal in the offset low friction mode at low values of offset. At high values of offset the seal works good but leakage is high. Thus, at this point it is not known particularly if the offset concept can be made to work to provide a low leakage, low friction seal as originally intended. More experimental work particularly at low offsets needs to be performed.

8) Additional data was obtained at various speeds for both the wavy seal and the parallel face seal. At very low speeds friction is quite large in both cases. There is a rapid decrease in friction with increasing speed for both the wavy and parallel face seals. The wavy seal friction is reduced much further by speed increases than the parallel face seal. There is strong evidence of microasperity lubrication in both cases, that is, friction decreases with increasing speed when no macro scale hydrodynamic lift is present. It is expected that the use of the wear test apparatus will help to resolve this question.

9) Tests using the existing seal as a nine-wave seal show poor performance. Friction is high. Later theory shows this to be expected and indicates that a wavy seal cannot be casually designed and expect good performance. Optimum wavy seal design principles must be adhered to.

Theoretical Results

1) The principles governing the waviness generator are

quite simple and similar to those for a poly phase electric motor. To this author's knowledge, this principle has not been previously applied to a mechanical device. There may be other applications for this principle.

2) The seal waviness model has been reworked using the Elrod algorithm to predict cavitation. Although compared to the previous model, little difference in prediction was observed for the three-wave seals, a great difference was noted for the non-optimum nine-wave seal above. The previous model overestimates load support. The Elrod algorithm based seal model is therefore more accurate and should be used hereafter. A small increase in computer time is needed for the new seal model, but no serious limitation is imposed.

3) A paper was written on optimum wavy seal design [14]. It has been shown that for seals operating under variable speeds and pressures, a relatively large number of waves must be used so that the relative tilt of the faces does not change under variable conditions. In the three-wave seal, results show that deflections change with pressure. This will lead to accelerated wear. It has been determined that about nine waves are required for sufficient stiffness for seals of the size herein. Further refinement in determining the optimum wavy seal configuration beyond the discussion in the previous report [8] has been provided. A new seal based on these principles is being designed.

4) The theory supporting the offset land concept is developed. Theory shows that an offset land seal with very low friction, wear and leakage can be designed.

Comparison of Theoretical and Experimental Results

- 1) Comparison of theory and experiment for three-wave seals at 6.9 MPa gas pressure is good.
- 2) The radial taper model provides a good prediction for the short-term effects of varying the radial taper. The effect of thermal rotation is properly accounted for. The long-term

performance is poorly predicted. It is thought that the wear model used is inadequate and it is expected that wear test results obtained on the friction and wear test apparatus will lead to improved predictions.

3) The high temperature seal model predicts the trend and transition point of the high temperature tests. The model cannot predict or explain the scatter of the data. It is believed that certain random processes may account for this scatter. A stochastic seal model is needed to better understand this behavior.

4) Some agreement between theory and experiment is observed for the offset land studies. More experimental data is needed to refine this comparison.

5) While predicting the general trend, the wavy seal model does a poor job on predicting wavy seal performance as a function of speed. It is thought that refined friction measurements will be helpful. However, it appears that other factors such as seal deflection may also be involved.

6) The refined wavy seal model does predict the high friction and low leakage observed for the nonoptimum nine-wave seal.

General

The experimental and theoretical foundations for the moving wave seal have been well established. It has been shown experimentally under somewhat ideal conditions that wear is insignificant. It has been shown that a waviness device and seal can be operated for a 500 hour test with no mechanical problem and no deterioration of purpose. It has been shown that the wavy seal model does a reasonable job of predicting performance although certain improvements are needed. In particular, a better understanding of the effect of actual surface roughness on leakage, wear mechanisms, and the change of friction coefficient under various operating conditions are needed. Experimental programs have been outlined to provide this needed information. Variables which govern optimum wavy seal performance are well understood.

References

1. Findlay, J. A., "Cavitation in Mechanical Face Seals," Transactions of the ASME, Journal of Lubrication Technology, April 1968, pp. 356-364.
2. Pape, J. G., "Fundamental Aspects of Radial Face Seals," Thesis WJHD-17, December 1969 (T. H. Delft, Netherlands), 172 pp.
3. Stanghan-Batch, B. and Iny, E. H., "A Hydrodynamic Theory of Radial Face Seals," Journal of Mechanical Engineering Science, Vol. 15, No. 1, 1973.
4. Lebeck, A. O., Teale, J. L., and Pierce, R. E., "Elastohydrodynamic Lubrication with Wear and Asperity Contact in Mechanical Face Seals," Annual Report ME-76(77)ONR-414-1, ONR Contract N-00014-76-C-0071, Bureau of Engineering Research, The University of New Mexico, Albuquerque, New Mexico, January 1977.
5. Lebeck, A. O., Teale, J. L., and Pierce, R. E., "Hydrodynamic Lubrication with Wear and Asperity Contact in Mechanical Face Seals," Annual Report ME-86(78)ONR-414-1, prepared for the Office of Naval Research under Contract No. ONRN-00014-76-C-0071, Bureau of Engineering Research, The University of New Mexico, Albuquerque, New Mexico, January 1978.
6. Lebeck, A. O., Teale, J. L. and Pierce, R. E., "Hydrodynamic Lubrication with Wear and Asperity Contact in Mechanical Face Seals," Annual Report ME-95(79)ONR-414-1, prepared for the Office of Naval Research under Contract No. ONR-N-00014-76-C-0071, Bureau of Engineering Research, The University of New Mexico, Albuquerque, New Mexico, January 1979.
7. Teale, J. L. and Lebeck, A. O., "An Evaluation of the Average Flow Model [1] for Surface Roughness Effects in Lubrication," ASME Paper 79-Lub-37, presented at the 1979 ASME-ASLE Lubrication Conference, Dayton, Ohio, October 16-18, 1979.
8. Lebeck, A. O. and Young, L. A., "The Wavy Mechanical Face Seal--Theoretical and Experimental Results," Annual Report ME-105(80)ONR-414-1, prepared for the Office of Naval Research under Contract ONR-N-00014-76-C-0071, Bureau of Engineering Research, The University of New Mexico, Albuquerque, New Mexico, January 1980.
9. Lebeck, A. O., "A Mixed Friction Hydrostatic Face Seal Model with Thermal Rotation and Wear," presented at the 1979 ASLE Annual Meeting, St. Louis, May 1979, ASLE Paper 79-AM-4C-3, to be published in the ASLE Transactions.

10. Snapp, R. B. and Sasdelli, K. R., "Performance Characteristics of High Pressure Face Seal with Radially Converging Interface Shapes," Paper E4, 6th International Conference on Fluid Sealing, February 27-March 2, 1973, Munich.
11. Lebeck, A. O., "A Mixed Friction Hydrostatic Face Seal Model with Phase Change," presented at the 1979 ASME-ASLE Joint Lubrication Conference, October 1979. ASME Paper 79-Lub-5, accepted for publication in Journal of Lubrication Technology.
12. Elrod, H. B., "A Cavitation Algorithm," presented at the Century 2 ASME-ASLE International Lubrication Conference (San Francisco: Aug. 1980) ASME Paper 80-C2/Lub-54.
13. Jakobsson, B. and Floberg, F., "The Finite Journal Bearing Considering Vaporization," Report No. 3, 1957, Institute of Machine Elements, Chalmers University, Gothenburg, Sweden.
14. Lebeck, A. O. and Young, L. A., "Design of an Optimum Moving Wave and Tilt Mechanical Face Seal for Liquid Applications," 9th International Conference on Fluid Sealing, The Netherlands, April 1-3, 1981.
15. Becker, K. M., "Measurements of Convective Heat Transfer from a Horizontal Cylinder Rotating in a Tank of Water," Int. J. Heat Mass Transfer, Vol. 6, 1963, pp. 1053-1062.
16. Patir, N. and Cheng, H. S., "An Average Flow Model for Determining Effects of Three-Dimensional Roughness on Partial Hydrodynamic Lubrication," Journal of Lubrication Technology, Trans. ASME, Series F, Vol. 100, January 1978, p. 2.

APPENDIX

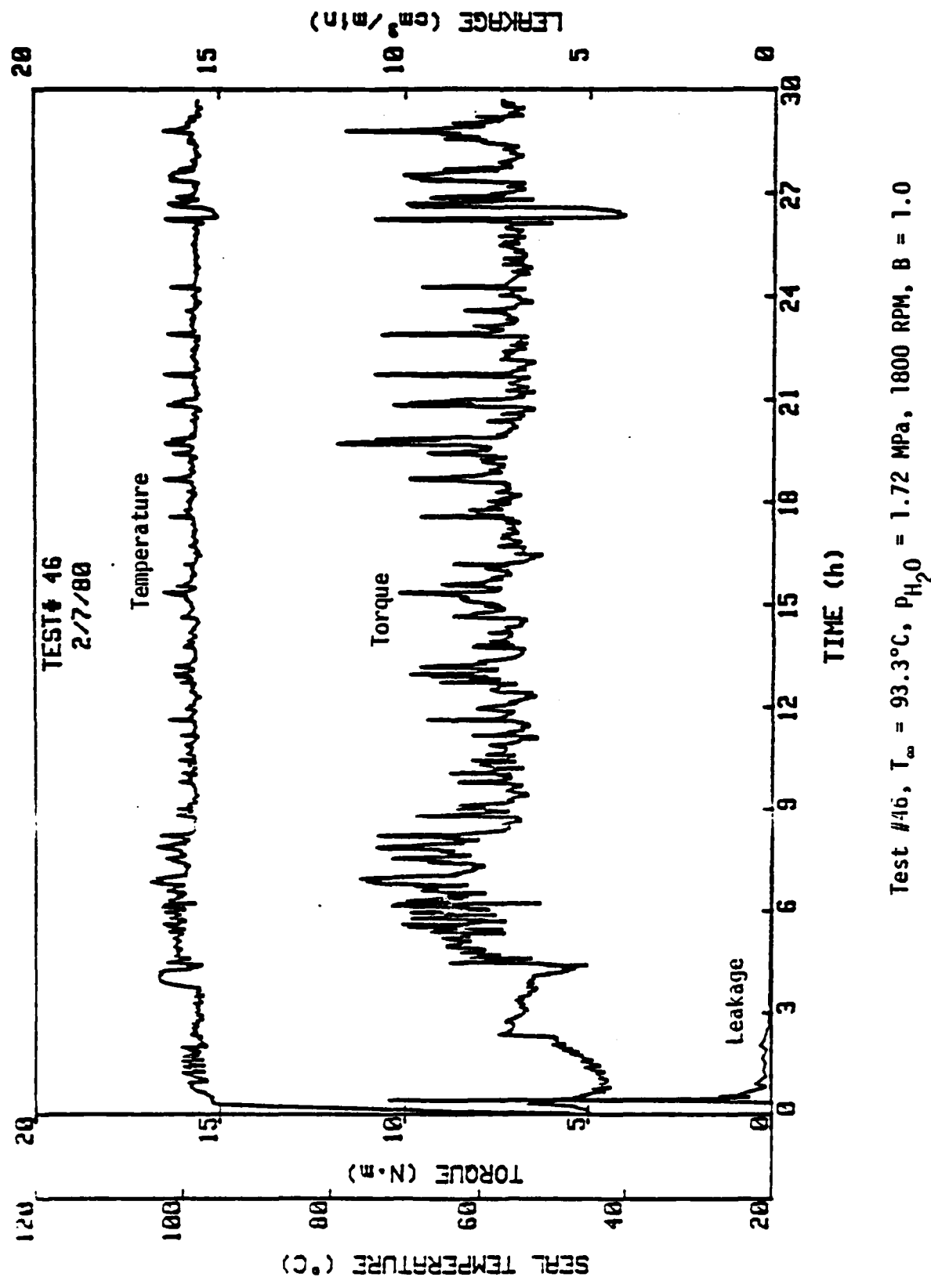
TEST # AND DATE	53	54	55	56	57	58	59	60	61	62	63	64	65
	2/24/80	3/5/80	3/14/80	3/11/80	3/17/80	3/24/80	3/27/80	3/27/80	3/29/80	4/1/80	4/15/80	4/17/80	
TYPE OF TEST	HOT	HOT	HOT	HOT	FLAT FACE 30° T.S.	HOT	HOT	HOT	HOT	HOT	RADIAL TAPER	RADIAL TAPER	
SPEED (RPM)	1800	1800	1800	1800	1800	1800	1800	1800	1800	1800	1800	1800	1800
SEALED PRESSURE (PSI)	238	238	238	238	500	238	238	238	238	238	500	500	600
TEST DURATION (HOURS)	46.5	72.0	26.8	43.7		1.2	0.8	44.2	46.0	4.5	1.7	24.0	64.0
WAVINESS PRESSURE (PSI)	0.0	0.0	0.0	0.0	0.0	0.0	0.0	0.0	0.0	0.0	0.0	0.0	0.0
COOLING WATER TEMPERATURE (°F)	100	200	280	330	100°	350	350	330	280	110 TO 340	110 TO 34.0	100°	100°
LEAKAGE INITIAL / FINAL (ML/MIN)	/	/	/	/	1.0	/	/	/	/	/	/	580	12.
BEARING HOUSING TEMPERATURE (°F)	110.64	109.03	111.25	111.06	113.6				111.20	110.14	96.2	101.6	125.5
SEAL FACE TEMPERATURE (°F)	144.27	209.57	285.31	336.03	118.3				339.87	294.27		94.1	100.2
SEAL TEMP. DIFF. (°F)	119.5	81.3	68.7	78.8	95.0				89.3	96.6		-3.2	17.5
INITIAL COKE (ML)	102.8	80.3	51.8	65.5	92.6				13.2	96.6		-3.56	2.6
PRIMARY RING #	5	7	7	7	8	7	9	9	9	9 (CAPPED)	7	9	10
AVERAGE WEAR (μm)					758 (ML)								
RADIAL CLEARANCE INITIAL / FINAL (μm)	26.3				29.9			11.3			25.0	22.2	
TRANSIENT CLEARANCE INITIAL / FINAL (μm)	16.9				33.5			15.9			14.6	25.0	22.2
TRANSIENT CAPTURE INITIAL / FINAL (μm)	0.0				1.1			0.0			13.4	22.2	13.3
RADIAL CLEARANCE SIDE #	-				1.1			0	0	0	4560	4.339	-321
RADIAL CLEARANCE SIDE # SIDE A SIDE B SIDE 2 SIDE 3 SIDE B SIDE 3 SIDE 2													
AVERAGE WEAR (μm)													

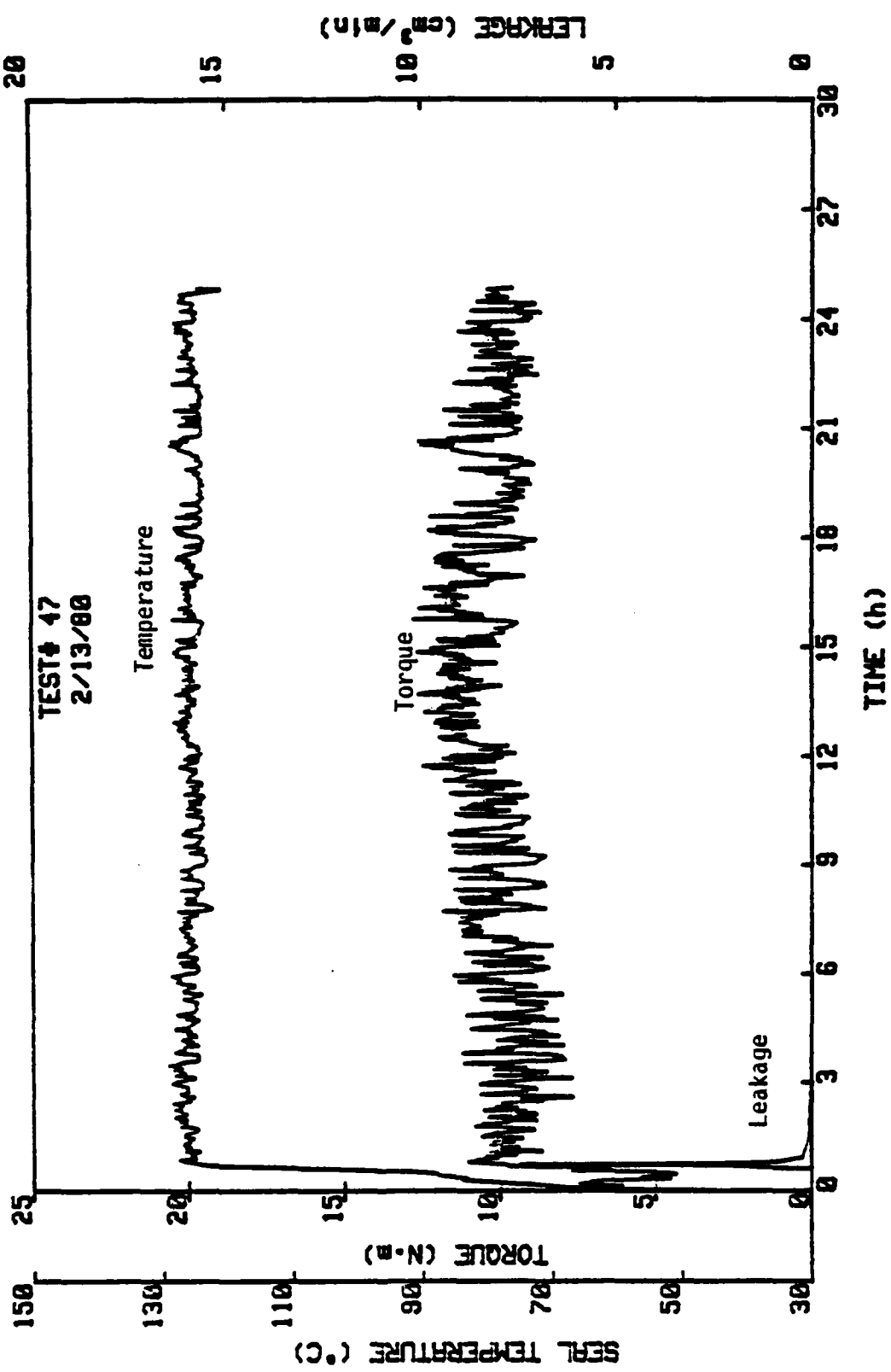
TEST # AND DATE	66	67	68	69	70	71	72	73	74	75	76	77	78
TYPE OF TEST	RADIAL TAPER	RADIAL TAPER	RADIAL TAPER	HOT	HOT	HOT	HOT	HOT	3 WAY	RADIAL TAPER	RADIAL TAPER	3 WAY	HOT
SPEED (RPM)	80±7.5 1800	80±7.5 1300	80±7.5 1300	80±7.5 1800	80±7.5 1800	80±7.5 1800	80±7.5 1300						
SEALED PRESSURE (PSI)	500	500	500	238	238	238	238	238	500	500	500	500	238
TEST DURATION (HOURS)	118.3	63.8	65.2	24.1	24.1	24.0	89.2	5.0	21.5	71.6	138.6	44.5	37.1
WAVINESS PRESSURE (PSI)	0.0	0.0	0.0	0.0	0.0	0.0	0.0	0.0	1000	0.0	0.0	800	3.0
COOLING WATER TEMPERATURE (°F)	100°	100°	100°	100	200	300	100	100° 375	100°	100°	100°	100°	100
LEAKAGE RATES	4.0	3.0	2.5						10	2.0	0.0	11	
FINAL THICKNESS	5.29	.80	.043	0.2	0.0	0.0	0.0	=1.0	2.7	0.0	.0072	4.7	1.0
BEARING HOUSING TEMPERATURE (°F)	121.0	126.2	121.0	101.2	99.6	114.3	103.3		118.5	120.4	120.6	120.8	111.9
SEAL FACE TEMPERATURE (°F)	103.3	107.8	112.2	114.4	208.6	307.8	106.0		103.3	118.4	122.6	102.3	116.8
FINAL TORQUE TORQUE THICKNESS (INCHES)	23.2	37.3	63.8	40.6	60.0	61.5	16.3		29.2	102.0	100.4	12.2	64.3
PRIMARY THICKNESS	8	10	11	10	10	10	10	10	10	10	9	10	10
AVERAGE WEAR (MICRS)										198.3	521.7		
RADIAL CLL THICKNESS THICKNESS (MICRS)	22.0	23.0	21.0	21.0					23.0	18.0	-	16.1	
ROTATIONAL CLL THICKNESS THICKNESS (MICRS)	25.0	25.0	24.0	22.4					24.0	26.0	-	18.1	
ROTATIONAL CLL THICKNESS THICKNESS (MICRS)	-4.0	-3.00	-7.50	-5.6					-11.0	-7.0	-	0.0	
ROTATIONAL CLL THICKNESS THICKNESS (MICRS)	-1.0	-2.05	-7.04						-7.0	-9.0	-		
ROTATIONAL CLL THICKNESS THICKNESS (MICRS)	2	3	3	2									
AVERAGE WEAR (MICRS)													

TEST # AND DATE	79	30	31	32	33	34	35	36	37	38	39	40	41	42	43
TYPE OF TEST	HOT	HOT	HOT	HOT	HOT	HOT	WAV.	WAV.	WAV.	WAV.	WAV.	WAV.	WAV.	WAV.	WAV.
SPEED (RPM)	82.75 1800	32.75 1500	32.75 1800	82.75 1800	32.75 1800	82.75 1800	1800	900	1800	2700	100	400	14		
SEALED PRESSURE (PSI)	233	233	233	233	238	238	500	500	500	500	500	500	500	500	500
TEST DURATION (HOURS)	12.2	10.0	12.0	11.7	3.8	2.1	24.5	48.5	44.3	44.8	49.3	72.4	20.6		
WAVENESS PRESSURES (PSI)	0.0	0.0	0.0	0.0	0.0	0.0	1000	1000	1000	1000	1000	1000	1000	1000	1000
COOLING WATER TEMPERATURE (°F)	150	200	250	350	300	375	100°	100°	100°	100°	100°	100°	100°	100°	100°
LEAKAGE PASTURE FINAL (MM)	0.0	0.0	0.0	0.0	0.1	0.0	0	2.	0	0	0	2	1.	3.	
BEARING HOUSING TEMPERATURE (°F)	104.5	106.5	105.8	119.4	110.3	117.9	128.5	106.2	128.6	123.1	110.5	89.6	93.7		
SEAL FACE TEMPERATURE (°F)	152.8	213.5	260.2	356.6	307.8	391.4	126.8	104.5	114.6	127.1	102.5	100.7	13.8		
FINAL TORQUE TORQUE CROSS SHEAR CROSS SHEAR PRIMARY RING #3	42.2 33.7	53.2 35.9	62.4 27.2	50.7 36.7	42.2 35.1	99.9 39.0	122.5 116.9	41.0 44.8	65.0 63.5	76.1 76.2	31.6 33.3	5.4 5.6	52.6 55.3		
AVERAGE WEAR (MM/M)	10	10	10	10	10	10	4	+	7	—	—				
RADIAL CLAW INITIAL FINAL (MM/M)															
TRANSPORT CLAW INITIAL FINAL (MM/M)															
RADIAL CLAW INITIAL FINAL (MM/M)															
RADIAL CLAW INITIAL FINAL (MM/M)															
AVERAGE WEAR (MM/M)															

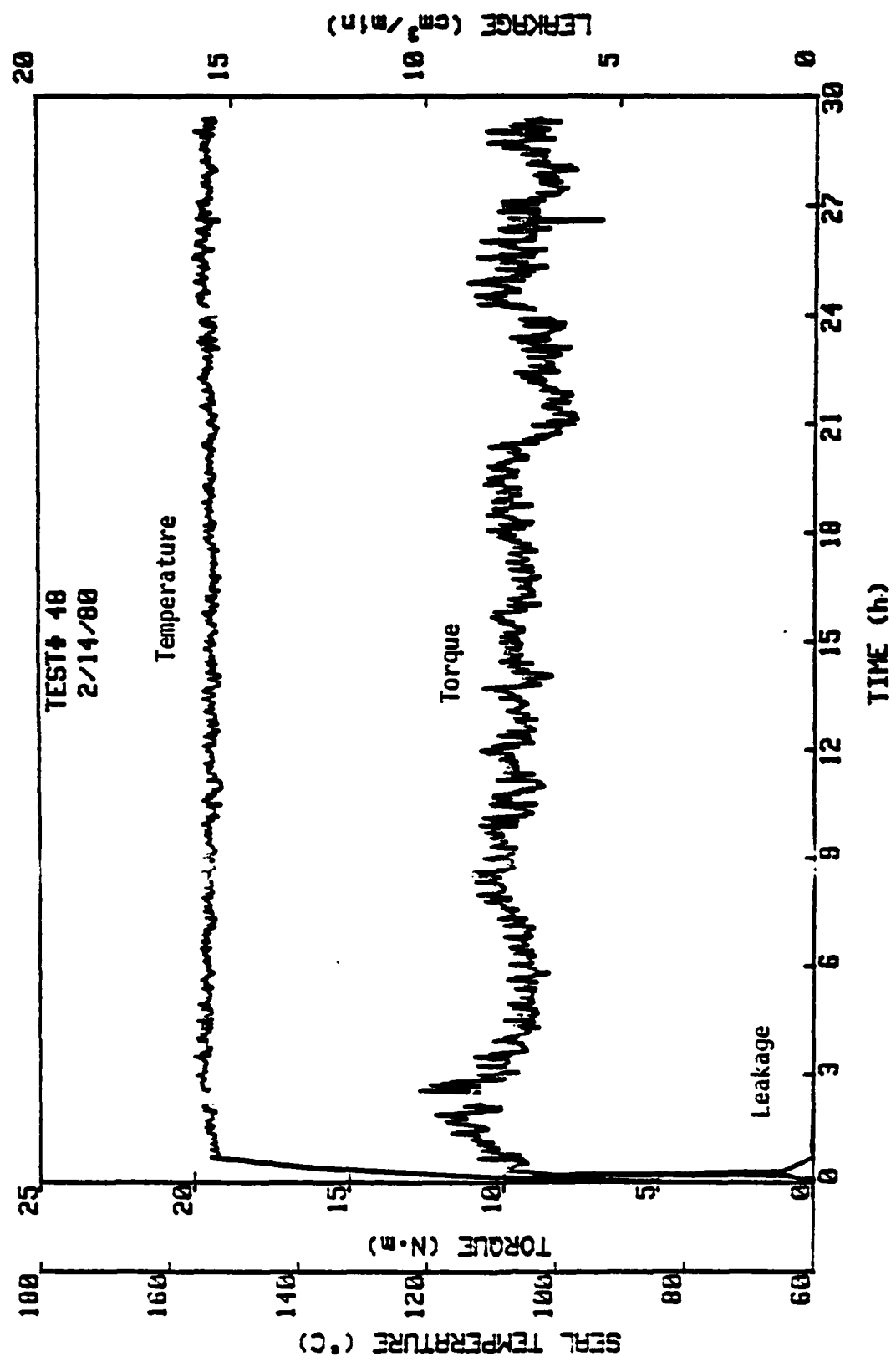
TEST # AND DATE	92	93	94	95	96	97	98	99	100	101	102	103	104
TYPE OF TEST	FLAT FACE	RADIAL TAPER 3% QTS	3 W.W.	3 W.W.	3 W.W.								
SPEED (RPM)	1.4	400	900	2700	3600	1800	1800	1800	1800	400	1.4	900	
SEALED PRESSURE (PSI)	500	500	500	500	500	500	500	500	500	500	500	500	
TEST DURATION (HOURS)	13.1	23.6	25.1	22.0	.8	66.7	15.6	4.1	24.4	47.9	47.8	48	29.7
WAVINNESS PRESSURE (PSI)	0.0	0.0	0.0	0.0	0.0	0.0	0.0	0.0	0.0	1000	1000	1000	1000
Cooling WATER TEMPERATURE (°F)	100°	100°	100	100	100	100	100	100	100	100	100	100	100
LEAKAGE INITIAL (MICRS)	0	0	0	0	0	0	88	20	42	3	-7	-2	-4
LEAKAGE FINAL (MICRS)	0	0	0	0	0	3.55	39	22	45.6	12.3	1.94	1.3	1.4
BEARING HOUSING TEMPERATURE (°F)	74.0	87.2	100.5	136.0	-	126.9	126.4	-	124.5	127.4	91.6	85.2	103.6
SEAL FACE TEMPERATURE (°F)	98.6	105.4	108.7	117.1	122	101.3	100.5	101	101	101	100.5	99.7	101.3
FINAL TEMPERATURE (INCLUDES COOLANT)	169	78.0	79.4	52.7	55	60.8	2.2	2.	8.6	10.9	5.55	27.3	65
PRIMARY STROKE (in)	6					9	12	12	12	12	9	9	7
AVERAGE WEAR (μm/in)													
RADIAL CLEARANCE INITIAL (μm/in)	24.0					12.0	18.0	18.0	17.0	18.0	19.0	24.0	18.0
RADIAL CLEARANCE FINAL (μm/in)	28.0					12.0	20.0	22.0	18.0	18.0	20.4	22.0	20.9
RADIAL CLEARANCE MAX (μm/in)	-100					26.0	15.0	15.0	19.0	14.0	17.0	18.0	15.0
SECONDARY RING #	5-26A					3.30	-	6.00	6.00				
RADIAL CLEARANCE INITIAL (μm/in)													
RADIAL CLEARANCE FINAL (μm/in)													
RADIAL CLEARANCE MAX (μm/in)													
AVERAGE WEAR (μm/in)													

TEST # AND DATE	105 11/13/80	106 11/17/80	107 11/26/80	108 12/2/80	109 1/12/81						
TYPE OF TEST	LAND SEAL $B=0.75$	LAND SEAL $B=0.75$	LAND SEAL $B=0.75$	LAND SEAL $B=0.75$		3 Wear. (Wear-ring Seal)					
SPEED (RPM)	1800	1800	1800	1800		1800					
SEALED PRESSURE (PSI)	500	500	500	500		500					
TEST DURATION (HOURS)	22.5	20.6	3.3	162.2		500					
WAVINESS PRESSURE (PSI)	0.0	0.0	0.0	0.0		1000					
COOLING WATER TEMPERATURE (°F)	100	100	100	100		100					
LEAKAGE INITIAL FINAL (μL/min)	~.01 .02	0.0 .003	7.0 71.9	5.0 14.3		2.5 1.54					
BEARING HOUSING TEMPERATURE (°F)	124.9	125.6	123.6	124.6		122.7					
SEAL FACE TEMPERATURE (°F)	125.9	125.7	100.5	100.9		102.8					
ETALON THERMOCOUPLE (mm)	117.2 117.0	121.4 122.7	9.5 2.8	5.6 2.8		11 11.3					
PRIMARY RING #	12	12	12	.12		9					
AVERAGE WEAR (μm)			21.7	6.7		-33					
RADIAL CLEARANCE INITIAL FINAL (μm)	20.0 15.3	20.0 14.0	16.0 18.0	19.0 18.0		17.0 12.0					
TEMPERATURE CLEARANCE INITIAL FINAL (μm)	20.0 13.0	19.0 22.0	19.0 22.0	24.0 22.0		20.0 12.0					
RADIAL CLEARANCE INITIAL FINAL (μm/deg)	-50 -1400	<12 -1430	412 -	412 -		412 -					
SECONDARY RING # SIDE A SIDE B SIDE C SIDE D SIDE A	2	2	2	2		3					
RADIAL CLEARANCE INITIAL FINAL (μm)											
TEMPERATURE CLEARANCE INITIAL FINAL (μm)											
RADIAL CLEARANCE INITIAL FINAL (μm/deg)											
AVERAGE WEAR (μm)											



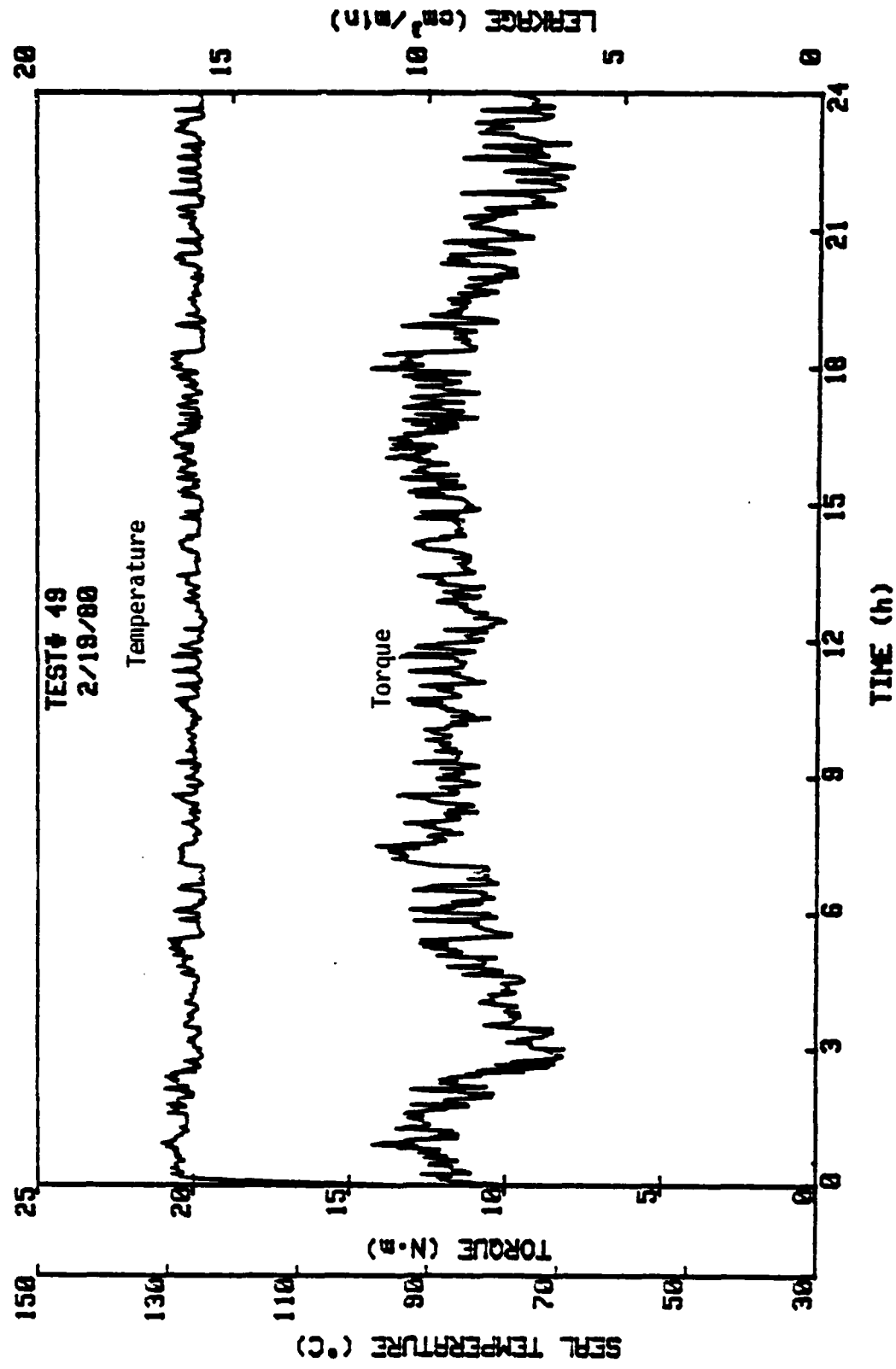


Test #47, $T_\infty = 121.1^\circ\text{C}$, $p_{\text{H}_2\text{O}} = 1.72 \text{ MPa}$, 1800 RPM, $B = 1.0$

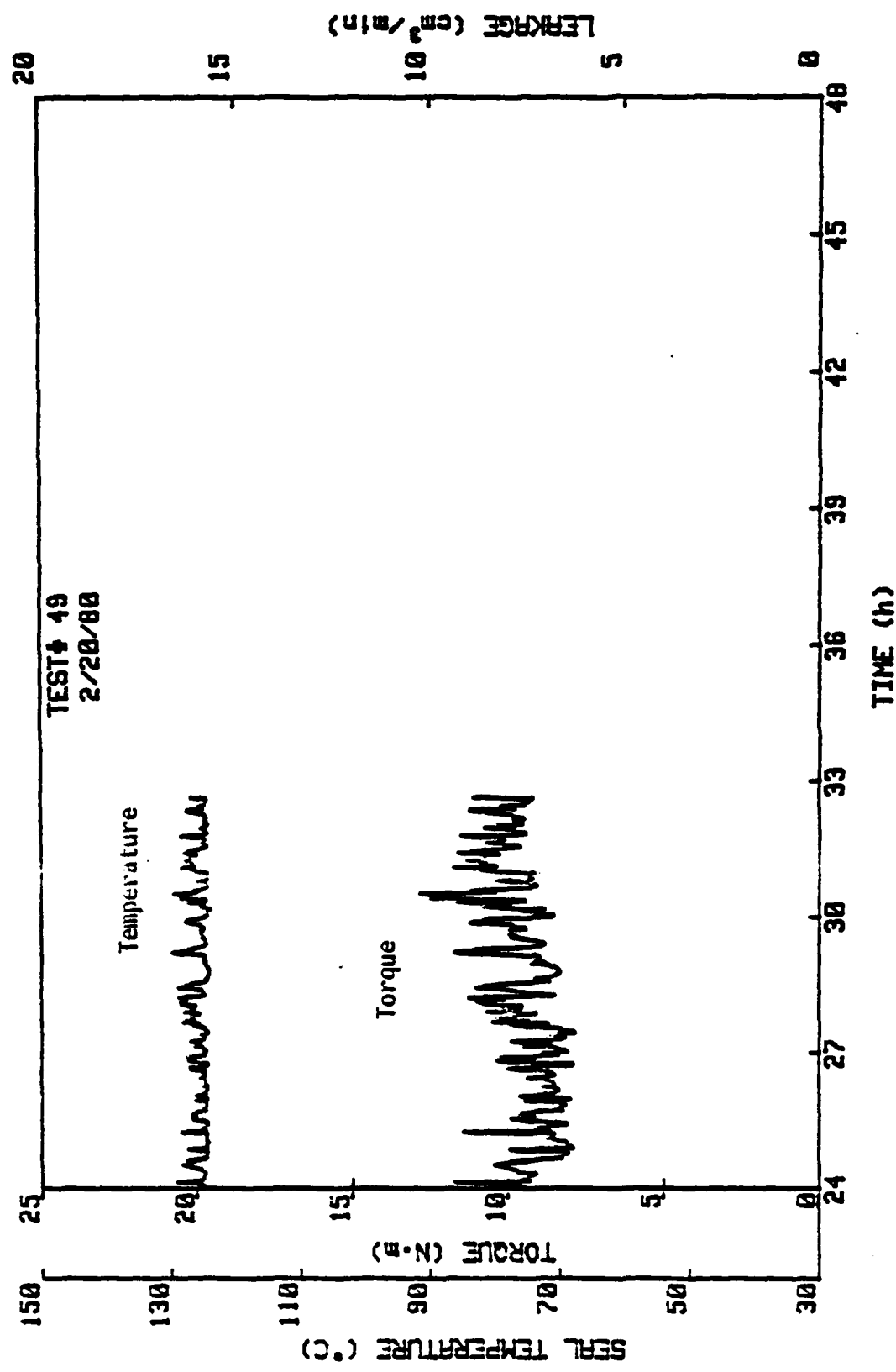


Test #48, $T_{\infty} = 148.9^{\circ}\text{C}$, $p_{\text{H}_2\text{O}} = 1.72 \text{ MPa}$, 1800 RPM, $\beta = 1.0$

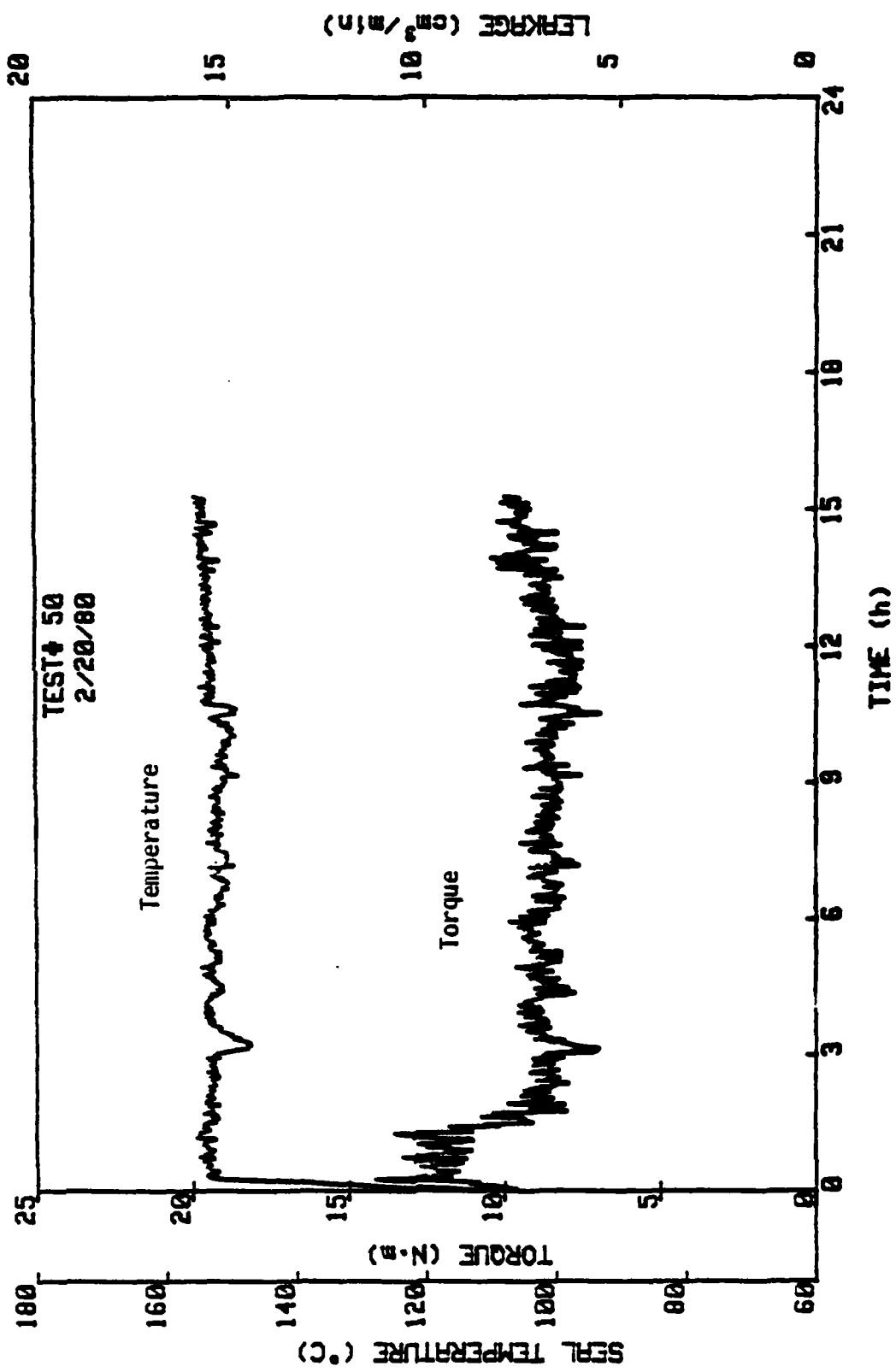
HEWLETT-Packard



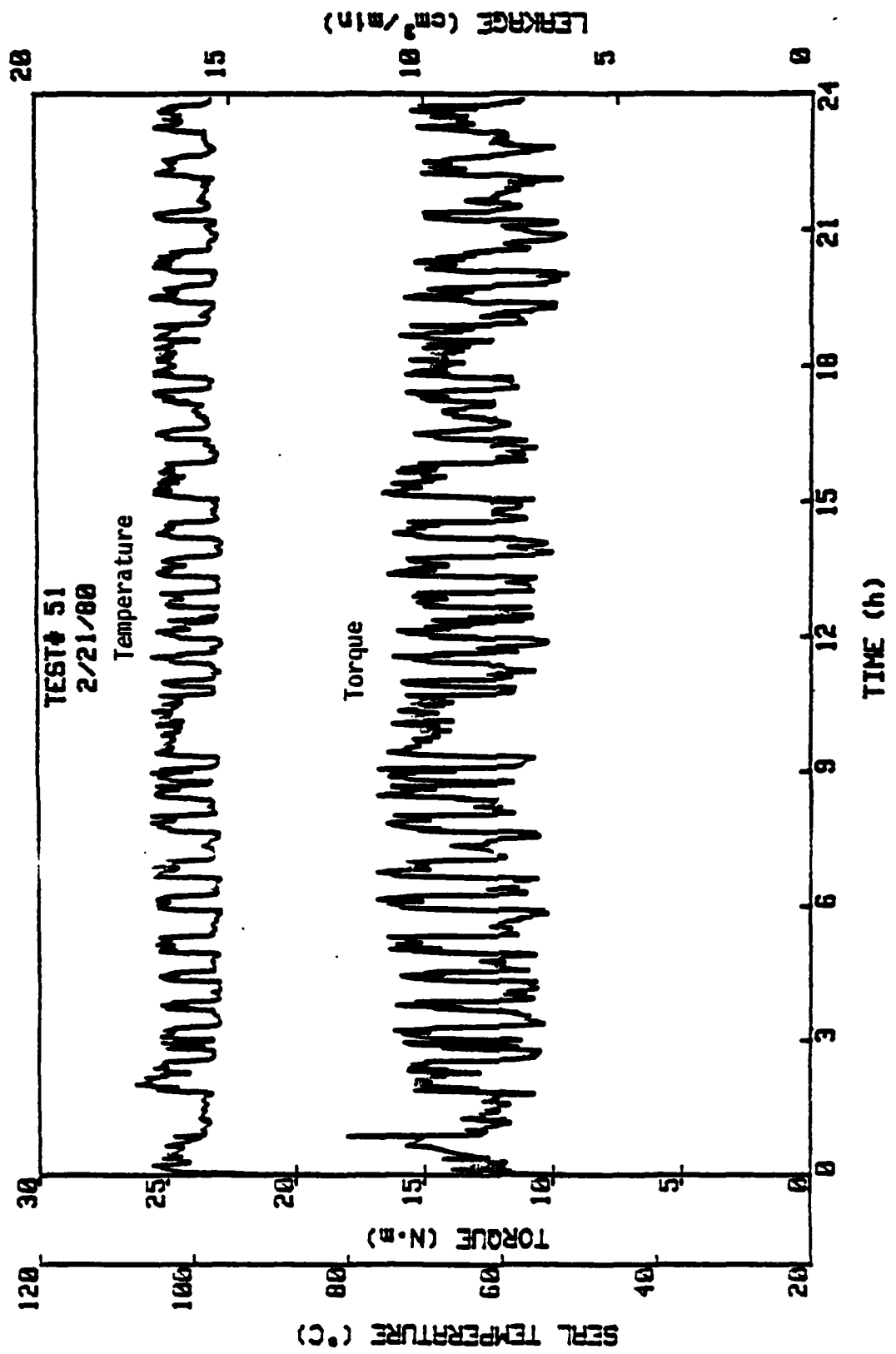
Test #49, $T_{\infty} = 121.1^{\circ}\text{C}$, $p_{\text{H}_2\text{O}} = 1.72 \text{ MPa}$, 1800 RPM, $B = 1.0$



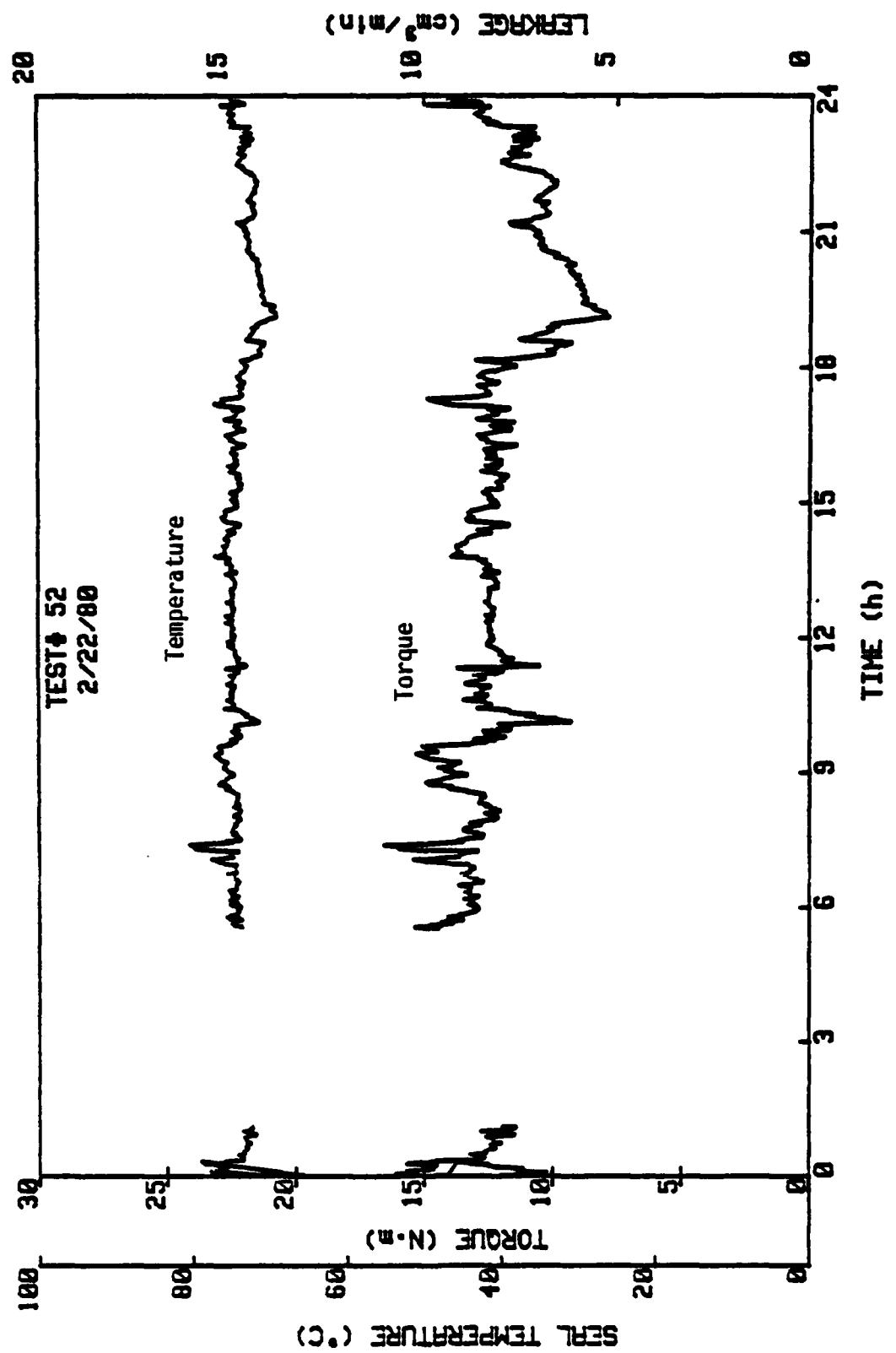
(Continued)



Test #50, $T_{\infty} = 148.9^\circ\text{C}$, $P_{\text{H}_2\text{O}} = 1.72 \text{ MPa}$, 1800 RPM, $B = 1.0$

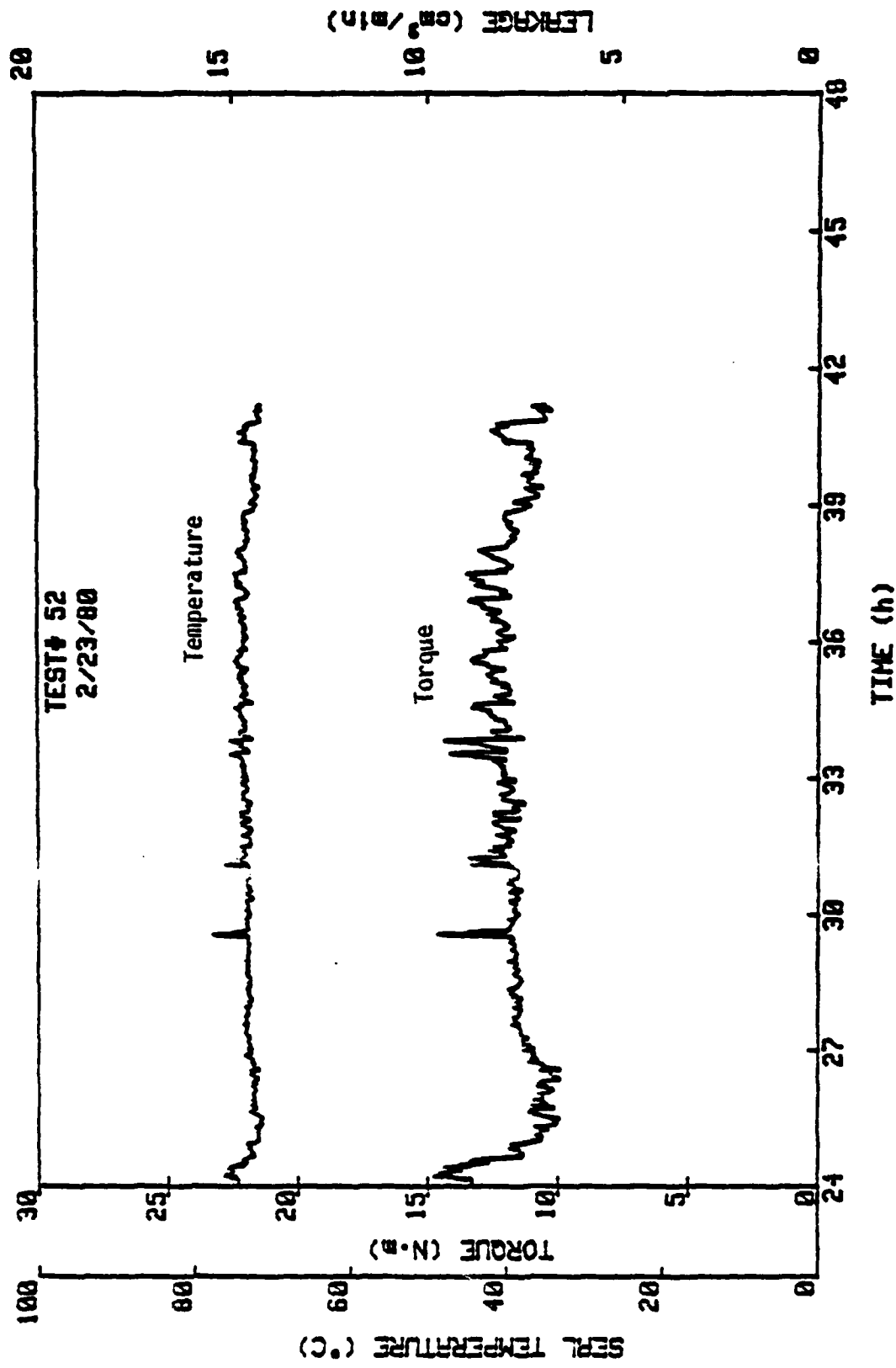


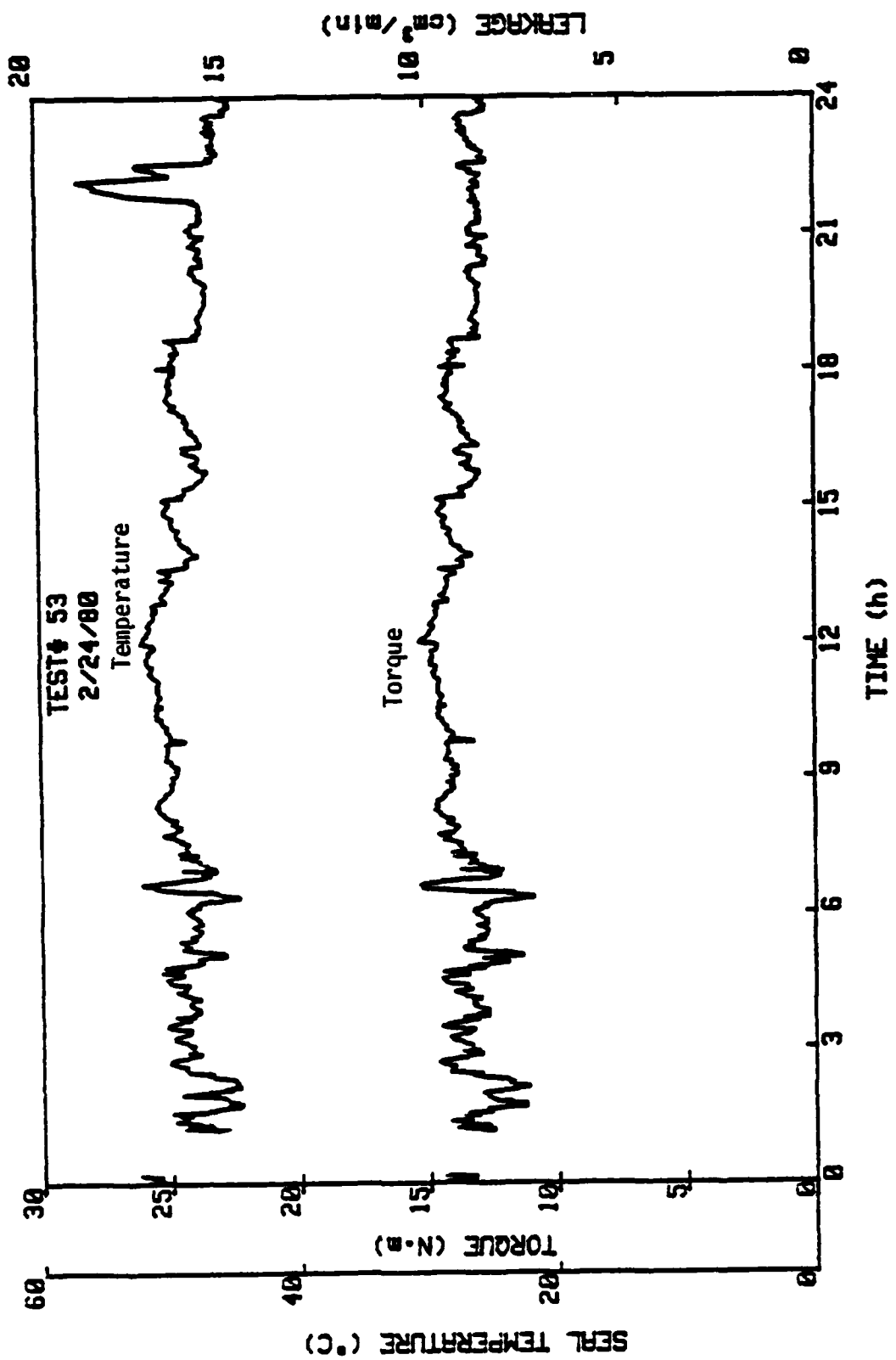
Test #51, $T_{\infty} = 93.3^{\circ}\text{C}$, $p_{\text{H}_2\text{O}} = 1.72 \text{ MPa}$, 1800 RPM, $B = 1.0$



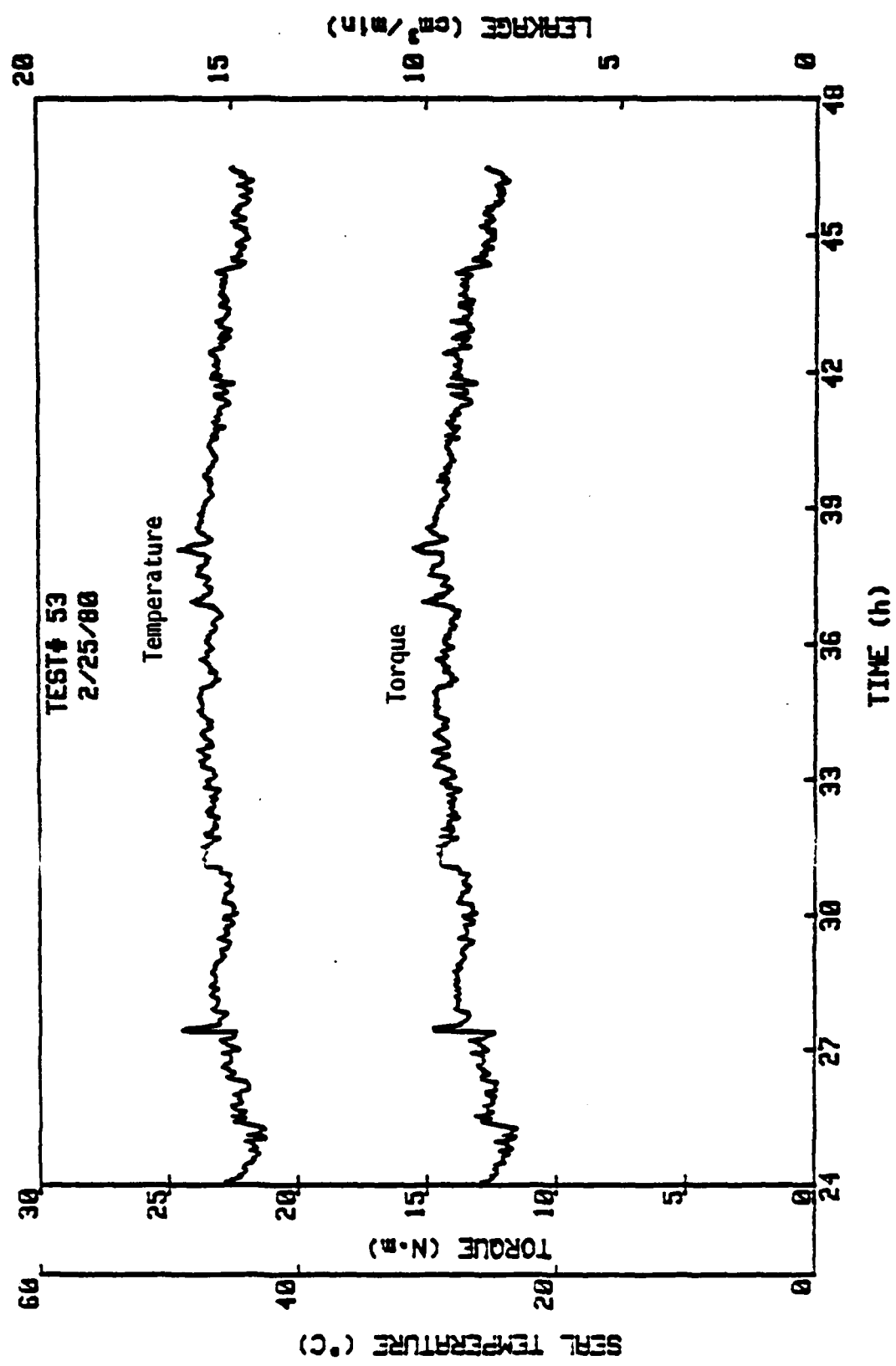
Test #52, $T_{\infty} = 65.6^{\circ}\text{C}$, $P_{\text{H}_2\text{O}} = 1.72 \text{ MPa}$, 1800 RPM, $B = 1.0$

(Continued)

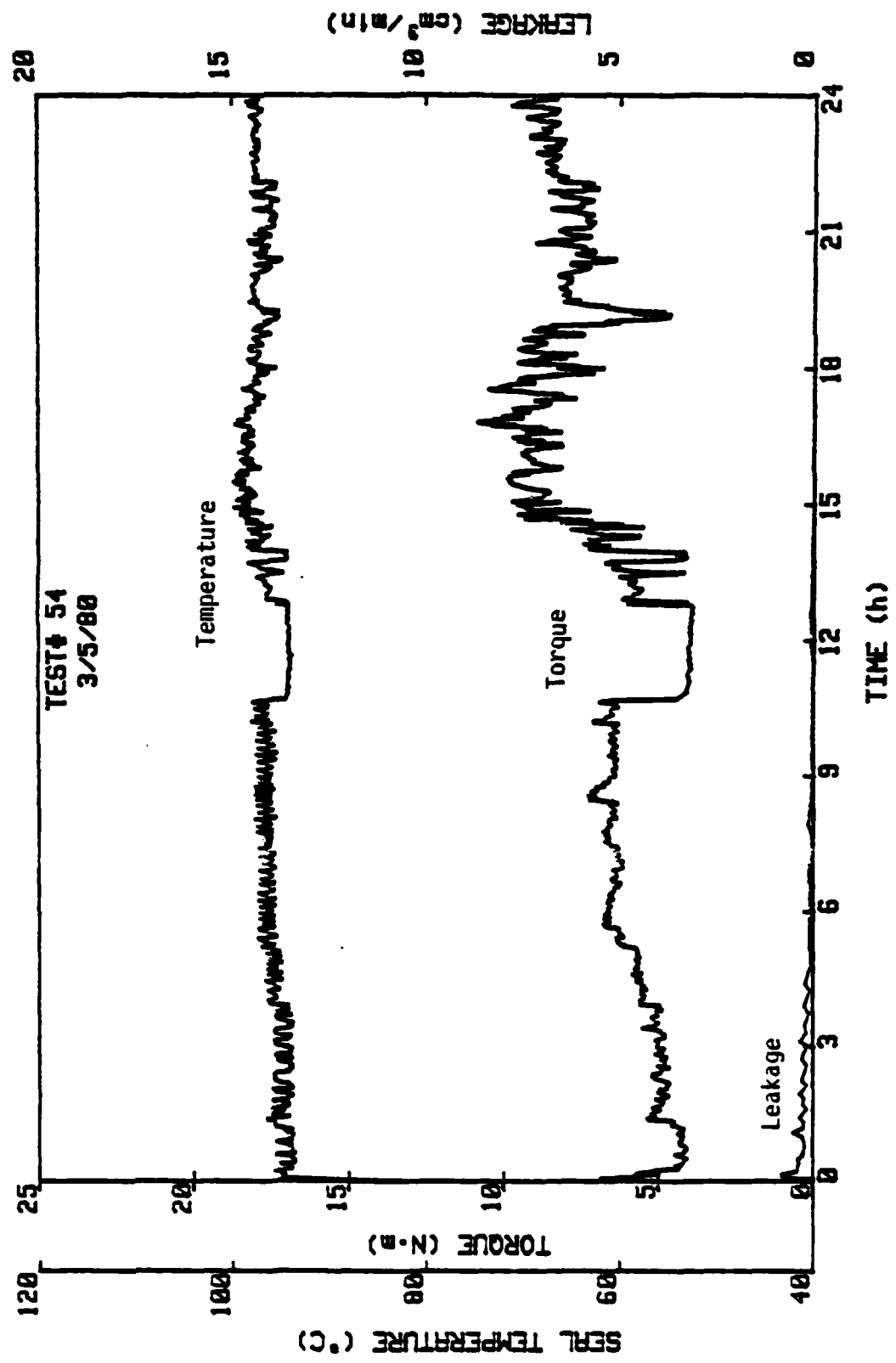




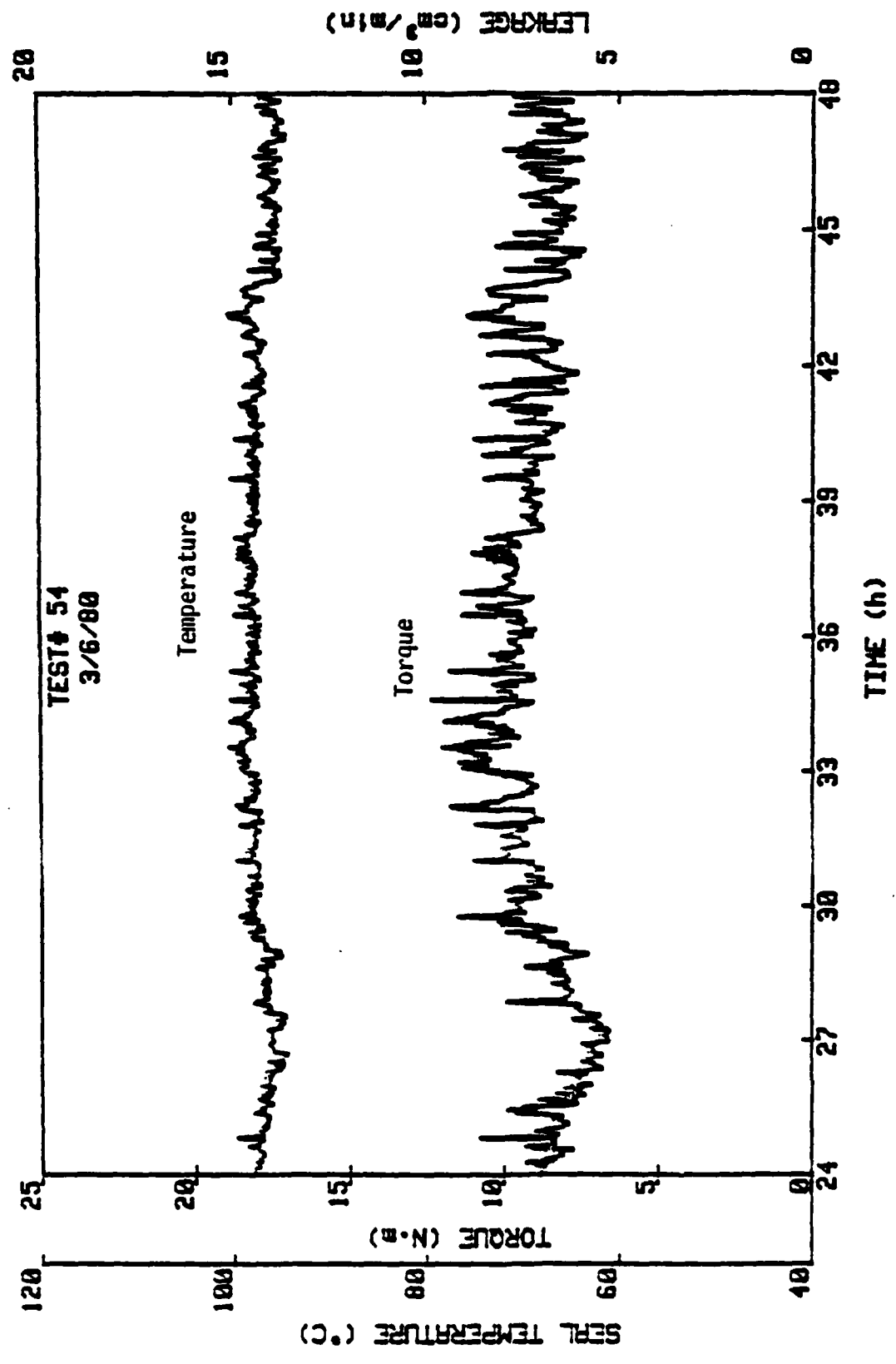
Test #53, $T_{\infty} = 37.8^{\circ}\text{C}$, $p_{\text{H}_2\text{O}} = 1.72 \text{ MPa}$, 1800 RPM, $B = 1.0$



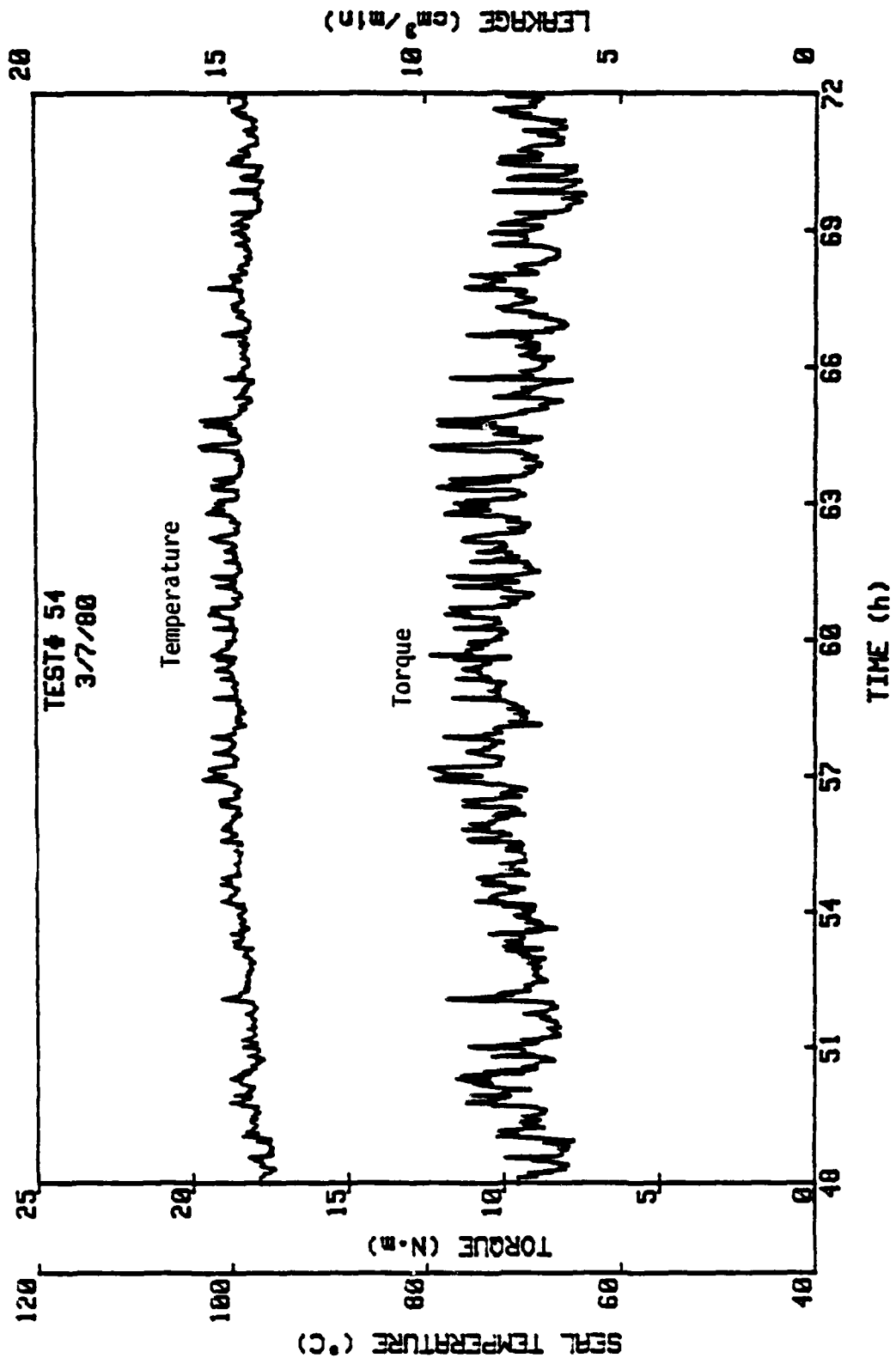
(Continued)



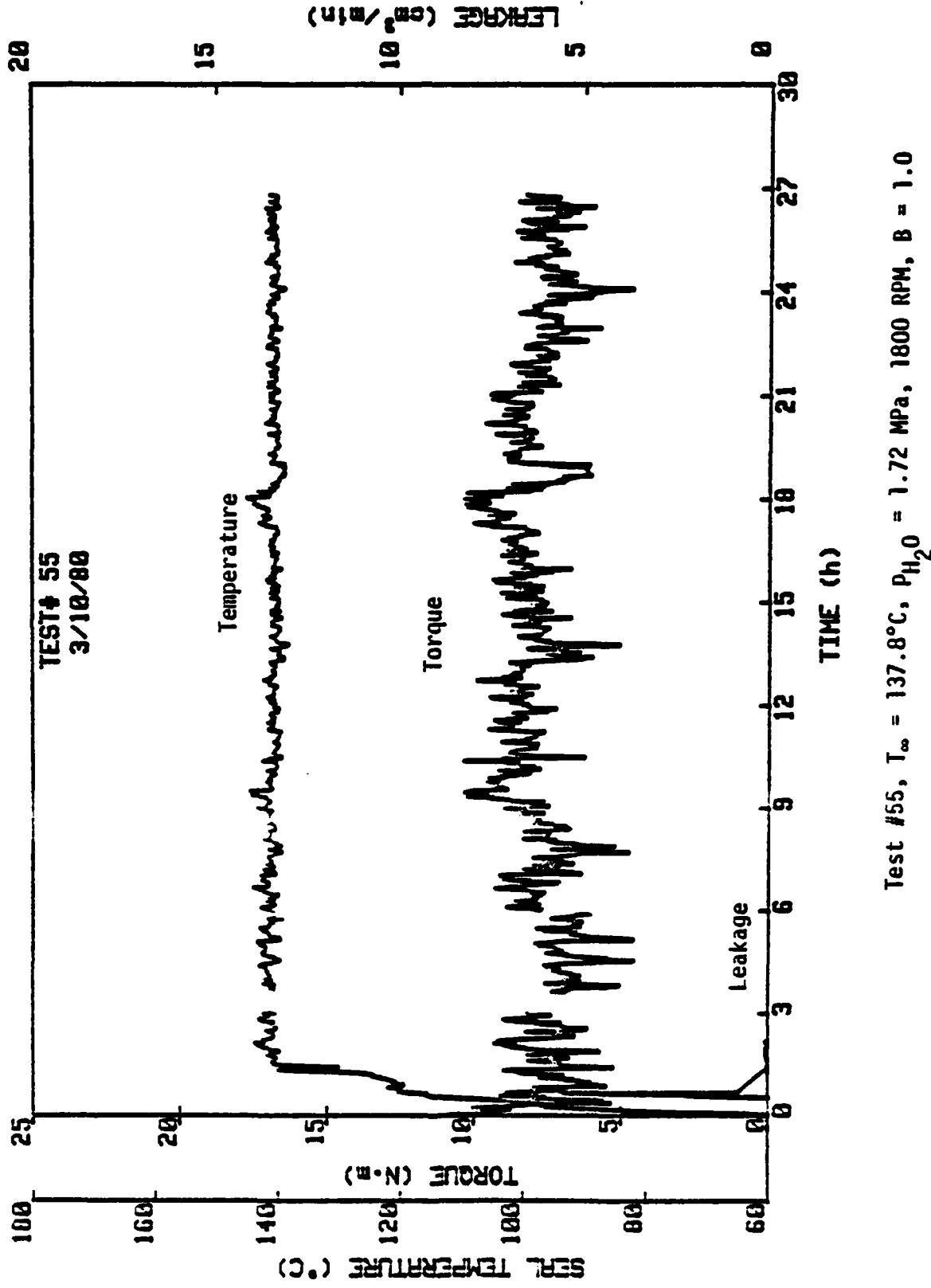
Test #54, $T_{\infty} = 93.3^{\circ}\text{C}$, $P_{\text{H}_2\text{O}} = 1.72 \text{ MPa}$, 1800 RPM, $B = 1.0$



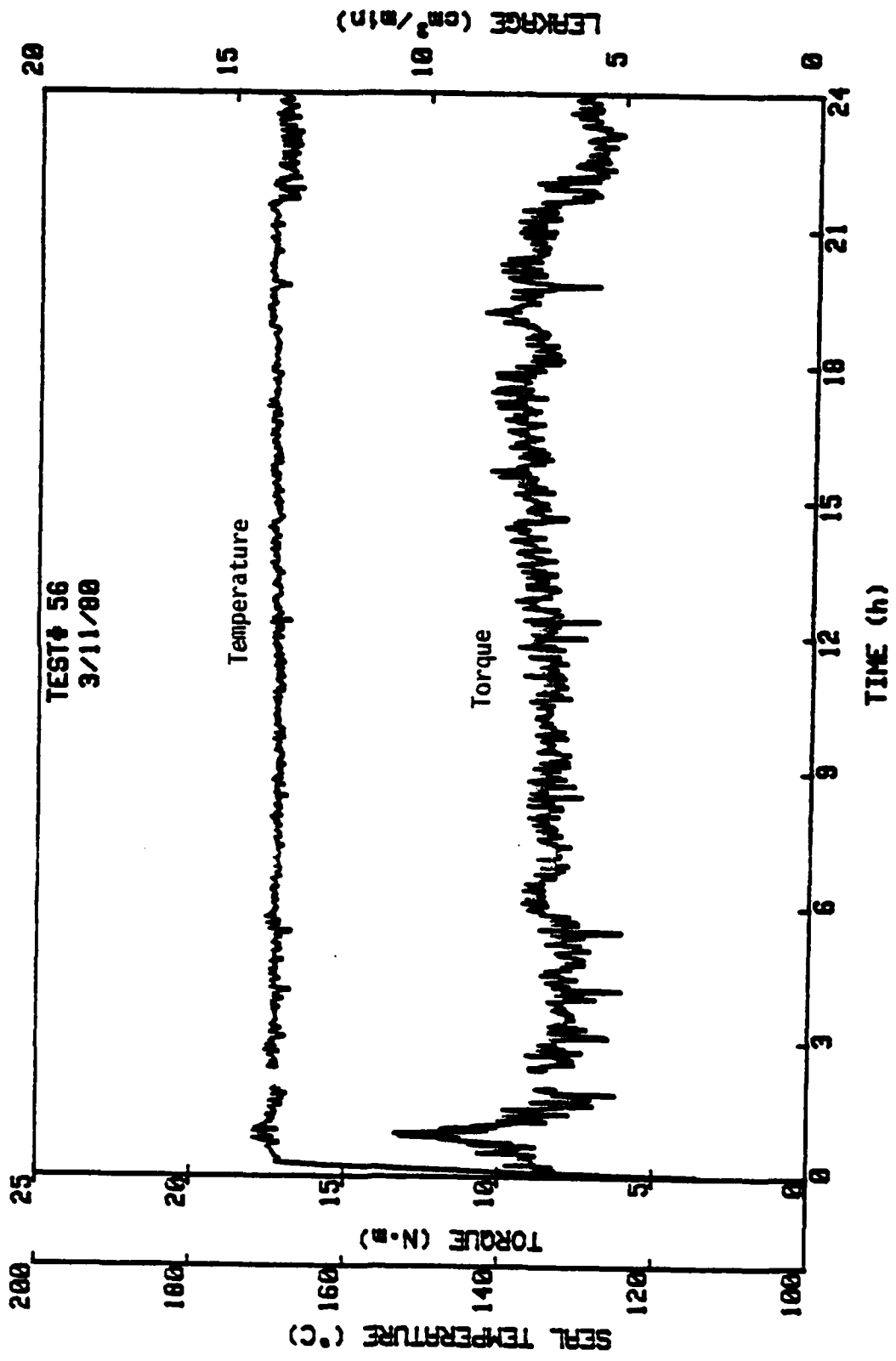
(Continued)



(Continued)

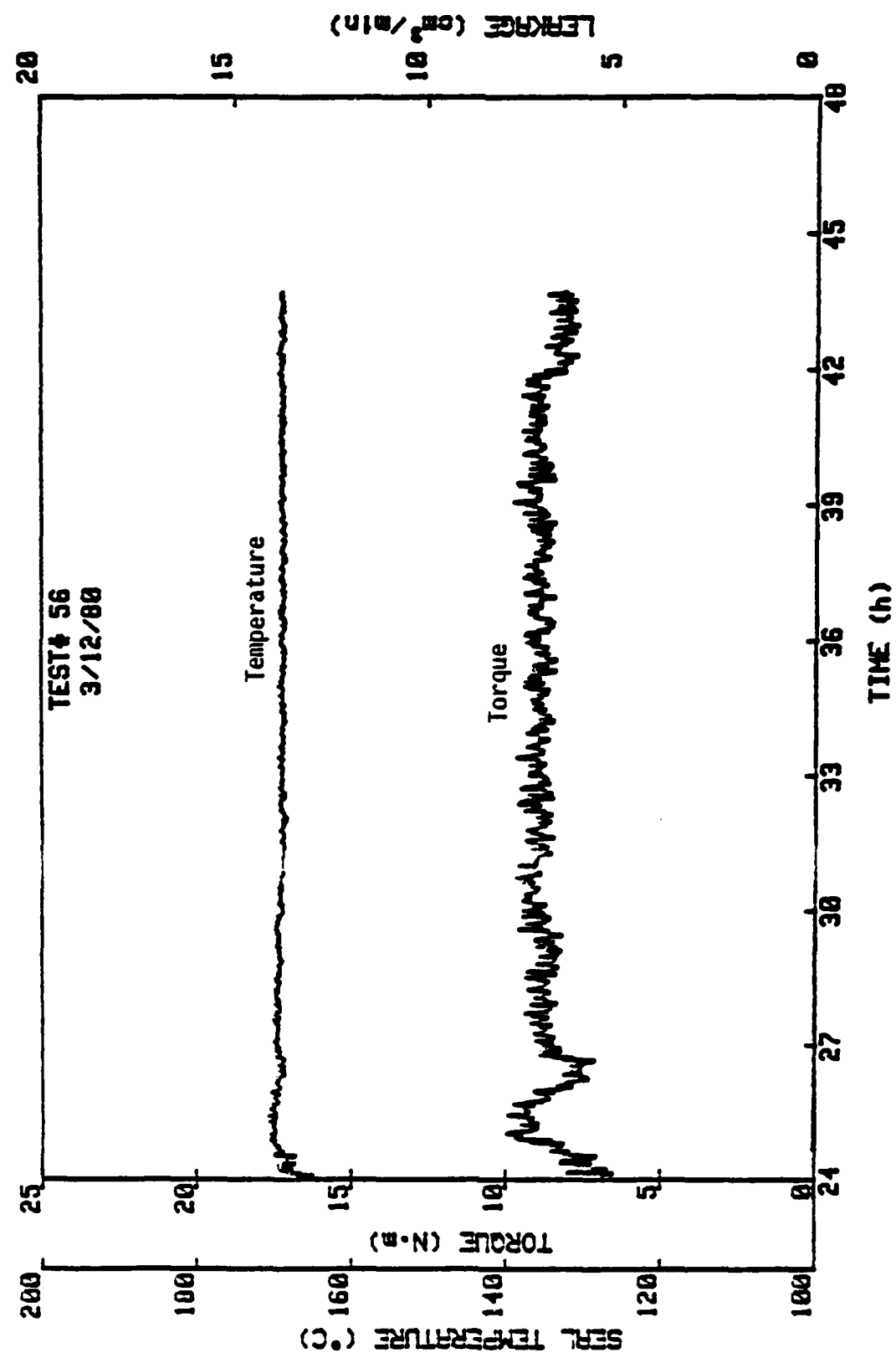


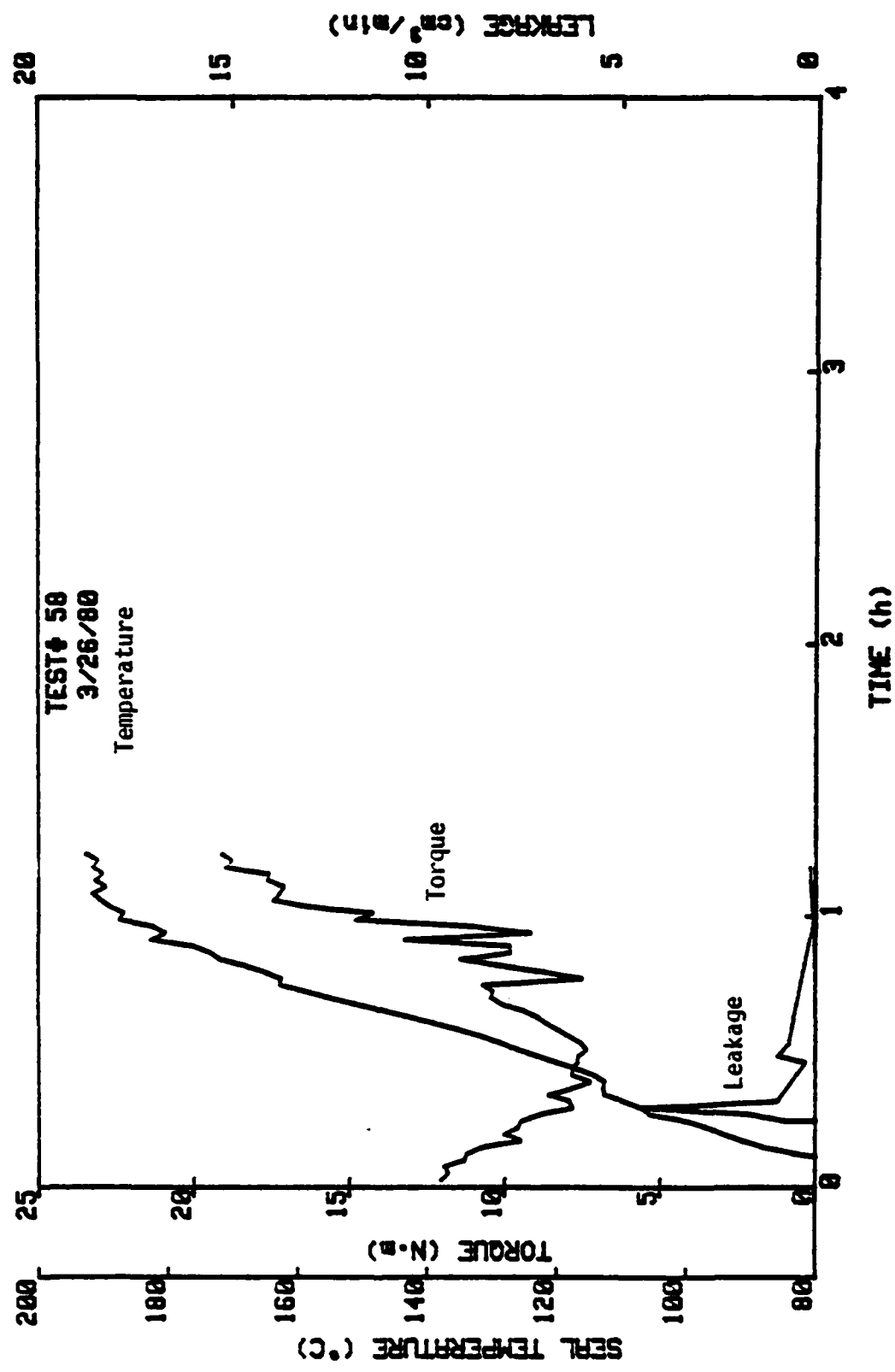
HEWLETT-Packard



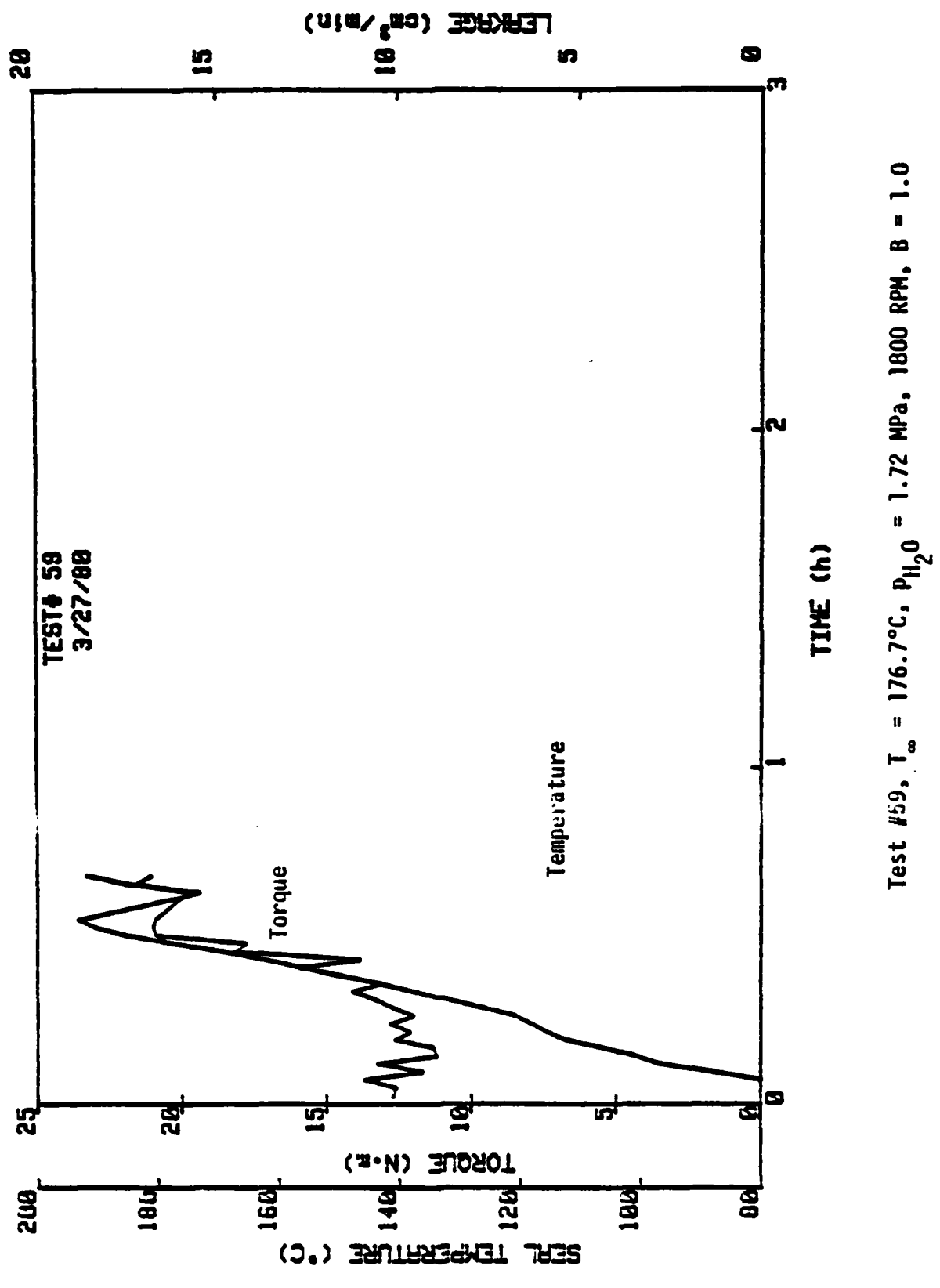
Test #56, $T_{\infty} = 165.6^{\circ}\text{C}$, $p_{\text{H}_2\text{O}} = 1.72 \text{ MPa}$, 1800 RPM, $B = 1.0$

(Continued)



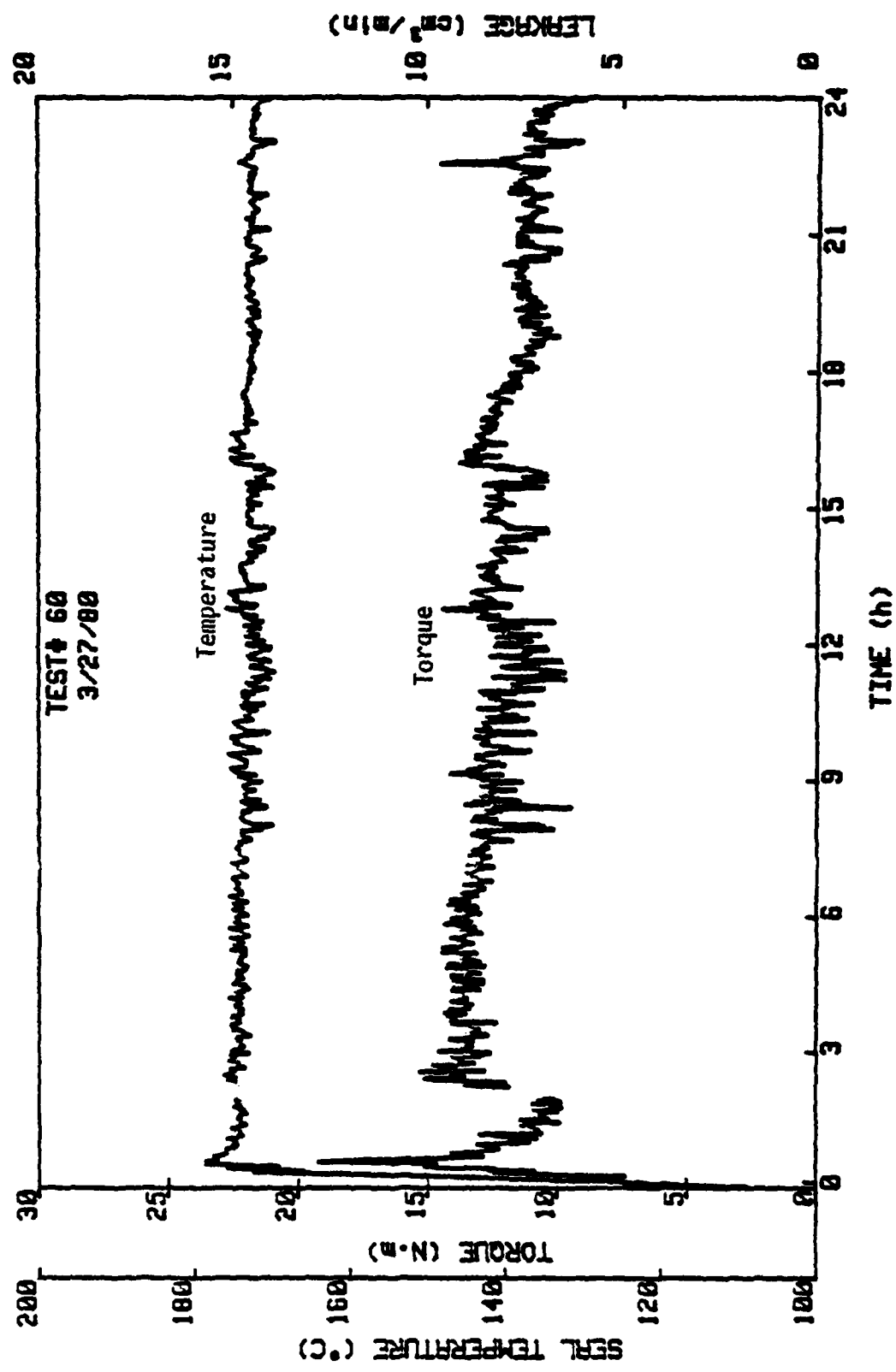


Test #58, $T_{\infty} = 176.7^{\circ}\text{C}$, $p_{\text{H}_2\text{O}} = 1.72 \text{ MPa}$, 1800 RPM, $B = 1.0$



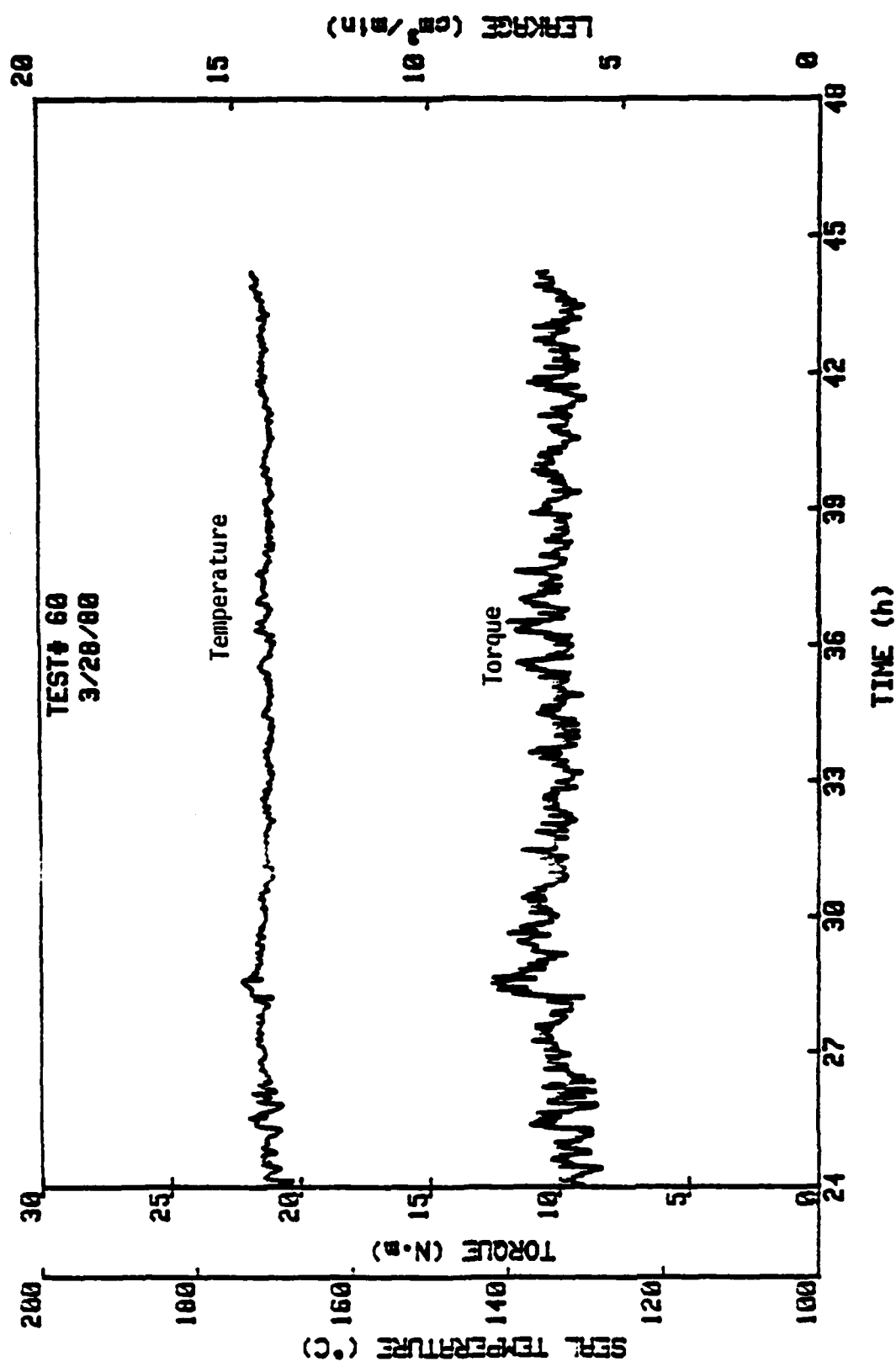
Test #59, $T_{\infty} = 176.7^{\circ}\text{C}$, $P_{\text{H}_2\text{O}} = 1.72 \text{ MPa}$, 1800 RPM, $B = 1.0$

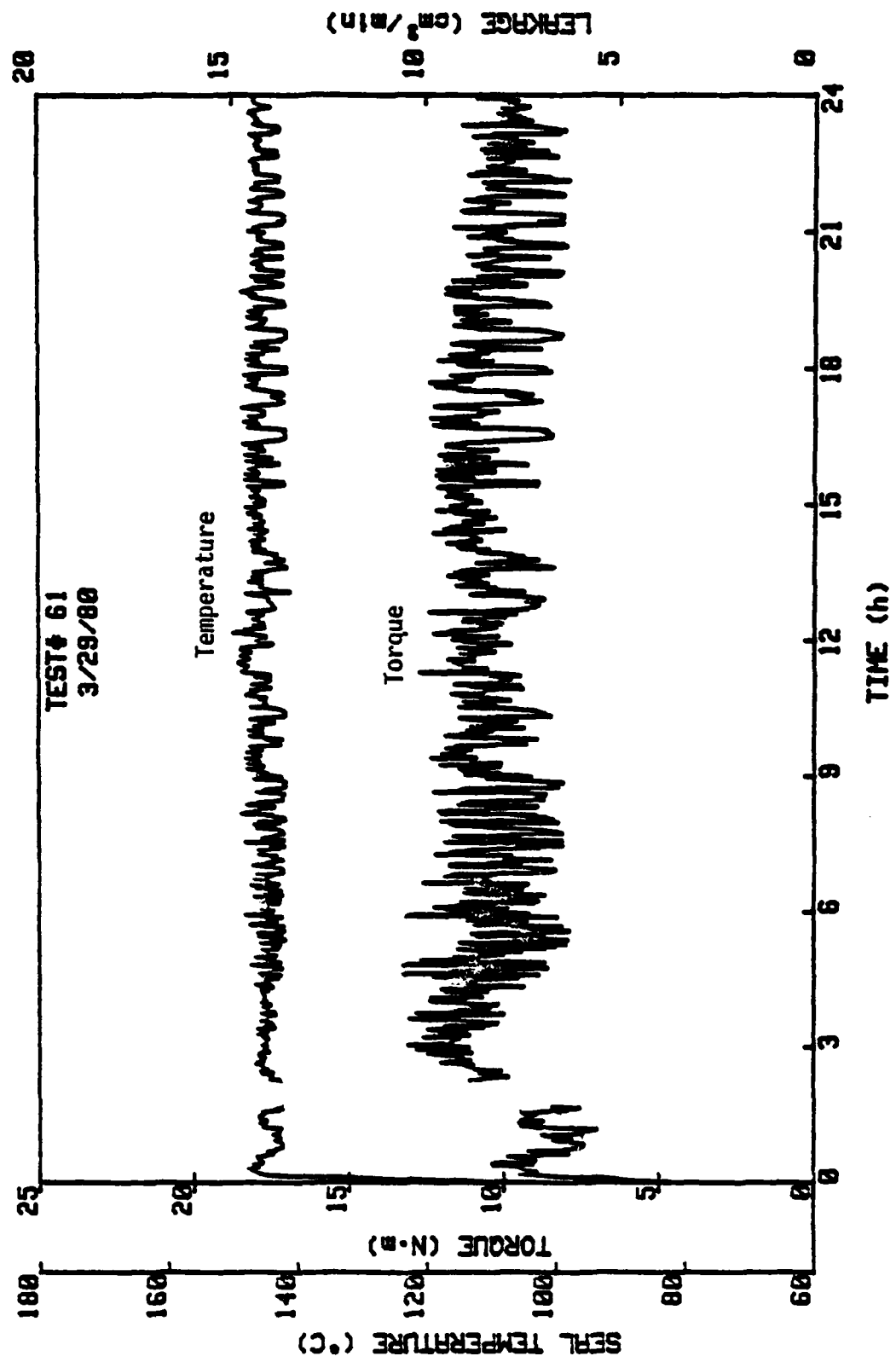
HEWLETT-Packard



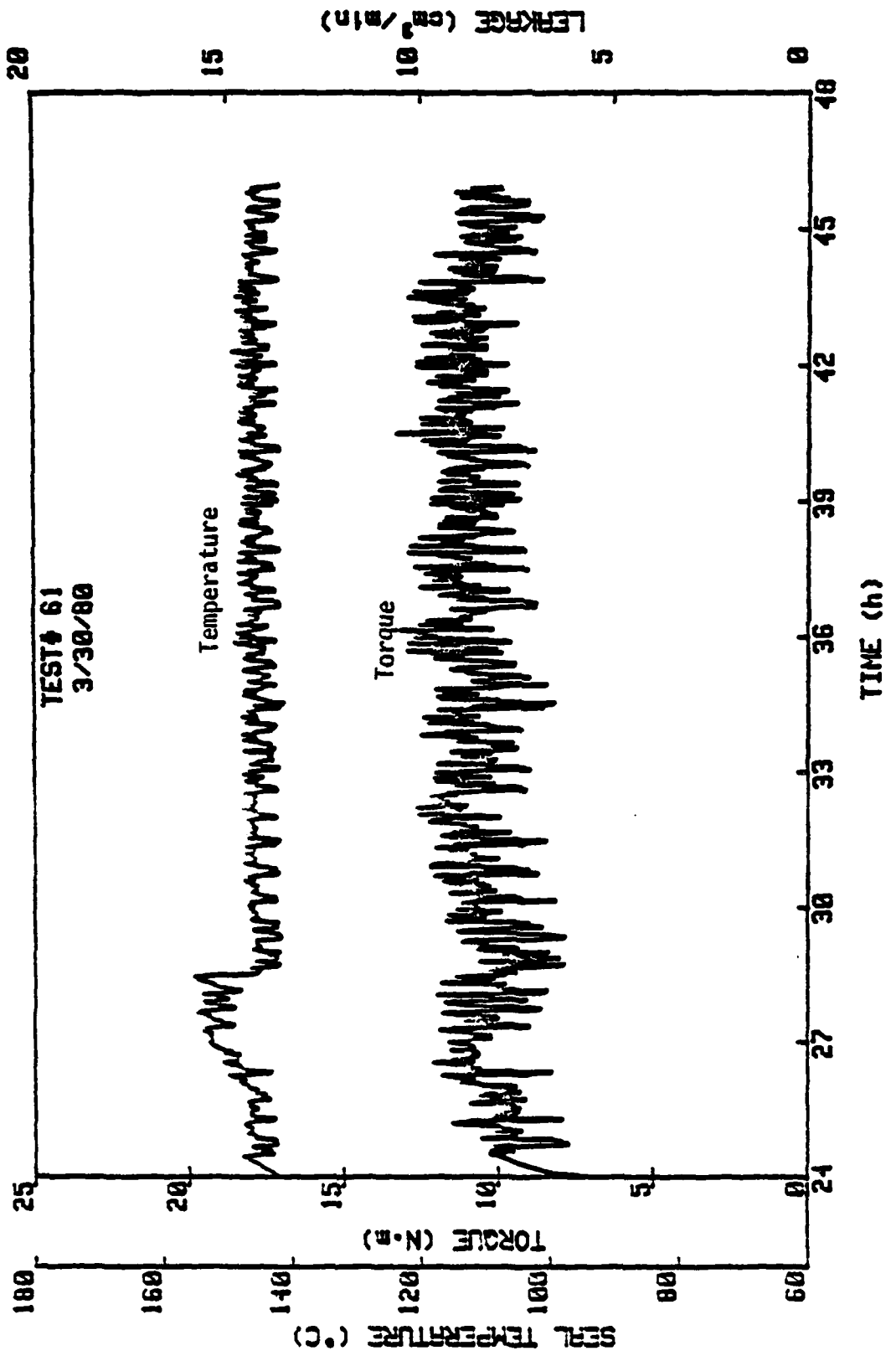
Test #60, $T_{\infty} = 165.6^{\circ}\text{C}$, $p_{\text{H}_2\text{O}} = 1.72 \text{ MPa}$, 1800 RPM, $\delta = 1.0$

(Continued)

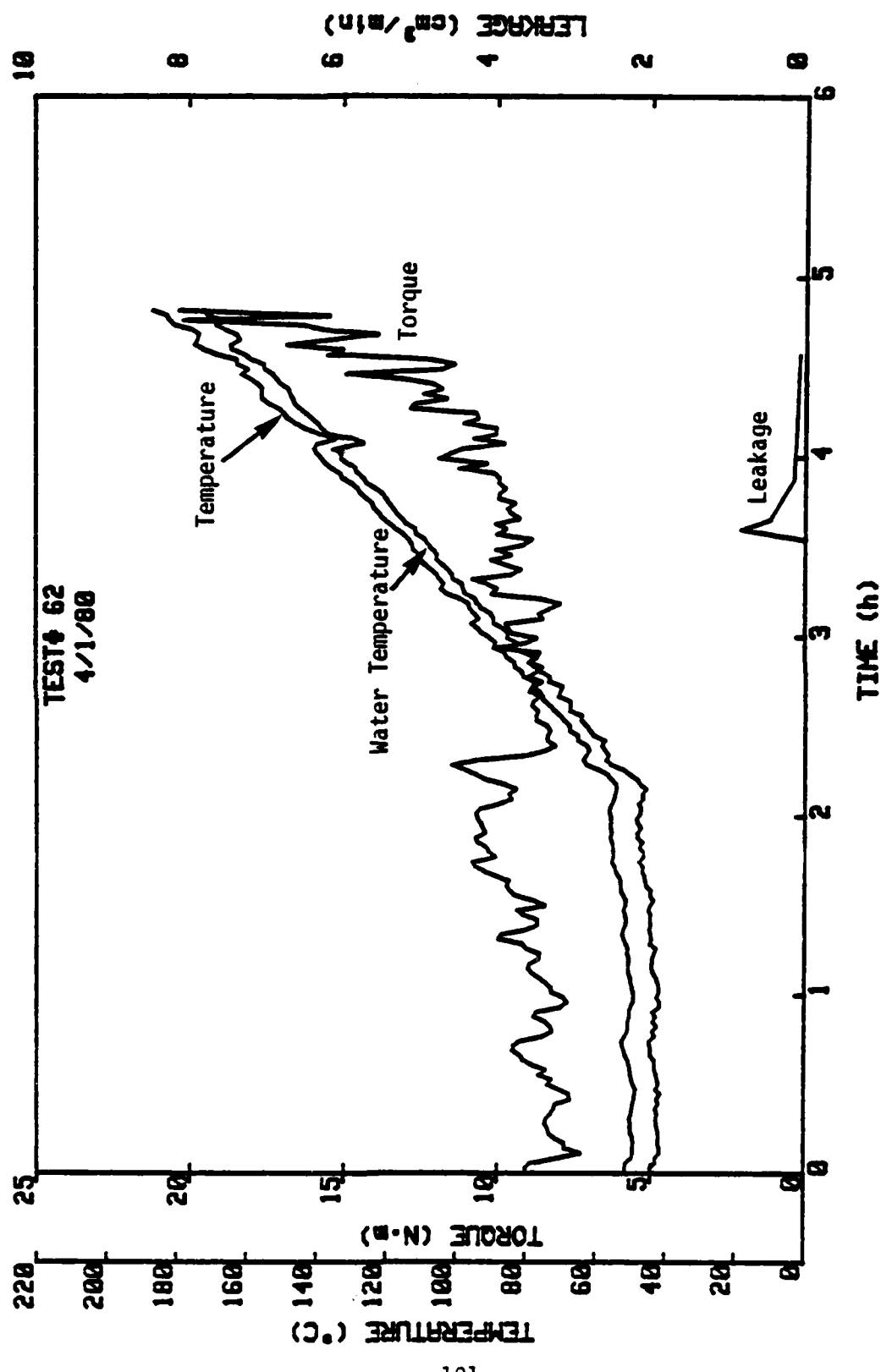




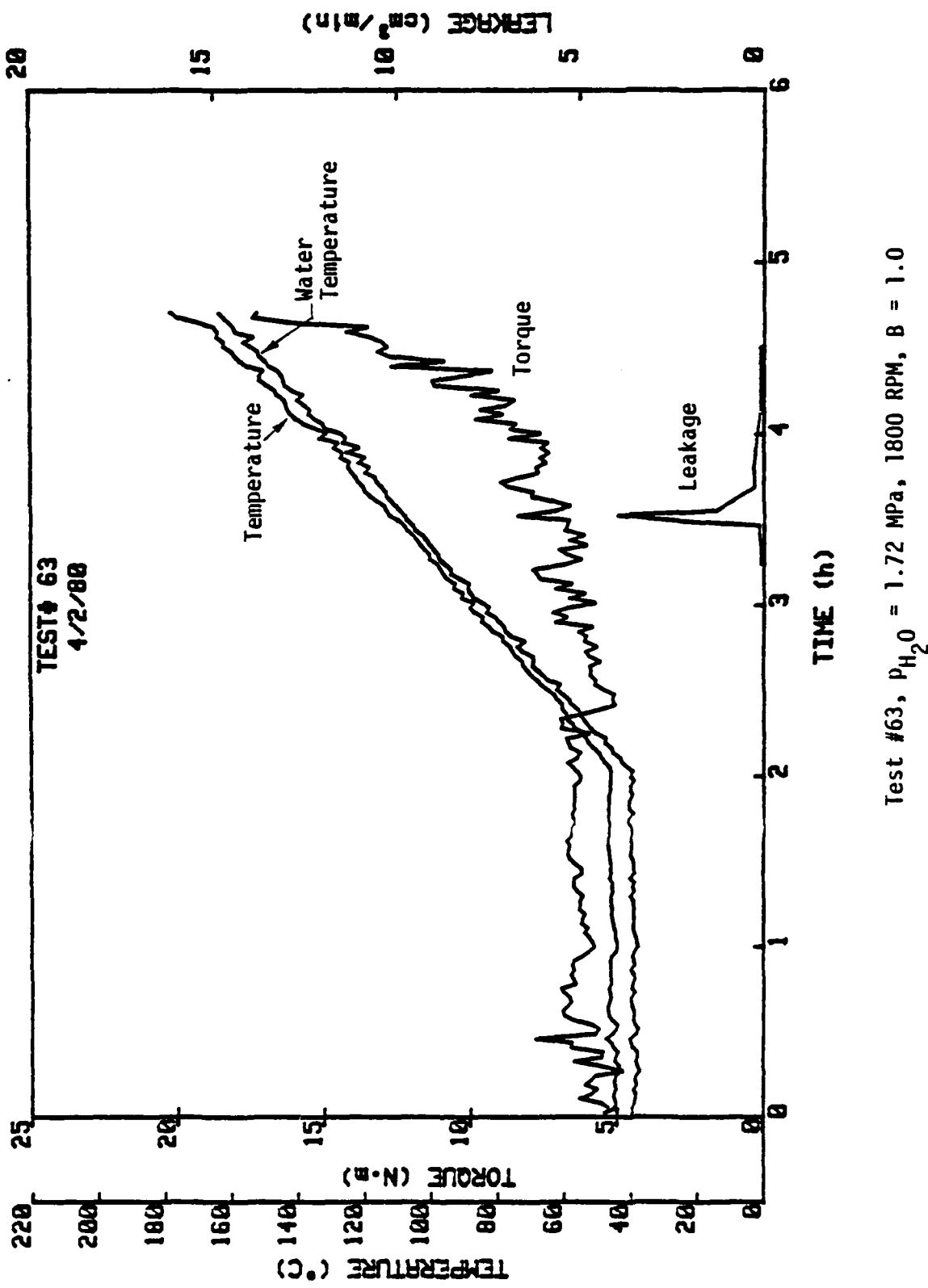
Test #61, $T_{\infty} = 137.8^{\circ}\text{C}$, $P_{\text{H}_2\text{O}} = 1.72 \text{ MPa}$, 1800 RPM, $B = 1.0$

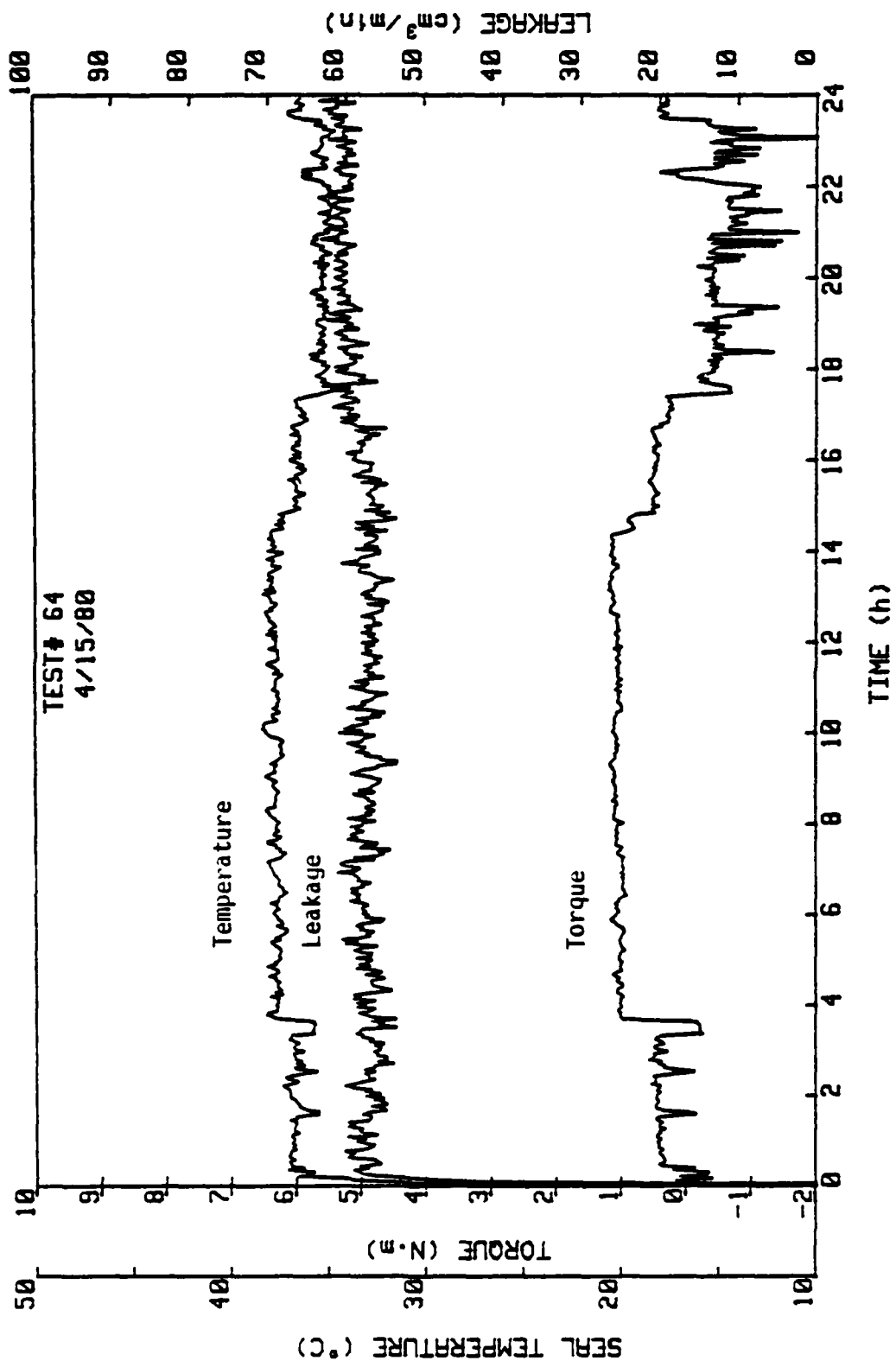


(Continued)

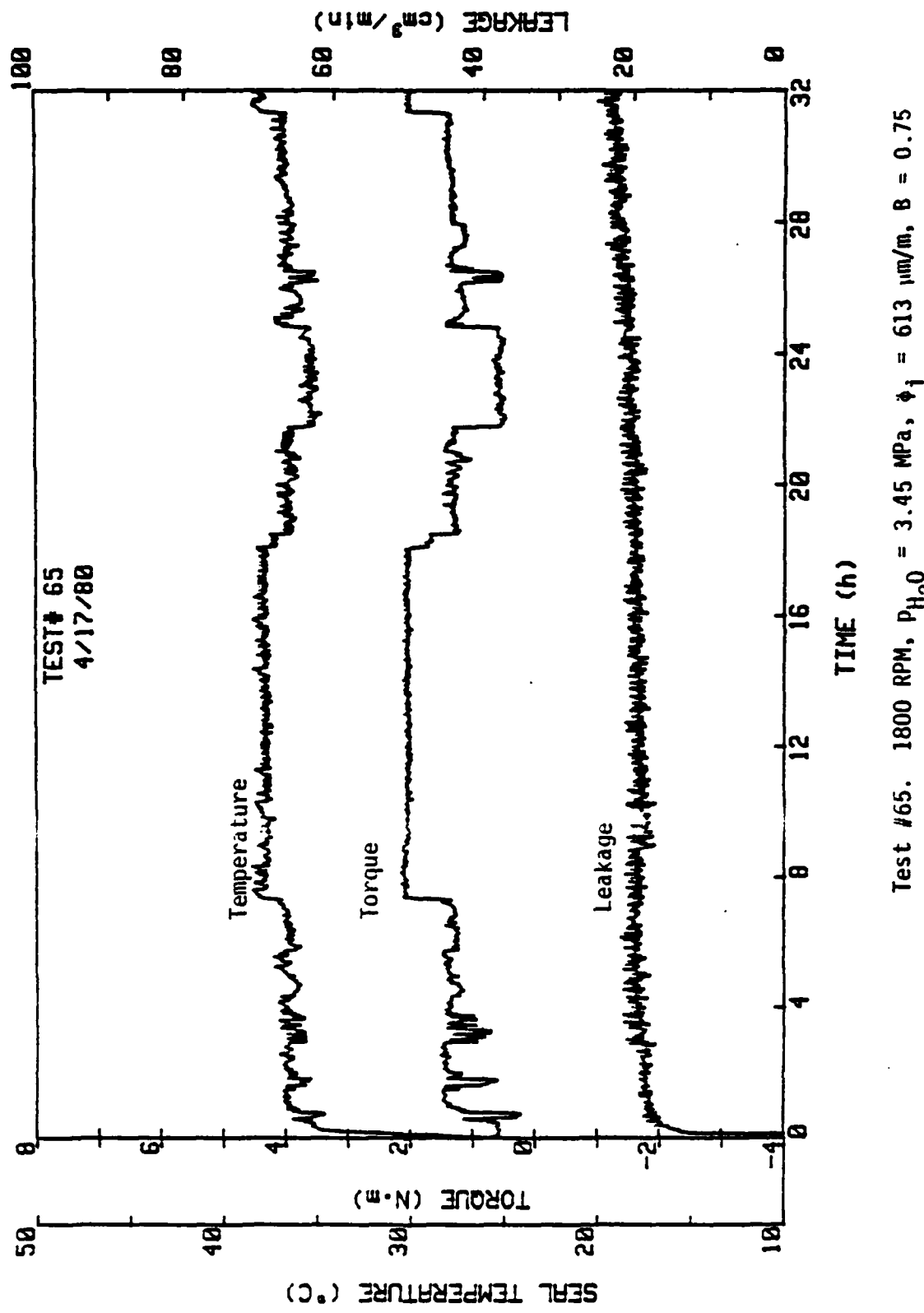


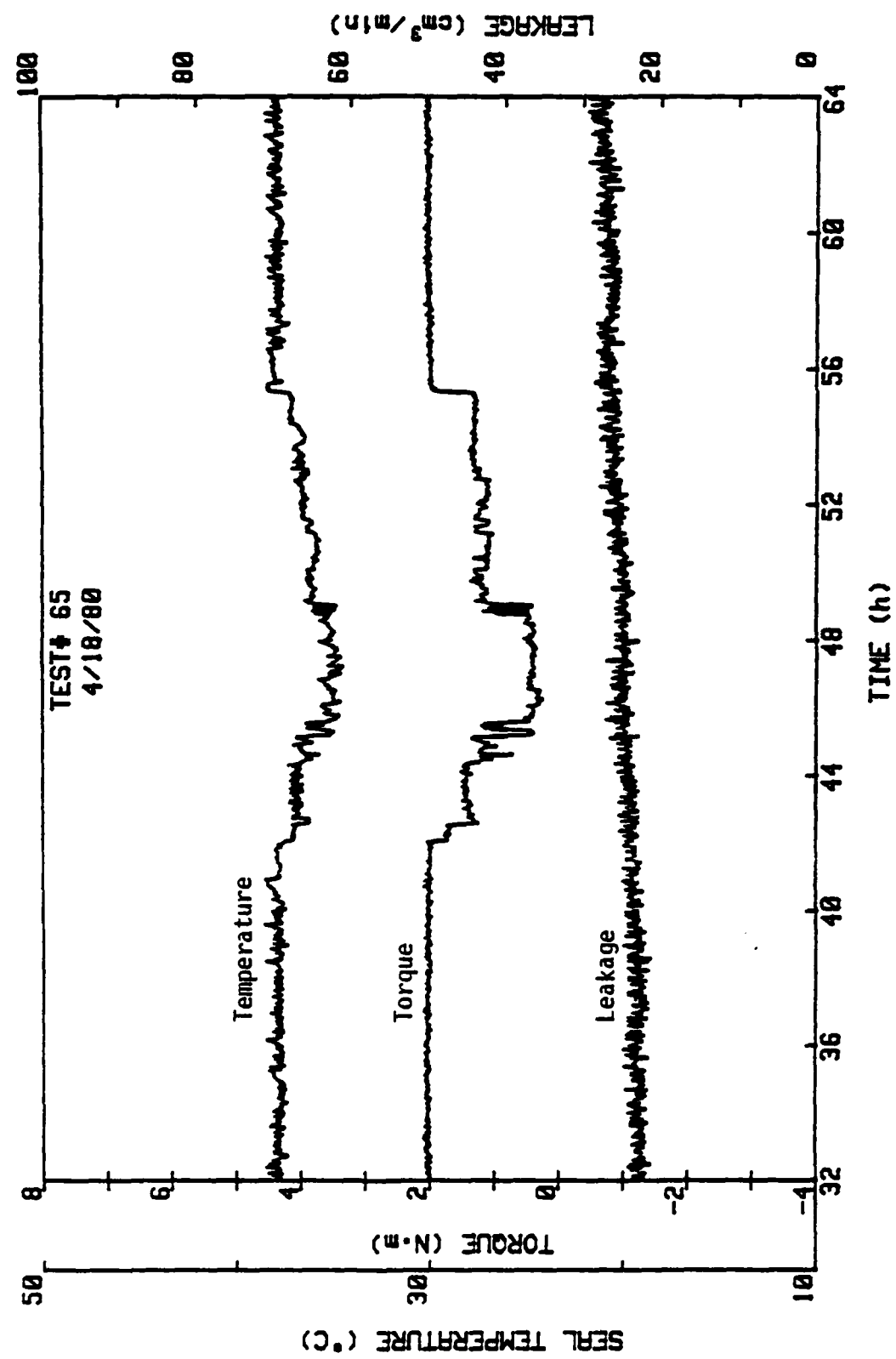
Test #62, $p_{\text{H}_2\text{O}} = 1.72 \text{ MPa}$, 1800 RPM, $B = 1.0$



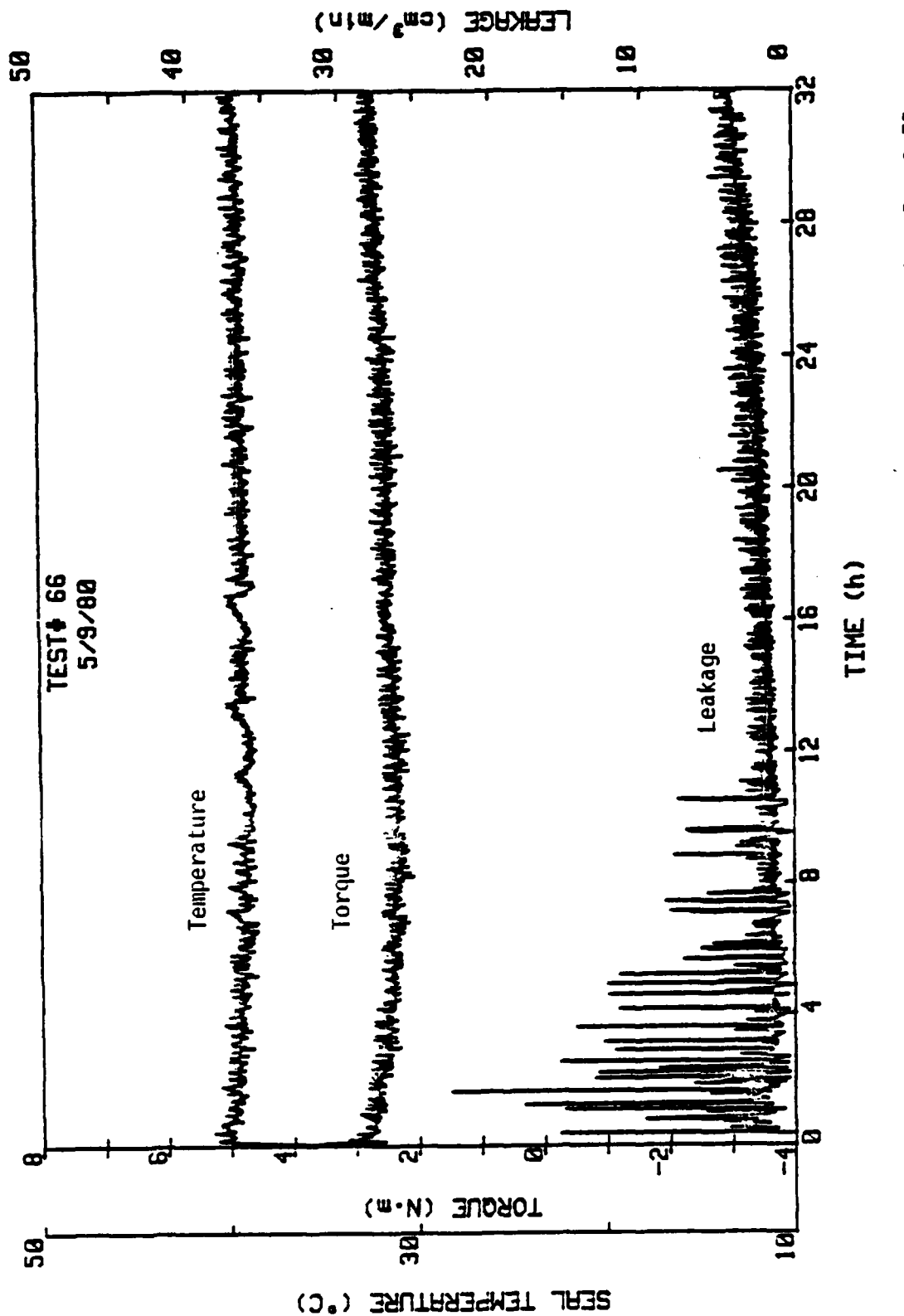


Test #64. 1800 RPM, $p_{\text{H}_2\text{O}} = 3.45 \text{ MPa}$, $\phi_1 = 1013 \mu\text{m/m}$, $B = 0.75$

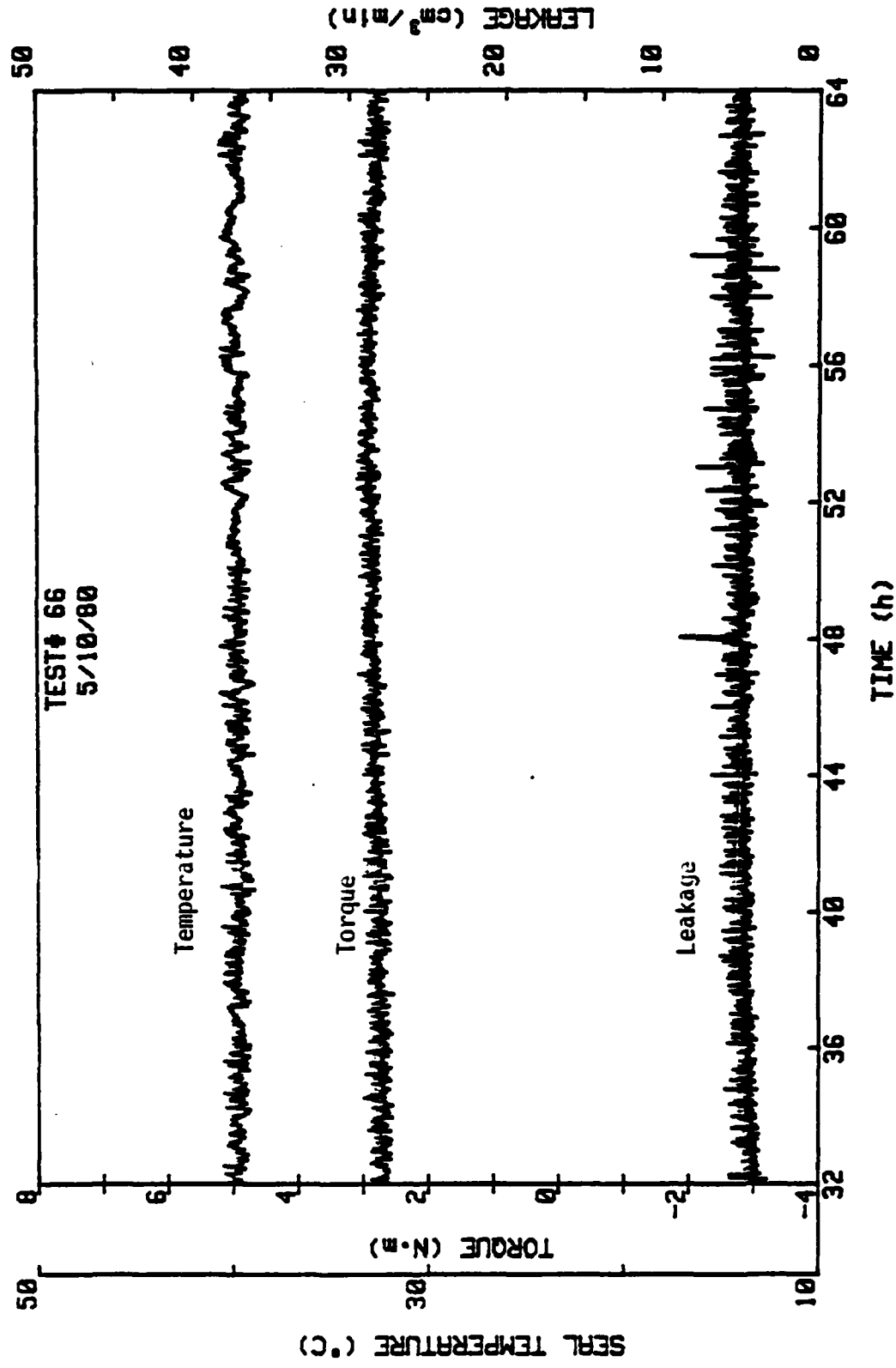




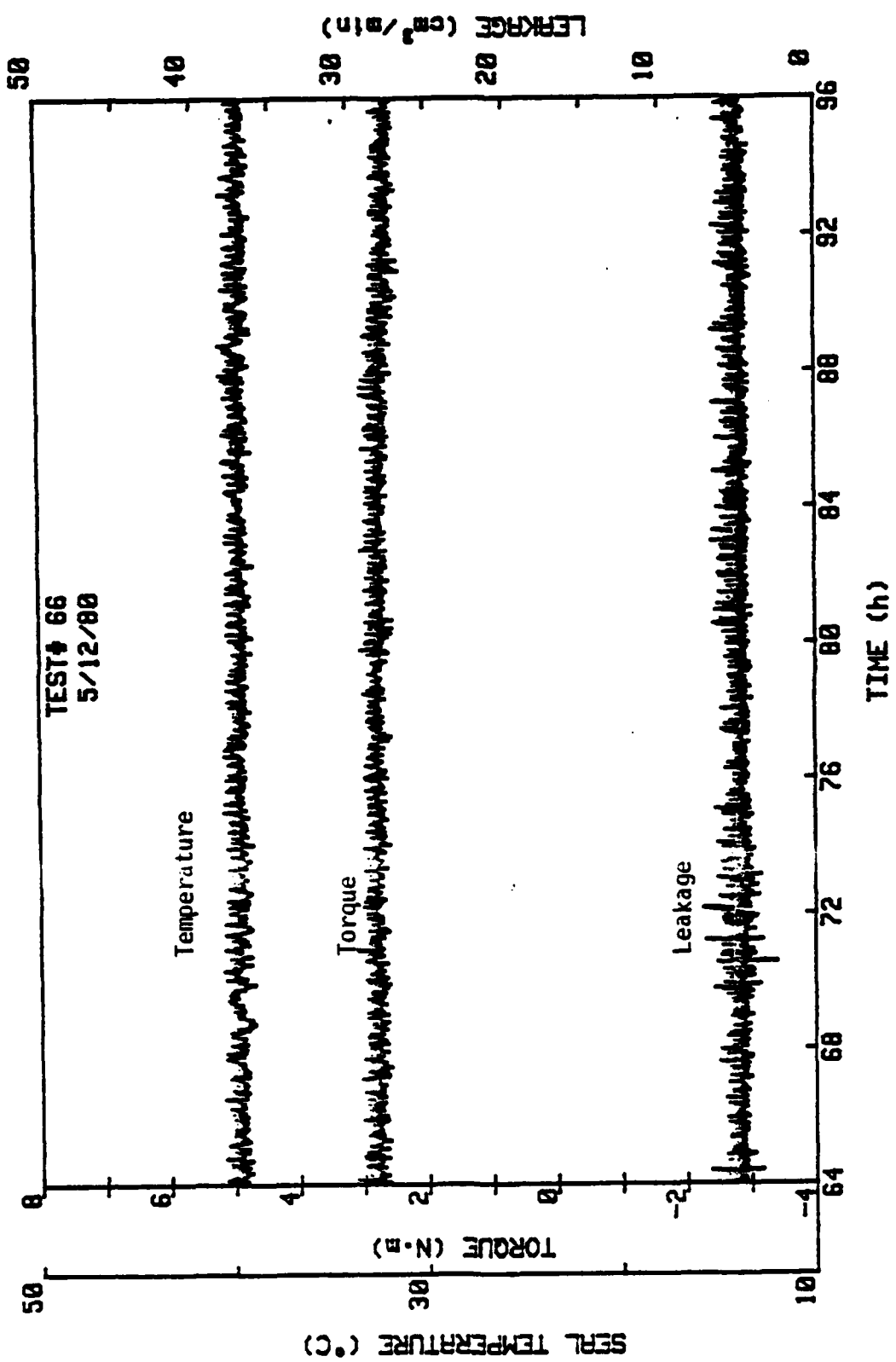
(continued)



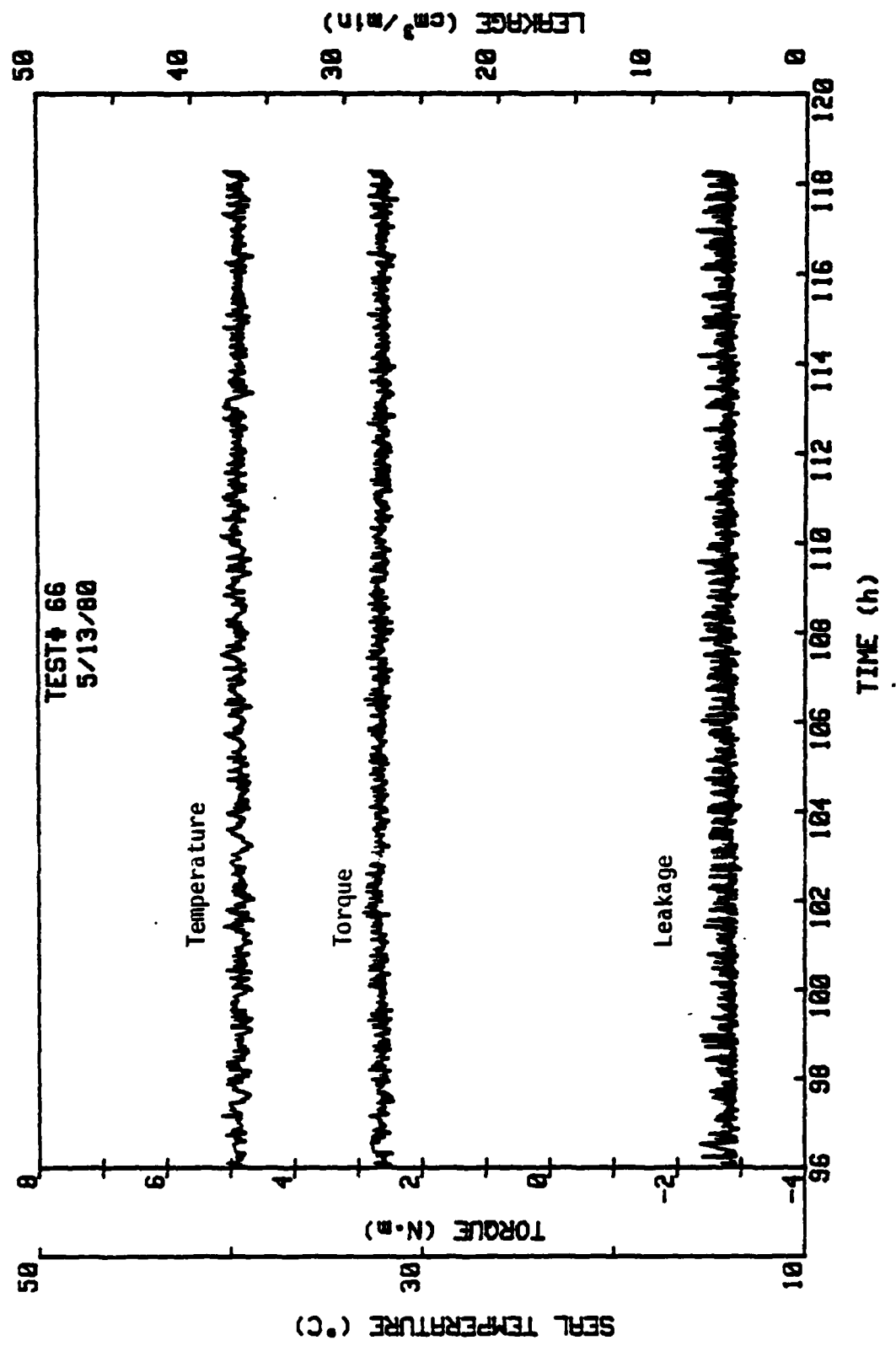
Test #66. 1800 RPM, $p_{H_2O} = 3.45 \text{ MPa}$, $\phi_i = 48 \mu\text{m/m}$, $B = 0.75$



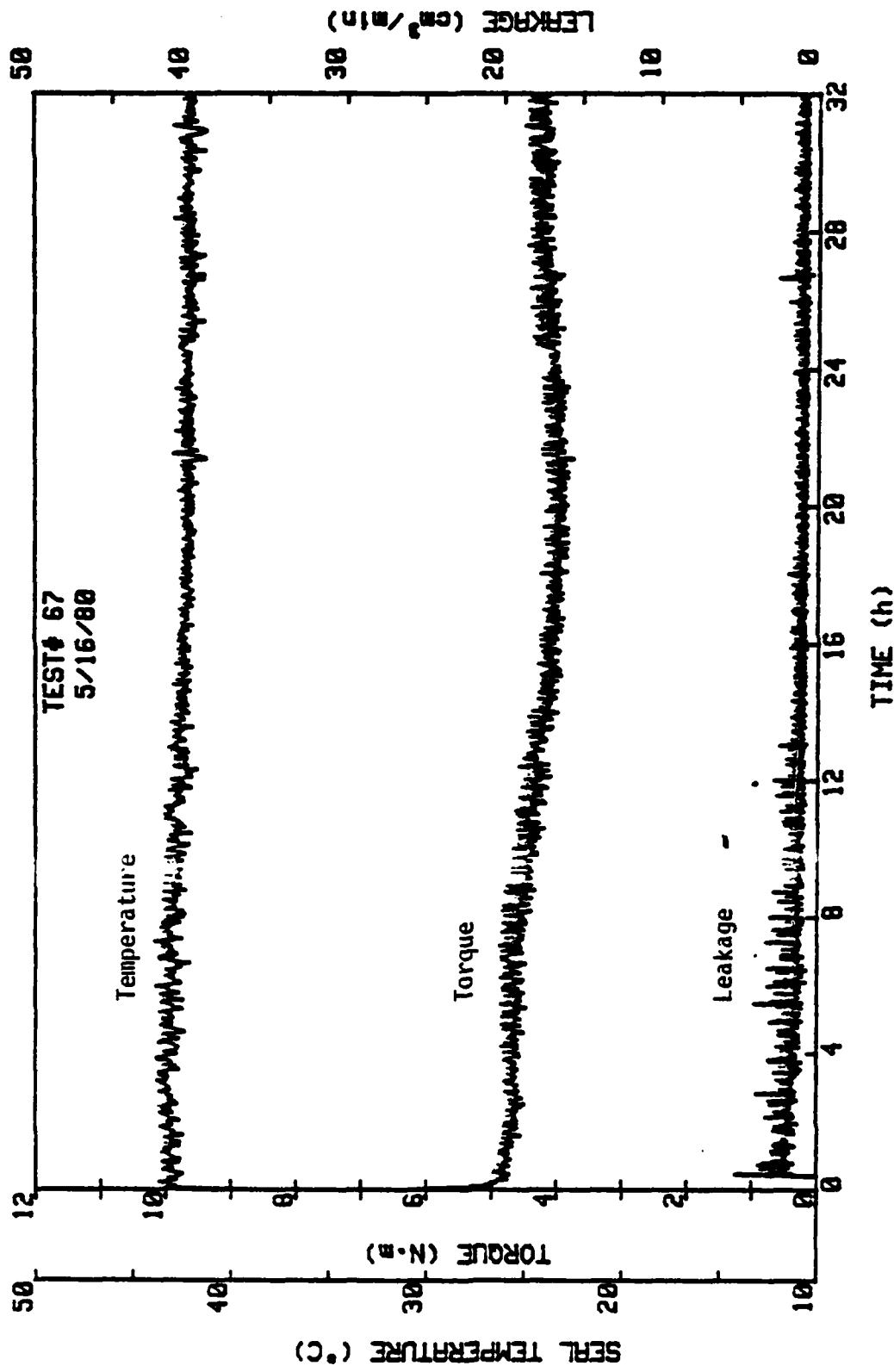
(continued)



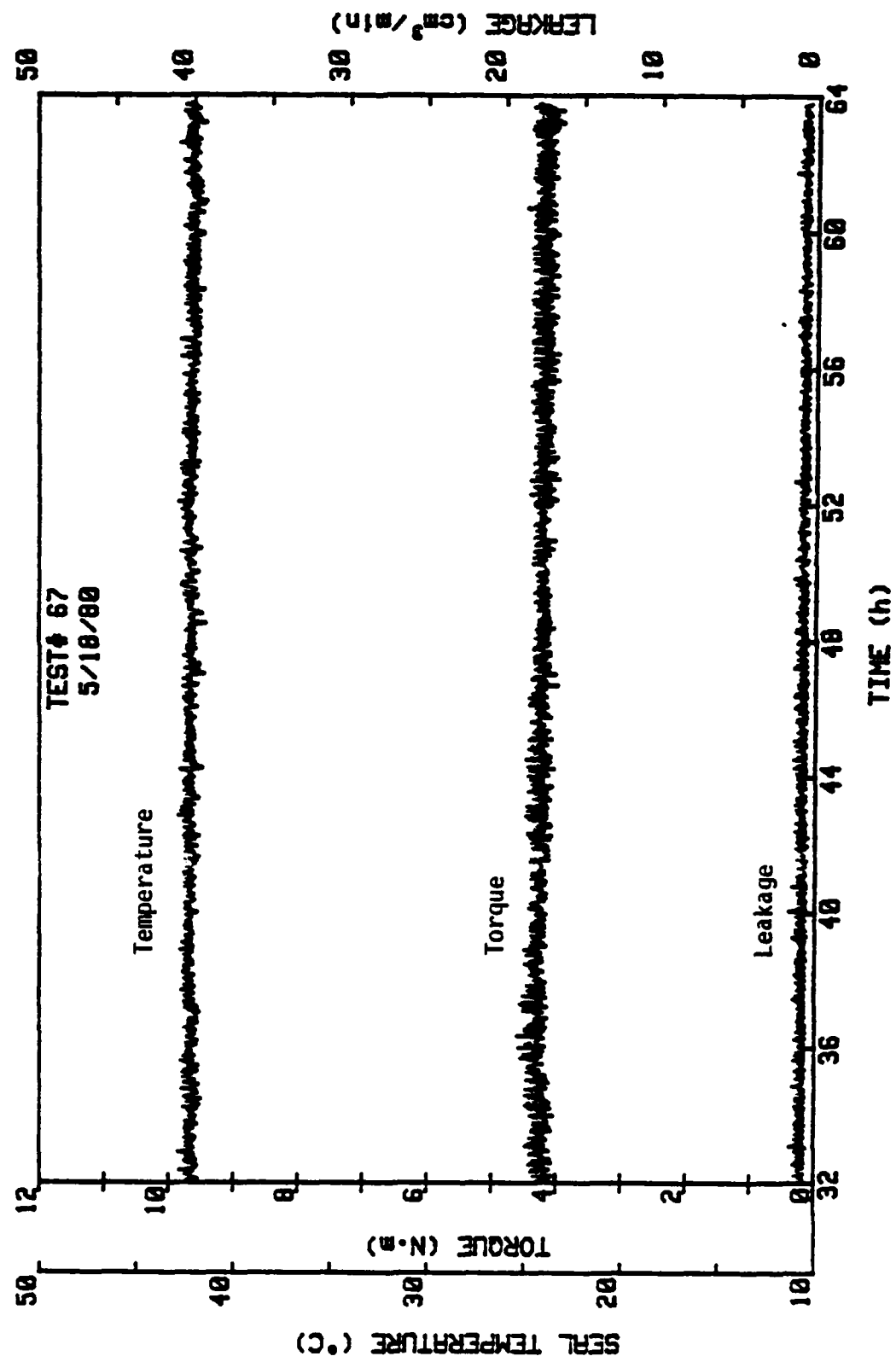
(continued)



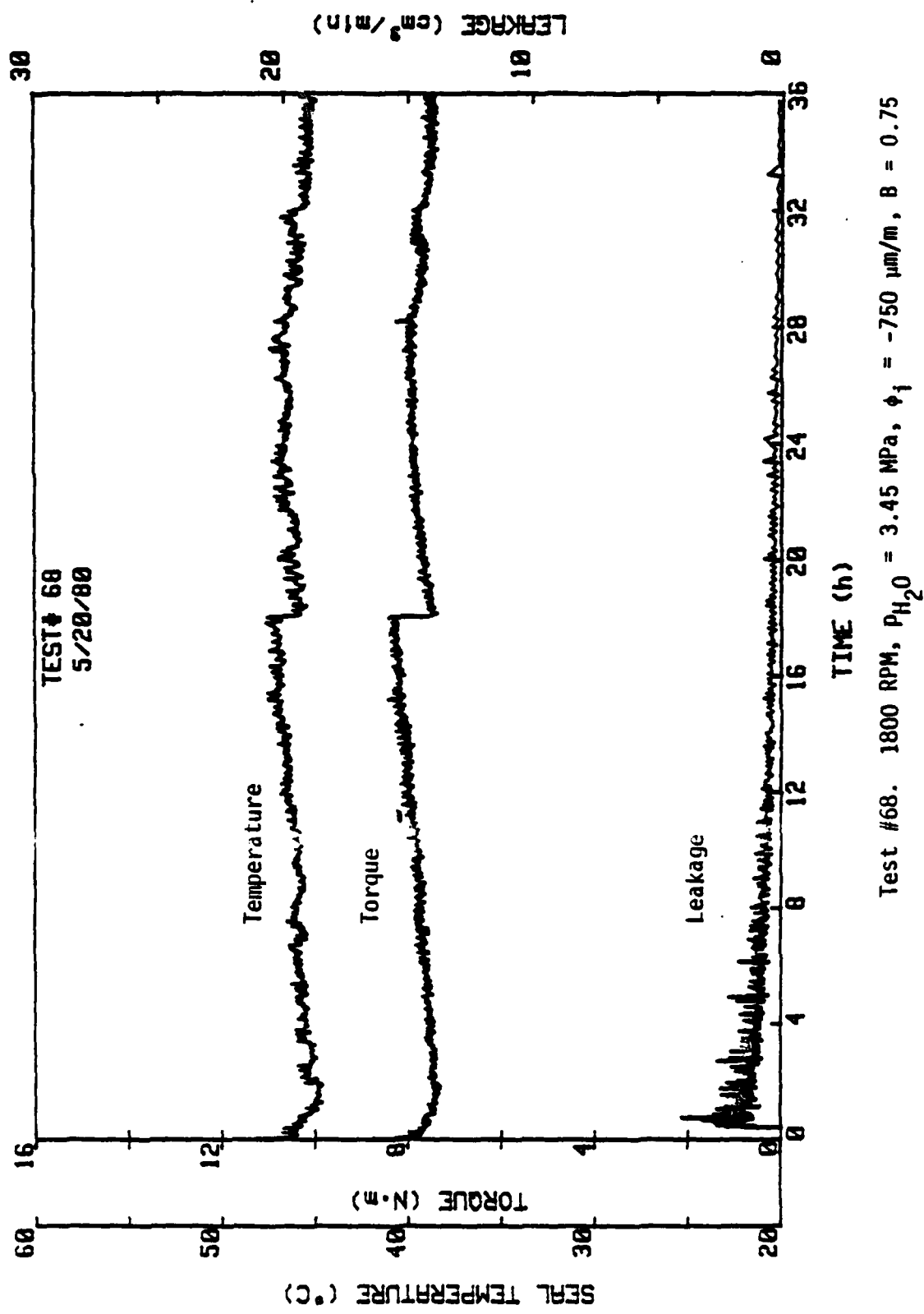
(continued)

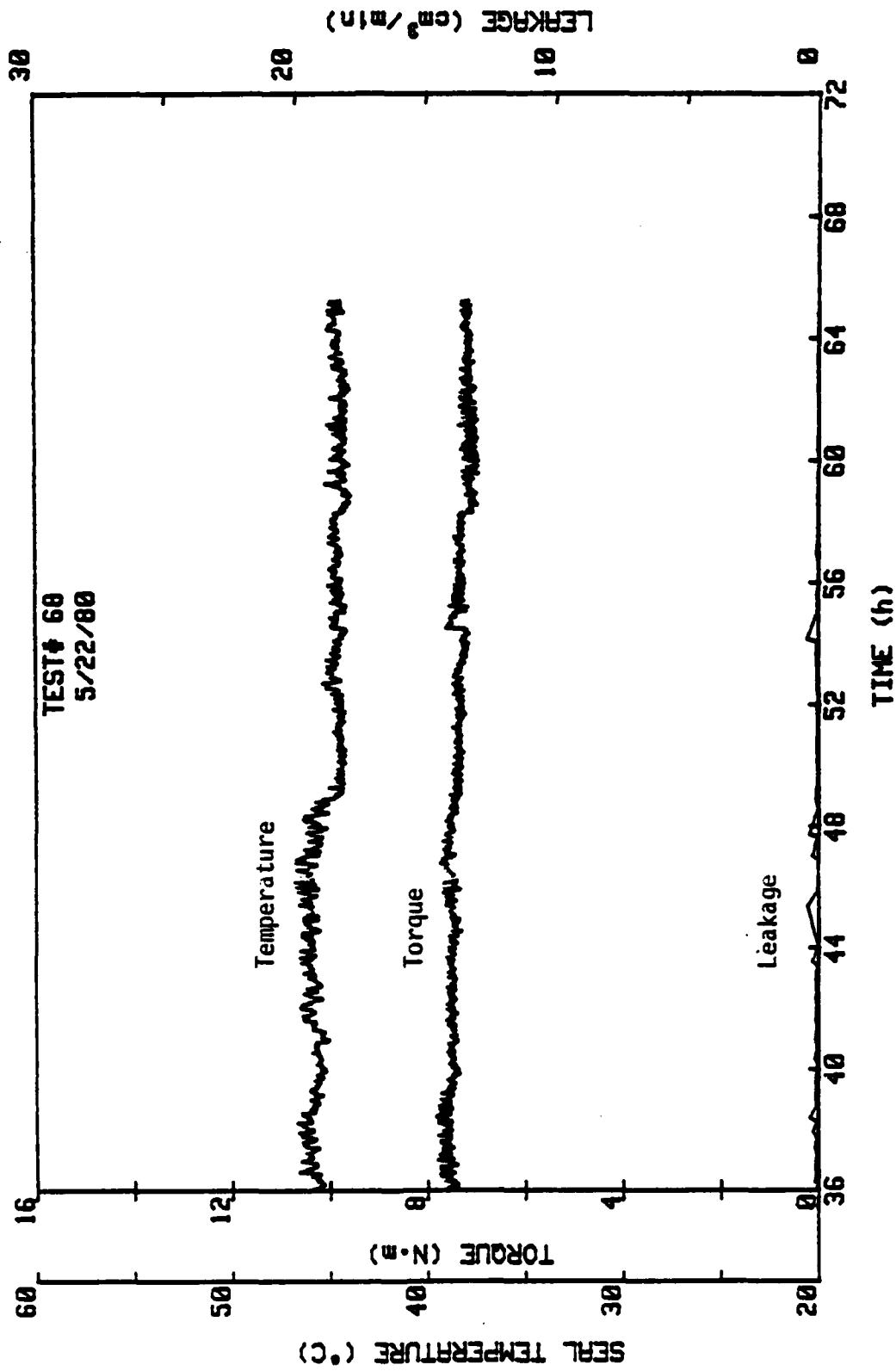


Test #67. 1800 RPM, $p_{H_2O} = 3.45$ MPa, $\phi_1 = -320 \mu\text{m/m}$, $B = 0.75$

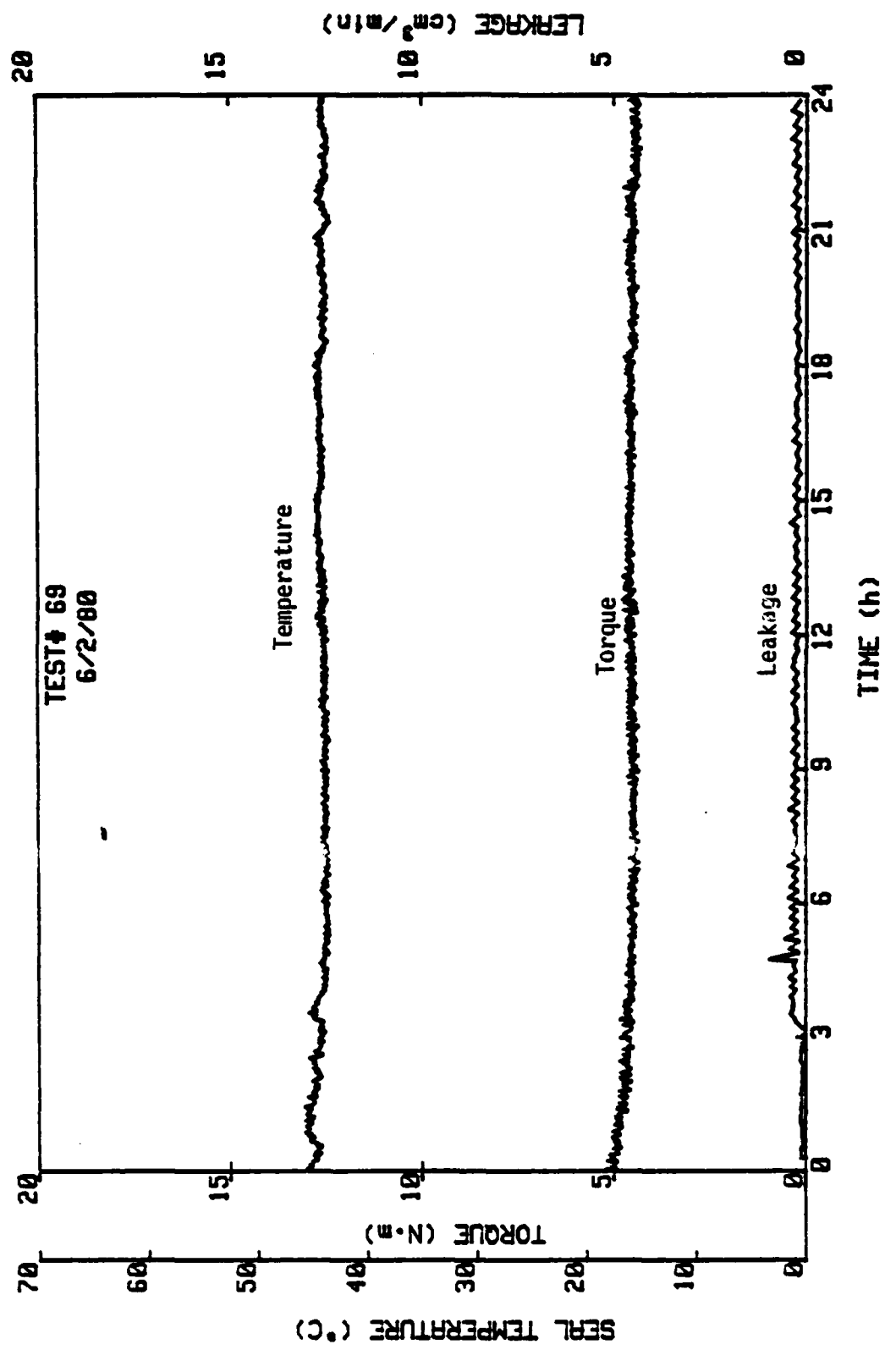


(continued)

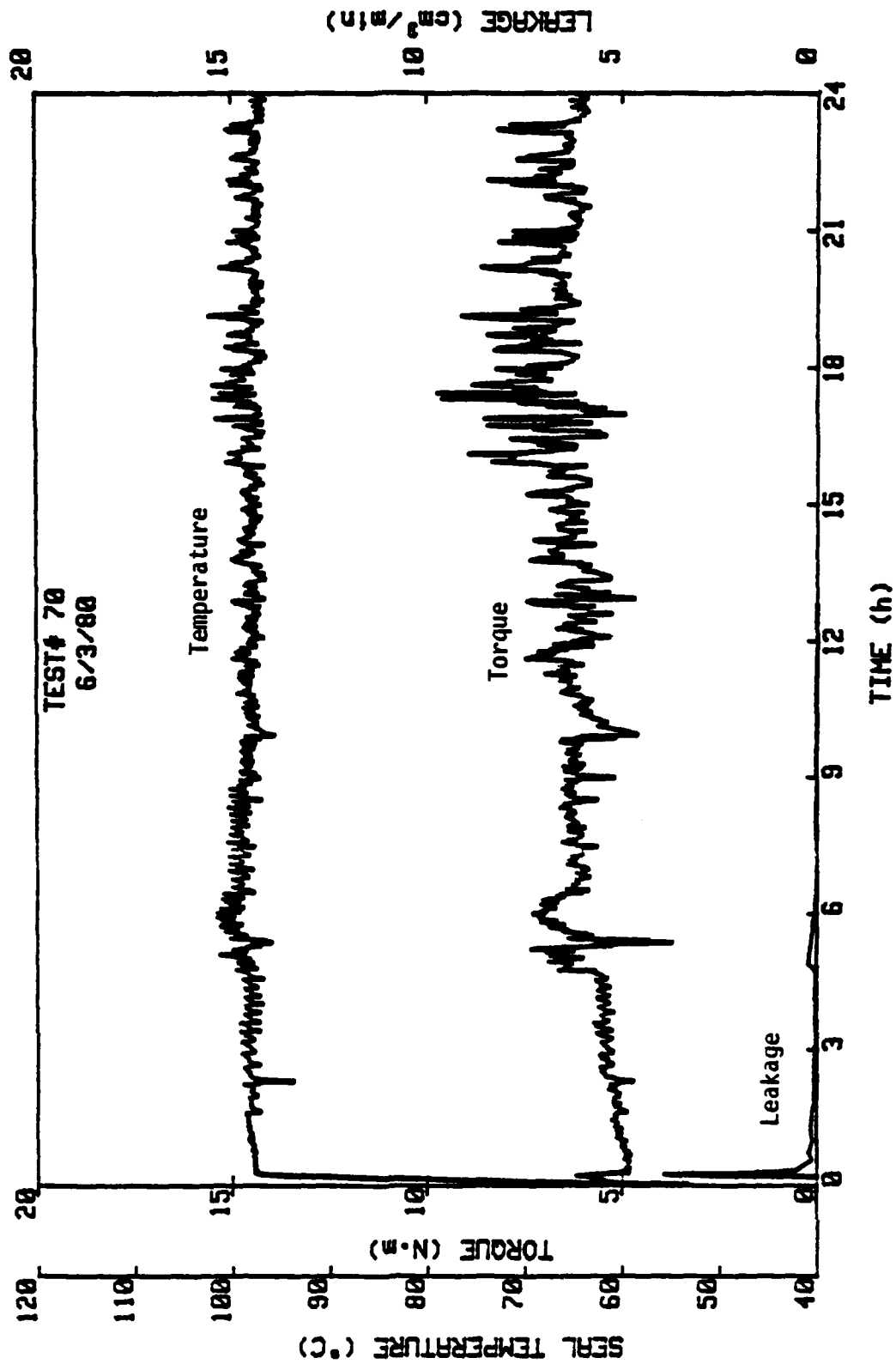




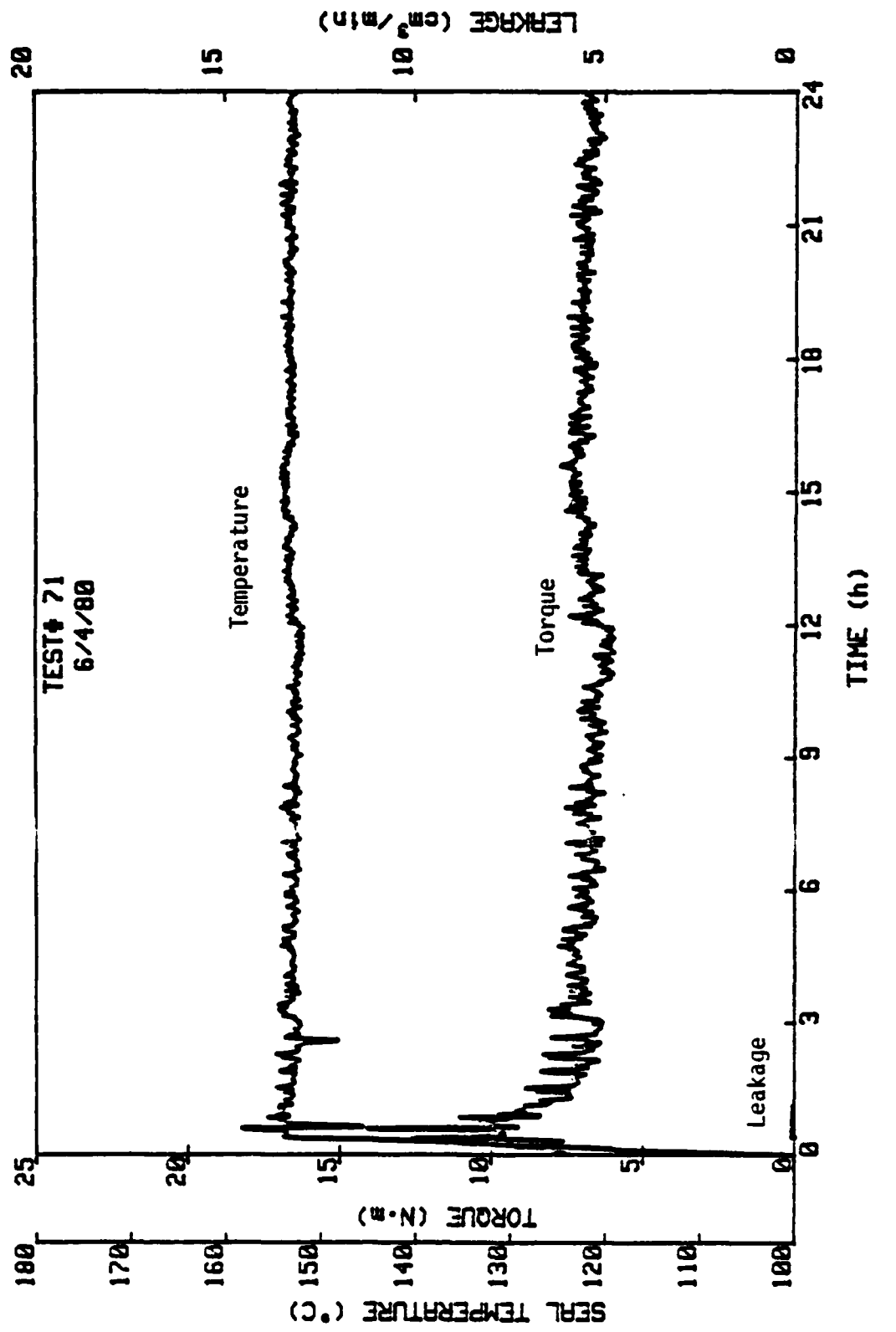
(continued)



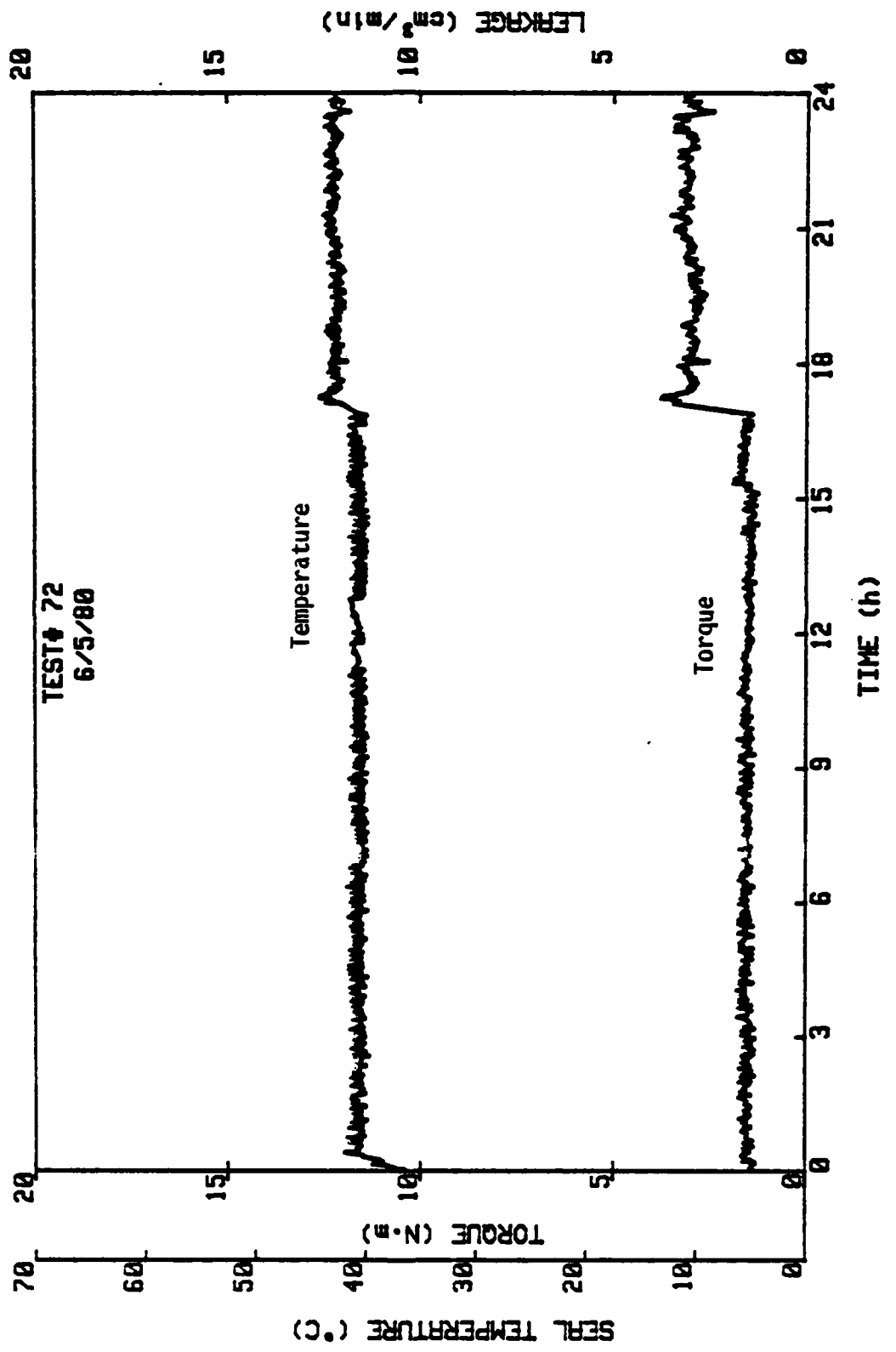
Test #69, $T_{\infty} = 37.8^{\circ}\text{C}$, $p_{\text{H}_2} = 1.72 \text{ MPa}$, 1800 RPM, $B = 0.75$



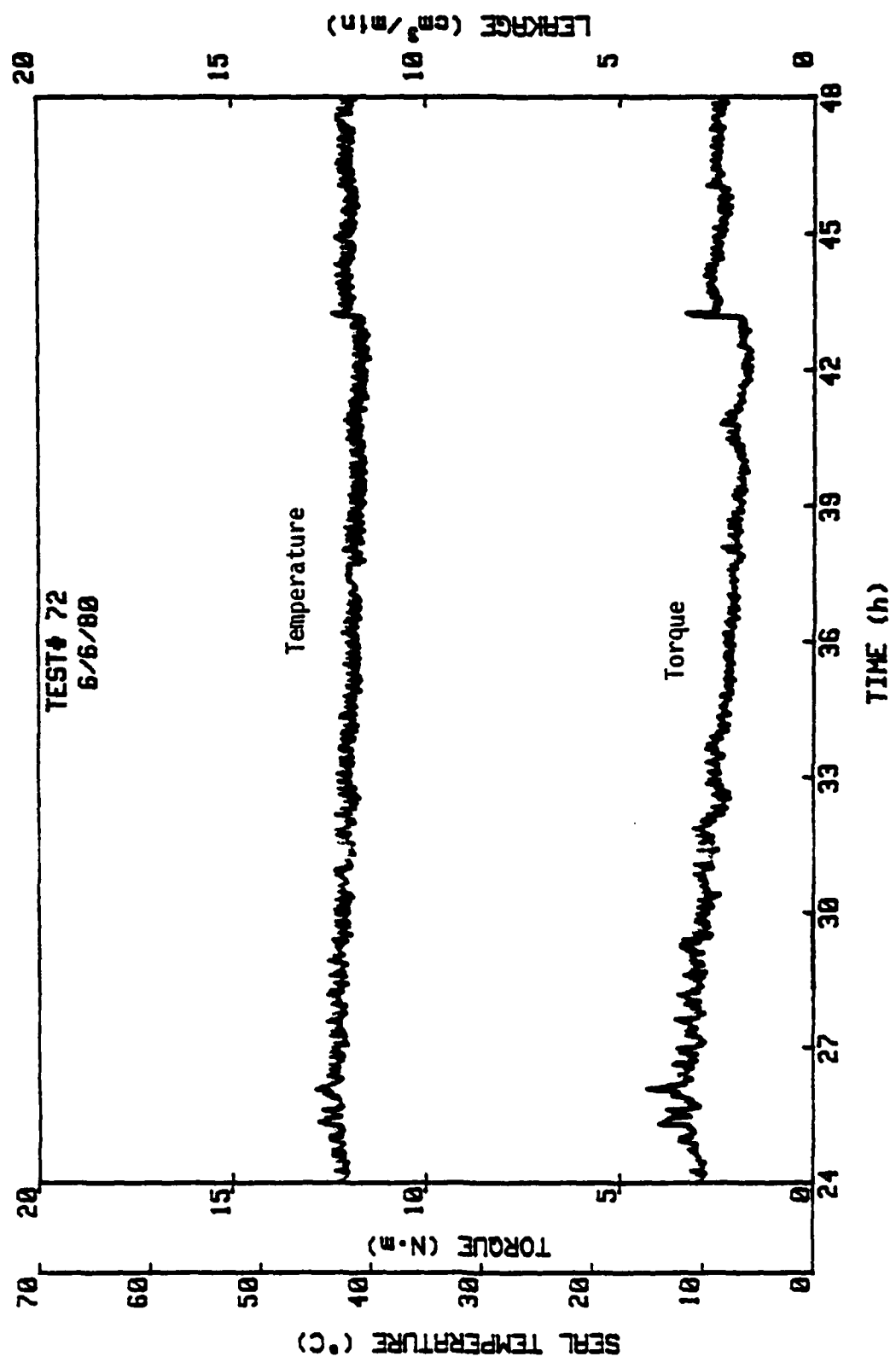
Test #70, $T_a = 93.3^\circ\text{C}$, $p_{H_2O} = 1.72 \text{ MPa}$, 1800 RPM, $B = 0.75$



Test #71, $T_{\infty} = 148.9^{\circ}\text{C}$, $p_{\text{H}_2\text{O}} = 1.72 \text{ MPa}$, 1800 RPM, $B = 0.75$

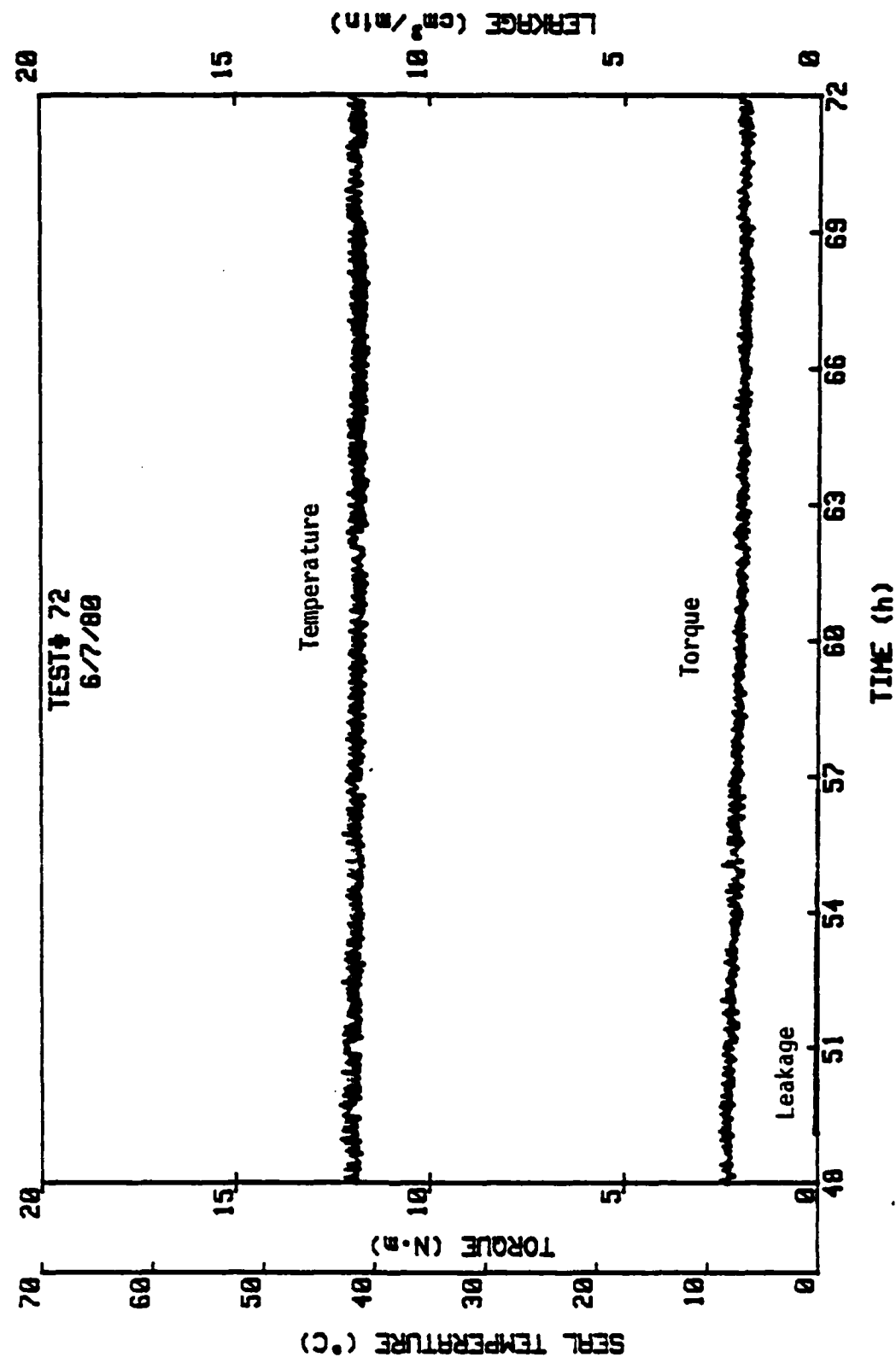


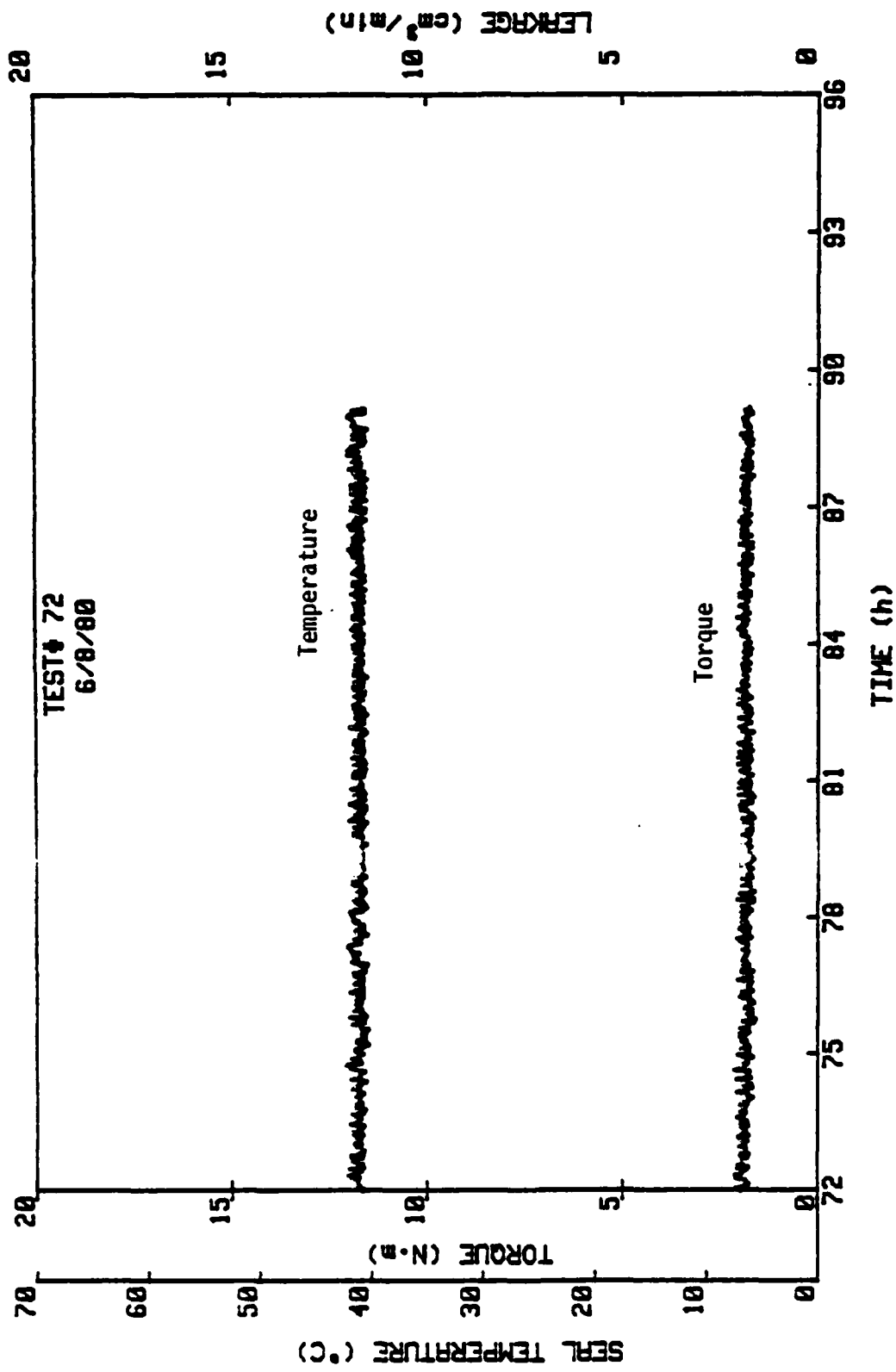
Test #72, $T_\infty = 37.8^\circ\text{C}$, $P_{\text{H}_2\text{O}} = 1.72 \text{ MPa}$, 1800 RPM, $B = 0.75$



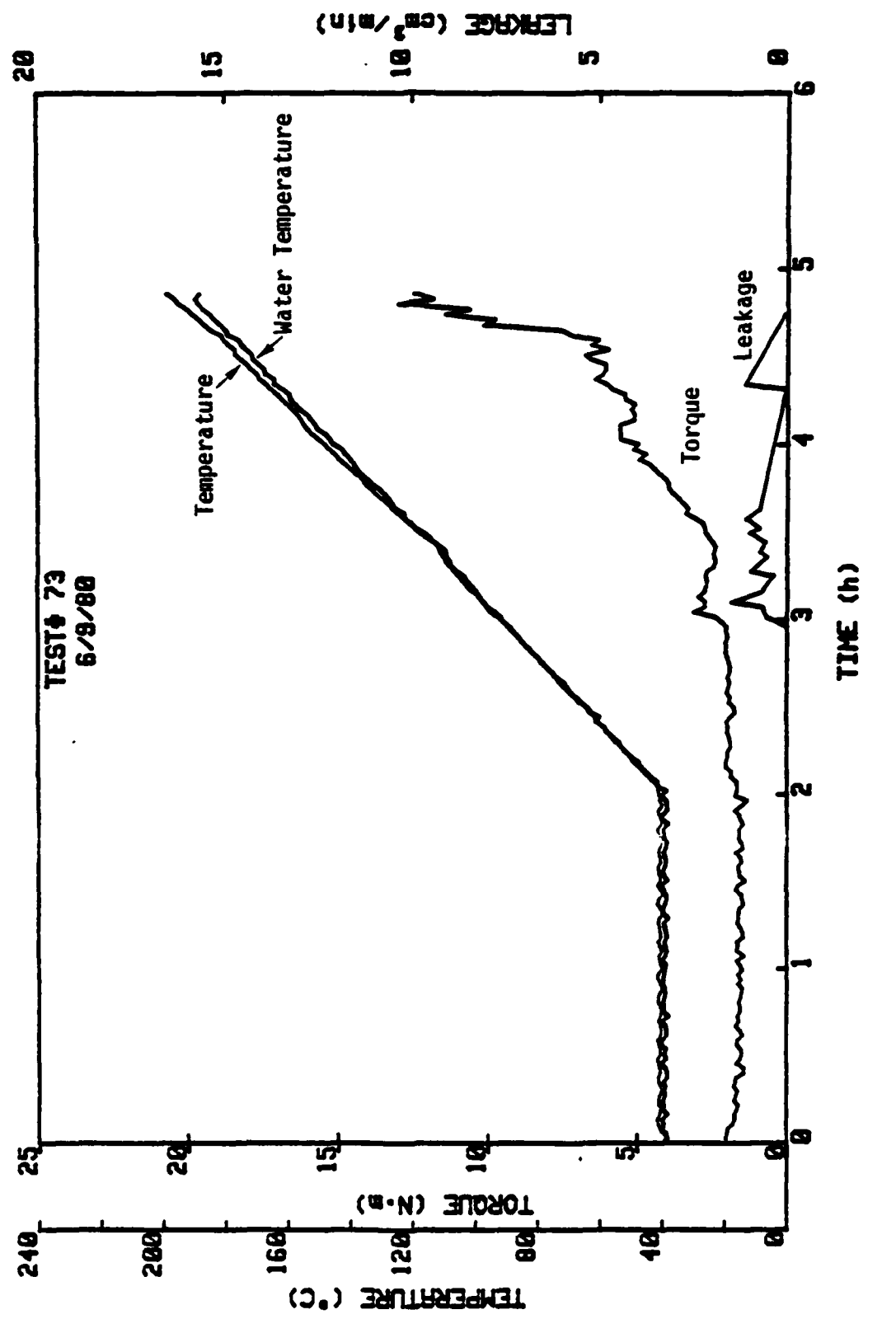
(Continued)

(Continued)

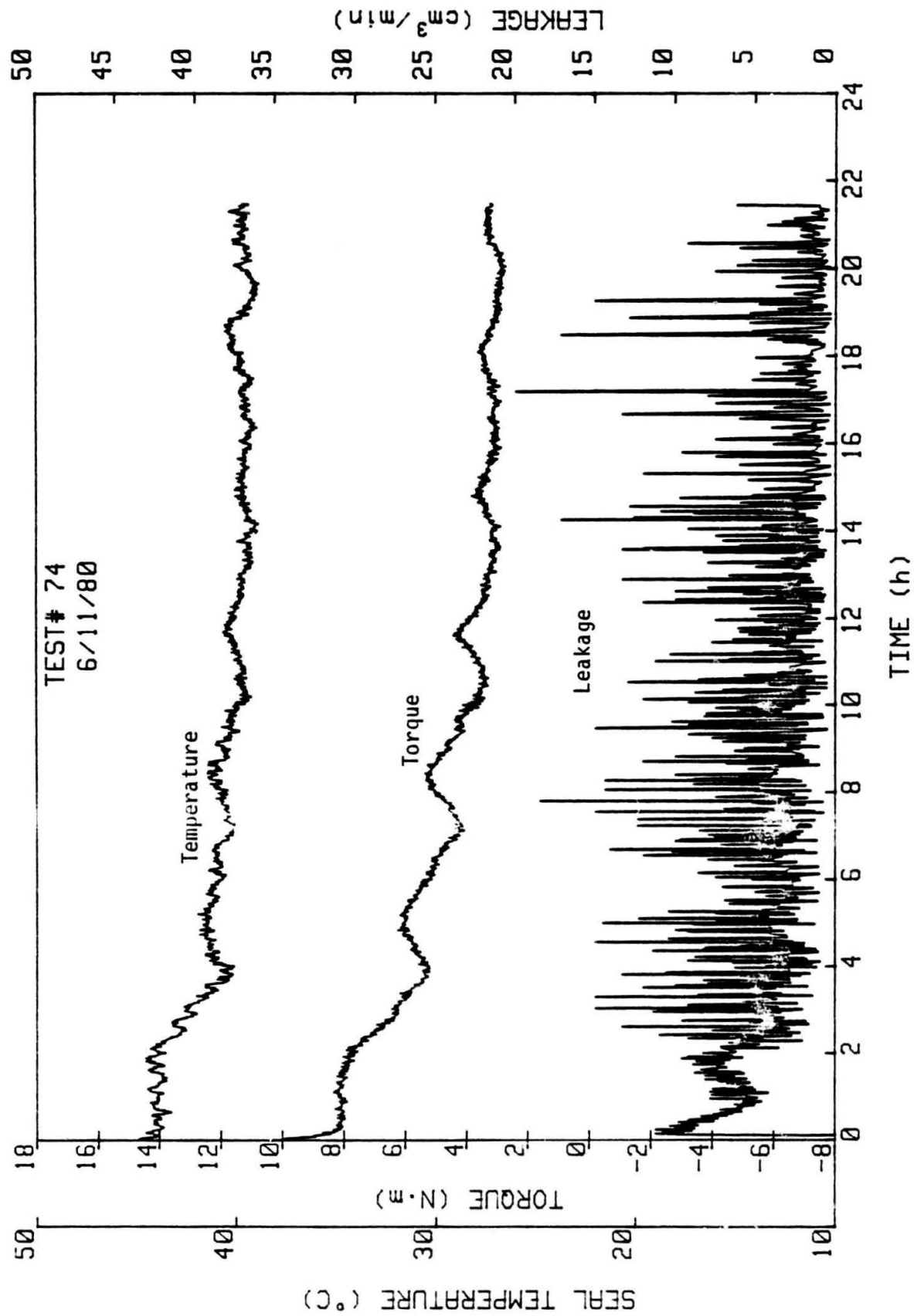




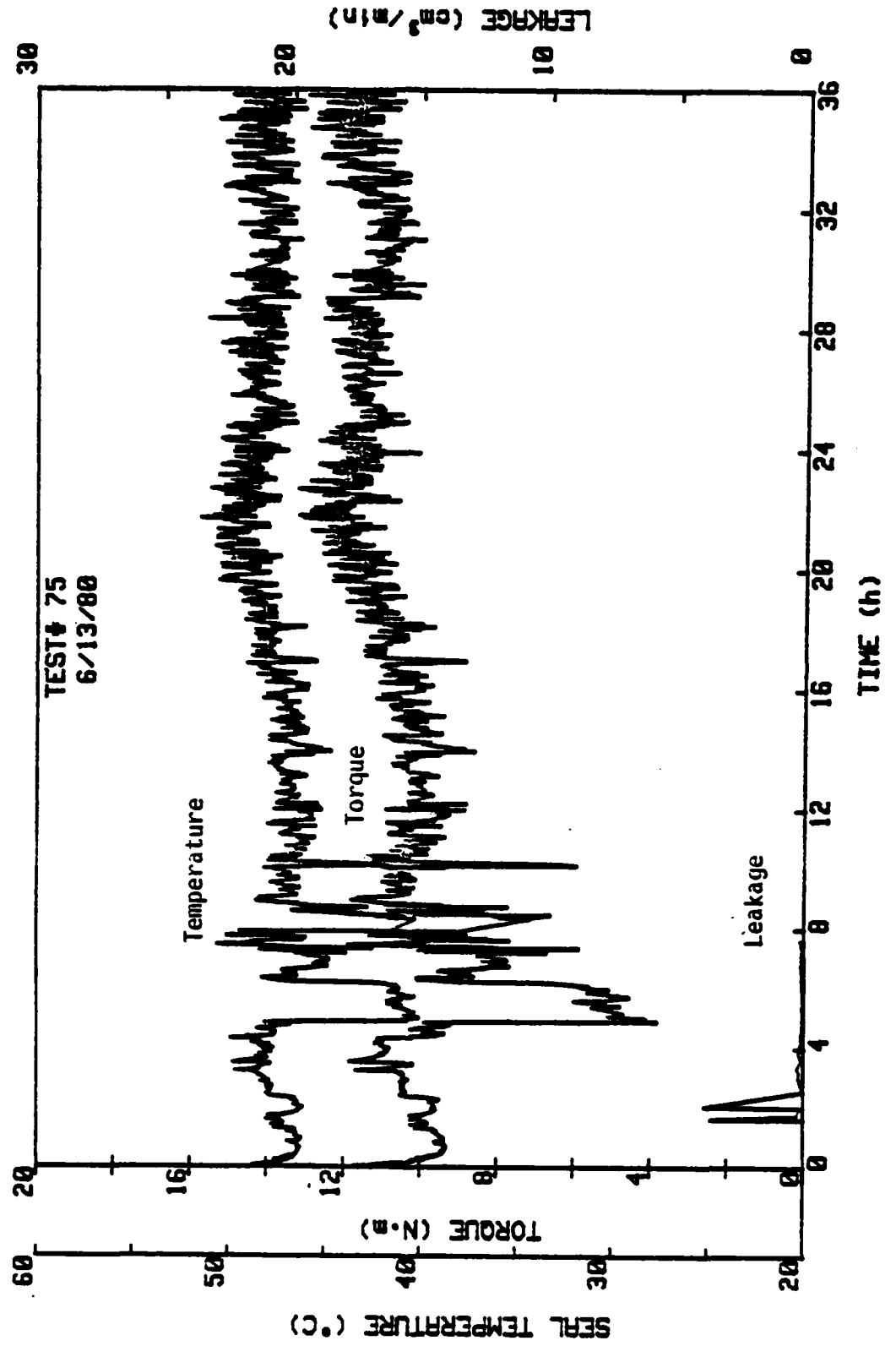
(Continued)



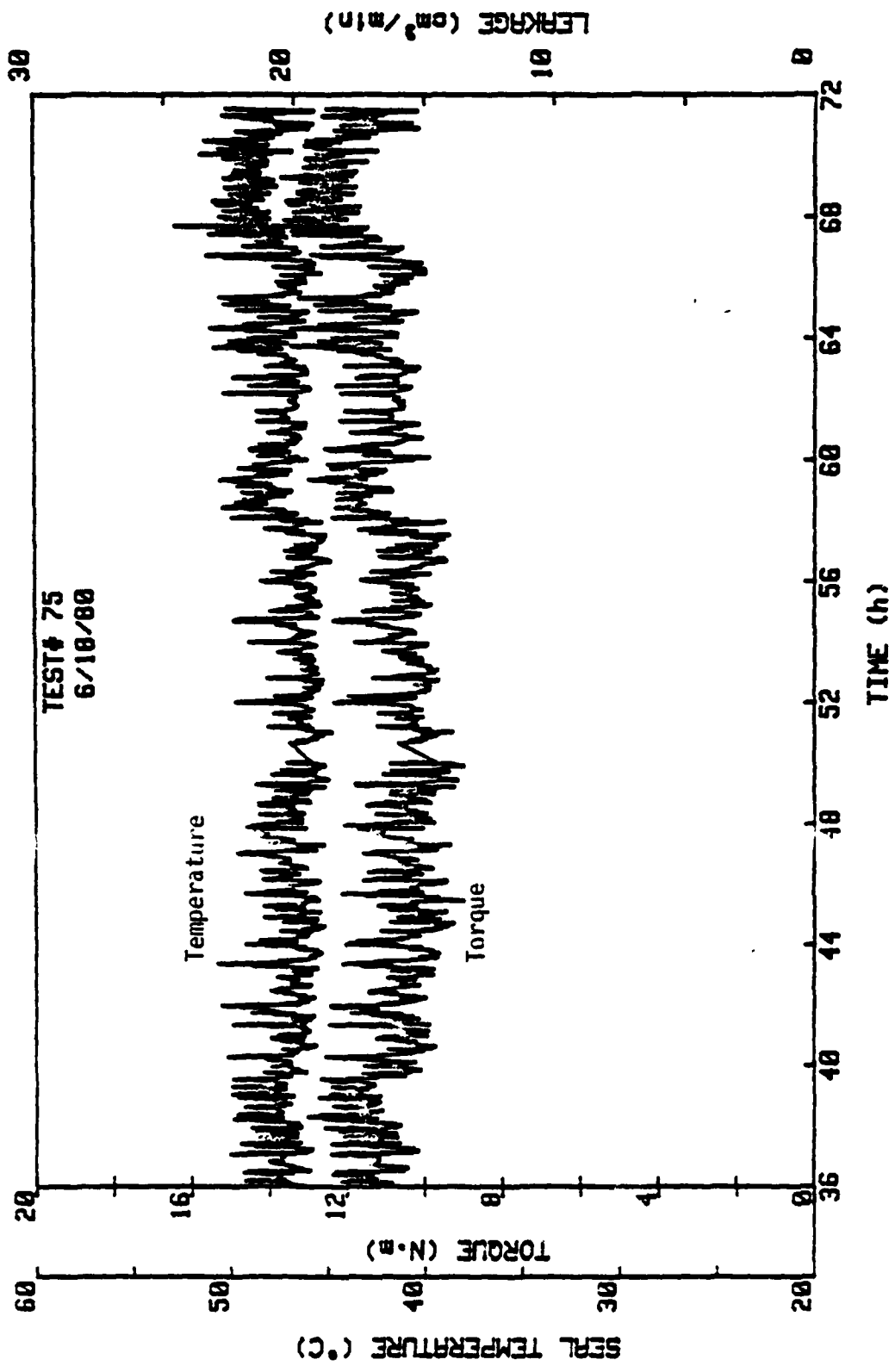
Test #73, $p_{H_2O} = 1.72 \text{ MPa}$, 1800 RPM, $B = 0.75$

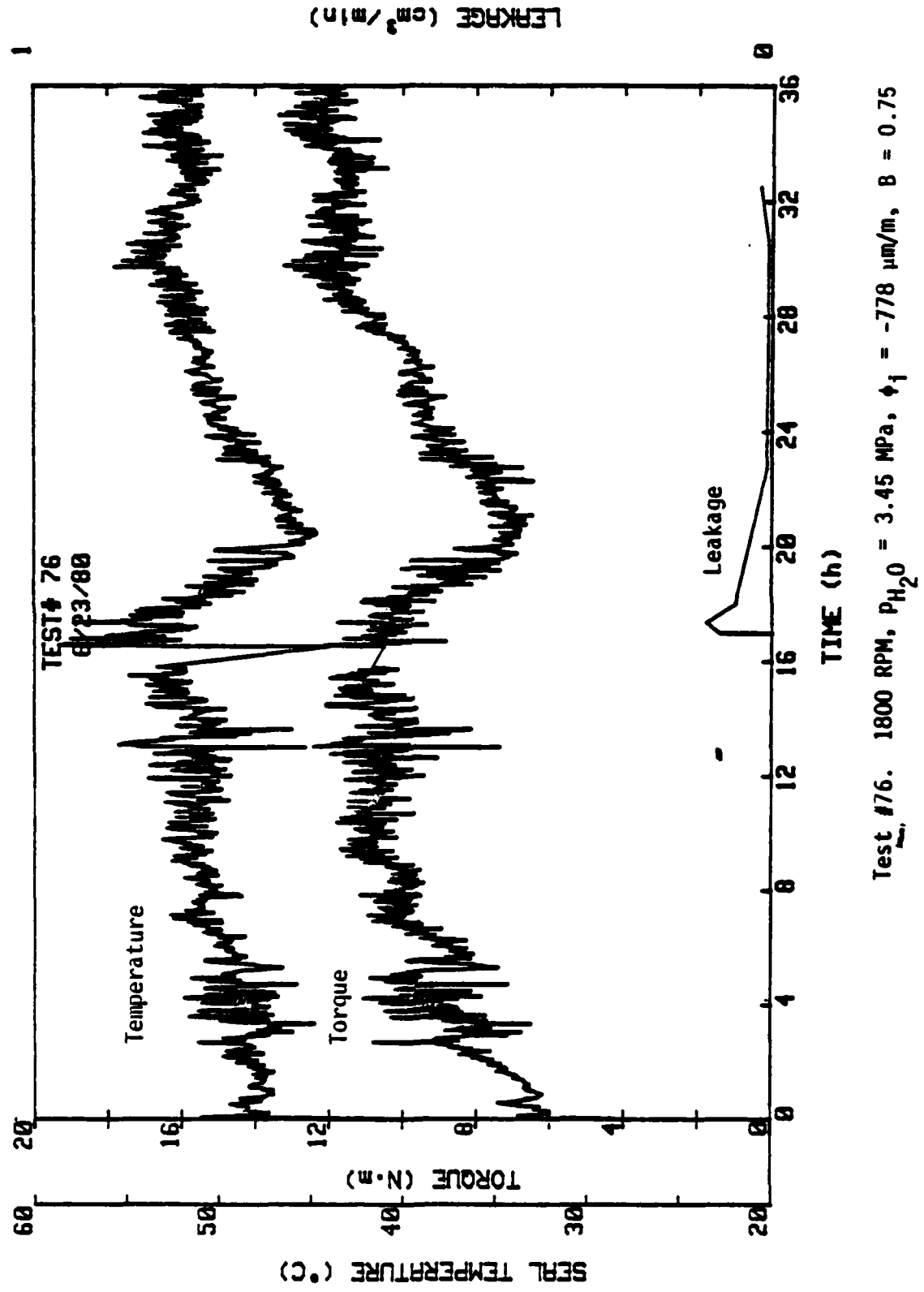


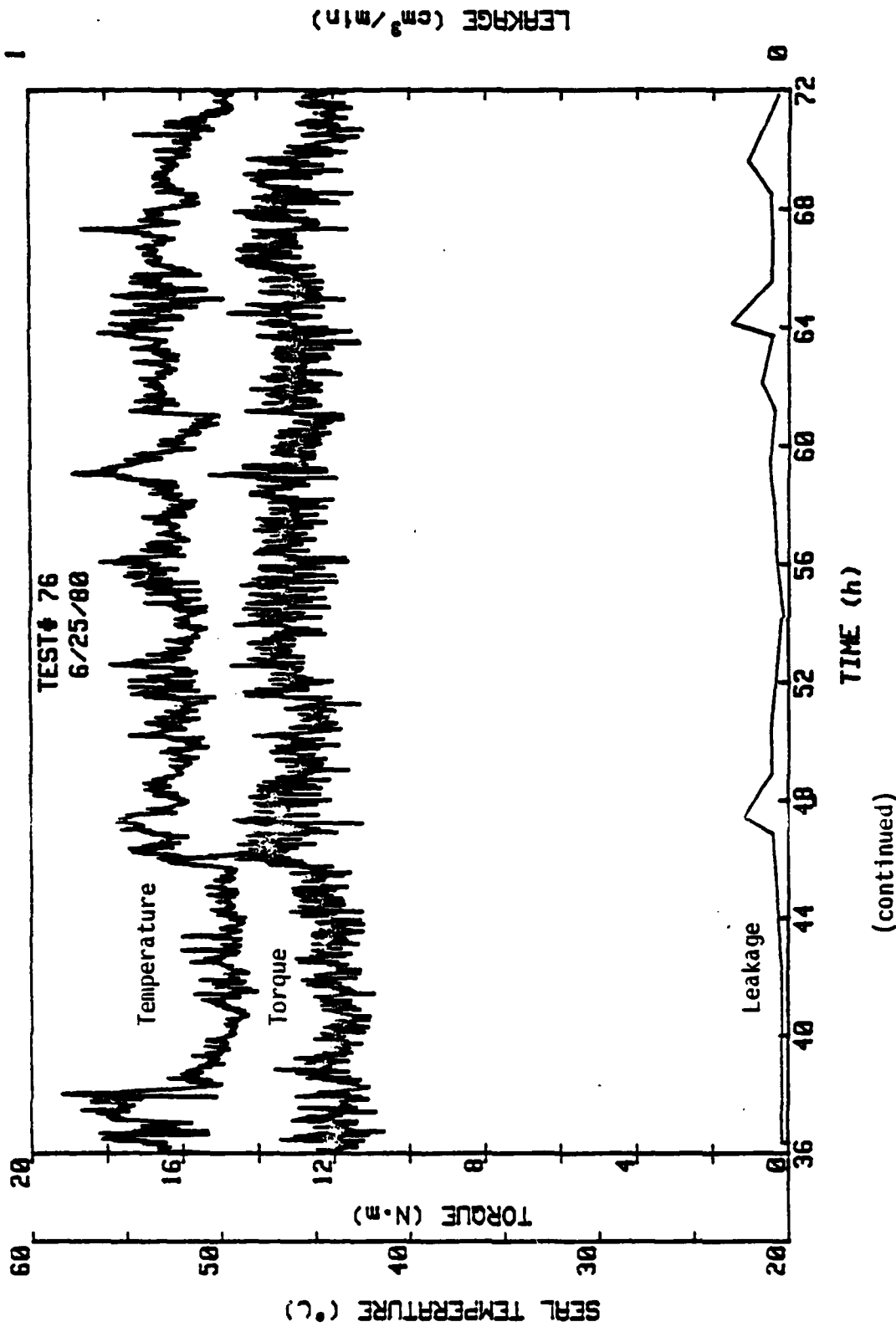
Test #74. 1800 RPM, $P_{\text{H}_2\text{O}} = 3.45 \text{ MPa}$, $P_g = 6.9 \text{ MPa}$, $n = 3$

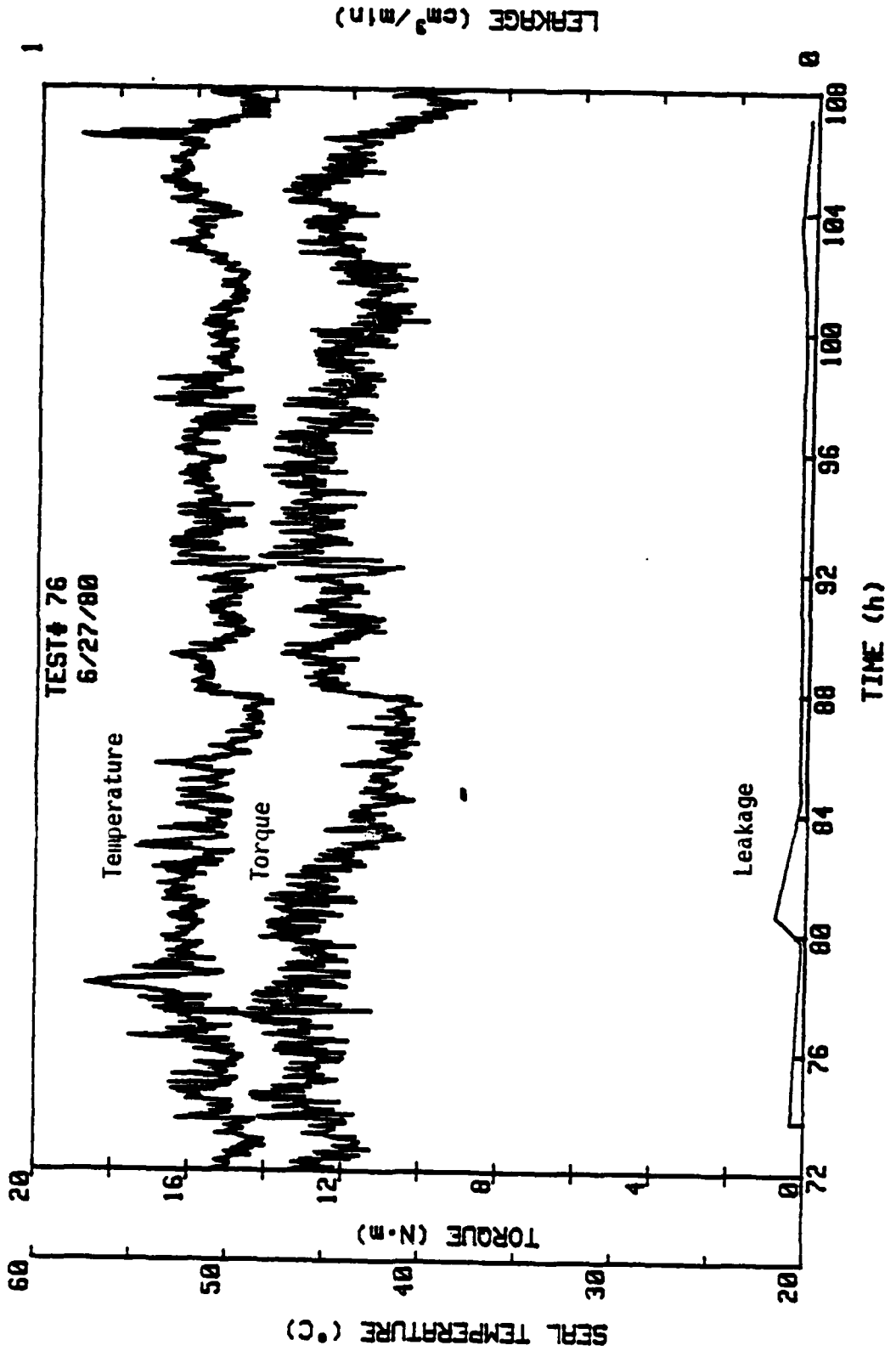


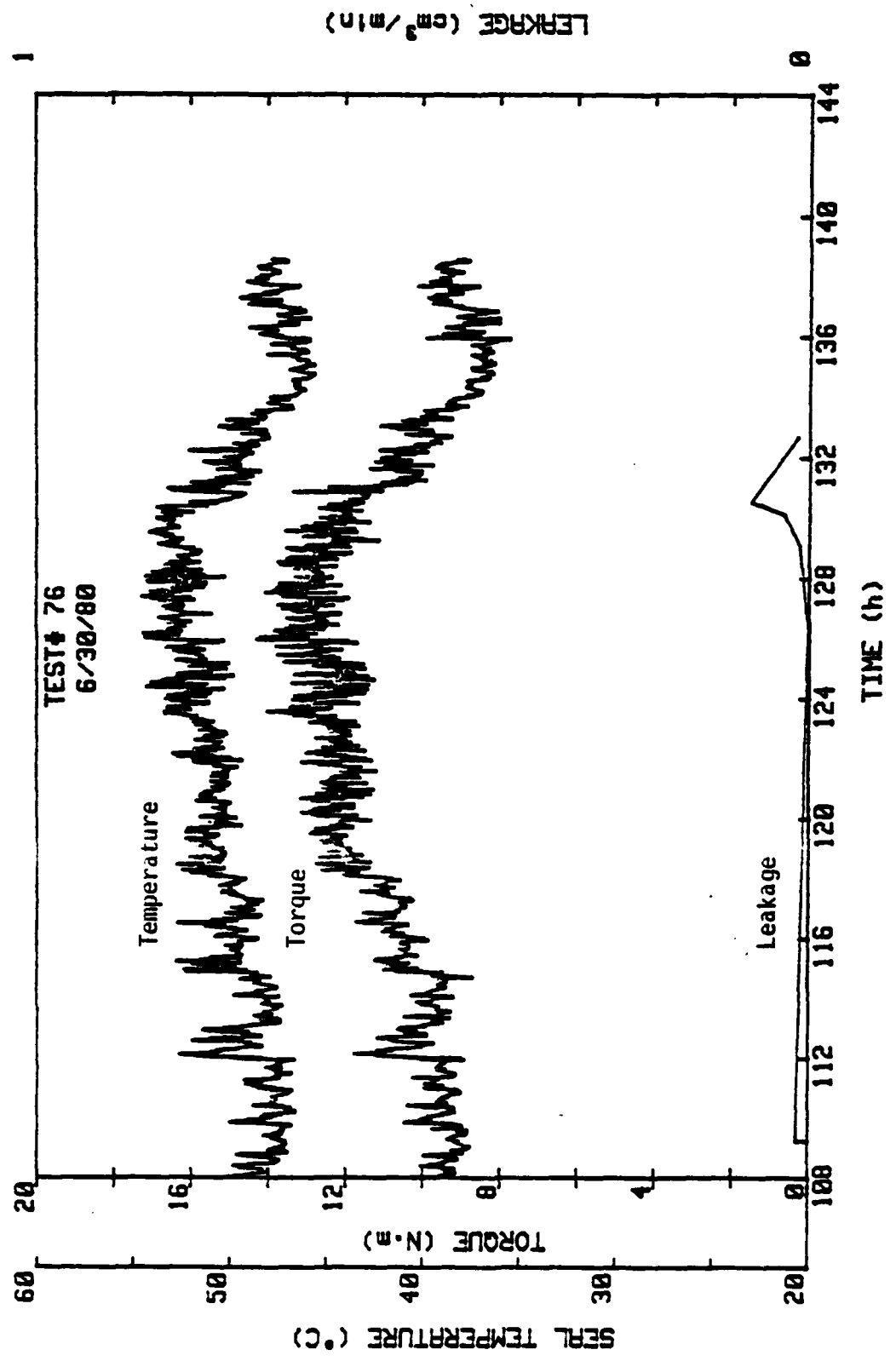
Test #75. 1800 RPM, $p_{\text{H}_2\text{O}} = 3.45 \text{ MPa}$, $\Phi_1 = -1110 \mu\text{m/m}$, $B = 0.75$



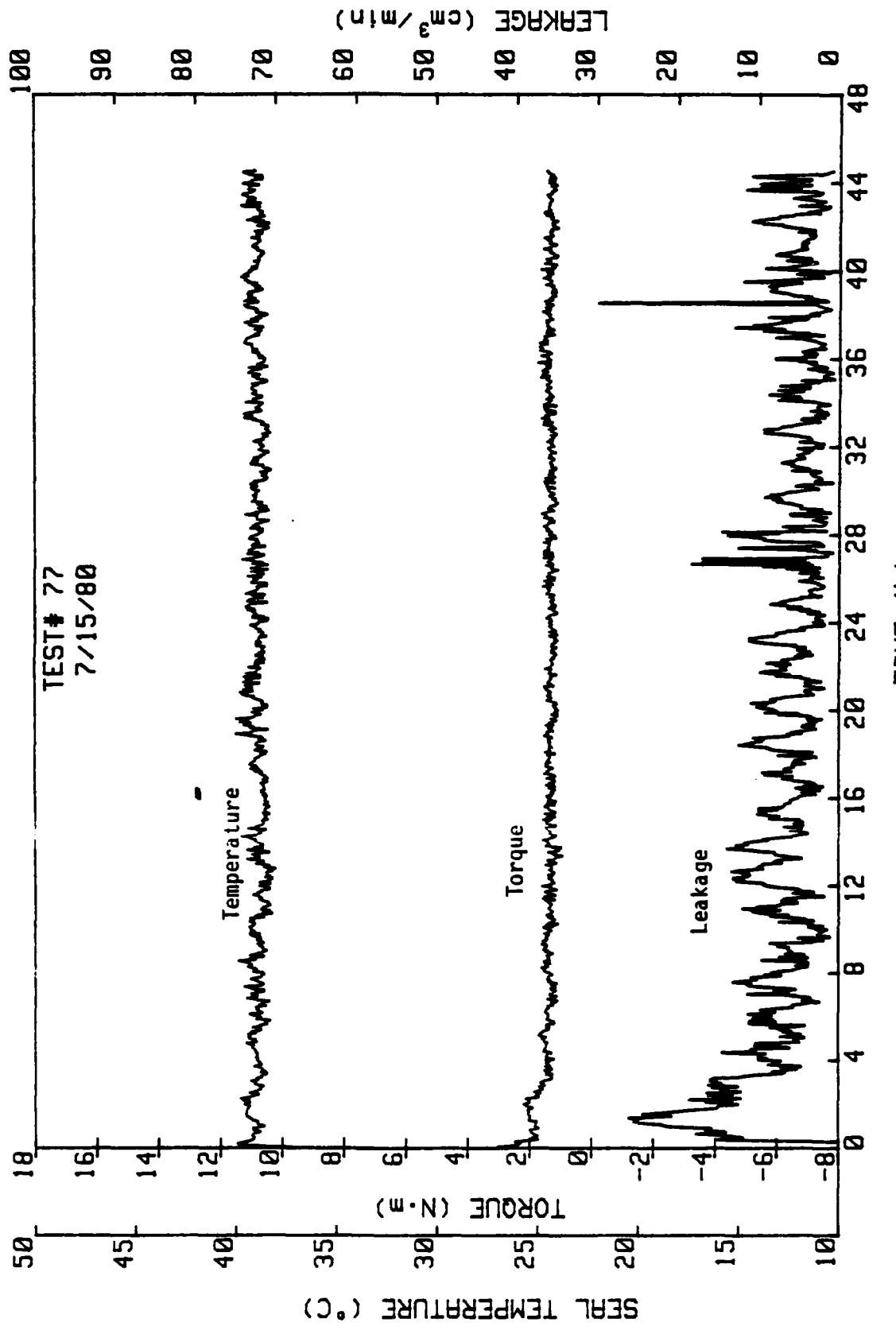




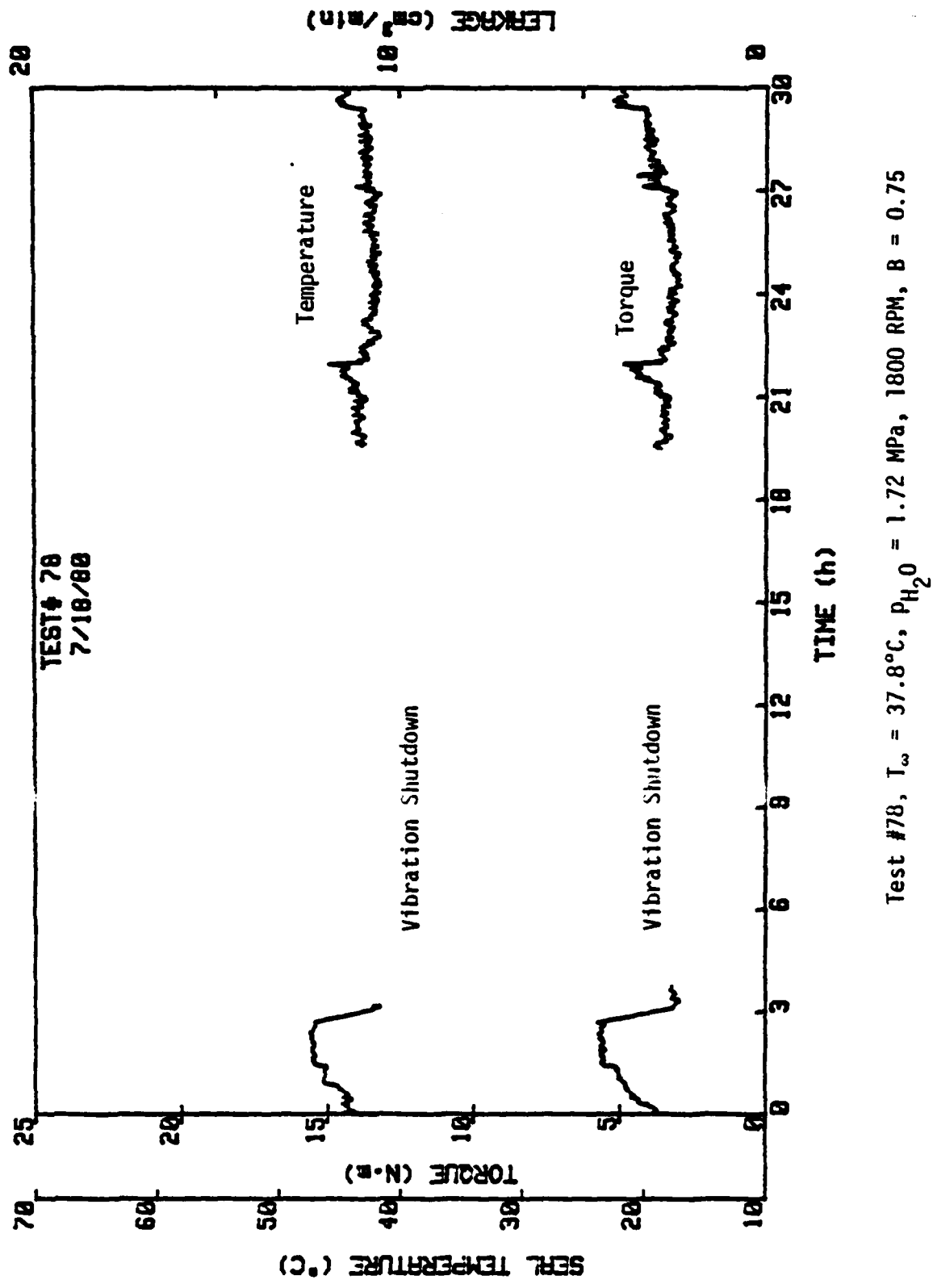


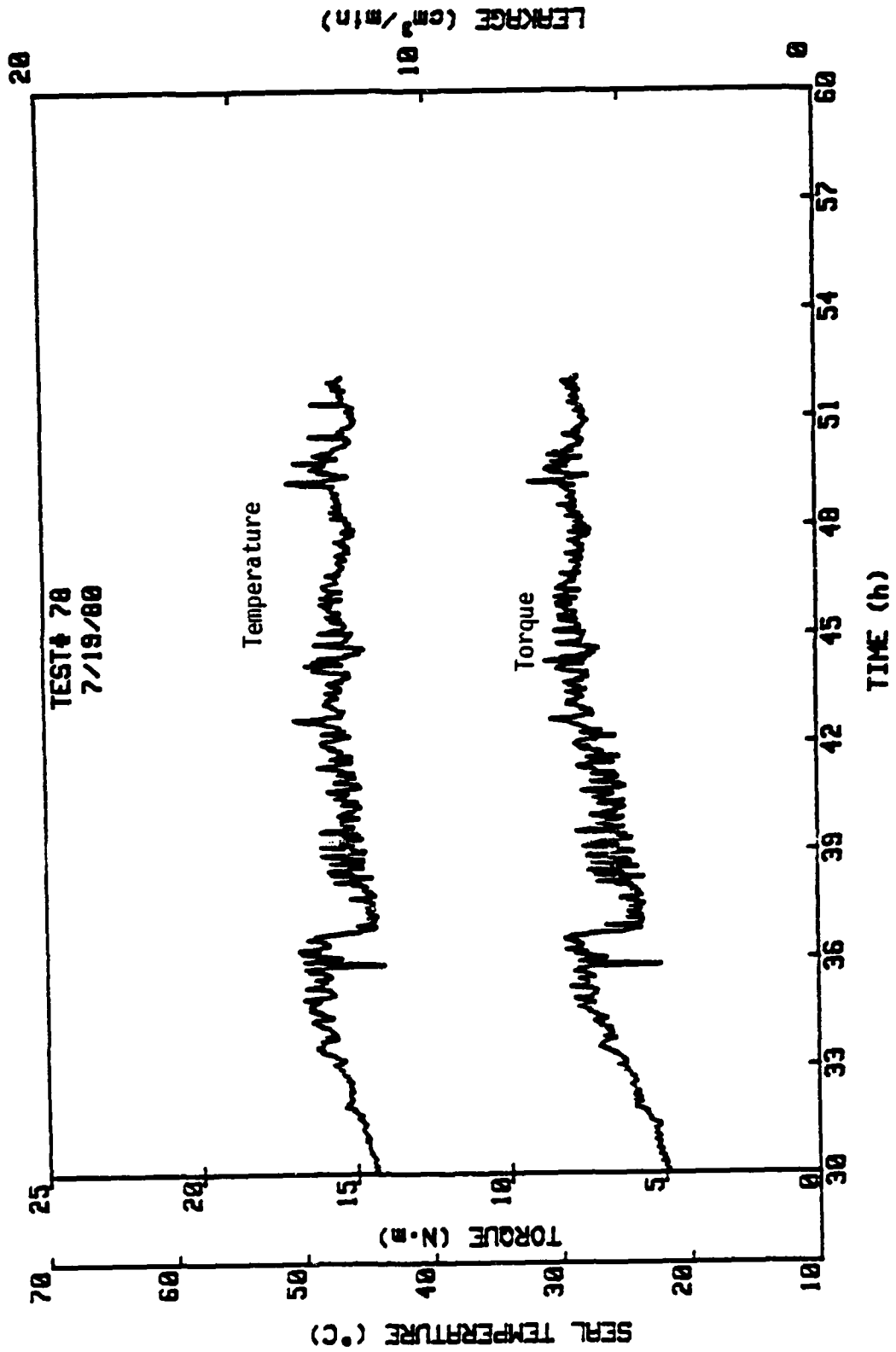


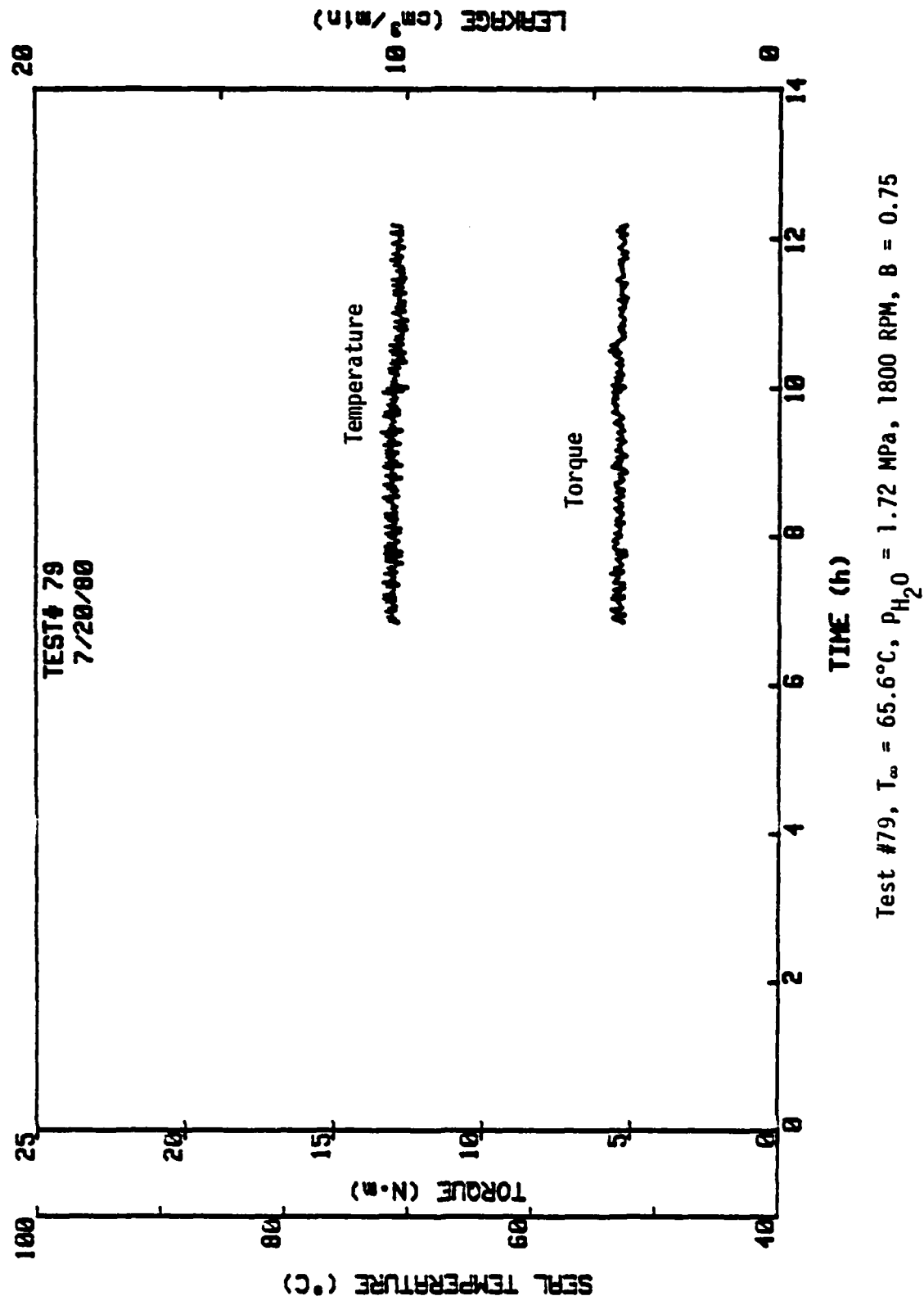
(continued)



Test #77. 1800 RPM, $P_{\text{H}_2\text{O}} = 3.45 \text{ MPa}$, $P_g = 5.52 \text{ MPa}$, $n = 3$

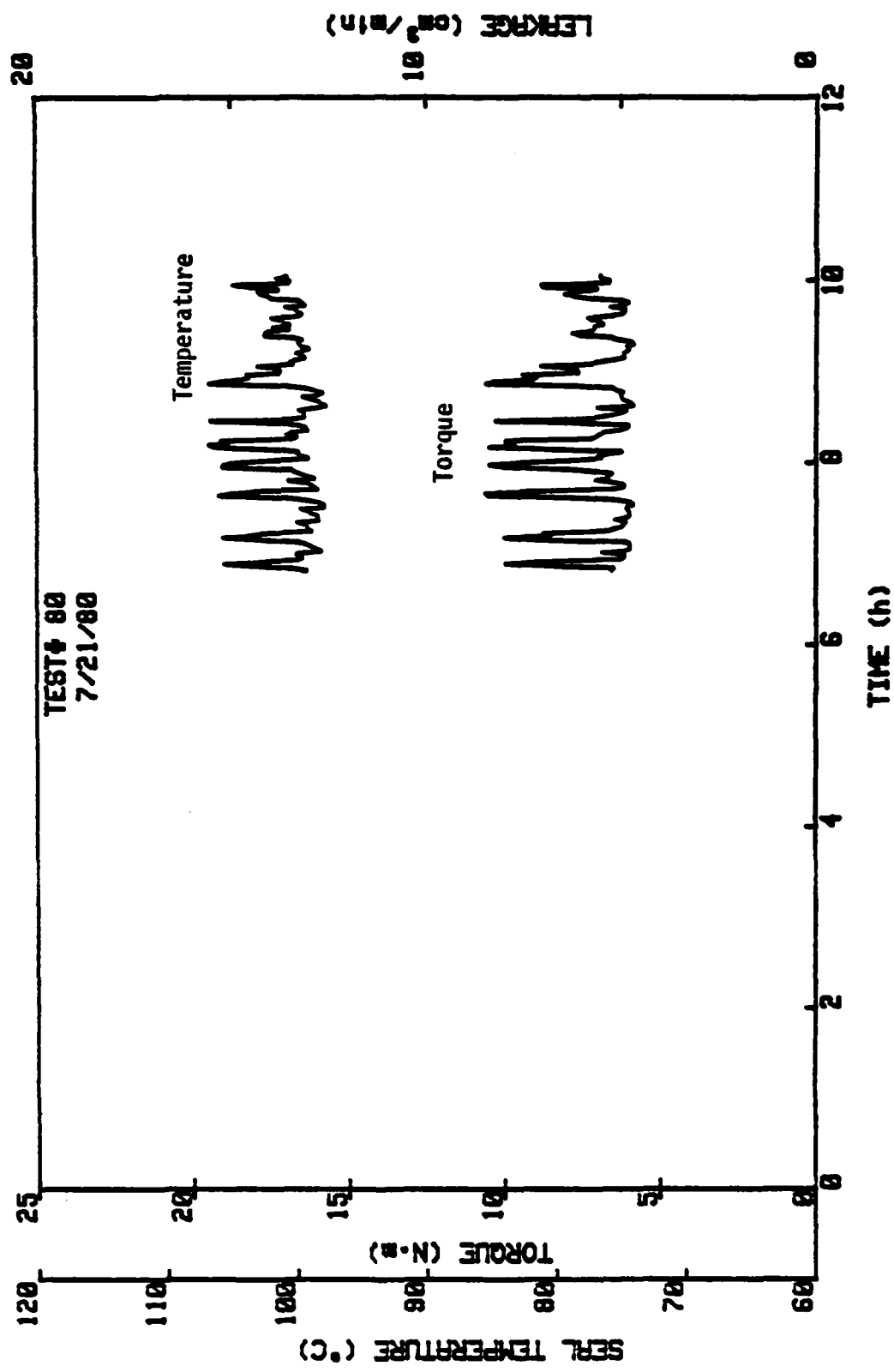




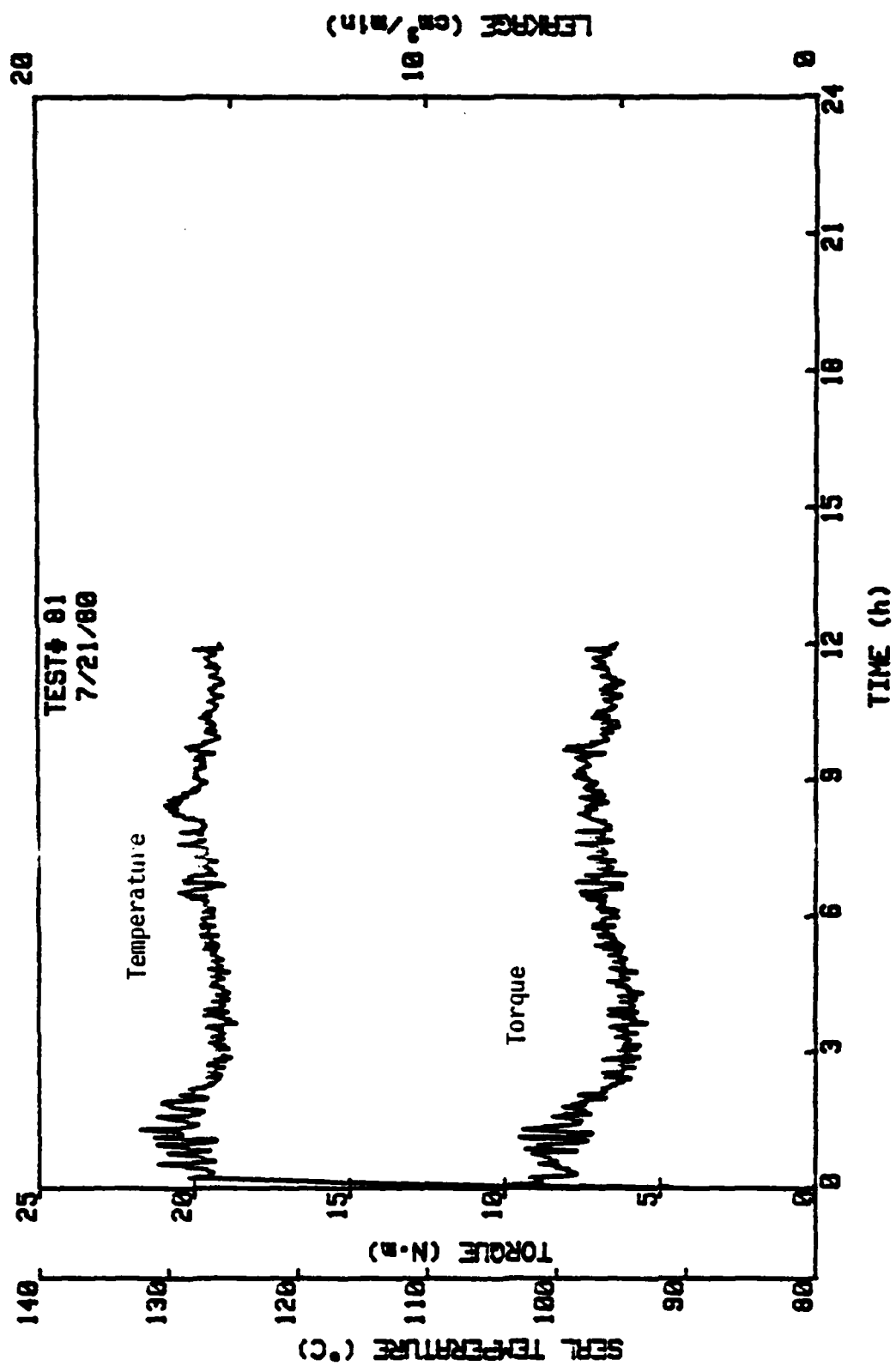


Test #79, $T_{\infty} = 65.6^{\circ}\text{C}$, $p_{\text{H}_2\text{O}} = 1.72 \text{ MPa}$, 1800 RPM, $B = 0.75$

 HEWLETT
PACKARD

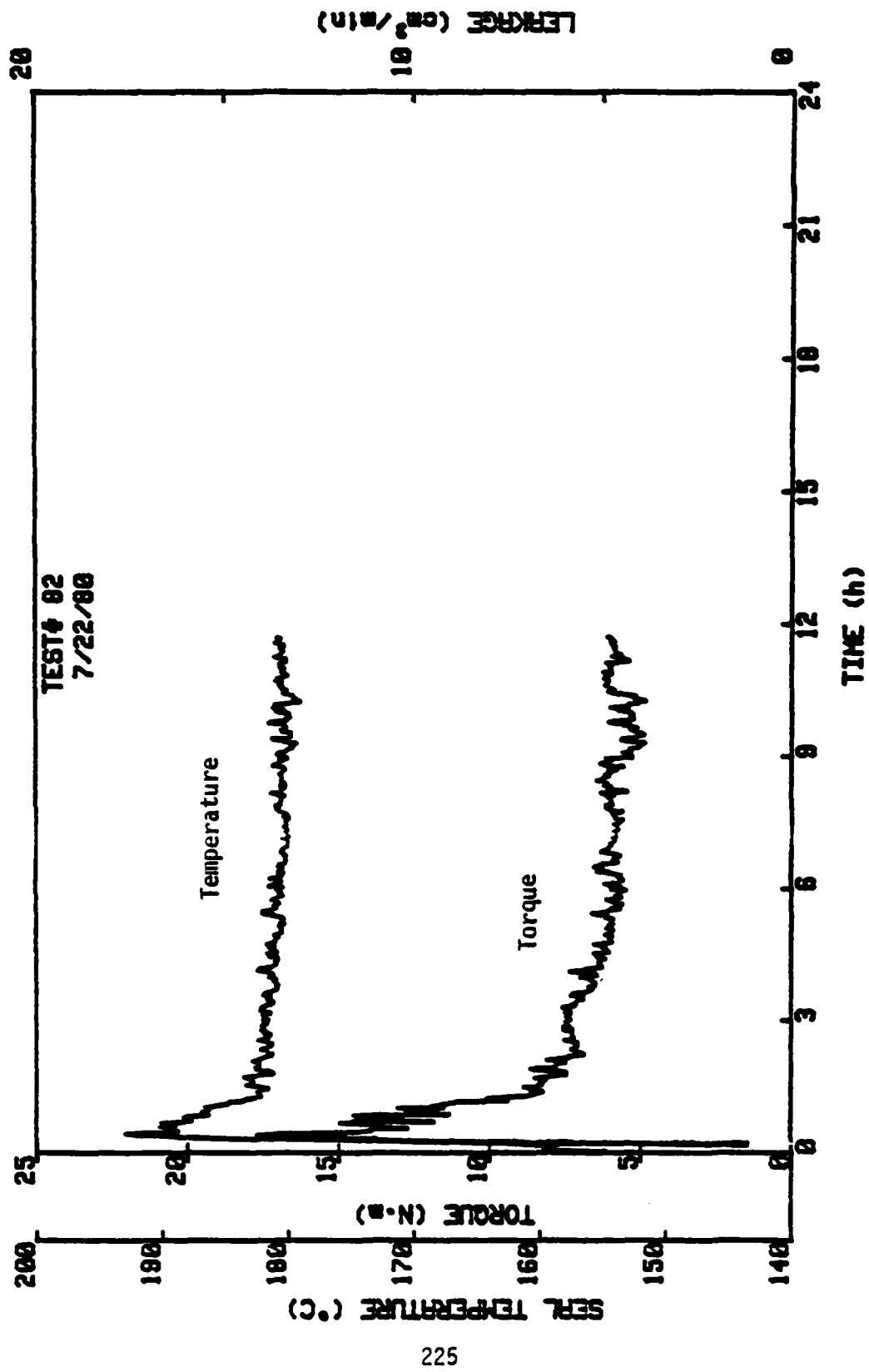


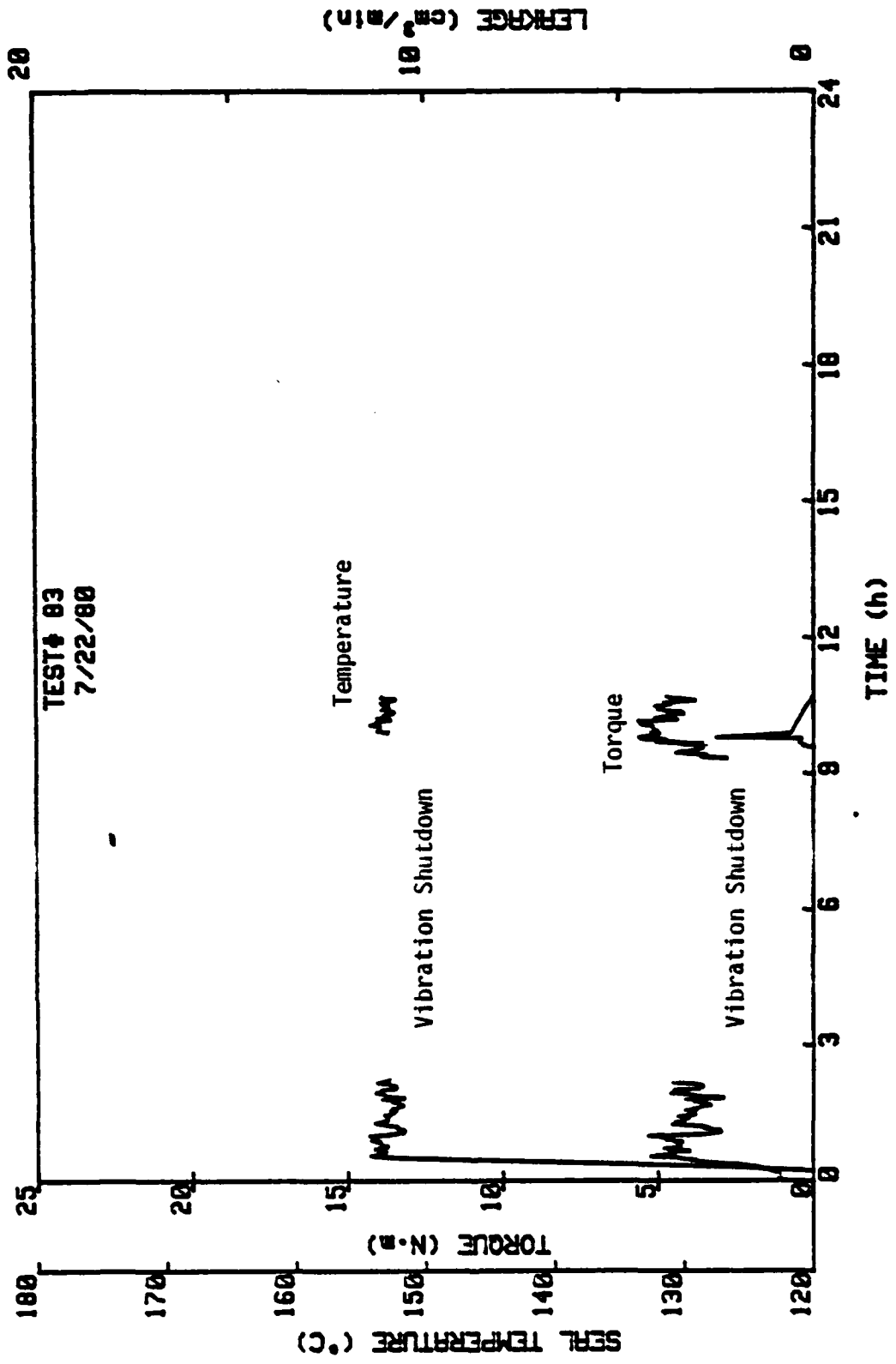
Test #80, $T_{\infty} = 93.3^{\circ}\text{C}$, $p_{\text{H}_2\text{O}} = 1.72 \text{ MPa}$, 1800 RPM, $B = 0.75$



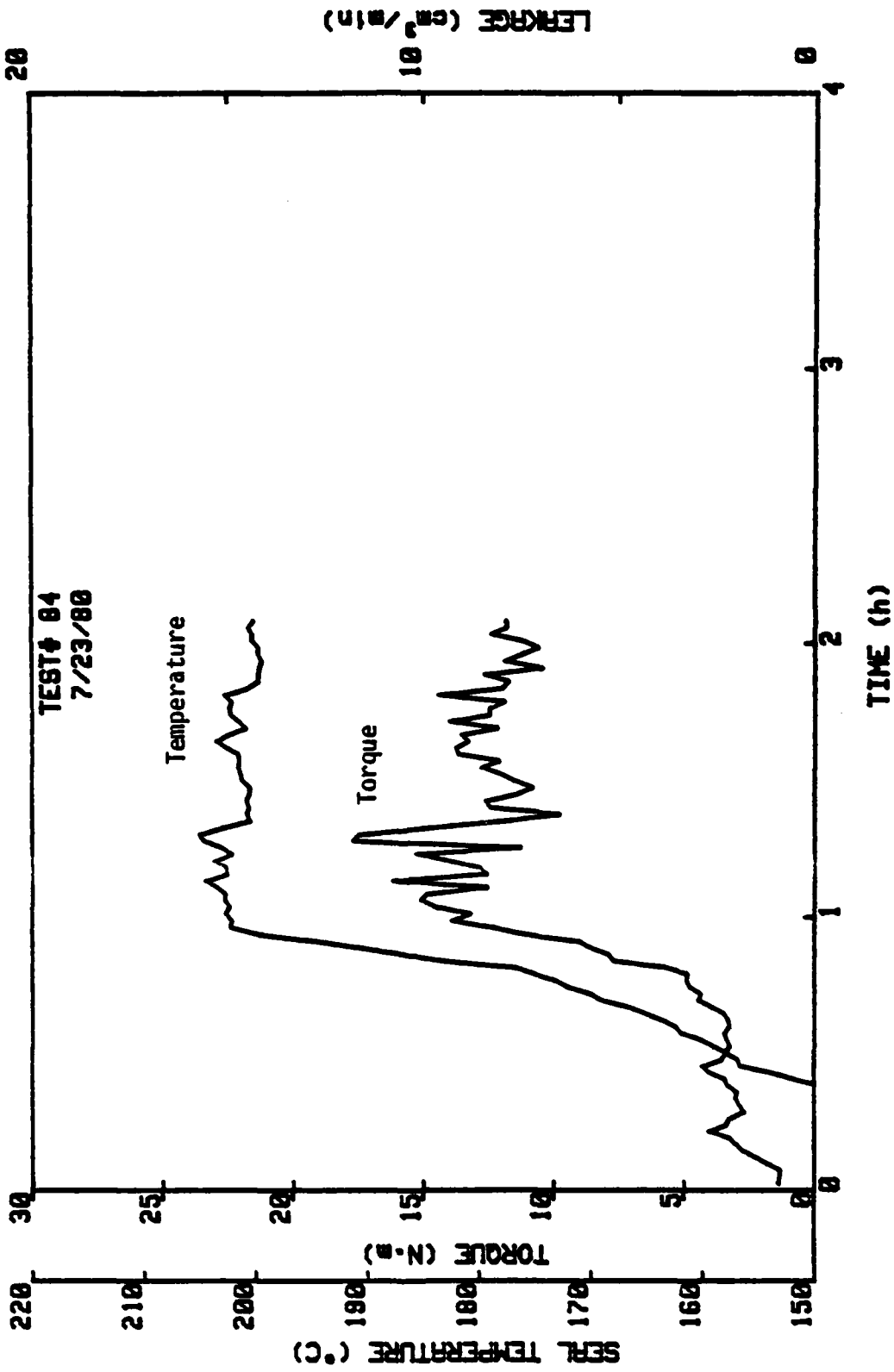
Test #81, $T_{\infty} = 121.1^{\circ}\text{C}$, $p_{\text{H}_2\text{O}} = 1.72 \text{ MPa}$, 1800 RPM, $B = 0.75$

HEWLETT
PACKARD

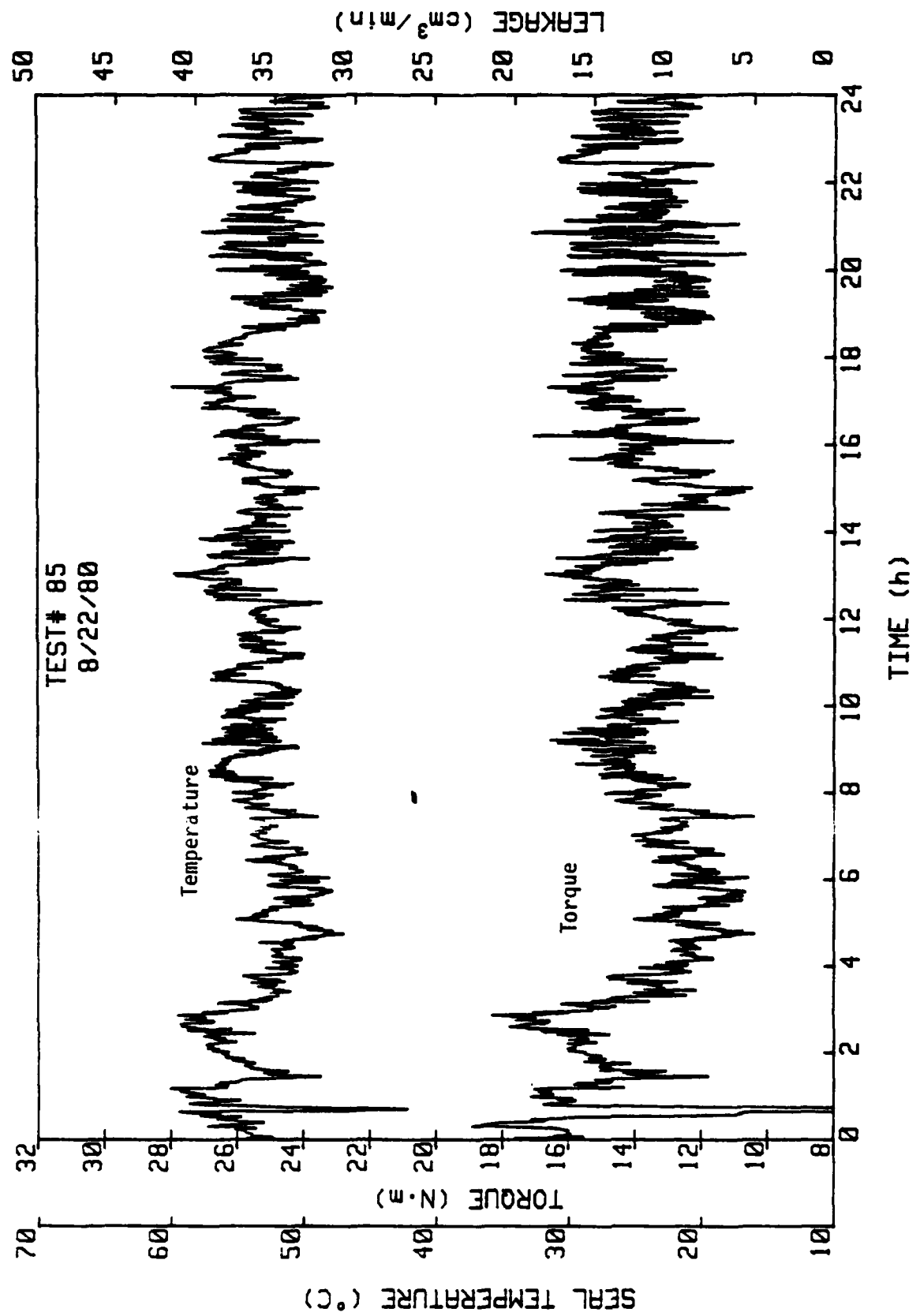




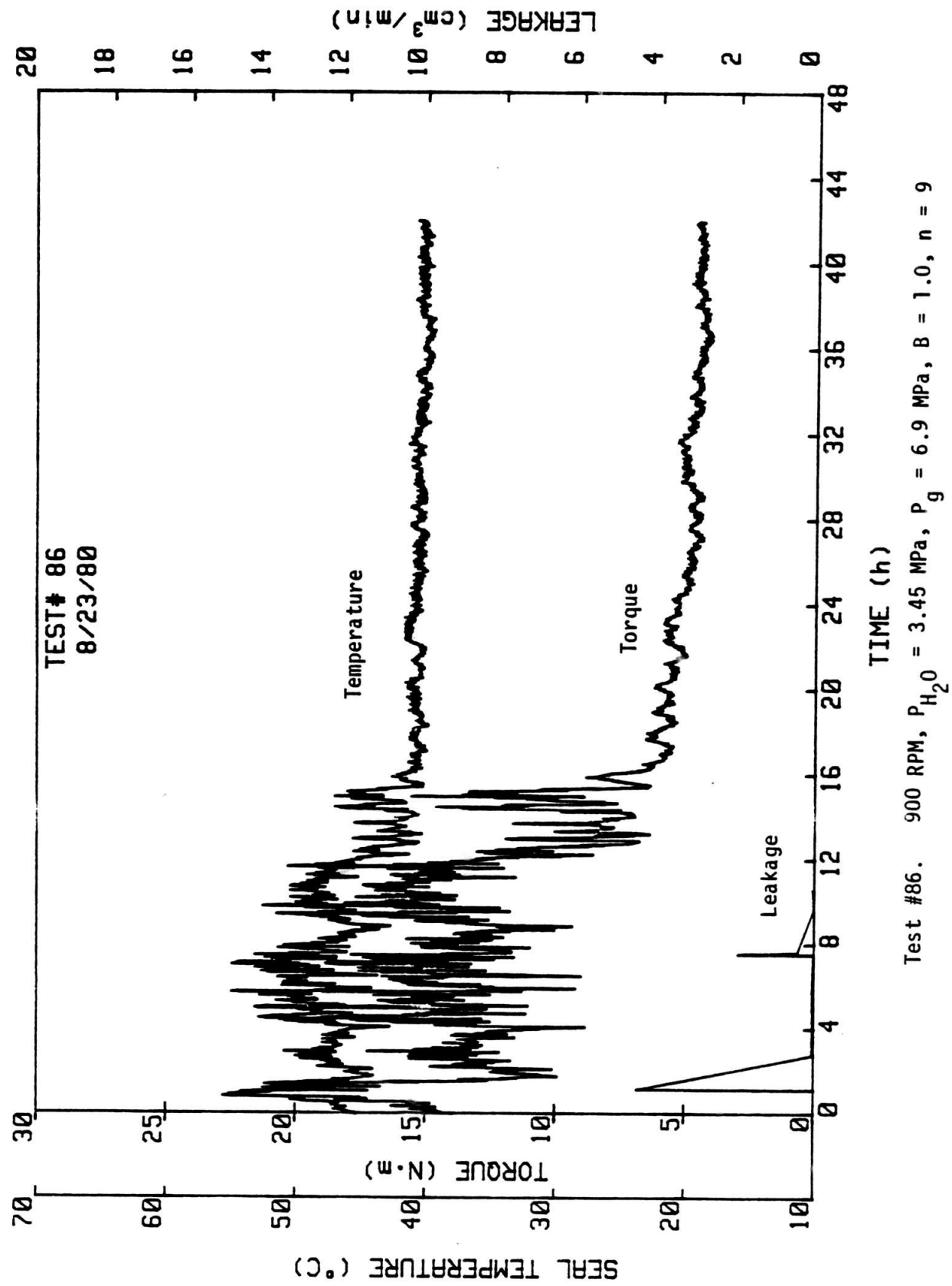
Test #83, $T_{\infty} = 148.9^{\circ}\text{C}$, $p_{\text{H}_2\text{O}} = 1.72 \text{ MPa}$, 1800 RPM, $B = 0.75$

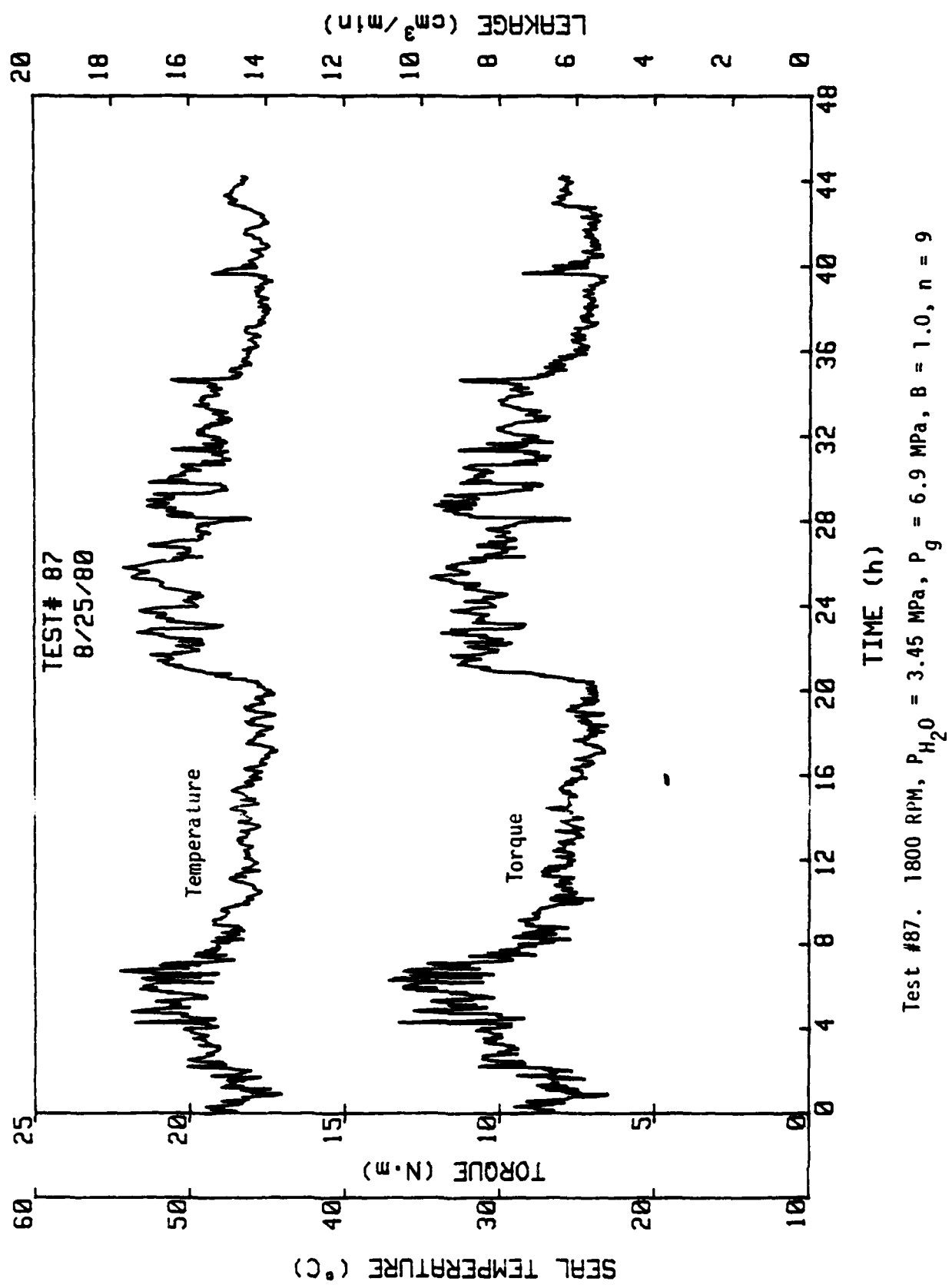


Test #84, $T_{\infty} = 190.6^\circ\text{C}$, $p_{\text{H}_2\text{O}} = 1.72 \text{ MPa}$, 1800 RPM, $\beta = 0.75$

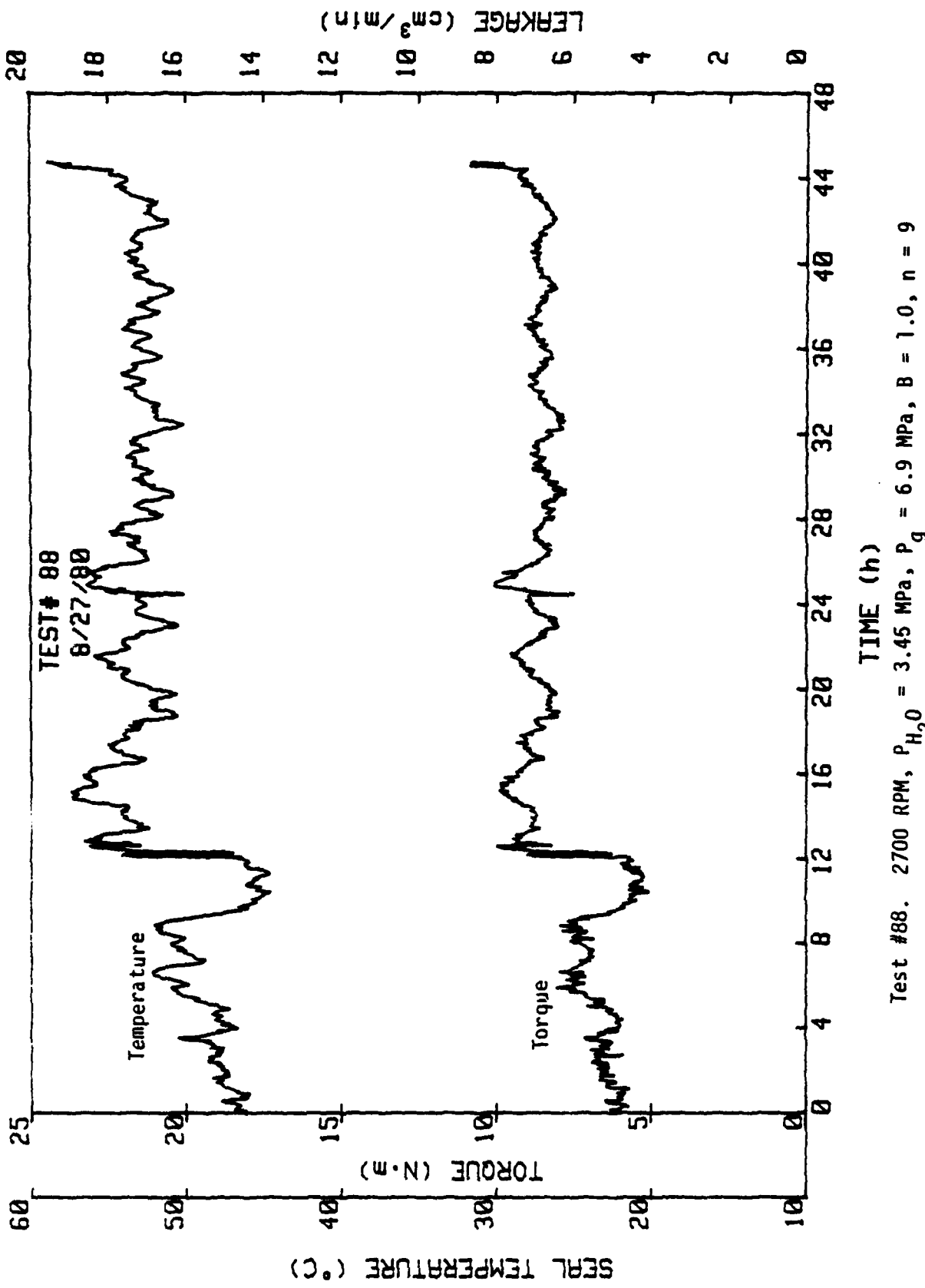


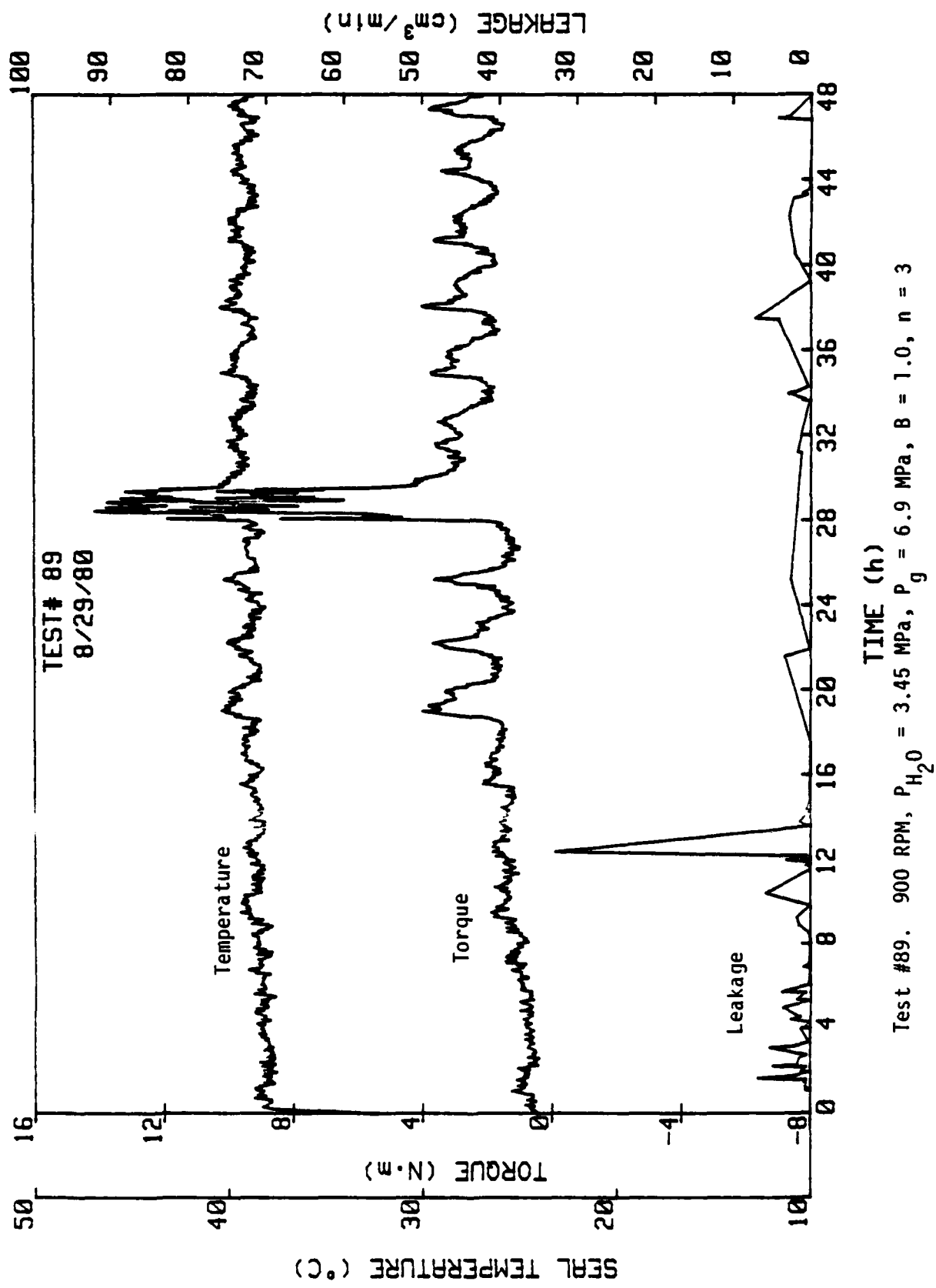
Test #85. 1800 RPM, $P_{H_2O} = 3.45 \text{ MPa}$, $P_g = 6.9 \text{ MPa}$, $B = 1.0$, $n = 9$

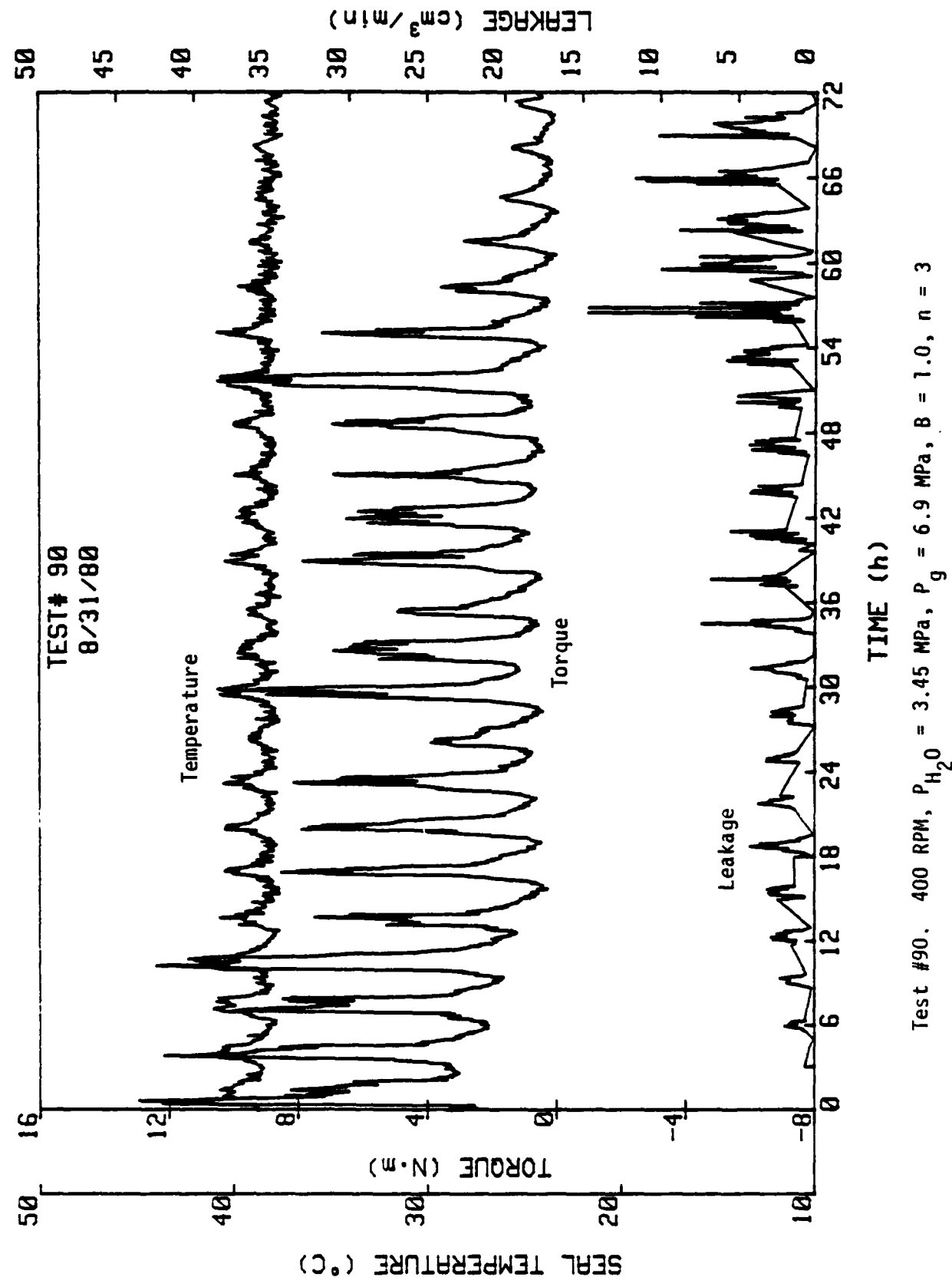


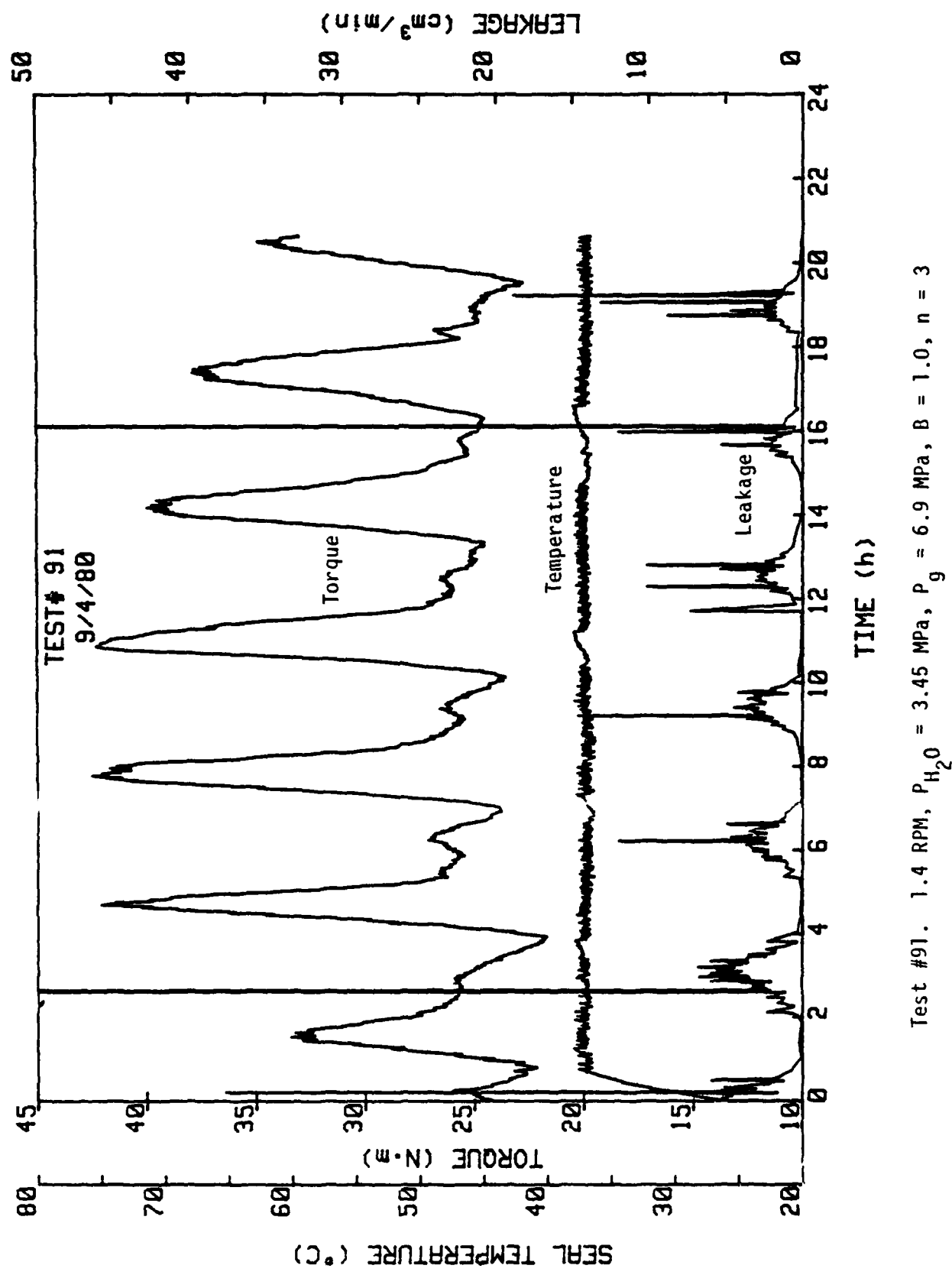


Test #87. 1800 RPM, $P_{H_2O} = 3.45 \text{ MPa}$, $P_g = 6.9 \text{ MPa}$, $B = 1.0$, $n = 9$

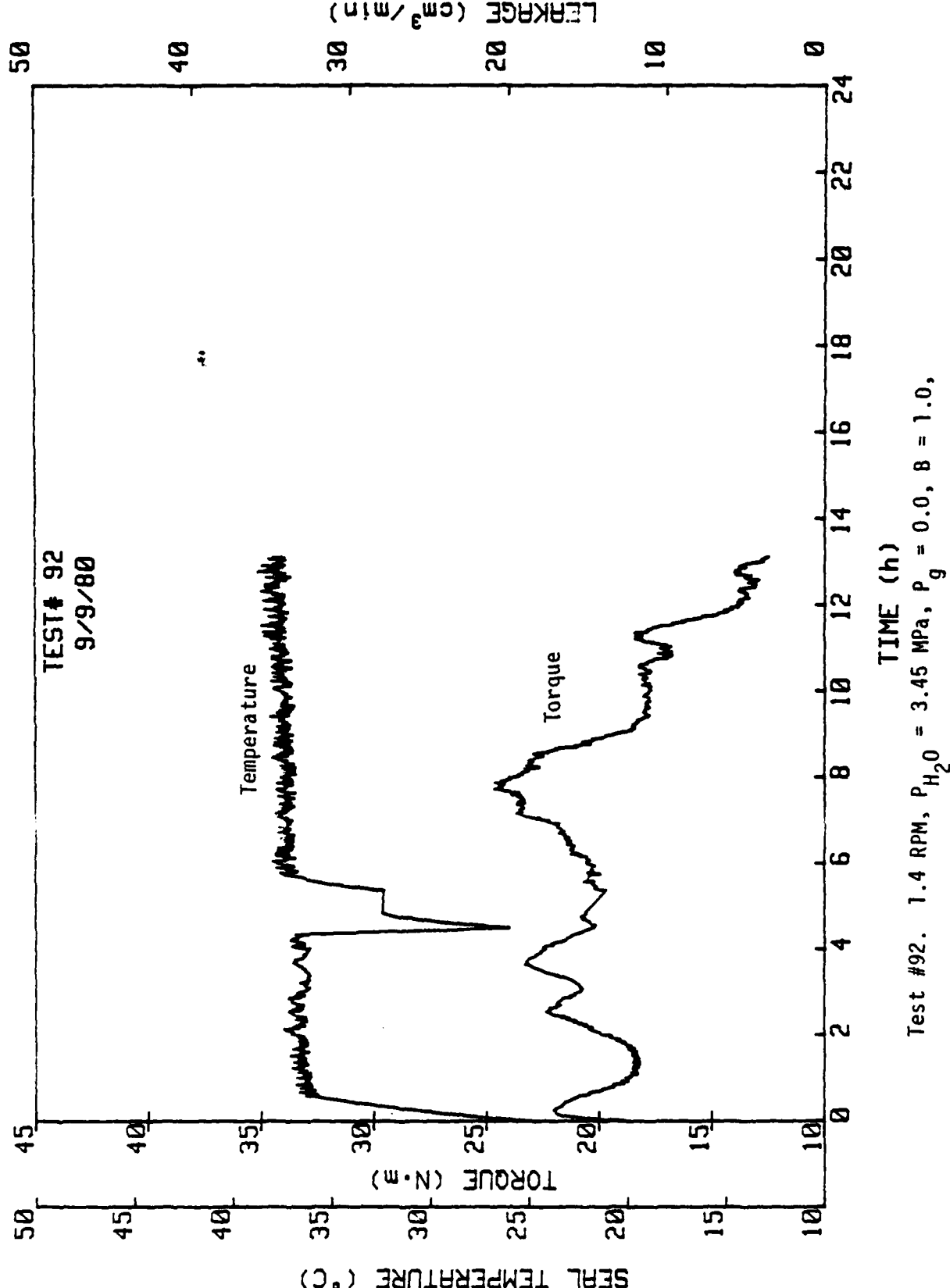


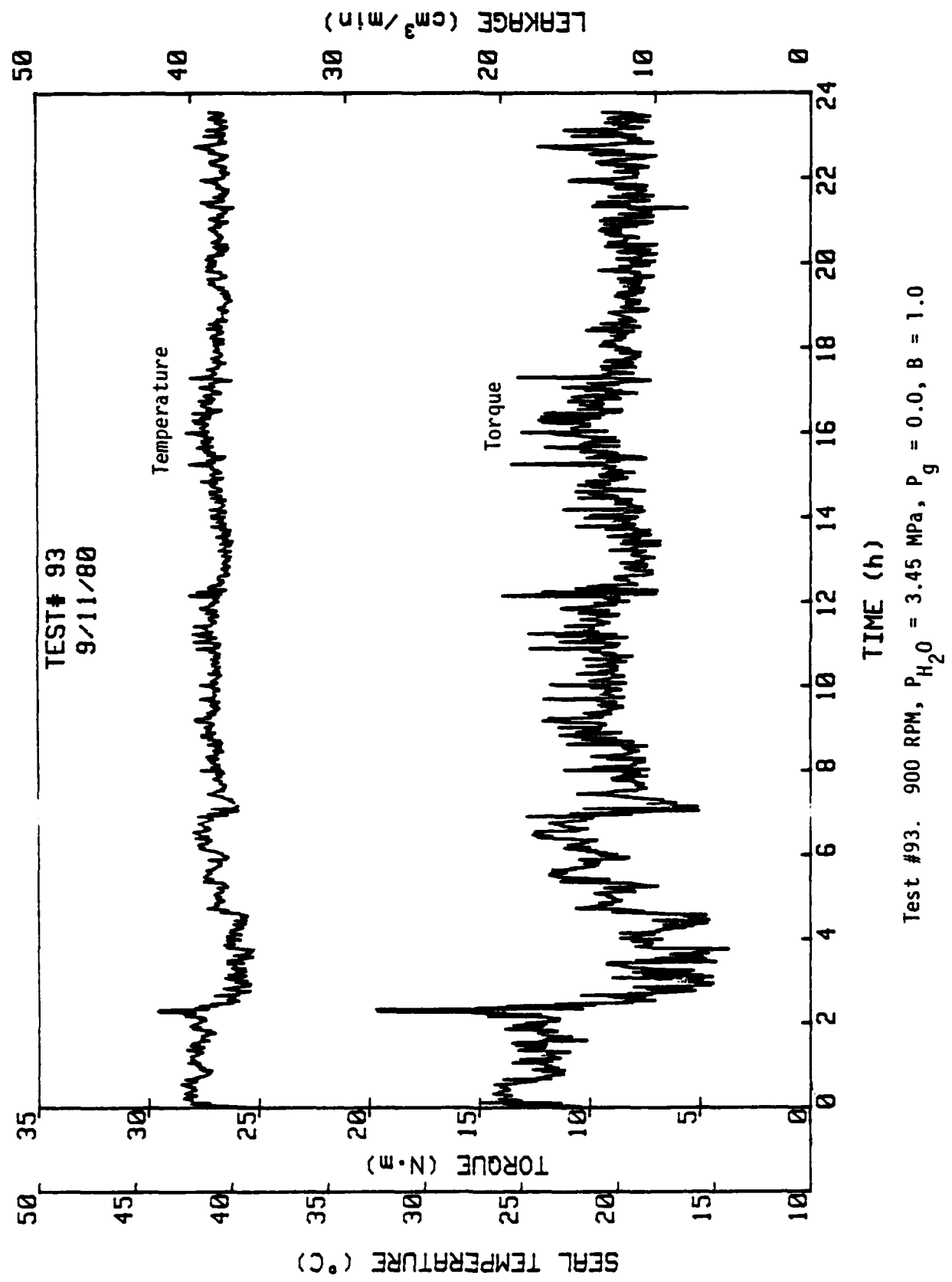


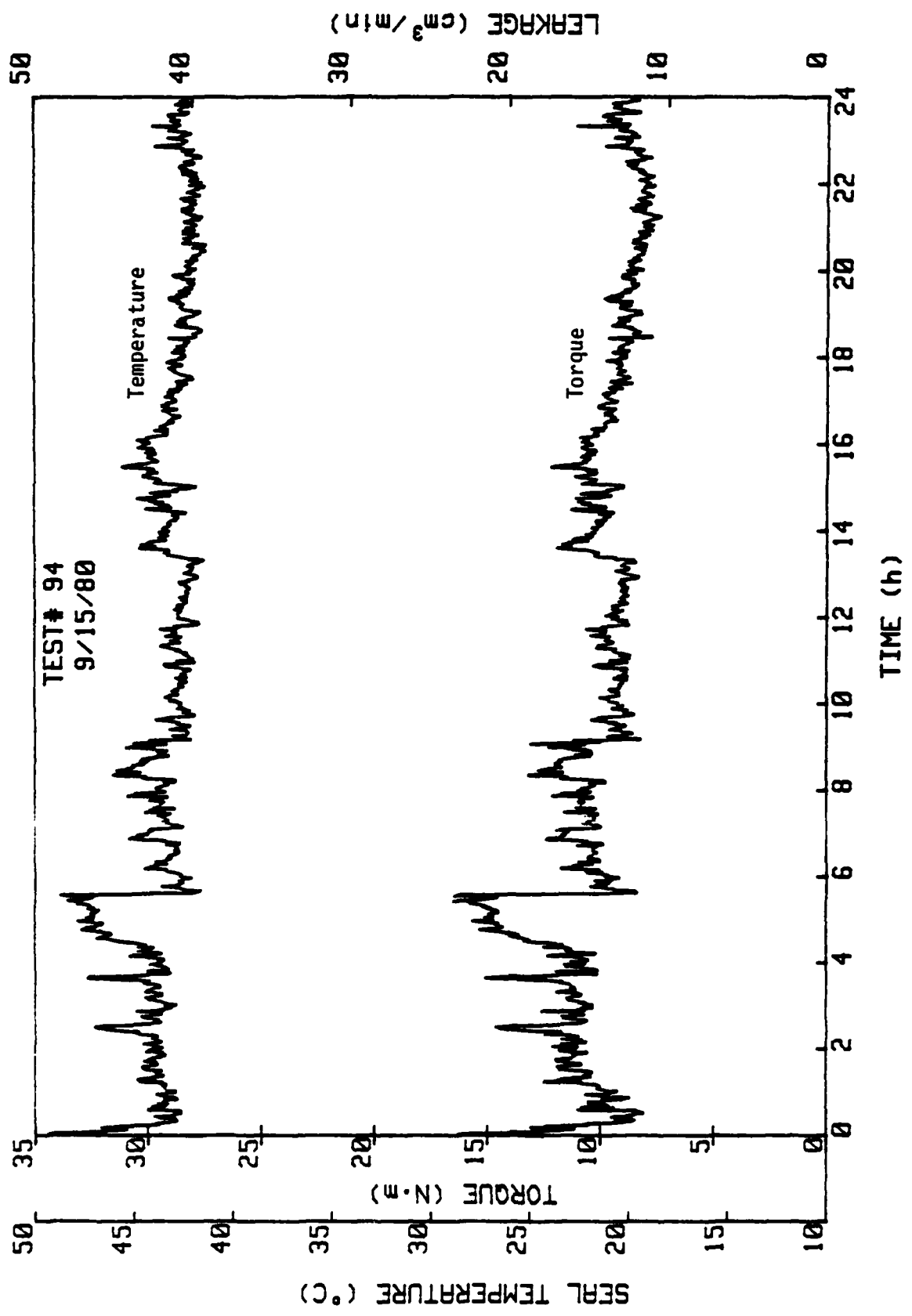


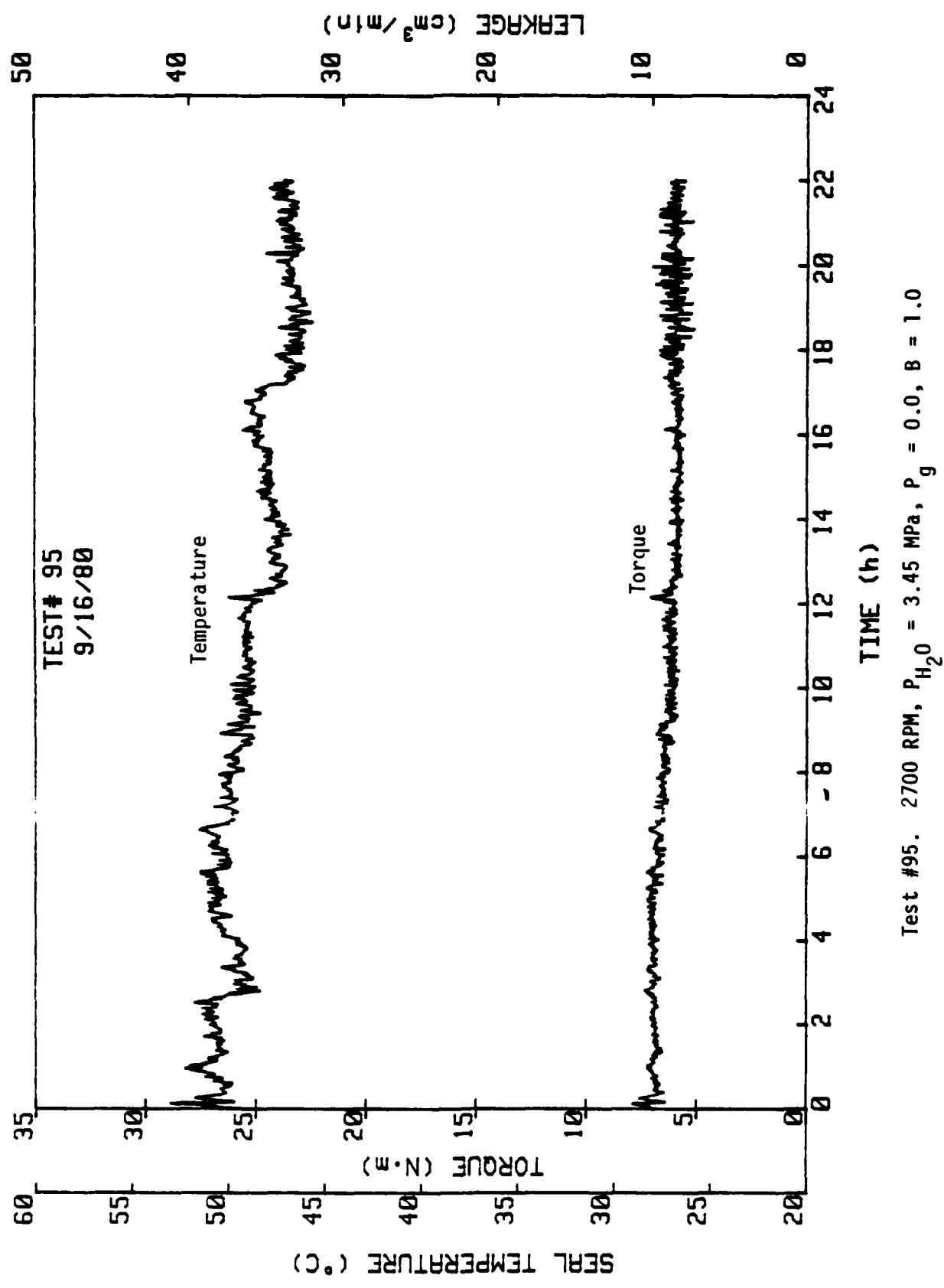


Test #91. 1.4 RPM, $P_{\text{H}_2\text{O}} = 3.45 \text{ MPa}$, $P_g = 6.9 \text{ MPa}$, $B = 1.0$, $n = 3$

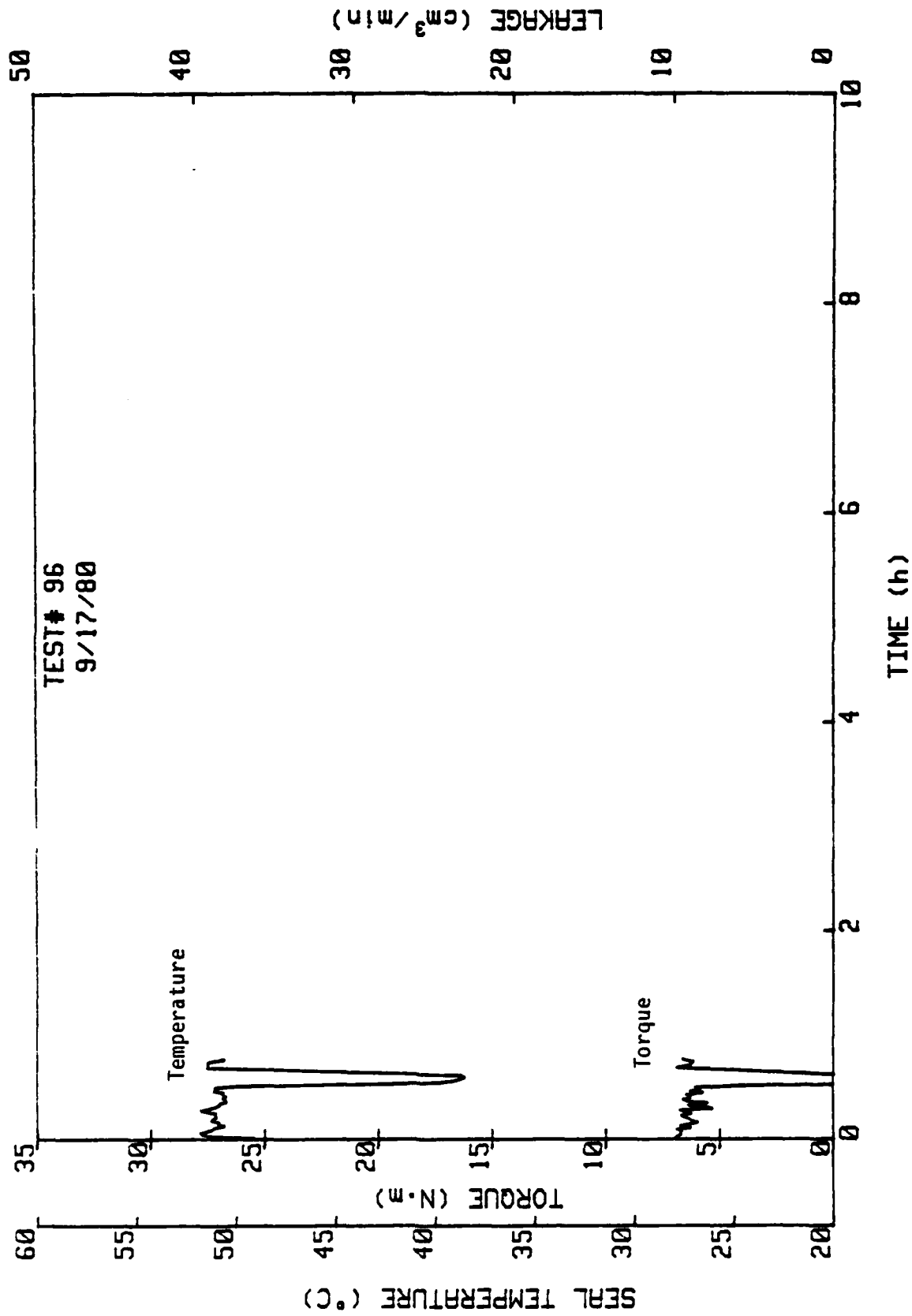




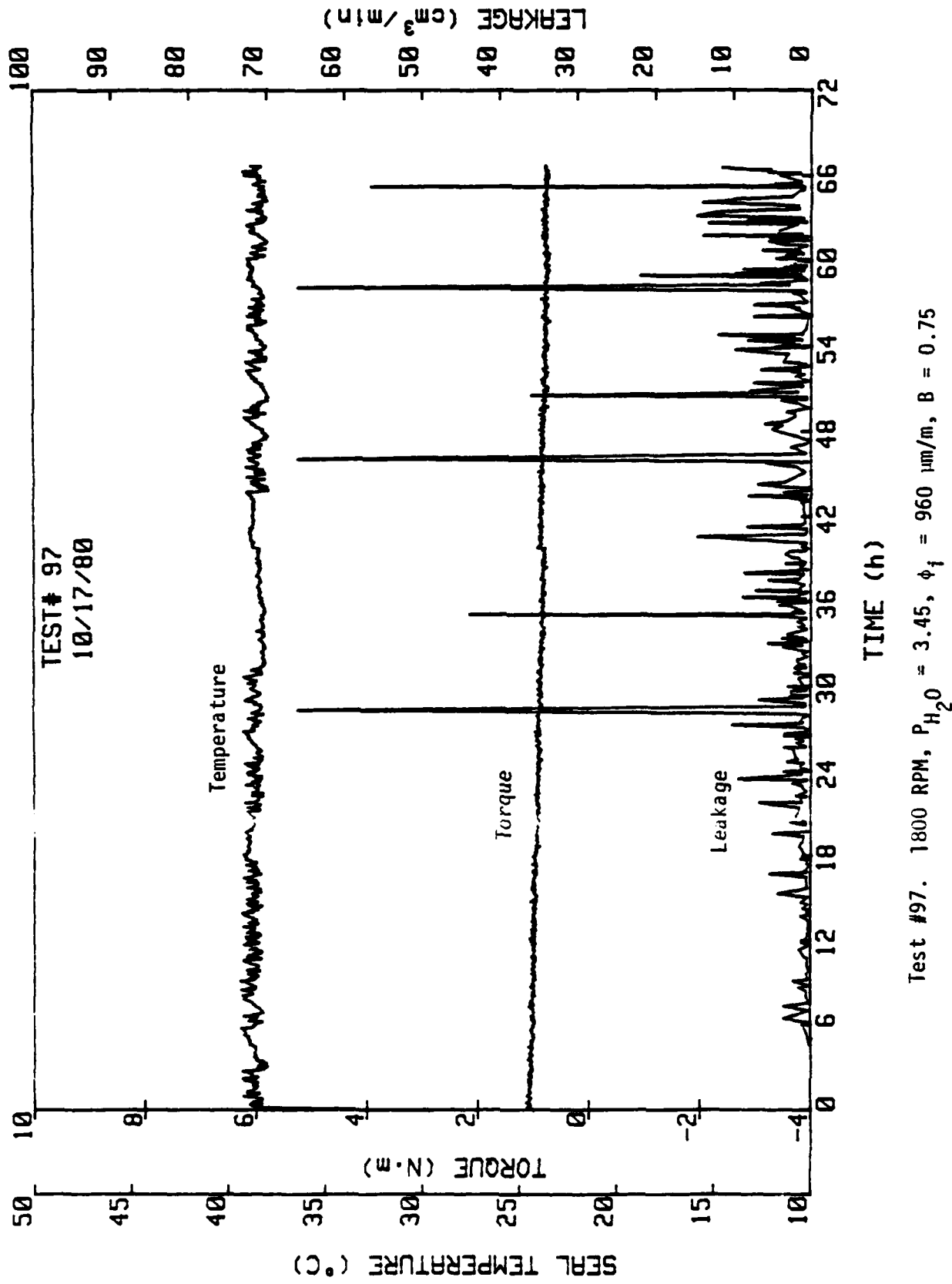




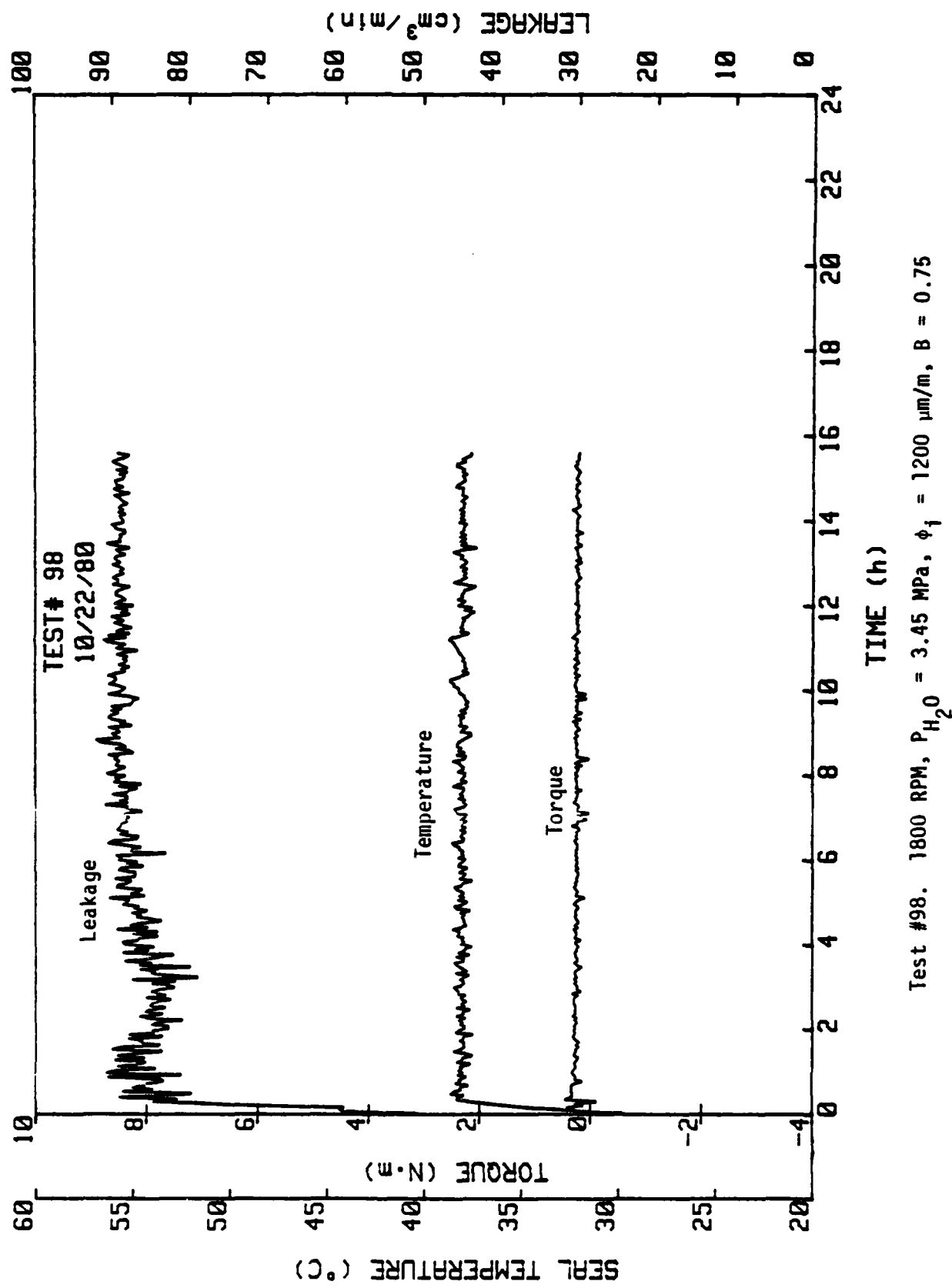
Test #95. 2700 RPM, $P_{H_2O} = 3.45 \text{ MPa}$, $P_g = 0.0$, $B = 1.0$

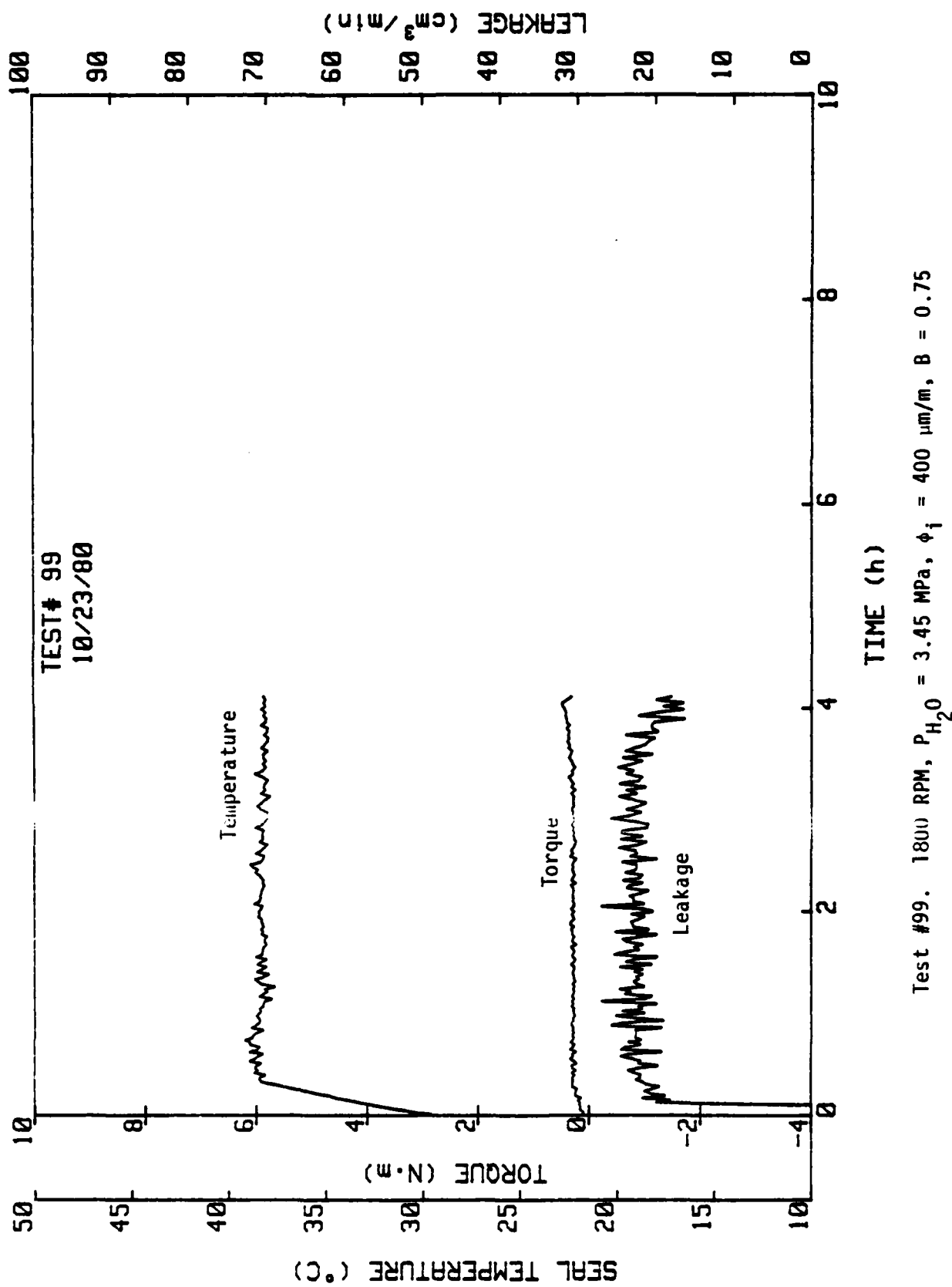


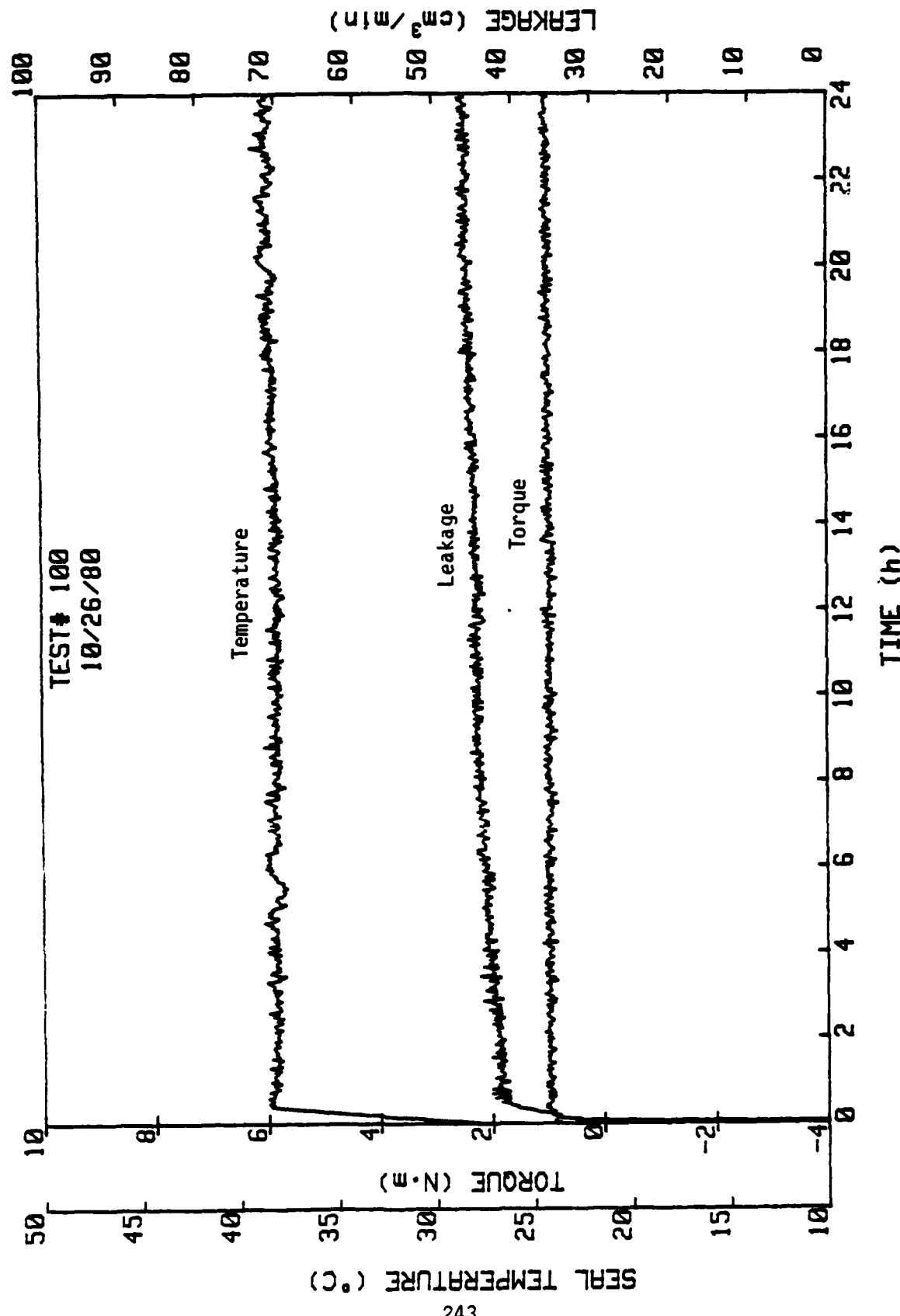
Test #96. 3600 RPM, $P_{\text{H}_2\text{O}} = 3.45 \text{ MPa}$, $P_g = 0.0$, $B = 1.0$



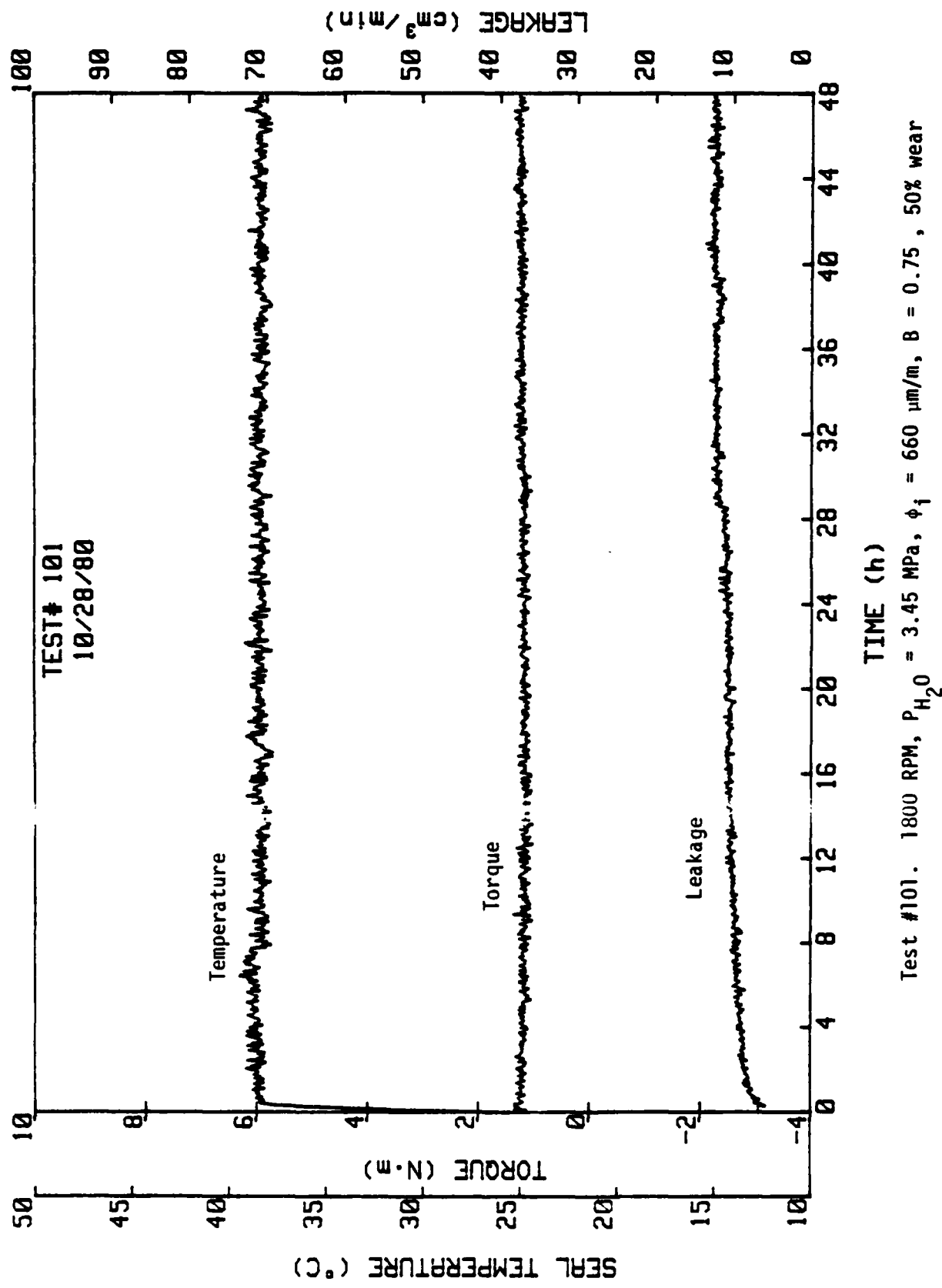
Test #97. 1800 RPM, $P_{H_2O} = 3.45$, $\phi_i = 960 \mu\text{m/m}$, $B = 0.75$



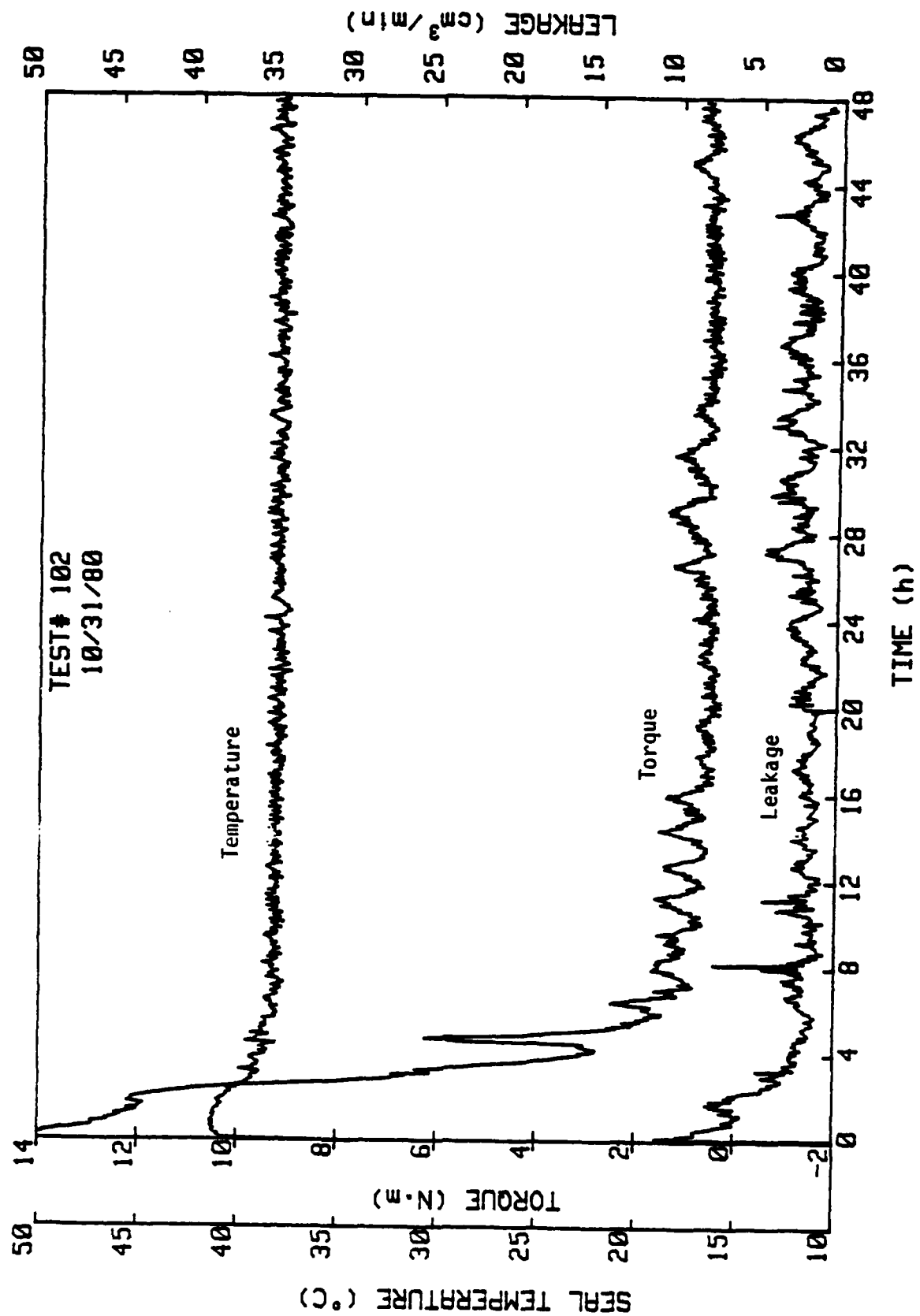


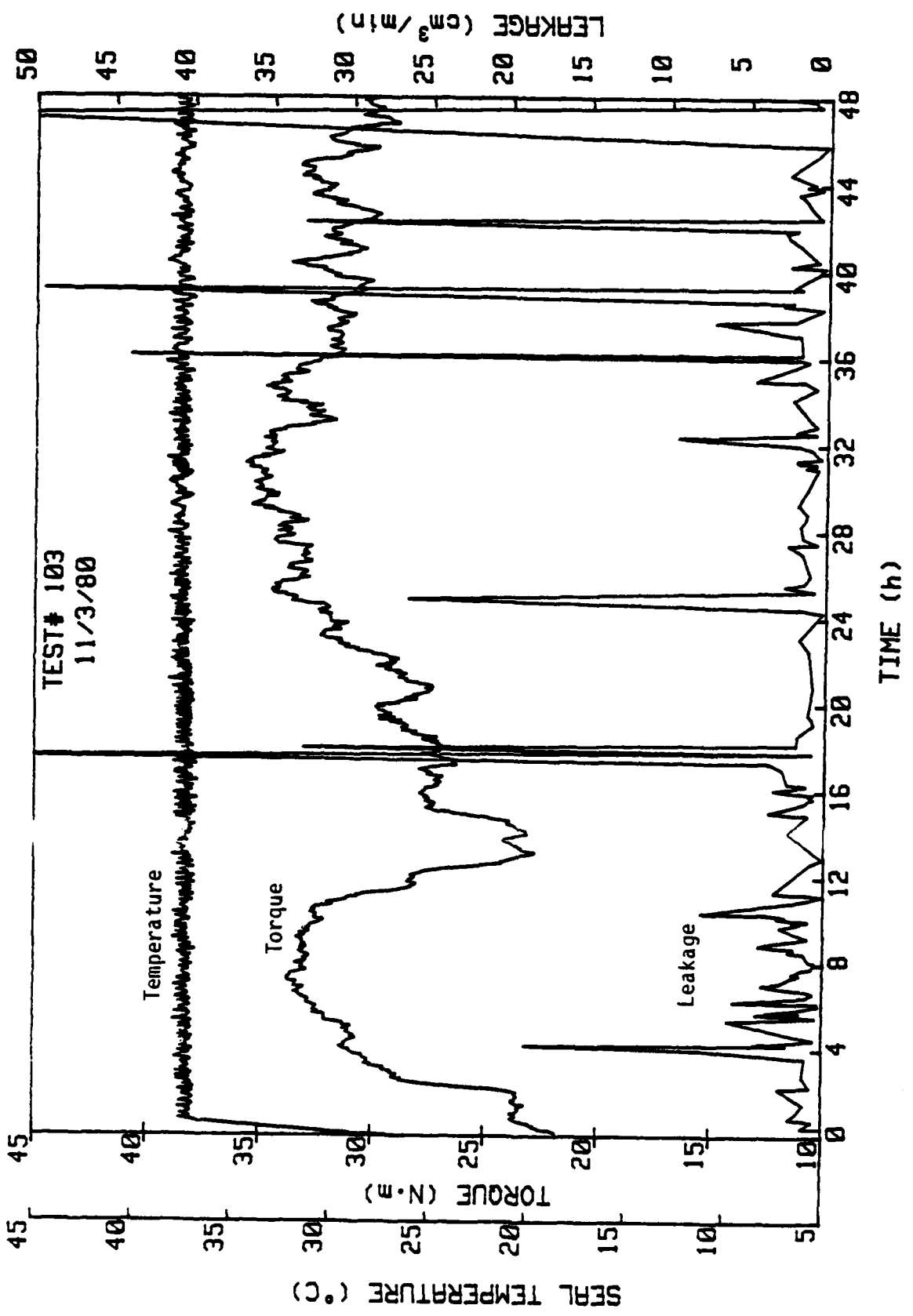


Test #100. 1800 RPM, $P_{H_2O} = 3.45$ MPa, $\phi_1 = 643 \mu\text{m}/\text{m}$, $B = 0.75$

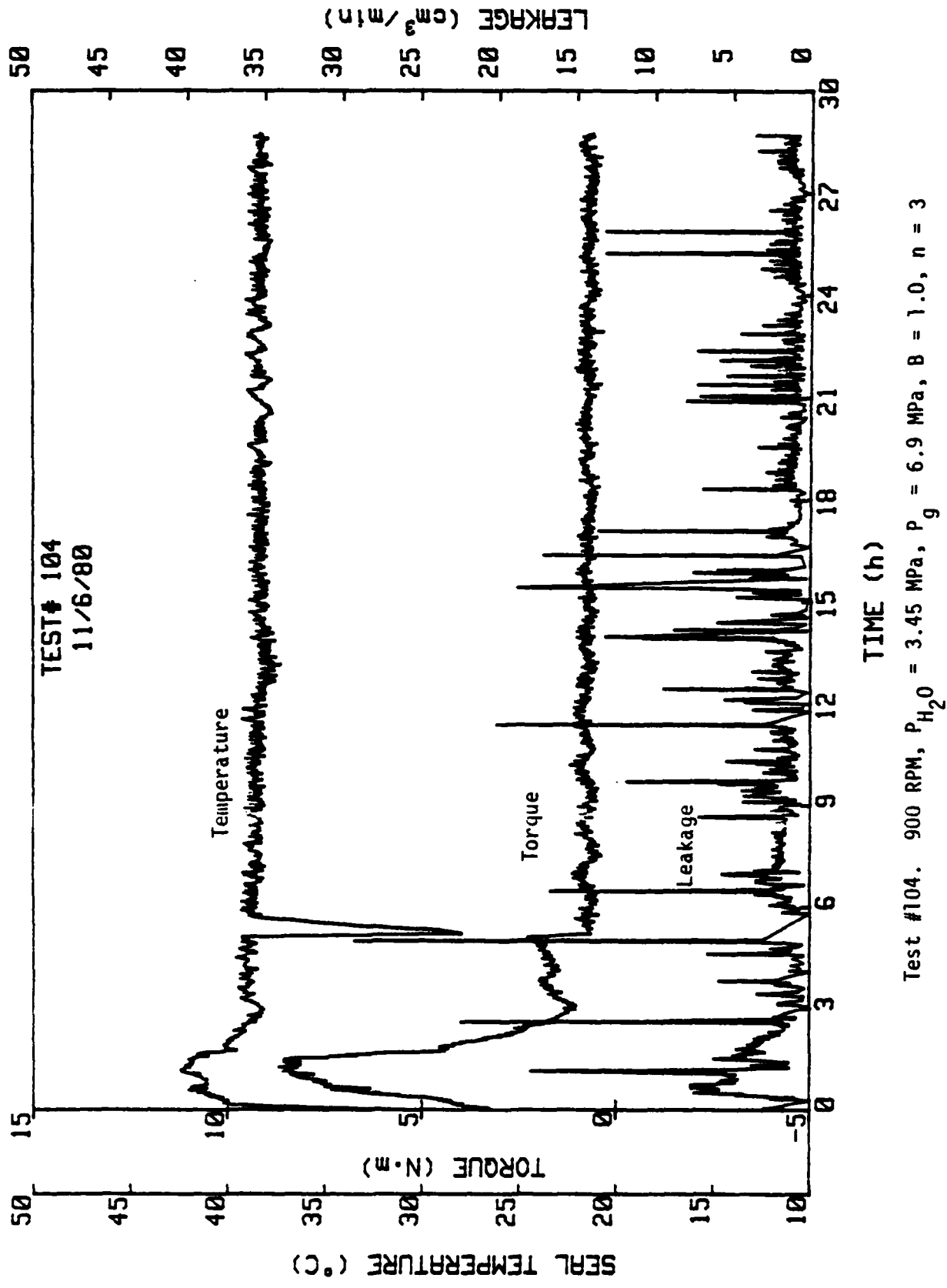


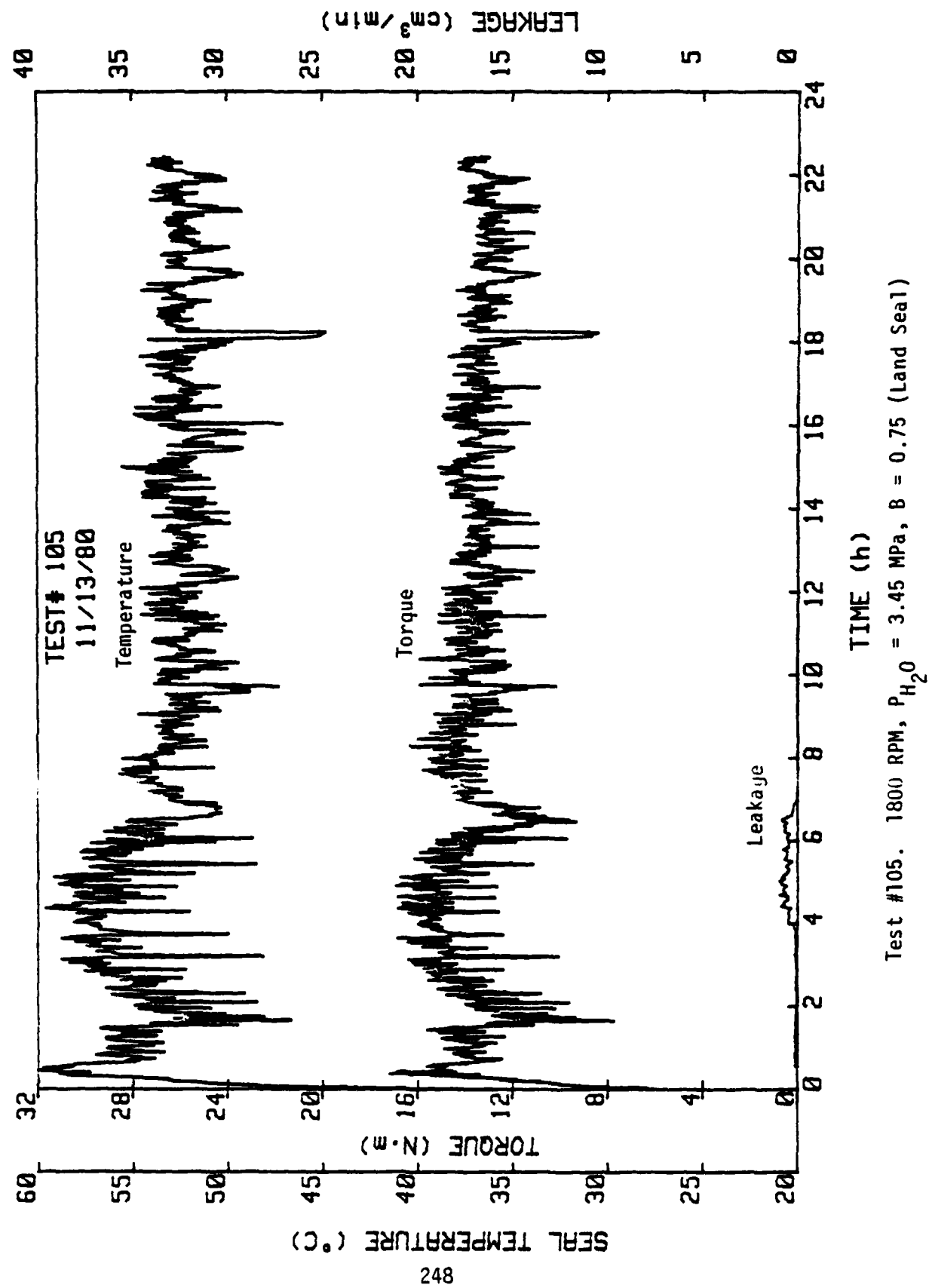
Test #101. 1800 RPM, $P_{H_2O} = 3.45$ MPa, $\phi_i = 660 \mu\text{m/m}$, $B = 0.75$, 50% wear

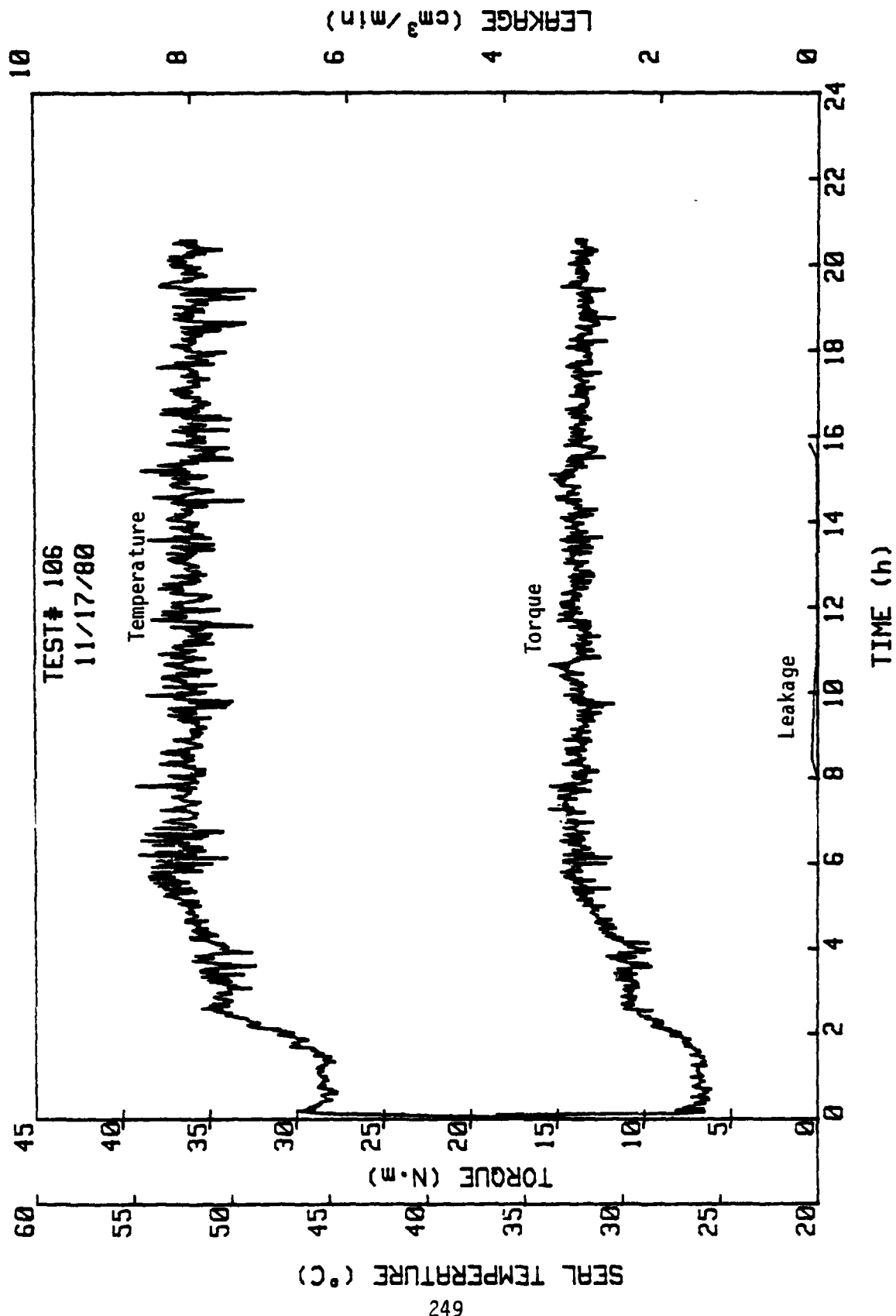




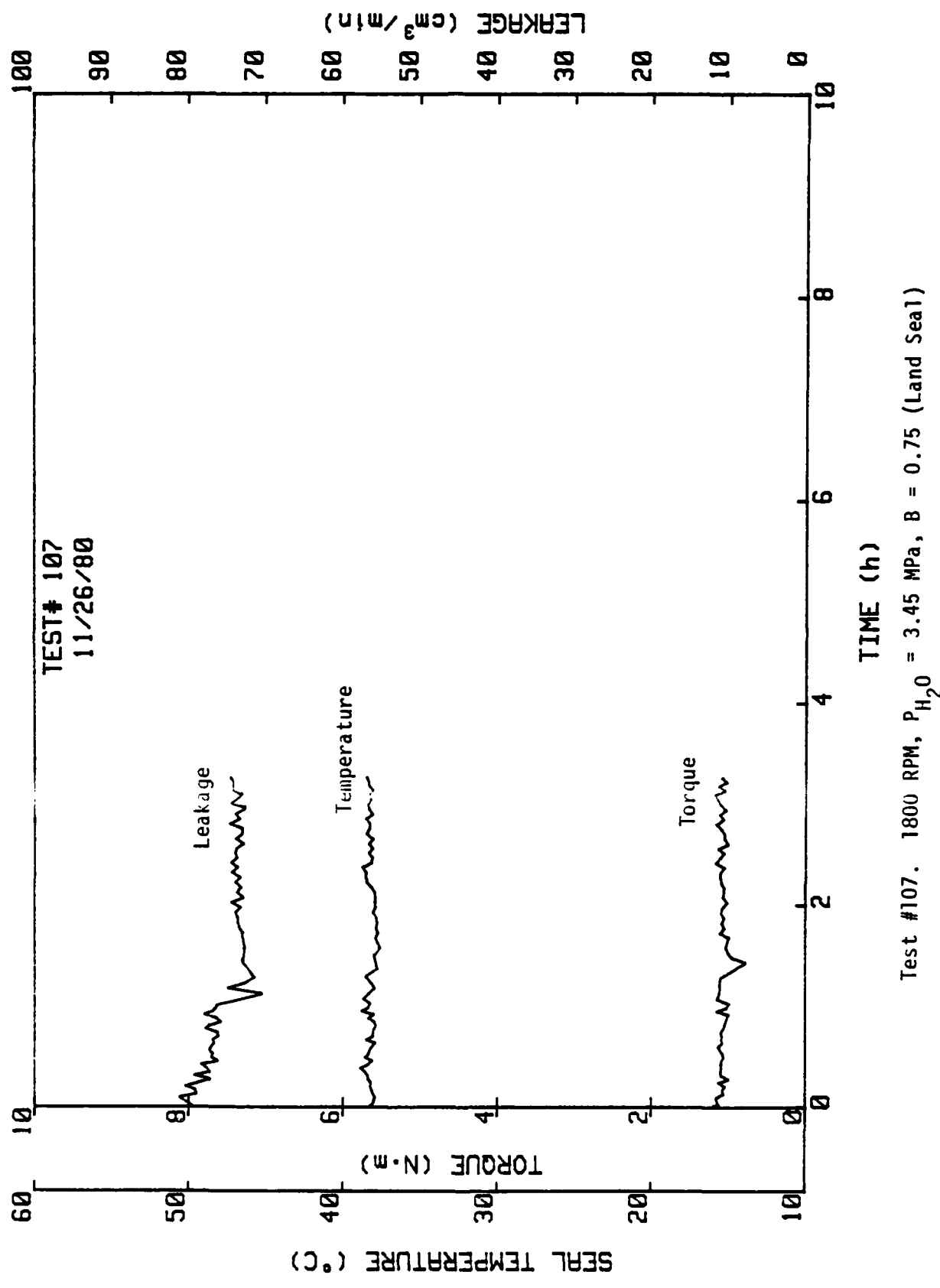
Test #103. 1.4 RPM, $P_{\text{H}_2\text{O}} = 3.45 \text{ MPa}$, $P_g = 6.9 \text{ MPa}$, $B = 1.0$, $n = 3$

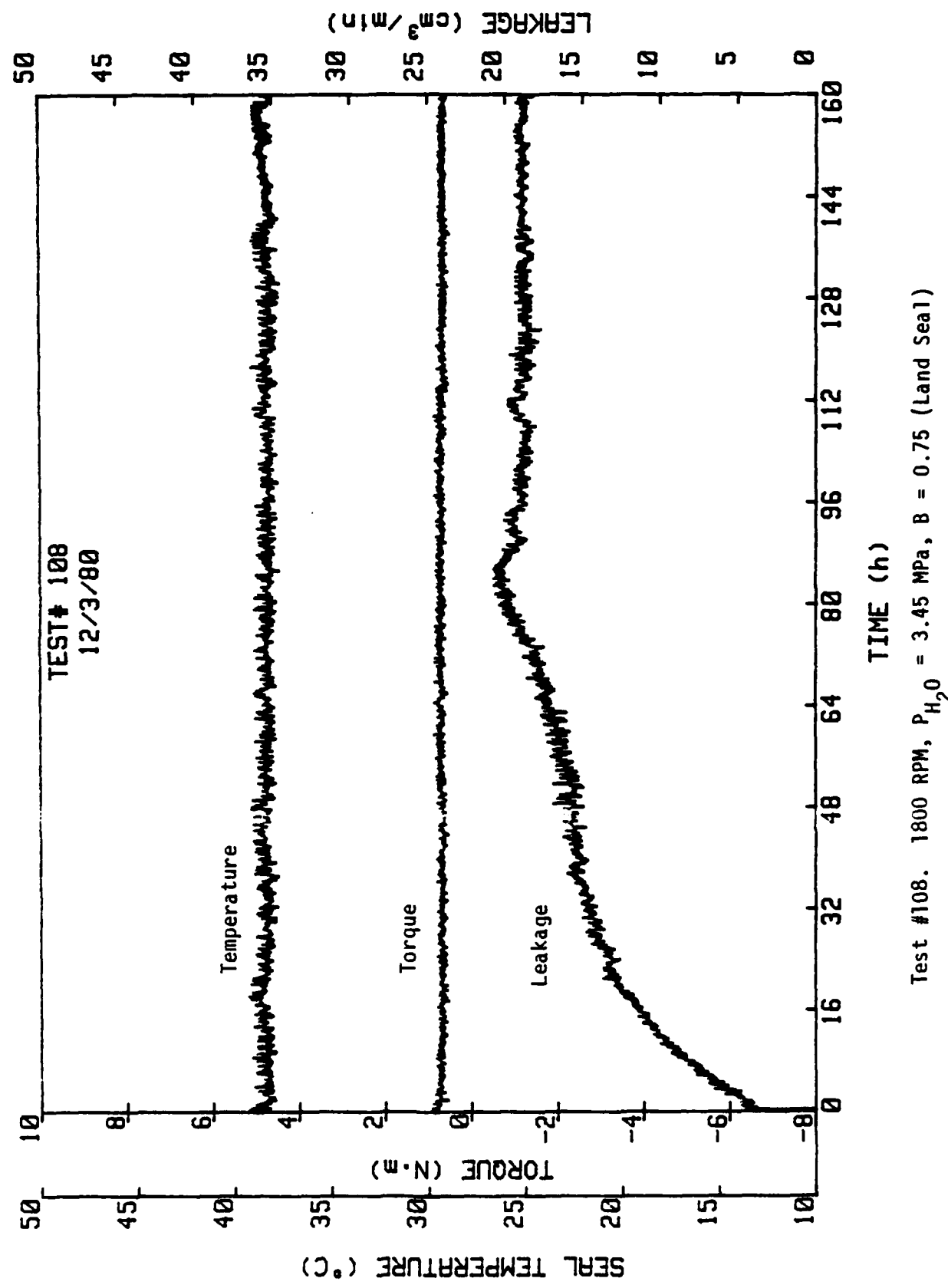


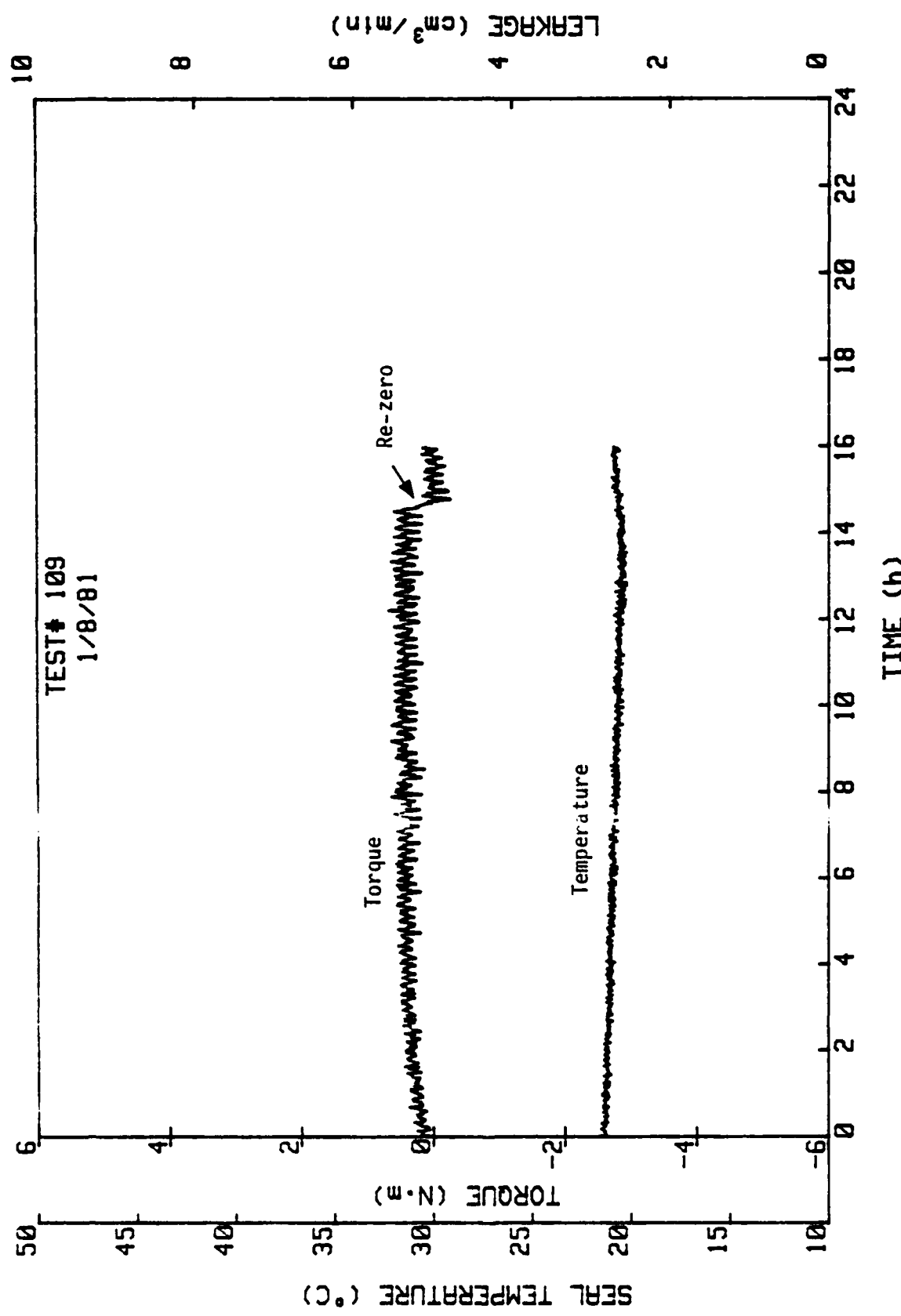




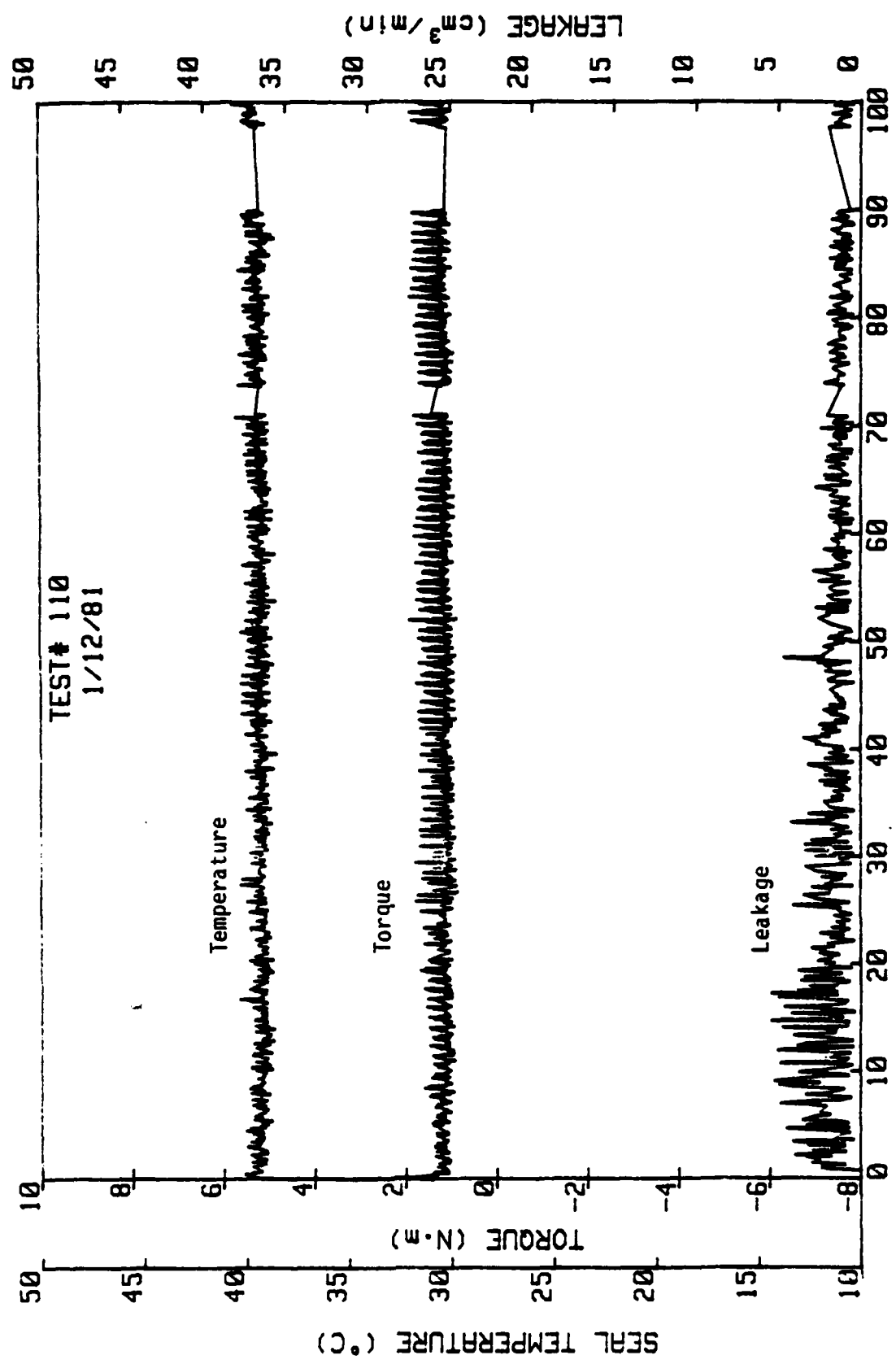
Test #106. 1800 RPM, $P_{H_2O} = 3.45 \text{ MPa}$, $B = 0.75$ (Land Seal)



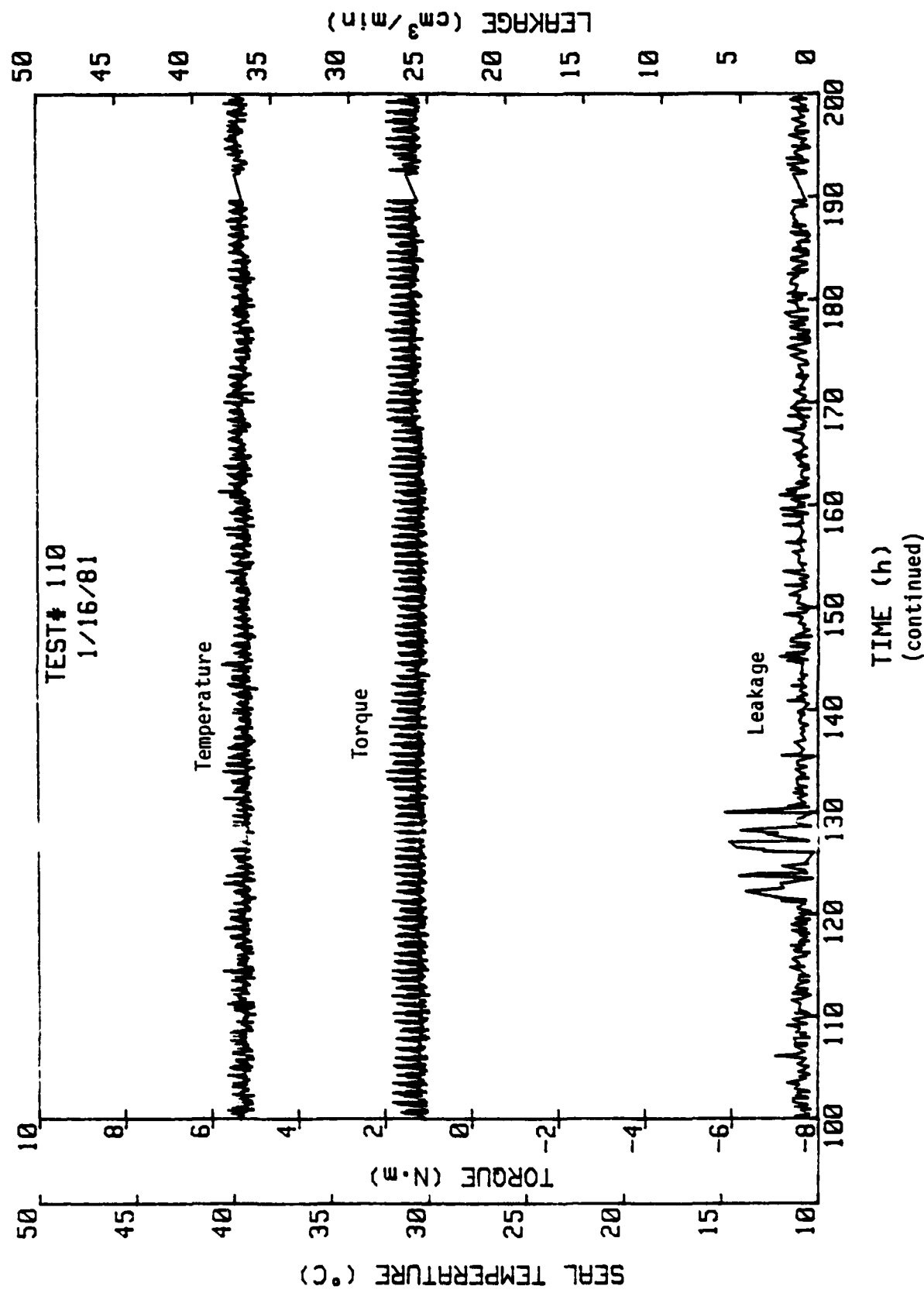




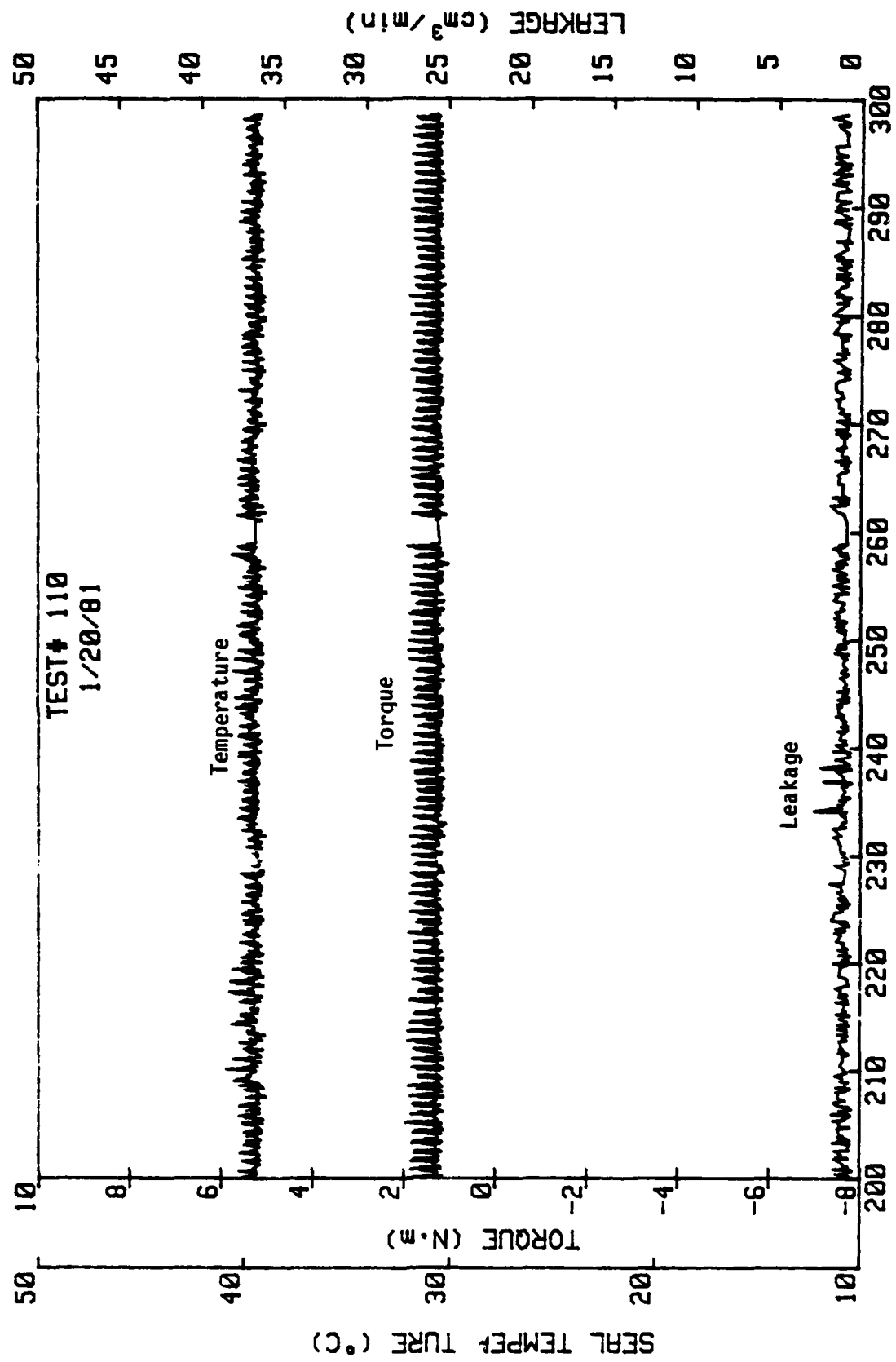
Test #109. Effect of waviness pressure on torque (0 RPM)

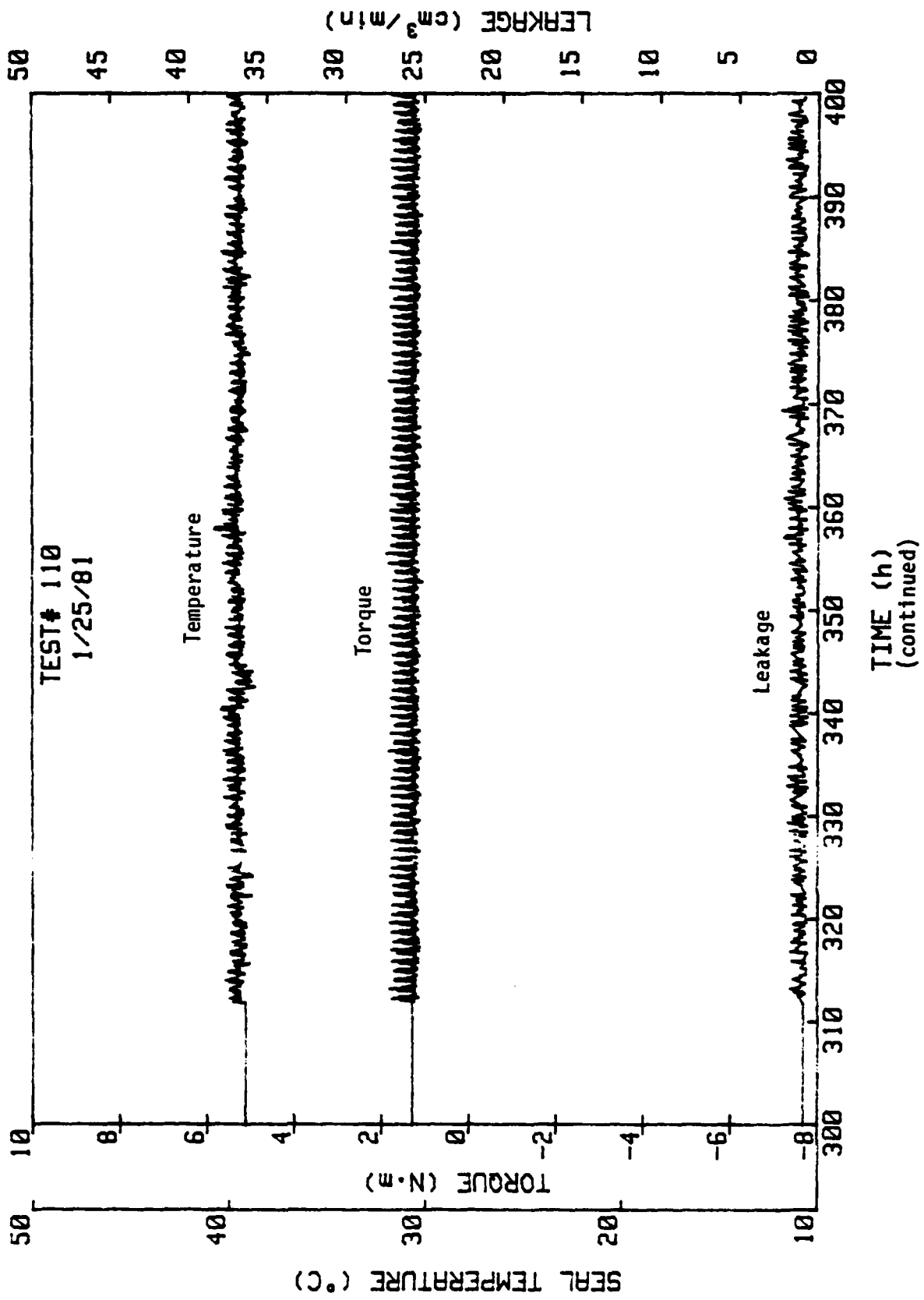


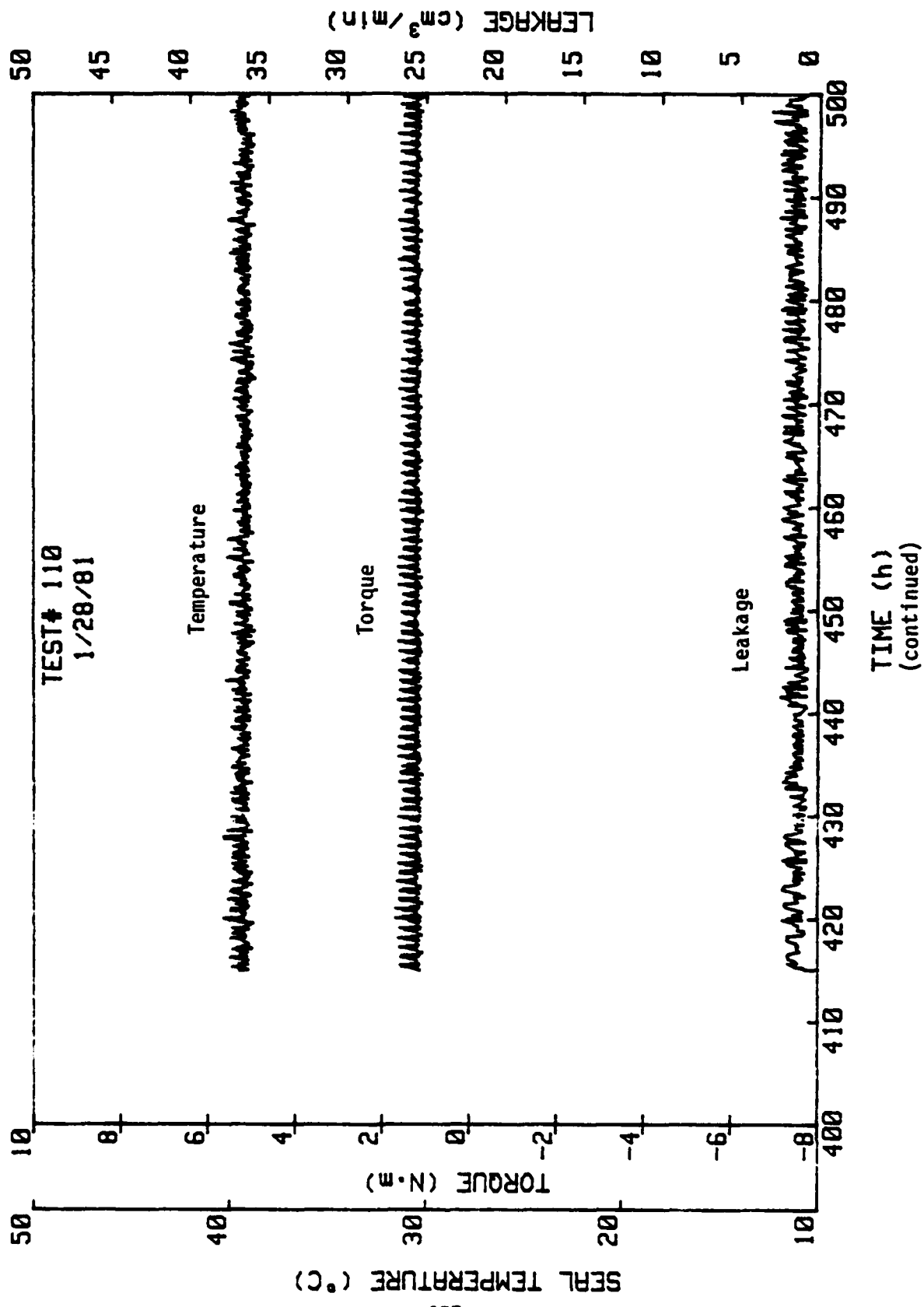
Test #110. 1800 RPM, $P_{\text{H}_2\text{O}} = 3.45 \text{ MPa}$, $P_g = 6.9 \text{ MPa}$, $n = 3$ (with new waviness generator)



(continued)







Distribution List

<u>Recipient</u>	<u>Number of Copies</u>
Office of Naval Research 800 N. Quincy Street Arlington, Virginia 22217 Attn: M. Keith Ellingsworth, Code 473	(3)
Defense Documentation Center Building 5 Cameron Station Alexandria, Virginia 22314	(12)
Naval Research Laboratory 4555 Overlook Avenue Washington, DC 20390 Attn: Technical Information Division Code 2627 Dr. Ravner, Code 6170	(6) (1)
U.S. Naval Postgraduate School Monterey, California 93940 Attn: Dept. of Mechanical Engineering	(1)
U.S. Naval Academy Annapolis, Maryland 21402 Attn: Dept. of Mechanical Engineering	(1)
Naval Air Systems Command Jefferson Plaza Washington, DC 20360 Attn: B. Poppert, Code 240E	(1)
Naval Sea Systems Command Crystal City, National Center #3 Washington, DC 20360 Attn: Frank Ventriglio, Code OSRT14	(1)
Naval Ships R&D Center Annapolis, Maryland 21402 Attn: Friction and Wear Branch J. F. Dray	(1)
Naval Air Engineering Center Lakehurst, New Jersey 08733 Attn: Mr. P. Senholzi	(1)
Naval Air Propulsion Test Center Trenton, New Jersey 08628 Attn: Mr. R. Valori	(1)

Distribution List (continued)

<u>Recipient</u>	<u>Number of Copies</u>
Naval Air Development Center Warminster, Pennsylvania 18974 Attn: Mr. A. Conte	(1)
National Science Foundation 1800 G Street, NW Washington, DC 20550 Attn: Dr. C. J. Astill	(1)
National Bureau of Standards Washington, DC 20234 Attn: Dr. W. Ruff	(1)
NASA Lewis Research Center 21000 Brookpark Road Cleveland, Ohio 44135 Attn: R. L. Johnson	(1)
Air Force Office of Scientific Research Washington, DC 20333 Attn: Directorate of Engineering Sciences	(1)
Air Force Aeropropulsion Laboratory Wright-Patterson Air Force Base, Ohio 45433 Attn: AFAPL/POD-1, Dick Quigley, Jr.	(1)
Army Research Office Durham, North Carolina 27706 Attn: Dr. E. A. Saibel	(1)
Office of Naval Research Branch Office 1030 East Green Street Pasadena, California 91106	(1)
Assistant Chief for Technology Office of Naval Research, Code 200 Arlington, Virginia	(1)
Prof. H. S. Cheng Department of Mechanical Engineering Northwestern University Evanston, Illinois	(1)
Crane Packing Company 6400 Oakton Street Morton Grove, Illinois 60053 Attn: Art Zobens	(1)

Distribution List - continued

<u>Recipient</u>	<u>Number of Copies</u>
Sealol, Inc. Box 2158 Providence, Rhode Island 02905 Attn: H. F. Greiner	(1)
Pure Carbon Company St. Marys, Pennsylvania 15857 Attn: R. R. Paxton	(1)
Franklin Research Institute 20th and Race Streets Philadelphia, Pennsylvania 19103 Attn: Harry C. Rippel	(1)
Naval Sea Systems Command Crystal City, National Center #3 Washington, DC 20360 Attn: Code 524, Dick Graham	(1)
Naval Ships R&D Center Annapolis, Maryland 21402 Attn: Al Harbaugh	(1)
Prof. Francis E. Kennedy, Jr. Thayer School of Engineering Dartmouth College Hanover, New Hampshire 03755	(1)
Mr. Clif Mussen PMS 396-223 Trident Submarine Ship Acquisition Project Naval Sea Systems Command Department of Navy Washington, DC 20362	(1)